

## N O T I C E

THIS DOCUMENT HAS BEEN REPRODUCED FROM  
MICROFICHE. ALTHOUGH IT IS RECOGNIZED THAT  
CERTAIN PORTIONS ARE ILLEGIBLE, IT IS BEING RELEASED  
IN THE INTEREST OF MAKING AVAILABLE AS MUCH  
INFORMATION AS POSSIBLE

CR/152380  
(R. voyage)

3

(NASA-CR-152380) PHASE 2 AND 3 WIND TUNNEL  
TESTS OF THE J-97 POWERED, EXTERNAL  
AUGMENTOR V/SIOL MODEL (De Havilland  
Aircraft Co. of Canada Ltd.) 148 p  
HC AC8/MF A01

N81-26076

Unclass  
CSCL C1A G3/02 28872



THE DE HAVILLAND AIRCRAFT OF CANADA LIMITED

NASA CR 152380

DHC-DND 80-1

PHASE 2 AND 3 WIND TUNNEL TESTS  
OF THE J-97 POWERED, EXTERNAL  
AUGMENTOR V/STOL MODEL

REVISED OCTOBER, 1980

DE HAVILLAND AIRCRAFT OF CANADA, LIMITED  
DOWNSVIEW, ONTARIO M3K 1Y5

DHC-DND 80-1

PHASE 2 AND 3 WIND TUNNEL TESTS  
OF THE J-97 POWERED, EXTERNAL  
AUGMENTOR V/STOL MODEL

NASA Contract No. NASW 2797

DSS Contract Serial No. 2SR77-00008

Prepared & Submitted by ..... D.B. Garland ..... J.L. Harris .....  
D.B. Garland J.L. Harris

Approved by ..... D.C. Whittley .....  
D.C. Whittley

## 1. SUMMARY

Further static and forward speed tests have been made in the 40- by 80- Foot Wind Tunnel at the Ames Research Center, NASA, of a large-scale, ejector-powered V/STOL aircraft model. Modifications had been made to the model following earlier tests primarily to improve longitudinal acceleration capability during transition from hovering to wing-borne flight. A rearward deflection of the fuselage augmentor thrust vector was shown to be beneficial in this regard. Other augmentor modifications were tested, notably the removal of both endplates, which improved acceleration performance at the higher transition speeds. The model tests again demonstrated minimal interference of the fuselage augmentor on aerodynamic lift. A flapped canard surface also showed negligible influence on the performance of the wing and of the fuselage augmentor.

2. CONTENTS

	<u>PAGE NOS.</u>
1. SUMMARY	1
2. CONTENTS	2
3. INTRODUCTION	4
4. DESCRIPTION OF MODEL AND TESTS	6
4.1 Model	6
4.2 Thrust Loading	8
4.3 Reference Pressure Ratio	9
4.4 Data Reduction	9
5. STATIC TEST RESULTS	12
6. FORWARD SPEED RESULTS	15
6.1 Presentation of Transition Performance	15
6.2 Basic Augmentor Configuration	17
6.3 Intermediate Augmentor Configurations	18
6.4 Augmentor-Sealed (Wing-Borne) Configuration	20
6.5 Summarized Acceleration Capability	21
6.6 Pitch Trim	21
6.7 Effect of Wing-Leading Edge Slat	22
6.8 Interference Effects of Fuselage Augmentor	22
6.8.1 Longitudinal	22
6.8.2 Lateral	24
6.9 Augmentor Exit Rake Results	24
6.9.1 Exit Distributions	24
6.9.2 Augmentor Inlet Vanes	25
6.10 Canard Characteristics and Interference Effects	27
6.10.1 Longitudinal	27
6.10.2 Lateral/Directional	28
7. CONCLUSIONS	29
8. REFERENCES	32
9. NOTATION	34
TABLES 1 - 8	37-55

PAGE NOS.

## TABLES

1	Geometry of J-97 Powered, External Augmentor V/STOL Model	36
2	Geometry of Fuselage Augmentor	37
3	Geometry of Wing Augmentor	38
4	Run History, VTOL 2 Tests	39 - 42
5	Run History, VTOL 3 Tests	43 - 46
6	Static Performance Summary	47 - 48
7	Transition Configurations Tested	49
8	Summary of Transition Performance	50 - 54

Figures 1-90

### 3. INTRODUCTION

Initial static and wind tunnel tests of the large-scale model of the DHC 'external-augmentor' V/STOL concept were undertaken in 1977-78 and reported in References 1, 2 and 3. Two further wind tunnel tests have now been completed, the results from which have been combined to form the present test report. The model is fully described in References 4 and 5. Descriptions of the concept together with an overview of test results have been published in References 6 and 7.

The objectives addressed in these latest tests were to investigate the effects of the following:

- (a) Vectoring of the fuselage augmentor thrust (the augmentor nozzles were deflected rearward by  $12\frac{1}{2}^{\circ}$ ).
- (b) Fuselage augmentor throttling (the diffuser area ratio was reduced from 1.6 to 0.5 at forward speed).
- (c) Thrust transfer from fuselage augmentor nozzles to a rear propulsion nozzle (individual fuselage augmentor nozzles were 'blanked-off' in several arrangements).
- (d) Removal of fuselage augmentor endplates at forward speed (normally required statically to maintain a high thrust augmentation ratio).
- (e) Fuselage augmentor inlet vanes (two different arrangements to improve flow into the augmentor at high forward speed).
- (f) Leading-edge slat on outboard wing panels (to eliminate a previously observed wing stall).

- (g) Canard surface interference on wing and fuselage augmentor.
- (h) 'Wing-borne' configuration (i.e. fuselage augmentor sealed and all fuselage augmentor nozzle thrust transferred to the rear propulsion nozzle, the wing augmentor remaining operational).

The research work described here was conducted by De Havilland Aircraft of Canada (DHC) in cooperation with the Ames Research Center, NASA: the work was funded jointly by the Canadian Department of National Defence and NASA and undertaken with the support of the facilities of the Ames Research Center.

#### 4. DESCRIPTION OF MODEL AND TESTS

##### 4.1 Model

A three-view drawing of the model is given in Figure 1. Photographs of the model in the 40- by 80- Foot Wind Tunnel at the Ames Research Center are reproduced as Figures 2 and 3. Tables 1, 2 and 3 list pertinent geometrical data.

The model geometry is the same as in the earlier tests, with the following exceptions:-

(a) Deflected fuselage augmentor nozzles.

The fuselage augmentor nozzles were 'twisted' through  $12\frac{1}{2}^{\circ}$  to provide an axial component of thrust to improve longitudinal acceleration during transition. Figure 4 shows how a 'twisted' segment was inserted into the basic nozzle to achieve the desired thrust deflection.

To maintain control over the flow at the augmentor endplates, the nozzle-to-endplate spacing has been retained at  $\frac{1}{4}$  pitch, hot. The inlet fairings and endplate locations have been modified accordingly, as shown in Figure 5. Two nozzles have been removed at the aft end of the augmentor to allow the rear endplate to remain within the existing augmentor door. This decreased the fuselage/wing thrust split ratio of 74/24 (References 1 through 3) to 68/24 which provides a favourable trend for improving transition.

(b) Hinged fuselage augmentor doors.

A revised door attachment scheme (Figure 6) was introduced to allow a wide range of diffuser area ratio and

yet still provide an essentially air-tight hinge. This feature will be most useful for future static tests when augmentor optimization will be pursued.

(c) Inlet turning vanes for fuselage augmentor.

Two designs of vanes were tested in an attempt to improve flow through the fuselage augmentor at forward speed. These are shown in Figure 7.

(d) Augmentor inlet cover plates.

As part of the transition studies, a longitudinally shortened augmentor was tested. Figure 8 shows how covers with inlet fairings were installed over the forward and rear quarters of the augmentor inlet leaving only the middle half of the augmentor operational. Nozzles under the covers were blanked-off. Augmentor endplates were removed and the augmentor door fixed at the required DAR by strut braces at the lower end of the doors.

(e) Leading edge slat for outboard wing panel.

A simple slat was attached to the outboard wing panels to extend the angle of attack range before leading edge stall occurred. Details are given in Figure 9.

(f) Canard surface.

A canard with leading edge slat and a plain flap (Figure 10) was mounted as shown in Figure 1. The flap was remotely controllable over the range  $0^\circ$  to  $30^\circ$  and the canard incidence could be manually set in increments of  $10^\circ$  in the range  $\pm 30^\circ$ .

(g) Sealed augmentor.

For tests representing the case where the fuselage augmentor was shut down, inlet covers were installed, the augmentor doors were removed and replaced with plywood panels in the 'closed door' position (see Figure 11). All the fuselage augmentor nozzles were blanked-off and a propulsion nozzle of equivalent area fitted to the rear end of the fuselage duct. The wing augmentor remained operational.

(h) Revised augmentor exit rake.

A new augmentor exit rake was made with pitot and static tubes inclined 15° to align with the expected fuselage augmentor efflux direction (Figure 12).

(i) Fuselage base instrumentation.

A false base was installed between the fuselage augmentors over the existing fuselage lower surface and extended between the augmentor ends. This was done in order to facilitate installation of static pressure taps and thermocouples as shown Figure 13. The pressure measurements were used to calculate the base thrust between the augmentors.

4.2 Thrust Loading

As noted in Reference 3, the design thrust loading for the model was 60 lb/ft<sup>2</sup>. At the elevated temperatures generated in the 40- by 80- Foot Wind Tunnel (up to 135°F) the maximum nozzle pressure ratio was limited to 2.5 (compared with the standard day design value of 3.5) and the thrust

loading was correspondingly reduced to 35 lb/ft.<sup>2</sup> Some of the later tests in the wind tunnel were further restricted by noise abatement requirements and an even lower thrust loading was necessary. The full scale, or equivalent, flight dynamic head is inversely proportional to the model thrust loading so that appropriate factors may be applied to the tunnel q to obtain equivalent full-scale dynamic head.

#### 4.3 Reference Pressure Ratio

The J97 engine thrust was set during tests by reference to a reading of the static pressure in the fuselage duct located just upstream of the first fuselage augmentor nozzle off-take (see location PF1 in Figure 14). This pressure is expressed as a Reference Pressure Ratio

$$RPR = \frac{P_{F1}}{P_a}$$

and is used throughout this report. The total pressure measured at the exit plane of the fuselage augmentor nozzles was approximately 9.6% greater than the reference static pressure, PF1. Hence with RPR = 2.30 (a value used for most of the forward speed tests) the average nozzle pressure ratio (NPR) was 2.52.

#### 4.4 Data Reduction

For all force and moment data, the thrust of the small trim nozzle in the rear fuselage was subtracted from the balance values. The inlet momentum drag of the J97 engine was not subtracted.

Wind tunnel boundary corrections were based on aerodynamic or effective lift (the total lift less the reactive lift components of the static augmented thrusts of the fuselage and wing augmentors). Effective lift coefficient is given by:

$$C_{L_{eff}} = C_L - C_{J_{AUG_F}} \cos(\alpha_u - \theta_{F,0}) - C_{J_{AUG_W}} \sin(\alpha_u + \delta_F) - C_{NA} \sin \alpha_u$$

The following boundary corrections were then made:

$$\alpha = \alpha_u + 0.3538 C_{L_{aero}}$$

$$C_D = C_{D_u} + 0.0062 (C_{L_{aero}})^2$$

The corrected coefficient data were then used to compute the force ratios

$$L/T_H, D/T_H, M/T_H \bar{c}$$

where  $T_H$  is the augmented thrust of the model in the "hovering" configuration, i.e. the sum of the fuselage augmentor thrust and the wing augmentor thrust. The former is the value determined from static test measurements with the nozzles deflected aft 12.5 degrees, all nozzles operating, endplates on and diffuser area ratio = 1.6. It includes a small loss due to negative base thrust (see Section 5). The wing augmentor thrust is the value determined from static test measurements with the wing/flap fairing off. This fairing gives rise to a small loss in thrust at large deflection angles (see Reference 8) which is discounted in the evaluation of  $T_H$ .

Note that the gross wing area used to define force and moment coefficients is the area of the complete wing, including the forward part containing the fuselage augmentor, plus the projected area of the complete wing within the fuselage. The gross area of the wing without the forward part is 98.80 sq. ft.

All force and moment coefficients are given about stability axes.

## 5. STATIC TEST RESULTS

For static tests in the wind tunnel working section, the model was mounted on the standard balance struts and was therefore about 18 feet above the tunnel floor, well out of ground effect. The overhead tunnel doors were opened wide to minimize recirculation effects and run times were kept short to reduce build-up of tunnel  $q$ .

The quantities of interest derived from the present static tests were the gross thrust augmentation ratio

$$\emptyset_{G_{F+B}} = \sqrt{L_{F+B}^2 + D_F^2} / X_{N_F}$$

and the average jet efflux angle

$$\theta_{F+B} = \tan^{-1} \left( \frac{-D_F}{L_{F+B}} \right)$$

where  $L_{F+B} = L - L_W$  ) suffix F relates to fuselage  
 $D_F = D - D_W + X_{N_R}$  ) augmentor  
 $L_W = \emptyset_{G_W} \cdot X_{N_W} \sin \delta_F$  } suffix W relates to wing  
 $D_W = -\emptyset_{G_W} X_{N_W} \cos \delta_F$  } augmentor  
{} the wing augmentor thrust components at the model static test attitude of  $\alpha = 0^\circ$

and  $X_{N_R}$  = the rear propulsion nozzle thrust, if any.

The fuselage augmentor nozzle thrust,  $X_{N_F}$ , was assumed to be 25/27 of the previously determined value for the VTOL 1 configuration (as in Reference 1), since two nozzles had been removed from each nozzle array for the present configuration (as shown in Figure 5).

The wing augmentor thrust terms,  $X_{N_W}$  and  $\emptyset_{G_W}$ , were the same as in the previous test (see Reference 2).

The subscript 'F + B', meaning 'fuselage augmentor plus base' , signifies that the base thrust effect is included in the calculated augmentation ratio and efflux angle. Base thrust data became available only in the VTOL 3 test program when the pressure instrumentation was added (see Figure 13). The base thrust arises from a small base pressure, negative in free-air, which is generated between the two fuselage augmentor effluxes. Subsequent static tests (Reference 8) have shown, however, that the negative base pressure causes an increase in thrust augmentation of the fuselage augmentor which almost offsets the base thrust. Nevertheless, the subscript 'F + B' is retained to indicate that the data refer to the complete 'fuselage augmentor plus base' configuration.

Figures 15 and 16 present  $\emptyset_{G_{F+B}}$  and  $\theta_{F+B}$  respectively versus RPR for each of the configurations tested. A summary of the results at RPR = 2.3 is given in Table 6.

For the basic augmentor, i.e., DAR = 1.6, endplates on and full set of 25 nozzles operating,  $\emptyset_{G_{F+B}}$  was determined to be about 1.50 to 1.57 in the VTOL 2 tests at RPR = 2.30. The scatter was partly due to the degree of endplate flow attachment generated by the jet efflux from the first and last nozzles of the array. The clearance between these nozzles and the endplates was initially too large and some experimentation was done in this area.

Cold flow tests at DHC had shown that a 15° efflux deflection (or thrust vectoring) of the fuselage augmentor

thrust would be obtained if the nozzle angle was a few degrees less ( $12.5^\circ$  was actually chosen for the J97 powered model). This arose from the augmentor internal flow having to cross the diffuser isobars non-orthogonally (viz.  $90 - 12.5 = 77.5^\circ$ , initially), as shown in Figure 17. The collected efflux angle data of Figure 16 indicate a deflection of about  $15^\circ$  for the basic augmentor.

The collected static test data also show the effects of diffuser area ratio, removing front or both endplates, blanking-off alternate nozzles, blanking-off all but the centre half of the nozzles, etc. These changes reflect naturally in the forward speed data.

Figure 18 shows a comparison between the deflected augmentor nozzle results of the present tests with those of the undeflected nozzle tests of the VTOL 1 augmentor (Reference 3). With base thrust effects included, the augmentation ratio  $\emptyset_{G_{F+B}}$  is seen to decrease by about 5 counts due to the nozzle deflection of  $12.5$  degrees.

Installation of the augmentor exit rake had no discernible effect on thrust augmentation ratio but caused small reductions in jet deflection angle (as shown in Figure 19). The reasons for this are not fully understood.

It should be noted that the derivation of  $\emptyset_{G_{F+B}}$  is more direct (and reliable) for configurations with  $\delta_F = 0^\circ$  because, in such cases, it is not necessary to make assumptions with respect to the thrust of the wing augmentor.

## 6. FORWARD SPEED RESULTS

### 6.1 Presentation of Transition Performance

An important area of interest at the present stage of development relates to the optimization of acceleration capability from hover to wing-borne flight during which the fuselage augmentor is progressively shut down and eventually sealed with appropriate folding doors. The rear propulsion nozzle is correspondingly increased in area to accept the transferred fuselage augmentor nozzle thrust. The angle of attack range during transition is important, too, as is the pitching moment. However, the moment is amenable to change by configuration layout and by appropriate 'blanking' of fuselage augmentor nozzles during transition.

A limited number of configurations have been tested in the wind tunnel to explore the effects of flap angle, diffuser area ratio, and thrust transfer on transition characteristics. These are listed in Table 7. The force data for these configurations are presented in Figures 20 through 48 in the format

$$\frac{L}{T_H} \text{ vs } \alpha'$$

$$\frac{L}{T_H} \text{ vs } \frac{D}{T_H}$$

$$\frac{L}{T_H} \text{ vs } \frac{M}{T_H c}$$

The denominator,  $T_H$ , is the take-off thrust in the hovering configuration as defined in Section 4.4.

These data relate to a fuselage augmentor with nozzle angle ( $\delta_N$ ) deflected  $12\frac{1}{2}^{\circ}$  rearward relative to the vertical datum of the aircraft. The data may be interpreted in either of two ways:

- (i) nozzle angle  $\delta_N = 12\frac{1}{2}^{\circ}$  and fixed, this being the basis of analysis (or interpretation) presented here.
- (ii) nozzle angle variable, in which case the results provide a set of data for one value of  $\delta_N$  only, in a possible range of  $-10^{\circ}$  to  $+40^{\circ}$ , say.

For a VTOL aircraft, it is necessary that  $T_H$  be greater than the take-off weight to allow for vertical acceleration and for excess thrust for control and trim purposes. When comparing the various transition configurations, a value of  $T_H/W = 1.10$  has been taken as a typical reference value. The drag ratio,  $D/T_H$ , during transition, is obtained from the wind tunnel data at a lift ratio given by

$$L/T_H = W/1.10W = 0.91$$

since  $L = W$  if negligible vertical acceleration is used once the VTOL aircraft has started to pick up forward speed. This also assumes that the hovering or take-off level of thrust is maintained during the transition maneuver.

From the drag ratio  $D/T_H$  the longitudinal acceleration is given by

$$\text{ACCEL}^{TN} = - D/W = - 1.10 \left( \frac{D}{T_H} \right) \quad (\text{acc}^n \text{ in g's})$$

This value of acceleration has been plotted to show transition performance (Figures 49 through 55) as a function of forward speed. In these figures the forward speed is the value equivalent to that for a VTOL aircraft having the same aerodynamic characteristics as the present model but operating at its design value of thrust loading,

$$\text{i.e. } \left( \frac{T_H}{S} \right)_{\text{Design}} = 60 \text{ lb/ft}^2$$

The wind tunnel model would have given this loading at standard day conditions with a J97 engine operating at its design pressure ratio (NPR = 3.5). Due to the high temperatures encountered in the wind tunnel the model was operated at a reduced power setting which generated a thrust loading less than the design value, as described in Section 4.2. The wind tunnel tests were conducted at correspondingly lowered wind speeds to generate the same jet thrust coefficient,  $C_J_{\text{AUG}}$ , as the 'full-scale aircraft'.

Table 8 gives a summary of transition performance, i.e. acceleration, angle of attack and pitching moment for  $\frac{T_H}{L} = 1.10$  and  $\frac{T_H}{S} = 60 \text{ lb/ft}^2$  as described above. The table also records the model configuration, its identification code and the figure number of the force data plot.

#### 6.2 Basic Augmentor Configuration

The 'basic' augmentor is that used for hovering. It generates the greatest thrust augmentation. In these tests therefore, the configuration is defined by all nozzles operating (but deflected  $12\frac{1}{2}^\circ$ ), endplates on and diffuser area ratio set to 1.60.

Tests were conducted with flap deflections of 0, 30 and 45°. The augmentor exit rake was installed for some tests and affected test results as described below. The effect of flap angle on acceleration and angle of attack in level flight is shown in Figure 49. It can be seen that a large flap deflection permits a greater acceleration but requires a large nosedown model attitude. A representative, practical deflection is probably about 30° and will allow acceleration up to about 130 knots (Figure 49(b), rake-off data) with a nose down attitude ( $\alpha$ ) not exceeding -13°.

Interference effects of the augmentor exit rake on performance at forward speed were unexpectedly large in the VTOL 2 tests (see Figure 50(a) and (b)) although much useful information on augmentor exit flow distribution was collected. (See Section 6.9.) In the VTOL 3 tests, the interference was smaller (Figure 50(c)) but the rake was removed for most of the tests.

### 6.3 Intermediate Augmentor Configurations

These fall into three categories

- (a) reductions in diffuser area ratio
- (b) removal of one or both endplates
- (c) thrust transfer (by blanking some augmentor nozzles and increasing propulsion nozzle area).

The tested configurations (see Table 7) often combined all three modifications as attempts were made to maximize acceleration capability and to simplify the augmentor configuration.

In the first category, reduction of DAR, Figures 51(a) and (b) show no favourable effect with the 'full nozzle set' augmentor at  $\delta_F = 45^\circ$  but some advantage at high speed with the 'alternate nozzles blanked' configuration. The acceleration data reflect the relative magnitudes of the major force components, viz. augmentor inlet momentum drag, propulsion nozzle thrust and drag due to lift. It should be noted that the nose down attitude is reduced as augmentor thrust is reduced (by throttling or thrust transfer). Aero-dynamic lift then replaces jet lift.

With augmentor endplates off, the effect of reducing DAR is very small. Figures 52(a), (b) and (c) show test results with the three different nozzle configurations, i.e. full nozzles, alternate nozzles and 'centre' nozzles.

The case with only the front endplate off (Figure 53) falls somewhere between the endplates on and endplates off test results. Reducing DAR with the full nozzle set at  $\delta_F = 30^\circ$  lowered the acceleration capability in the speed range of interest.

In the second category, removal of one or both endplates, a significant improvement in acceleration performance was produced by removing the front endplate. (See Figures 54(a) and (b)). It is presumed that the increased deflection of the fuselage augmentor efflux (see Section 5) gave rise to this improvement. There was some benefit obtained by removing both endplates, a result of some considerable practical significance.

In the third category, thrust transfer, a benefit was recorded above about 100 knots (see Figure 55(a)) with alternate nozzles blanked-off and with  $\delta_F = 30^\circ$ . There was no improvement, however, with the flap set at  $45^\circ$ , (Figure 55(b)). The best results were obtained with the "centre nozzles" configuration and endplates off (Figure 55(c)). Inlet fairings or covers over the blanked-off nozzles at the front and back of the augmentor (Figure 8) had no effect on the test data.

Some representative test data of intermediate transition configurations are given in Figure 56 in the more usual force coefficient format. These may be compared with the wing-borne data shown in Figure 61.

#### 6.4 Augmentor Sealed (Wing-Borne) Configuration

This configuration is one where all the fuselage augmentor nozzle area has been blanked-off and replaced with equivalent propulsion nozzle area in the rear fuselage. The wing augmentor was operating as usual but the fuselage augmentor doors were "retracted" (in practice, replaced with plywood panels to simulate the retracted position, see Figure 11). The fuselage augmentor inlets were sealed with close-fitting light alloy covers, simulating intake doors on a VTOL aircraft in the closed position.

The test data (Figure 57) show an acceleration capability of about 0.4g at 100 knots. Performance is best at the lower flap angles but angle of attack becomes rather large in that case. A good compromise would be  $\delta_F = 40^\circ$

at  $\alpha = + 10^\circ$  at 100 knots. The corresponding lift coefficient is  $C_L = 1.6$  and the equivalent wing loading is  $W/S = 54.5 \text{ lb}/\text{ft}^2$  based on gross wing area.

#### 6.5 Summarized Acceleration Capability

The maximum recorded accelerations for the best configurations are shown in Figure 58 together with the associated angles of attack. Also shown are the accelerations available within arbitrarily chosen  $\alpha$  limits of  $\pm 10^\circ$ . These test data applied to a full-scale aircraft would allow acceleration to 110 knots in about 10 seconds, covering about 1000 feet horizontally in the process. At 110 knots, transition from jet-borne to wing-borne flight could be achieved with a constant flap angle of  $30^\circ$  without exceeding the  $\pm 10^\circ$  attitude limitations.

#### 6.6 Pitch Trim

The major components of the pitching moment arise from the deflected wing augmentor flap (nose down moments) and the fuselage augmentor inlet flow (nose up moment). At low forward speed the resultant moment would be minimized by appropriate choice of aircraft layout and trimmed out by jet reaction methods (using either the fuselage augmentor or separate 'puff-pipes'). At higher speeds, a tailplane or canard surface would provide the primary trim control.

Pitching moments of the present model layout are shown in Figure 59 to give an idea of present magnitudes and are compared with the available contribution from the present canard surface (or an equivalent tailplane) at an effective surface lift coefficient of 1.0.

### 6.7 Effect of Wing Leading-Edge Slat

The outer wing panels showed a pronounced leading edge stall during the VTOL 1 tests, the stalling angle being a function of flap angle primarily. For the subsequent wind tunnel tests, a simple L/E slat (see Figure 9) was added. It provided excellent control of flow over the wing, as indicated by tufts, up to  $\alpha = 24^\circ$  or so. The flow on the slat upper surface was also attached. Test data are reproduced in Figure 60. The improvement due to slat is evident at the larger angles of attack. This is more clearly seen when the test data are plotted with the reactive thrust components removed (see Section 6.8, Figure 74).

### 6.8 Interference Effects of Fuselage Augmentor

#### 6.8.1 Longitudinal

In the VTOL 3 wind tunnel tests some runs were made with the fuselage augmentor nozzles blanked-off and the augmentor closed and sealed (see Figure 11). A conical propulsion nozzle of equal area was fitted to allow for transfer of the augmentor nozzle thrust. The interference effects of the fuselage augmentor could then be obtained directly by difference between 'augmentor-on' and 'augmentor-sealed' configurations. (Unfortunately, there was insufficient test time available to examine directional characteristics with augmentor-sealed.)

The longitudinal data, in coefficient form, for the augmentor-sealed or 'wing-borne' configuration are

given in Figure 61 for flap angles of  $15^\circ$ ,  $30^\circ$  and  $45^\circ$ .

The "effective lift coefficient" is given in Figure 62 for the same flap angles and for the three jet coefficients,  $C_{J_{N_W}}$ , at which the tests were made. Cross-plots of  $C_{L_{eff}}$

at  $\alpha = 0^\circ$  versus  $\delta_F$  and  $C_{J_{N_W}}$  are given in Figure 63.

Lift curve slopes are plotted in Figure 64. Note that effective lift is defined as "total lift minus static, augmented lift", as defined in Section 4.4.

In Figure 65 is given  $C_{L_{eff}}$  versus  $\alpha$  for the 'augmentor-on' configuration, the jet-borne configuration with basic augmentor, i.e. full nozzle set, DAR = 1.6 and endplates on. The comparisons in Figures 66 and 67 show very small interference effects of the fuselage augmentor on lift.

Drag data for the wing-borne configuration are given in Figure 68 in the form  $C_{D_{eff}}^2$  versus  $C_{L_{eff}}^2$  for the three flap angles and three jet coefficients. The slope of these curves is approximately  $1/\pi A$ . The effect of flap angle is fairly small, as shown in Figure 69.

The definition of  $C_{D_{eff}}$  parallels that of  $C_{L_{eff}}$ , i.e.  $C_{D_{eff}} = C_D - C_{J_{AUG_F}} \sin(\alpha_u - \theta_F + \beta) - C_{J_{AUG_W}} \cos(\alpha_u + \delta_F) - C_{J_{N_R}} \cos \alpha_u$ .

The comparative drag data with augmentor operating are given in Figures 70, 71 and 72 for the VTOL 1, 2 and 3 tests respectively. A comparison of the three tests

is given in Figure 73. The slope is seen to be about  $1/\pi A$  provided the outboard wing leading-edge slat is on, as more clearly indicated in Figure 74.

#### 6.8.2 Lateral

Some indication of the effect of fuselage augmentor on lateral data can be obtained from the effects of changing power setting, or  $C_J^{AUG}$ . Figures 75(a) and (b) show a small dependence on  $C_J^{AUG}$  of all three lateral/directional coefficients.

The effect of thrust vectoring the fuselage augmentor efflux was small (Figure 76) as was the effect of removing the augmentor endplates (Figure 77).

### 6.9 Augmentor Exit Rake Results

#### 6.9.1 Exit Distributions

The fuselage augmentor exit rake (see Figure 12) was installed for some of the runs to obtain exit total and static pressure distributions, from which were calculated velocity distributions. These, in turn, provided integrated thrust and mass flow data. Due to turbulence in the exit flow the rake thrust readings are higher than the true (balance) values (this was discussed in Reference 3). However, for comparative purposes the rake data are quite valuable.

The longitudinal distribution of exit thrust is first shown (Figures 78 and 79) for the VTOL 2 and VTOL 3 tests respectively with 'basic' augmentor. The degree of flow attachment at front and rear endplates is indicated by

the thrust level at each end of the augmentor at  $q = 0$ . At forward speed the exit thrust increases noticeably especially the rear 70% of the augmentor length. The VTOL 2 results show some thrust reduction over the front 30%, an effect also noted in the VTOL 1 tests. The VTOL 3 results show a general improvement over VTOL 2 both in the front and rear portions of the augmentor for reasons not fully understood.

A summation of the longitudinal thrust distribution gives the total rake thrust which may be divided by the fuselage augmentor nozzle thrust to give an augmentation ratio  $\phi_{G_{RAKE}}$ . The magnitude is high, due to turbulence, but the variation with RPR and forward speed is indicative of the real trends. Figure 80 shows results for the basic augmentor from both VTOL 2 and VTOL 3 tests.

The effect of angle of attack is quite small (Figure 81) especially for the VTOL 3 configuration (even though nominally the same as the VTOL 2 configuration).

#### 6.9.2 Augmentor Inlet Vanes

During the VTOL 1 wind tunnel tests (Reference 3) some degradation in fuselage augmentor exit velocity distribution had been recorded at forward speed (using the exit rake). This was tentatively attributed to a flow separation near the front inlet region. Subsequent tests (in VTOL 2 and VTOL 3) with inlet vanes arranged to improve flow attachment on the high-curvature inlet regions were not successful in improving exit distributions significantly. However,

surface and stand-off tufts showed a notable change of flow direction and improvement in flow smoothness when the front endplate was removed (Run 8 of VTOL 3). The exit rake, unfortunately, was not installed for these tests. Further tuft studies in the region just ahead of the front endplate showed a flow separation from the outer edge of the front endplate (when installed) which was carried up over the wing leading-edge and into the fuselage augmentor. This is illustrated in Figure 82. The problem is believed to be much alleviated with the front endplate removed.

## 6.10 Canard Characteristics and Interference Effects

### 6.10.1 Longitudinal

Tests to investigate the magnitude of interference generated by a canard surface were made in both VTOL 2 and VTOL 3 wind tunnel programs.

Longitudinal data in coefficient format are given in Figures 83 and 84. In Figure 85 the lift and moment data are plotted versus  $\alpha$  for the two canard incidences,  $i_c = \pm 10^\circ$ . The generated pitching moment increment for  $\Delta i_c = 20^\circ$  was  $\Delta C_M = 0.090$ . With a canard moment arm of  $l_c/c = 0.92$ , the corresponding lift increment would be  $\Delta C_L = 0.10$ . However, the measured increment was only 0.05, indicating that the downwash from the canard caused a download on the wing in the manner described in Reference 9, for example. Interference of this type may also reduce the net canard pitching moment if the downwash affects mostly that part of the wing ahead of the moment reference centre.

Figure 86 shows the effect of canard incidence change for the power-off, augmentor open configuration. These results are similar but contain several anomalous variations.

From the intersection points of the canard on/off pitching moment curves, where the canard angle of attack is zero, the upwash at the canard location can be obtained from

$$\epsilon_c = -(\alpha_w + i_c)$$

The available data are plotted in Figure 87 and show  $\frac{\partial \epsilon_c}{\partial \alpha} \approx 0.5$  from the VTOL 3 tests for the configuration tested at  $C_{J_{AUG}} \approx 1.25$ . The effect of  $C_J$  on upwash at the canard is very small, as indicated by the intersections in Figures 83(a), (b) and (c).

Figure 88 shows the effect of canard flap deflection on  $C_L$ ,  $C_D$  and  $C_M$ .

#### 6.10.2 Lateral/Directional

Lateral data were collected with the canard at a high lift setting, viz.  $i_c = + 10^\circ$  and  $\delta_c = + 30^\circ$ . A comparison, with canard-off data, (Figure 89) shows a small increase in  $C_l$  and a larger increase in  $C_n$ .

Figure 90 shows no change in the effect of yaw on longitudinal coefficients when the canard was installed. The comparison tests were made with  $\alpha = 0$  and  $\delta_F = 30^\circ$  with positive and negative lift on the canard. There was no observable effect of the canard on the augmentor performance.

## 7. CONCLUSIONS

- (i) Rearward deflection of the fuselage augmentor nozzle thrust direction by about  $15^{\circ}$  resulted in much improved longitudinal acceleration capability.
- (ii) Reducing diffuser area ratio was not an effective means of increasing acceleration capability for the configuration with all augmentor nozzles operating. Some benefit at high speed was noted for the case where one half of the augmentor nozzles were operating. With augmentor endplates removed the effect of reducing DAR was small but favourable.
- (iii) Removing the front augmentor endplate had a beneficial effect on acceleration due to the rearward deflection of fuselage augmentor efflux caused thereby.
- (iv) Removing both endplates, a significant practical case, also caused an improvement in acceleration, especially at high forward speed.
- (v) Thrust transfer from fuselage augmentor to rear propulsion nozzle was most beneficial when the front and rear quarters of the augmentor were shut down and augmentor endplates were removed. This configuration provided a good acceleration capability to full scale speeds in excess of 140 knots.

- (vi) The wing-borne configuration or jet-flap mode (i.e. fuselage augmentor sealed and thrust transferred to the rear propulsion nozzle) demonstrated excellent acceleration capability at low speed - nearly 0.4g with  $\delta_F = 40^\circ$  and  $\alpha = + 10^\circ$  at 100 knots full-scale.
- (vii) Interference effects of the fuselage augmentor on lift characteristics of the model were again shown to be minimal. The influence of intake momentum on drag and pitching moment was as expected. Similar effects on lateral/directional derivatives are strong but well ordered. Further study is required in this area.
- (viii) Tests of a canard surface mounted below the wing chord datum showed no adverse effects on the fuselage augmentor operation. The downwash from the lifting canard apparently unloads the wing somewhat. The upwash at the canard due to the wing gave a value of  $(\partial e_c / \partial \alpha)$  about 0.5.
- (ix) A leading-edge slat added to the outer wing panels extended the low induced drag characteristics of the model to high angles of attack. The induced drag factor 'k' was approximately 1.0 over a wide range of angle of attack and jet coefficient both 'jet-borne' and 'wing-borne'.

- (x) A fuselage augmentor exit rake showed an increase of exit thrust with forward speed and quite small effects of angle of attack. The exit thrust at the front end of the augmentor at forward speed was generally lower than that in the static case. This was believed to be due to rough inlet flow which was caused by a flow separation emanating from the front augmentor endplates.

8. REFERENCES

1. Garland, D.B. Static Tests of the J97 Powered External Augmentor V/STOL Wind Tunnel Model.  
DHC Report DHC-DND 77-4, February 1978.
2. Aoyagi, K. Wind-Tunnel Investigation of a Large-Scale VTOL Aircraft Model with Wing Root and Wing Thrust Augmentors.  
NASA TM 78589, September 1979.
3. Garland, D.B. Phase I Wind Tunnel Tests of the J97 Powered, External Augmentor V/STOL Model.  
DHC Report DHC-DND 79-4, September 1979 (also NASA CR 15255).
4. Garland, D.B. Description and Test Specification for J97 Powered, External Augmentor V/STOL Wind Tunnel Model.  
DHC Report DHC-DND 77-3, December 1977.
5. Garland, D.B. Specification for Phase 2 Static and Wind Tunnel Tests of J97 Powered, External Augmentor V/STOL Model (with Phase 3 Test Specification Addendum).  
DHC Report DHC-DND 78-2, November 1978.
6. Garland, D.B. Transition Characteristics of the External Augmentor V/STOL Aircraft Concept.  
Proc. V/STOL Aircraft Aerodynamics Symposium, Naval Postgraduate School, Monterey, California, May 1979.
7. Whittley, D.C. Large Scale Model Tests of a New Technology V/STOL Concept.  
AIAA Paper No. 80-0233, January 1980.

8. Gilbertson, F.L.  
Love, R.H.      Static Tests of the J-97 Powered,  
                  External Augmentor V/STOL Model  
                  at the Ames Research Center, NASA  
                  DHC-DND 80-2 April 1980
9. Paulson, J.W.  
Thomas, J.L.      Summary of Low-Speed Longitudinal  
                  Aerodynamics of Two Powered, Close-  
                  Coupled Wing-Canard, Fighter  
                  Configurations.  
  
                  NASA TP 1535,  
                  December 1979.

9. NOTATION

$A$	= aspect ratio
$\bar{c}$	= mean aerodynamic chord (m.a.c.) (ft.)
$c_D$ ,	= corrected drag coefficient
$c_{D_{eff}}$	= effective drag coefficient (see Section 6.8.1)
$c_{D_U}$	= uncorrected drag coefficient
$c_{J_{AUG}}$	= $T_M/qS$
$c_{J_{AUG_F}}$	= $x_{AUG_F}/qS$
$c_{J_{AUG_W}}$	= $x_{AUG_W}/qS$
$c_{J_{NF}}$	= $x_{N_F}/qS$
$c_{J_{NR}}$	= $x_{N_R}/qS$
$c_{J_{NW}}$	= $x_{N_W}/qS$
$c_L$	= lift coefficient
$c_{L_{aero}}$	= $c_{L_{eff}}$ , effective lift coefficient (see Section 4.4)
$c_{L_T}$	= tail (or canard) lift coefficient
$c_l$	= rolling moment coefficient
$c_m$	= pitching moment coefficient (see Table 1)
$c_n$	= yawing moment coefficient
$c_y$	= side force coefficient
$D$	= balance drag force (lb)
$D_F$	= drag component of fuselage augmentor thrust (lb) ( $q = 0$ )
$D_R$	= drag component of rear nozzle thrust ( $q = 0$ ) (lb)

$D_w$	= drag component of wing augmentor thrust ( $q = 0$ ) (lb.)
DAR	= diffuser area ratio
DHC	= The De Havilland Aircraft of Canada, Limited
E/P	= endplate
$i_c$	= canard incidence (degs.)
$k$	= induced drag factor = $\frac{dC_{D,eff}/dC_{L,eff}^2}{1/\pi A}$
L	= lift force (lb.)
$L_F$	= lift component of fuselage augmentor thrust ( $q = 0$ ) (lb.)
$L_R$	= lift component of rear nozzle thrust ( $q = 0$ ) (lb.)
$L_W$	= lift component of wing augmentor thrust ( $q = 0$ ) (lb.)
L/E	= leading-edge
M	= pitching moment (lb.ft.)
mac	= mean aerodynamic chord ( $= \bar{c}$ ) (ft.)
NPR	= fuselage augmentor nozzle pressure ratio
p	= fuselage augmentor nozzle pitch (ins.)
$p_a$	= ambient pressure (psia)
Pf1	= reference pressure in J97 exhaust duct (psia)
q	= wind tunnel dynamic head ( $lb/ft^2$ )
RPR	= reference pressure ratio ( $Pf1/p_a$ )
S	= gross wing area ( $ft^2$ )
t/c	= thickness/chord ratio
$T_H$	= $(X_{AUG_F} + X_{AUG_W} + X_{BASE})$ at $q = 0$ , DAR = 1.6 (lb.)
W	= aircraft weight (lb.)
$X_{AUG_F}$	= fuselage augmentor thrust ( $= \emptyset_{G_F} \cdot X_{N_F}$ ) (lb.)
$X_{AUG_W}$	= wing augmentor thrust ( $= \emptyset_{G_W} \cdot X_{N_W}$ ) (lb.)
$X_{BASE}$	= fuselage base thrust between fuselage augmentors (lb.)

$x_{N_F}$	= fuselage augmentor nozzle thrust
$x_{N_R}$	= rear (propulsive) nozzle thrust
$x_{N_W}$	= wing augmentor nozzle thrust
$\alpha$	= wing angle of attack, corrected for tunnel wall constraint (degs.)
$\alpha_u$	= uncorrected angle of attack (degs.)
$\beta$	= sideslip angle (degs.)
$\delta_c$	= canard flap deflection angle (degs.)
$\delta_F$	= wing augmentor flap deflection angle (degs.)
$\delta_N$	= fuselage augmentor nozzle deflection angle (degs.) (measured from z axis)
$\gamma_c$	= downwash angle at canard location (degs.)
$\theta_{F+B}$	= average jet efflux angle of fuselage augmentor (degs.) (see page 11)
$\phi_{G_{F+B}}$	= $(x_{AUG_F} + x_{BASE})/x_{N_F}$ at $q = 0$
$\phi_{G_{RAKE}}$	= Fuselage augmentor exit thrust as obtained by rake survey / $x_{N_F}$
$\phi_{G_W}$	= $x_{AUG_W}/x_{N_W}$ at $q = 0$

**TABLE 1 GEOMETRY OF J-97 POWERED, EXTERNAL  
AUGMENTOR V/STOL MODEL**

<u>Wing</u>	
Area, gross	141 ft <sup>2</sup>
Area, net	97 ft <sup>2</sup>
Span	15.25 ft.
Aspect ratio	1.65
t/c	6%
m.a.c.	12.68 ft.
Chord on Fuselage Centreline	16.92 ft.
<u>Fuselage</u>	
Overall length	approx. 28 ft.
<u>Fin</u>	
Area	22.4 ft <sup>2</sup>
Span (above fuselage top)	4.33 ft.
Aspect ratio	0.84
<u>Canard</u>	
Area (exposed/gross)	15.0/24.2 ft <sup>2</sup>
Span	8.83 ft.
Aspect ratio	3.23
Tail volume coefficient (gross)	0.158

Moment reference centre (wing leading edge joint, on wing chord datum)  
 Distance ahead of rear strut location  $\bar{x} = 44.0"$   
 (also equal to 47.2% of m.a.c.)

TABLE 2 GEOMETRY OF FUSELAGE AUGMENTOR

<u>Augmentor</u>	
Chordwise length	= 92 in.
Throat width ( $L_T$ )	= 10.5 in.
Exit width ( $L_E$ )	= } variable
Diffuser area ratio ( $L_E/L_T$ )	= }
Length (min) (L)	= 34 in.
Mean nozzle width ( $\bar{t}$ )	= 0.457 in.
Augmentor length ratio ( $L/\bar{t}$ )	= 74
<u>Nozzles</u>	
Total geometric exit area (per side)	= 42.3 in. <sup>2</sup>
Number of nozzles (per side)	= 25
Area (per nozzle)	= 1.693 in. <sup>2</sup>
Aspect ratio (AR)	= 60
Span ( $b_N$ )	= 10.12 in.
Thickness at exit ( $t_N$ )	= 0.167 in.
Pitch (p)	= 3.68 in.
Pitch ratio ( $p/\bar{t}$ )	= 8.0

TABLE 3 GEOMETRY OF WING AUGMENTOR

Span (per wing)			= 69.5 in.
Total nozzle area (per wing)			= 11.5 in. <sup>2</sup>
Bay spans	24.25	22.75	22.5 in.
Nozzle area/bay	4.88	3.73	2.88 in. <sup>2</sup>
Mean nozzle width $\bar{t}$	0.201	0.164	0.128 in.
Number of nozzles (N)	15	17	22
Area per nozzle ( $A_N$ )	0.325	0.219	0.131 in. <sup>2</sup>
Pitch (p)	1.60	1.32	1.01 in.
Nozzle span (b)	3.61	2.96	2.29 in.
Nozzle thickness (t)	.091	.074	.057 in.
Nozzle aspect ratio (AR)	40	40	40
Throat (mid span) ( $L_T$ )	4.17	3.40	2.65 in.
Exit (mid span) ( $L_E$ )	6.67	5.44	4.24 in.
Diffuser area ratio $L_E/L_T$	1.60	1.60	1.60
Nozzle inlet area/exit area	5.0	5.0	5.0
Augmentor length (mid span) (L)	17.3	14.7	12.1 in.
$L/\bar{t}$	86	90	95

TABLE 4

## RUN HISTORY VTOL-2 TESTS (T-538)

Sheet 1

RUN NO.	MODEL CONFIGURATION						TEST CONDITION				REMARKS	
	$\delta_F$	WING SLAT	CANARD i C	DAR	E/P'S	AUG. NOZZLES	AUG. INLET	EXIT RAKE	RPR	q	$\alpha$	$\beta$
1	30° OFF	OFF	1.6	ON	FULL	ST'D	OFF	-	0	~	~	Weight Tare
2								~	0	0	0	
3								2.3	5	~		
4									10			
5									15			
6									15			Run 5 cont'd.
7									25			
8									40			
9		ON							10			
10									25			
11									40			
12							ON	~	0	0	0	
13									5	~		
14									10			
15								2.3	0	0	0	E/P Adjustments
16								~	0	0	0	
17									0			
18								2.3	5	~	0	Repeat of Run 13
19									10			Repeat of Run 14
20									15			
21									25			
22									40			
23									~	25	0	

ORIGINAL POOR QUALITY

TABLE 4

## RUN HISTORY VTOL-2 TESTS (T-538)

SHEET 2

RUN NO.	MODEL CONFIGURATION						TEST CONDITION				REMARKS		
	$\delta_F$	WING SLAT	CANARD i <sub>C</sub>	DAR	E/P'S	AUG. NOZZLES	AUG. INLET	EXIT RAKE	RPR	q	$\alpha$	$\beta$	
24	30	ON	OFF	1.6	ON	FULL	ST'D	ON	~	10	0	0	
25									2.3		~		
26									1.5		~		
27													
28										40			
29										10			
30										5			
31	0°					ST'D	OFF	~	0	0	0		
32									2.3	15	~		
33										25			
34										40			
35									~	40	0		
36									~	25			
37									~	10			
38									~	0	0	Nozzle Welded	
39									2.3	15	~	Repeat of Run 32	
40								ON	~	0	0	Rake On But No Data	
41									2.3	15	~		
42									~	0	0	Repeat of Run 40	
43									2.3	25	~		
44										40			
45	45°								2.3	5	~	0	
46										10			

TABLE 4

RUN HISTORY VTOL-2 TESTS (T-538)

SHEET 3

RUN NO.	$\delta_F$	MODEL CONFIGURATION						TEST CONDITION				REMARKS
		WING SLAT	CANARD i <sub>c</sub>	DAR	E/P'S	AUG. NOZZLES	EXIT RAKE	RPR	q	$\alpha$	$\beta$	
47	45°	ON	OFF	1.6	ON	FULL	ST'D	ON	2.3	15	~	0
48										25		
49									40			
50									2.3	10	~	0
51									~	0	0	
52									2.3	25	~	
53									40	~		
54	30°		0°						2.3	15	~	0
55									25			
56									40			
57			OFF						2.3	15	~	0
58									25			
59									40			
60				0.5					~	0	0	
61									2.3	40	~	
62									25			
63									15			
64	45°								2.3	15	~	0
67				0.5	FULL				~	0	0	
68									2.3	40	~	
69									25			

TABLE 4

RUN HISTORY VTOL-2 TESTS (T-538)

SHEET 4

RUN NO.	$\delta_F$	WING SLAT	CANARD i <sub>C</sub>	MODEL CONFIGURATION					TEST CONDITION				REMARKS
				DAR	E/P's	AUG. NOZZLES	AUG. INLET	EXIT RAKE	RPR	q	$\alpha$	$\beta$	
70	45°	ON	OFF	0.5	ON	FULL	ST'D	ON	2.3	15	~	0	
71											10		
72										5			

TABLE 5 RUN HISTORY VTOL-3 TESTS (T-542) SHEET 1

MODEL CONFIGURATION							TEST CONDITION				REMARKS			
RUN NO.	$\delta_F$	WING SLAT	CANARD i <sub>c</sub>	DAR	E/P'S	AUG. NOZZLES	ST'D	INLET	EXIT RAKE	RPR	q	$\alpha$	$\beta$	
1	30°	ON	OFF	1.6	ON	FULL	ST'D	ON	~	0	0	0	0	
2										2.3	40	~		
3										25				
4										15				
5														Weight Tare
6														
7							FRONT OFF							
8														DUFF RUN
9														
10														
11														
12														
13							OFF							
14														
15														
16														
17														
18														
19														
20														
21														
22							FRONT OFF							
23														

ORIGINAL  
POOR PAGE  
QUALITY

TABLE 5

## RUN HISTORY VTOL-3 TESTS (T-542)

SHEET 2

RUN NO.	MODEL CONFIGURATION						TEST CONDITION				REMARKS	
	$\delta_F$	WING SLAT	CANARD i_c	DAR	E/P's	AUG. NOZZLES	AUG. INLET	EXIT RAKE	RPR	q	$\alpha$	$\beta$
24	30°	ON	OFF	1.0	FRONT OFF	FULL	ST'D	OFF	2.3	25	~	0
25										15		
26				1.6	ON					~	0	0
27								2.3	40	~		
28										25		
29										15		
30										10		
31						HALF ALTERNATE		~		0	0	0
32								~		0	0	0
33								2.3	40	~		
34										25		
35										15		
36										15	0	~
37										25		
38										40		
39										2.0	32	~
40											0	0
41		ON									-	-
42			-10°							2.0	20	~
43											0	~
44										1.0	~	0
45			+10°							2.0	20	~

 $\delta_c = 0^\circ$  and variable

TABLE 5

RUN HISTORY VTOL-3 TESTS (T-542)

SHEET 3

RUN NO.	$\delta_F$	WING SLAT	CANARD i <sub>C</sub>	MODEL CONFIGURATION				TEST CONDITION				REMARKS
				DAR	E/P's	AUG. NOZZLES	AUG. INLET	EXIT RAKE	RPR	q	$\alpha$	
46									2.0	20	0	~
47	30°	ON	+10°	1.6	ON	HALF ALTERNATE	ST'D	OFF	2.0	20	0	~ $\delta c = 30^\circ$
48									1.0	~	0	POWER-OFF
49									~	0	0	
50									2.0	32	~	
51										20		
52										12		
53									~	0	0	0
54									2.0	32	~	
55										20		
56										12		
57										20	0	~
58									~	0	0	0
59									2.0	32	~	
60										20		
61										12		
62									~	0	0	0
63									2.0	32	~	
64										20		
65										12		
66									~	0	0	0
67									2.0	32	~	
68										20		
69										12		

TABLE 5

## RUN HISTORY VTOL-3 TESTS (T-542)

SHEET 4

RUN NO.	$\delta_F$	MODEL CONFIGURATION					TEST CONDITION					REMARKS
		WING SLAT	CANARD i <sub>c</sub>	DAR	E/P'S	AUG. NOZZLES	AUG. INLET	EXIT RAKE	RPR	q	$\alpha$	
70	30°	ON	OFF	1.0	OFF	HALF CENTRE	COVERS ON	OFF	~	0	0	0
71									2.0	32	~	
72										20		
73										12		
74				1.6					~	0	0	0
75									2.0	32	~	
76										20		
77				0.5					~	0	0	0
78									2.0	32	~	
79										20		
80											12	
81	30°				FUSELAGE AUGMENTOR SEALED			~	0	0	0	
82									2.0	32	~	
83										20		
84										12		
85											WEIGHT TARE	
86	45°									2.0	0	0
87										2.0	32	~
88											20	
89											12	
90	15°									2.0	32	~
91											20	
92											12	

TABLE 6 - STATIC PERFORMANCE SUMMARY - VTOL 2 TESTS

Sheet 1

RUN NO.	$\delta_F$	DAR	RAKE	NOZZLES	END-PLATES	REMARKS	AT RPR = 2.3 $\phi_{GF+B}$	AT RPR = 2.3 $\phi_{F+B}$
2	30	1.6	OFF	FULL	ON		1.54	13.8
12	30	"	ON	"	"		1.57	12.2
15	"	"	"	"	"	Inlet Gaps Sealed with RTV	1.50	13.3
16	"	"	"	"	"	Reduced Nozzle/End-Plate Clearance	1.52	11.3
17	"	"	"	"	"	"	1.54	11.4
31	0	"	OFF	"	"		1.51	15.0
38	"	"	"	"	"	Some Inlet Fairing Screws Tightened	1.51	14.8
40	"	"	ON	"	"	Some Force Data Not Acquired	1.51	12.2
42	"	"	"	"	"	Repeat of Run 40	1.51	13.0
51	45	"	"	"	"	ALTERNATE	1.48	4°
60	30	0.5	"	"	"		0.87	2°
67	45	"	"	FULL	"		0.86	10.0

TABLE 6 - STATIC PERFORMANCE SUMMARY - VTOL 3 TESTS  
(Cont'd.)

Sheet 2

RUN NO.	$\delta_F$	DAR	RAKE	NOZZLES	END-PLATES	REMARKS	AT RPR = 2.3	
							$\bar{\rho}_{GF+B}$	$\Theta_{F+B}$
1	30	1.6	ON	FULL	ON		1.55	14.6
7	"	"	OFF	"	FRONT OFF		1.42	22.7
13	"	"	"	"	BOTH OFF		1.37	15.5
18	"	1.0	"	"	"		1.26	12.9
22	"	"	"	FRONT OFF			1.27	13.8
26	"	1.6	"	"	ON		1.55	15.8
31	"	"	ALTERNATE	"			1.41	8.3
32	"	"	"	"		Rear Calibration Nozzle Installed	1.46	9.3
49	"	"	"	"	FRONT OFF		1.32	20.0
53	"	"	"	"	BOTH OFF		1.24	15.0
58	"	1.0	"	"	"		1.24	9.6
62	"	0.5	"	"	"		0.93	10.0
66	"	1.0	CENTRE	OFF	Inlet Covers Off		1.08	11.3
70	"	"	"	"	Inlet Covers On		1.08	12.6
74	"	1.6	"	"	"		1.08	13.7
77	"	0.5	"	"	"		0.86	14.5

**TABLE 7**  
**TRANSITION CONFIGURATIONS TESTED**  
**(T538 & T542; VTOL 2 AND 3 TESTS)**

FUSELAGE AUGMENTOR CONFIGURATION			DIFFUSER AREA RATIO			
NOZZLES	END-PLATES	REMARKS	1.6	1.0	0.5	0
FULL SET	ON		0, 0R 30, 30R 45R			
	FRONT OFF		30	30		
	BOTH OFF		30	30		
½ ALTERNATE	ON		30, 30R 45R		30R 45R	
	FRONT OFF		30			
	BOTH OFF		30	30	30	
¼ CENTRE	BOTH OFF	NO INLET COVERS		30		
	BOTH OFF	WITH INLET COVERS	30	30	30	
AUGMENTOR SEALED	REMOVED	POWER ON				15 30 45
	REMOVED	POWER OFF				0 30

NOTES: (i) NUMERALS SHOWN REFER TO FLAP ANGLES TESTED.  
(ii) LETTER 'R' INDICATES EXIT RAKE ON.

TABLE 8 SUMMARY OF TRANSITION PERFORMANCE,  $T_H/L = 1.10$ ,  $T_H/S = 60$  LB/ft<sup>2</sup>

IDENT. NO.	RUN NO'S	CONFIGURATION						FULL-SCALE $V_\infty$ (KNOTS)						FIG. NO.
		$\delta_1$	NOZZ..	DAR	RAKE	LND- PLATES	OTHER	50	71	87	112	142		
2.1	3-8	30°	FULL	1.6	OFF	ON	ACCEL IN ALPHA M/THT	.292 2.0	.237 5.2	.198 8.3	.094 11.6	.077 14.3	20	
2.2	9-11	30°	FULL	1.6	OFF	ON	WING SLAT ADDED	-	.249 6.2	-	.088 11.1	.083 13.2	21	
2.3	18-22	30°	FULL	1.6	ON	ON		-	.095	-	.070	.035		
2.4	28-30	30°	FULL	1.6	ON	ON	INLET VANES ON	.314 7.3	.220 8.1	.154 11.2	.017 13.5	.182 15.2	22	
2.5	32-34	0°	FULL	1.6	OFF	ON		-	-	.022	.068	.253	23	
2.6	41-44	0°	FULL	1.6	ON	ON		-	-	3.8	3.0	0.5		24
2.7	45-49	45°	FULL	1.6	ON	ON		-	-	-	2.6	0.4		
											.110	.155	200	
														25

TABLE 8 SUMMARY OF TRANSITION PERFORMANCE.  $T_{H/L} = 1.10$ ,  $T_{H/S} = 60$  LB/ft<sup>2</sup>

IDENT. NO.	RUN NO'S	CONFIGURATION						FULL-SCALE V <sub>∞</sub> (KNOTS)						FIG. NO.
		δ <sub>F</sub>	NOZZ.	DRAH	RAKE	END- PLATES	OTHER	50	71	87	112	142		
2-8	50-53	45°	ALT.	1.6	ON	ON	ACCEL IN ALPHA M/T <sub>H</sub> τ	-	.105	-	.028	.160	.26	
2-9	57-59	30°	ALT	1.6	ON	ON		-	2.2	-	.124	.160	.26	
2-10	61-63	30°	ALT	0.5	ON	ON		-	.015	-	.046	.065		
2-11	64-66	45°	ALT	0.5	ON	ON		-	-	-	.064	.038		
2-12	68-72	45°	FULL	0.5	ON	ON		-	-	-	.25	.51	.27	
3-1	24	30°	FULL	1.6	ON	ON		-	-	-	.065	.050	.015	
3-2	9-12	30°	FULL	1.6	OFF	FRONT OFF		-	-	-	.038	.110		
								-	-	-	.067	.071	.32	
								-	-	-	.125	.31	.28	
								-	-	-	.035	.065	.156	
								-	-	-	.030	.020	.073	
								-	-	-	.59	.37	.56	
								-	-	-	.030	.160	.250	
								-	-	-	.028	0	.072	
								-	-	-	1.9	.45	.52	
								-	-	-	.050	.085	.145	
								-	-	-	.028	.045	.135	
								-	-	-	.154	.033	.127	
								-	-	-	.103	.133	.150	
								-	-	-	.115	.105	.075	
								-	-	-	.248	.215	.116	
								-	-	-	.70	.50	.83	
								-	-	-	.092	.080	.055	
								-	-	-	.248	.215	.116	
								-	-	-	.70	.50	.83	
								-	-	-	.092	.080	.055	

TABLE 8 SUMMARY OF TRANSITION PERFORMANCE,  $T_H/L = 1.10$ ,  $T_H/S = 60$  LB/ft<sup>2</sup>

IDENT. NO.	RUN NO.'S	CONFIGURATION					FULL-SCALE V <sub>∞</sub> (KNOTS)				FIG. NO.	
		$\delta_T$	NOZZ.	DAR	RAKE	END- PLATES	OTHER	50	71	87	112	
3-3	14-16	30°	FULL	1.6	OFF	BOTH OFF	ACCEL IN ALPHA M/T <sub>H</sub> $\tau$	-	-	.132 5.5	.050 8.0	.088 11.0
3-4	19-21	30°	FULL	1.0	OFF	BOTH OFF	-	-	-	.121 4.3	.050 8.0	.083 10.2
3-5	23-25	30°	FULL	1.0	OFF	FRONT OFF	-	-	-	.105 3.3	.044 7.0	.088 10.2
3-6	27-30	30°	FULL	1.6	OFF	ON	-	-	-	.040 .135	.006 .115	.055 .085
3-7	33-35	30°	ALT.	1.6	OFF	ON	-	-	-	.259 8.0	.171 8.7	.061 11.8
3-8	50-52	30°	ALT	1.6	OFF	FRONT OFF	-	-	-	.132 4.0	.088 4.2	.050 8.9
3-9	54-56	30°	ALT	1.6	OFF	BOTH OFF	-	-	-	.080 .030	.062 .030	.075

TABLE 8 SUMMARY OF TRANSITION PERFORMANCE,  $T_H/L = 1.10$ ,  $T_H/S = 60 \text{ LB/ft}^2$

IDENT. NO.	RUN NO'S	CONFIGURATION					FULL-SCALE $V_\infty$ (KNOTS)					FIG. NO.	
		$\delta_F$	NOZZ.	DAR	RAKE	END- PLATES	OTHER	50	71	87	112	142	
3-10	59-61	30°	ALT	1.0	OFF	BOTH OFF	ACCEL IN ALPHA M/TH $\bar{c}$	-	-	.118	.118	.039	40
3-11	63-65	30°	ALT	0.5	OFF	BOTH OFF		-	-	9.5	0.7	4.5	
								-	-	.008	.033	.092	
3-12	67-69	30°	CENTRE	1.0	OFF	BOTH OFF		-	-	.094	.114	.055	41
								-	-	.12.8	3.2	2.6	
								-	-	.026	.069	.136	
3-13	71-73	30°	CENTRE	1.0	OFF	BOTH OFF	INLET COVERS ON	-	-	.132	.143	.086	42
								-	-	11.3	3.0	3.2	
								-	-	.029	.073	.137	
3-14	75,76	30°	CENTRE	1.6	OFF	BOTH OFF		-	-	.12.6	4.2	2.4	43
								-	-	.010	.054	.126	
3-15	78-80	30°	CENTRE	1.6	OFF	BOTH OFF		-	-	-	.149	.088	44
								-	-	-	4.0	2.0	
								-	-	-	.037	.105	
3-16	82-84	30°	—	—	OFF	BOTH OFF	FUSELAGE AUGMENTOR SEALED	-	-	.143	.171	.121	45
								-	-	13.5	4.2	2.1	
								-	-	.030	.085	.157	
								-	-	.054	.126	.210	

TABLE 8 SUMMARY OF TRANSITION PERFORMANCE,  $T_H/L = 1.10$ ,  $T_H/S = 60 \text{ LB/ft}^2$

IDENT. NO.	RUN NO'S	CONFIGURATION						FULL-SCALE $V_\infty$ (KNOTS)				FIG. NO.
		$\delta_F$	NOZZ.	WALL	WALKL	END- PLATES	OTHER	50	71	87	112	
3-17	87-89	45°	—	—	OFF	BOTH OFF	ACCEL IN ALPHA M/TH ε	—	—	.347	363	294
								—	—	14.2	3.4	3.2
								—	—	.104	.190	.292
3-18	90-92	15°	—	—	OFF	BOTH OFF		—	—	.396	446	451
								—	—	24.5	15.8	9.2
								—	—	.020	.026	.075



Fig. 1

# DHC EXTERNAL AUGMENTOR V/STOL CONCEPT

G.A. OF J-97 POWERED MODEL

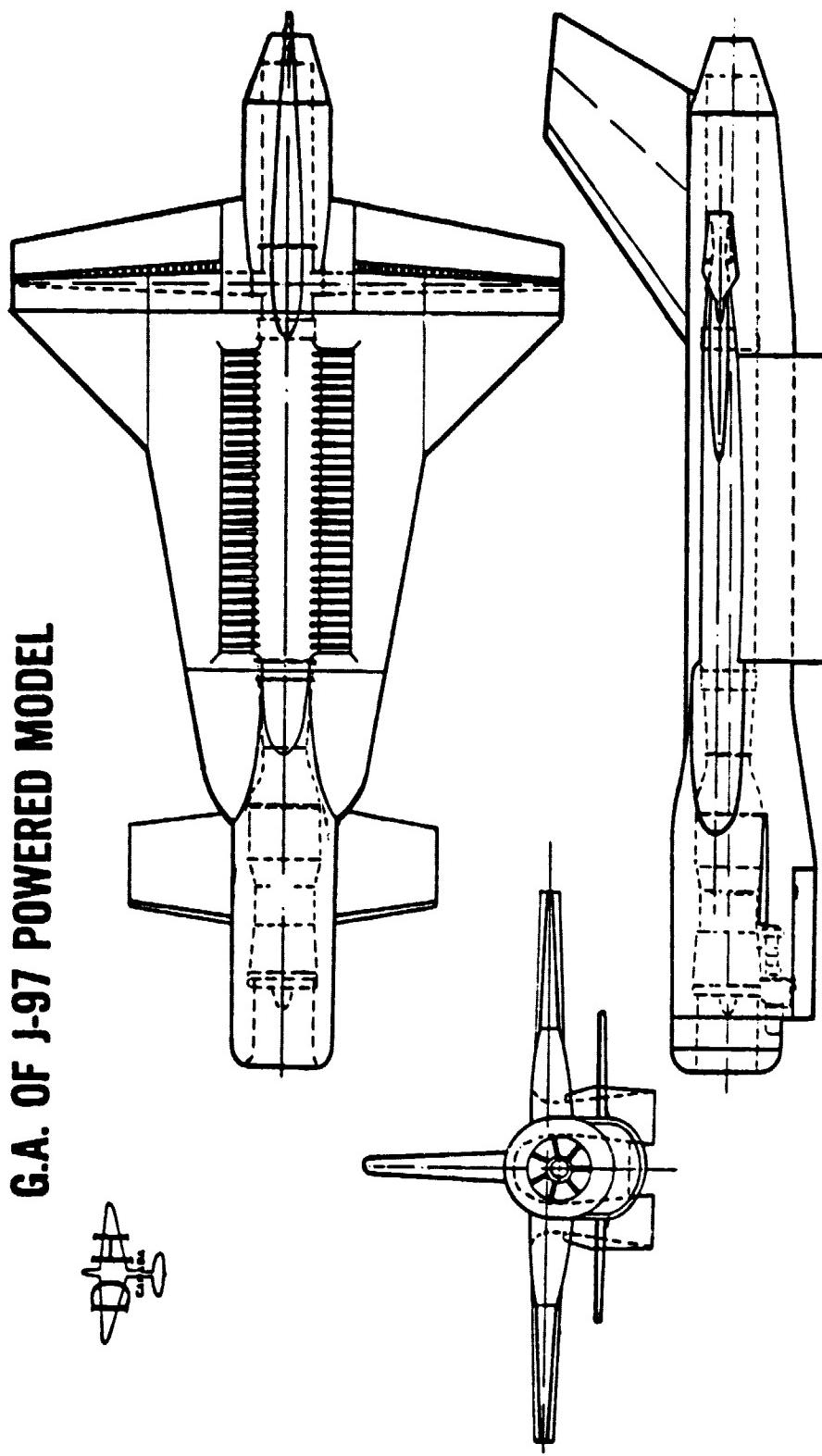
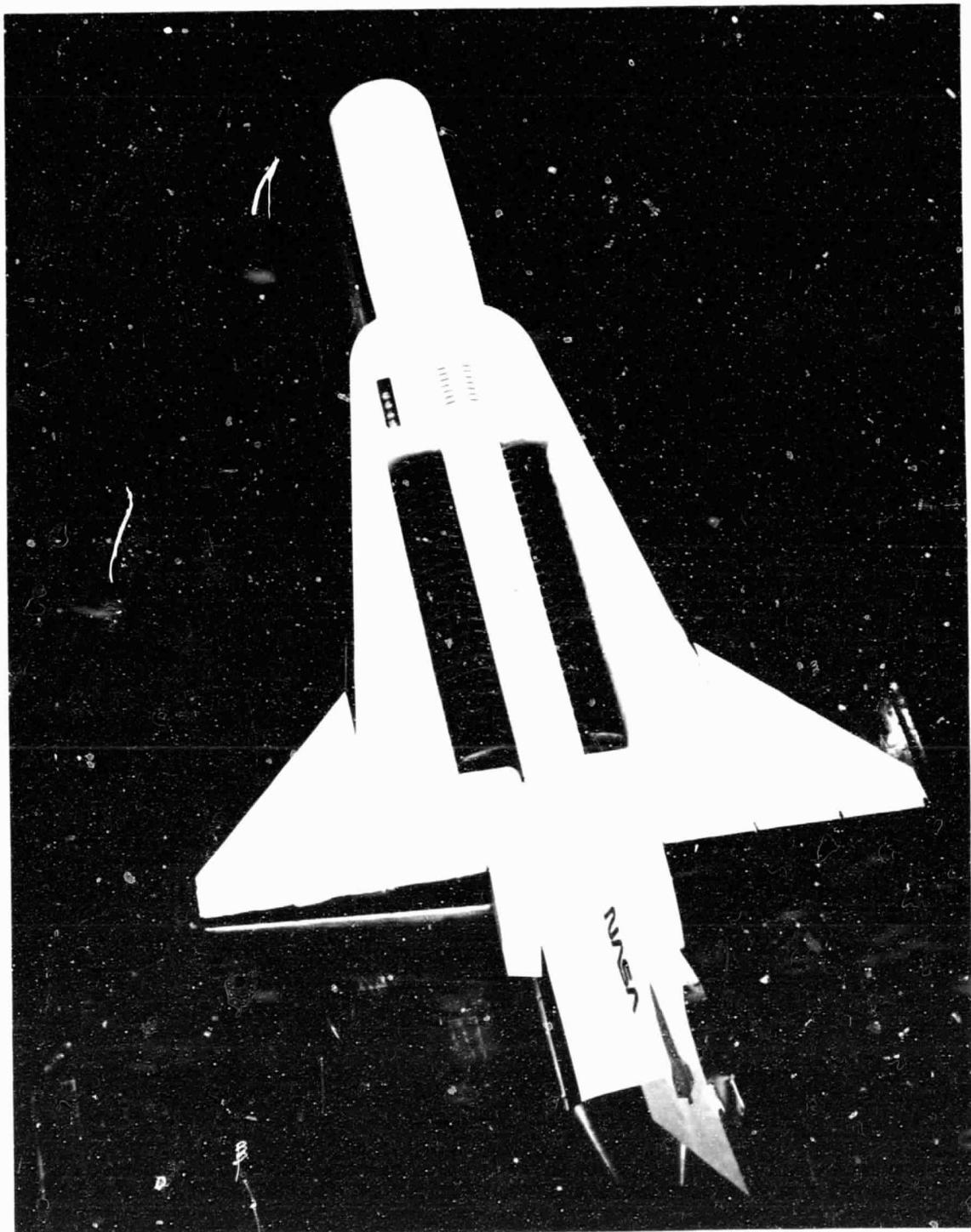




Fig. 2



ORIGINAL PAGE IS  
OF POOR QUALITY

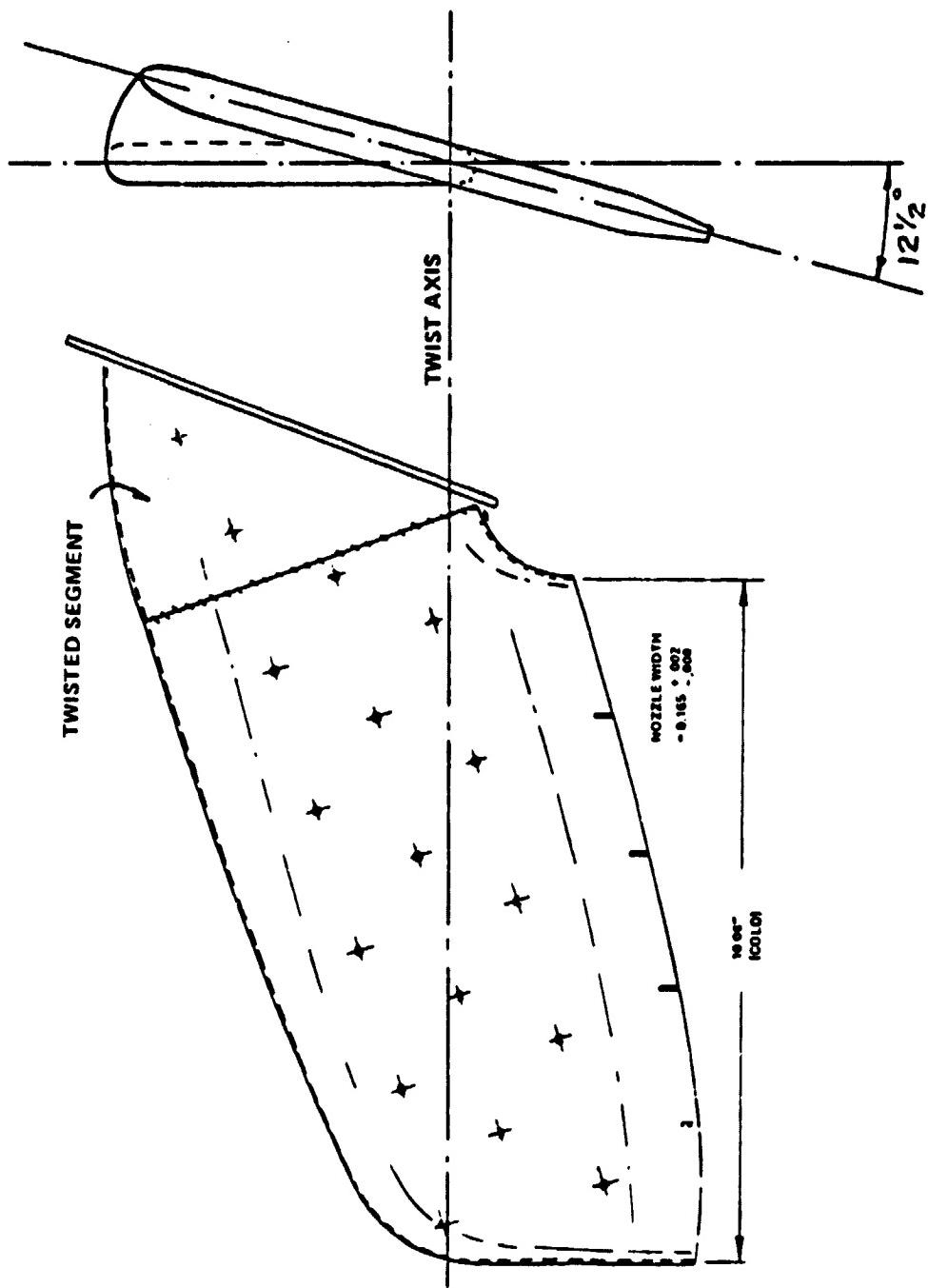
OVERHEAD VIEW OF MODEL IN TUNNEL



REAR VIEW OF MODEL IN TUNNEL



Fig. — 4



FUSELAGE AUGMENTOR NOZZLE, TWISTED 12 1/2°



Fig. 6

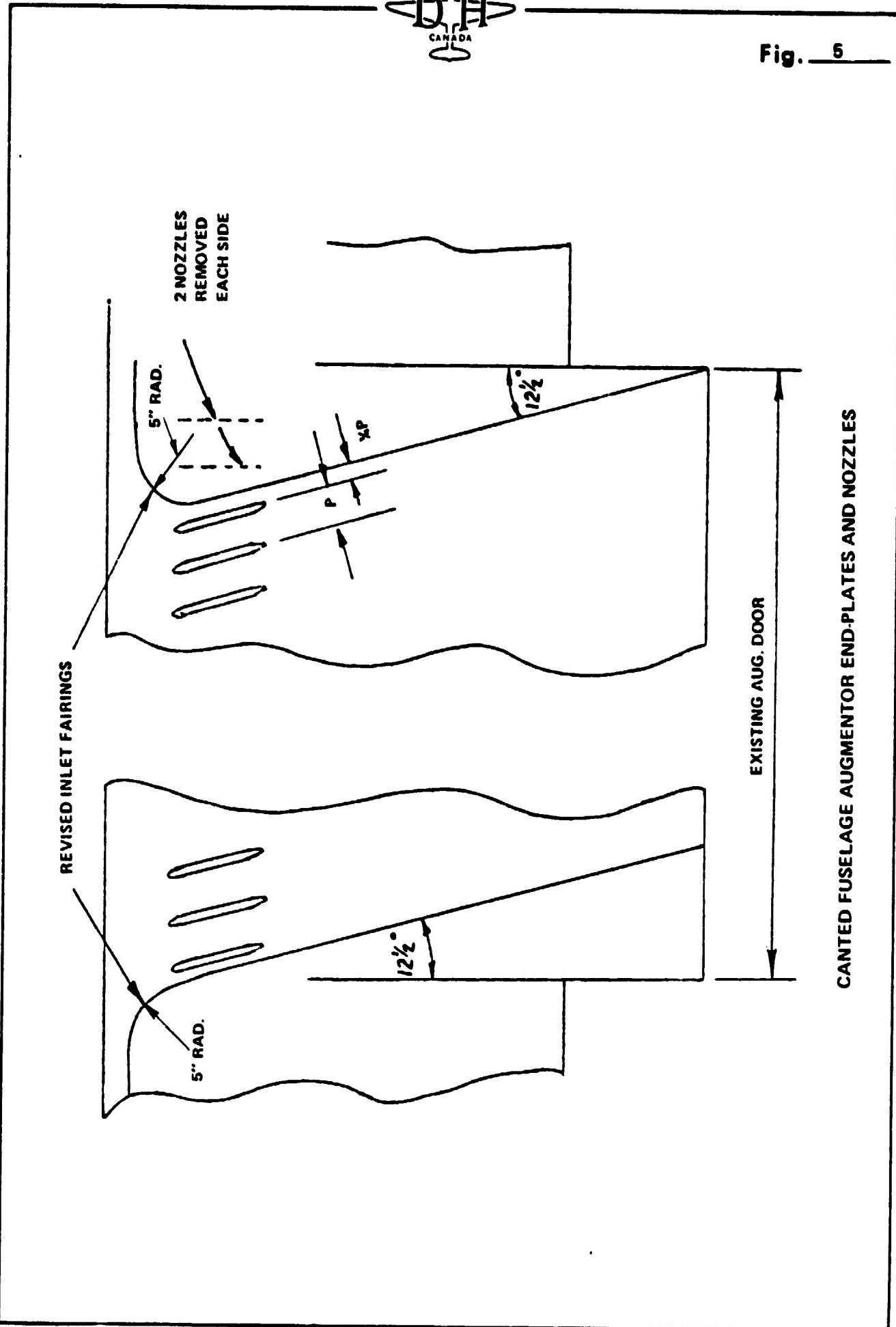
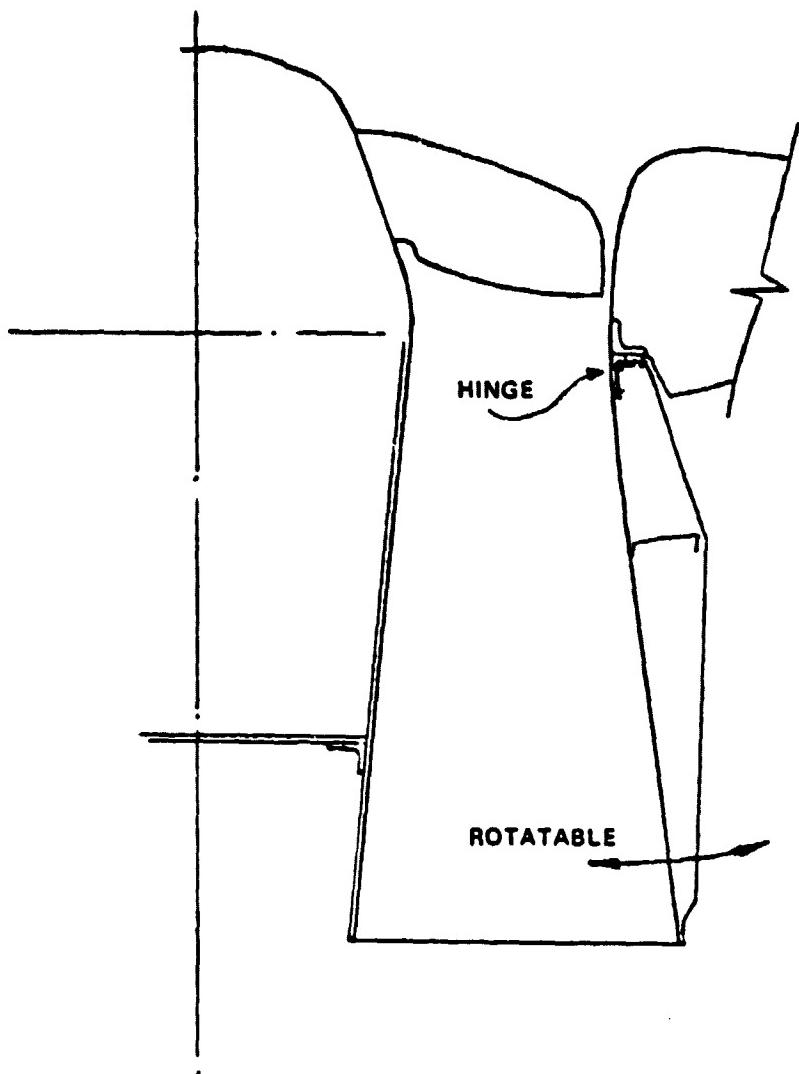
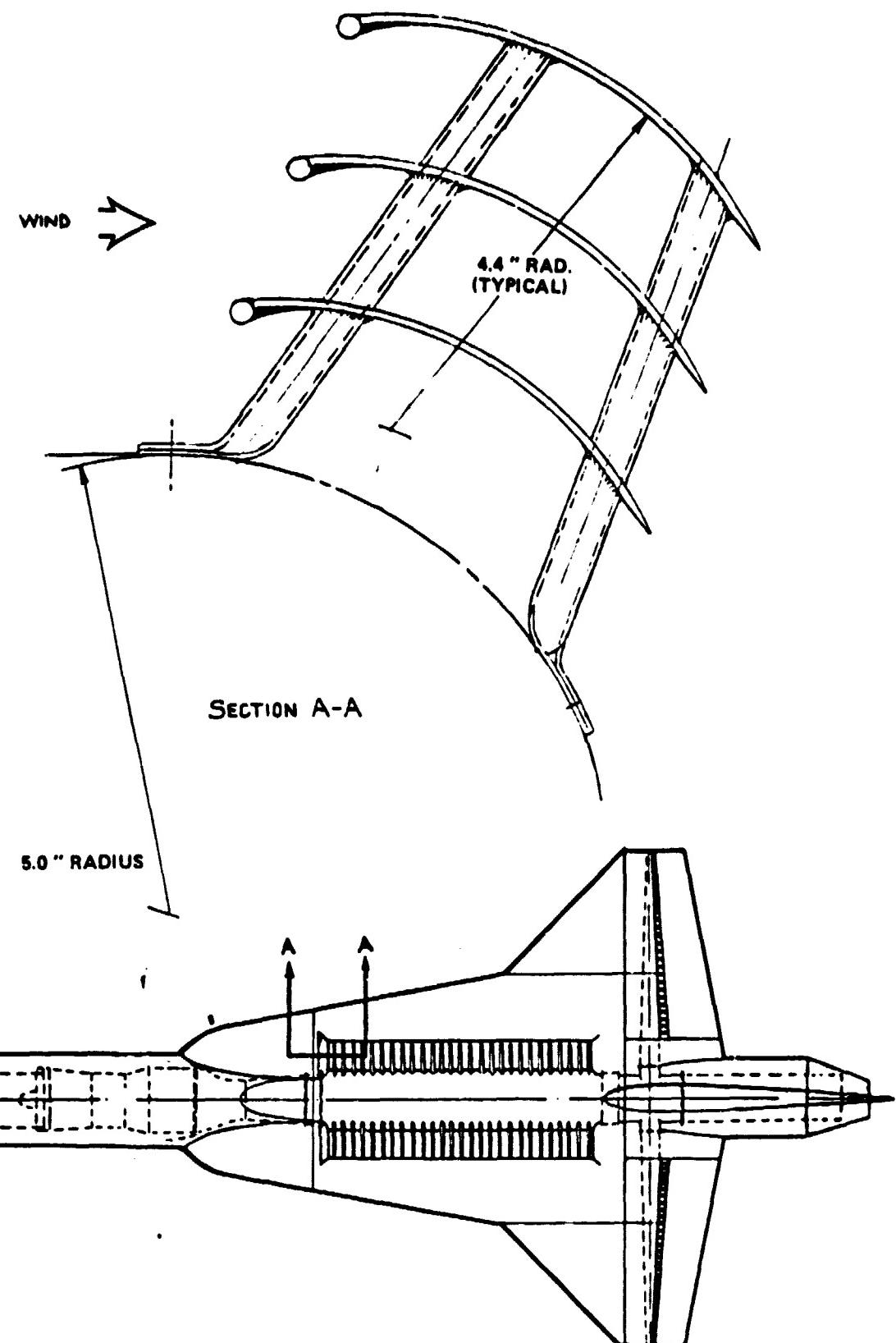




Fig. 6



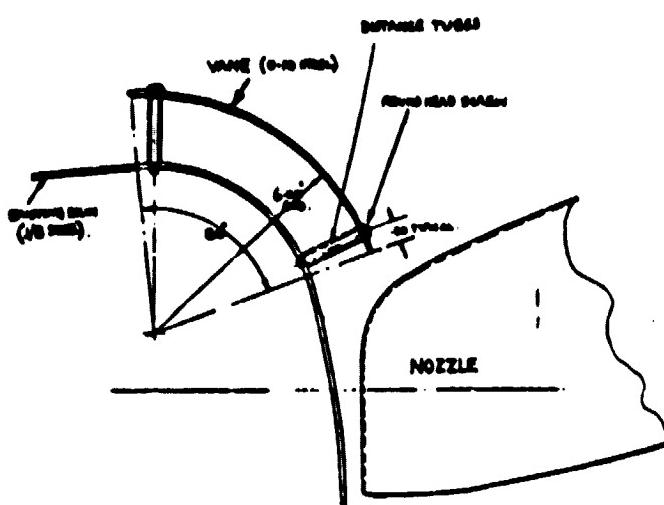
HINGED FUSELAGE AUGMENTOR DOOR



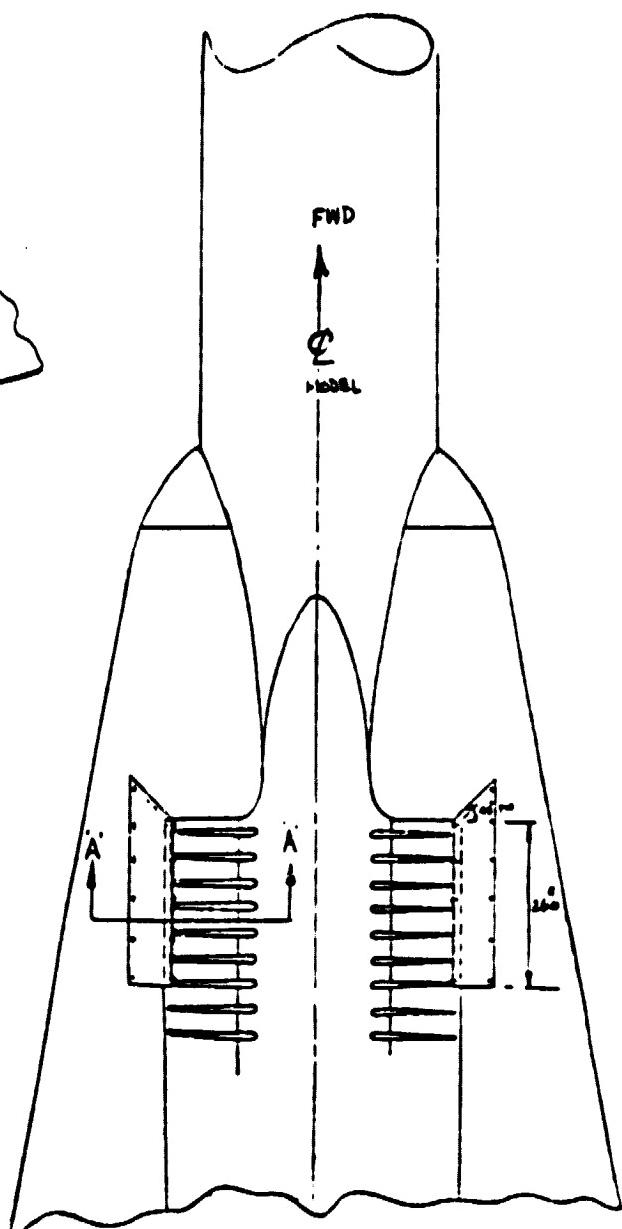
INLET FLOW-TURNING VANES (VTOL-2 TESTS)



Fig. 7(b)



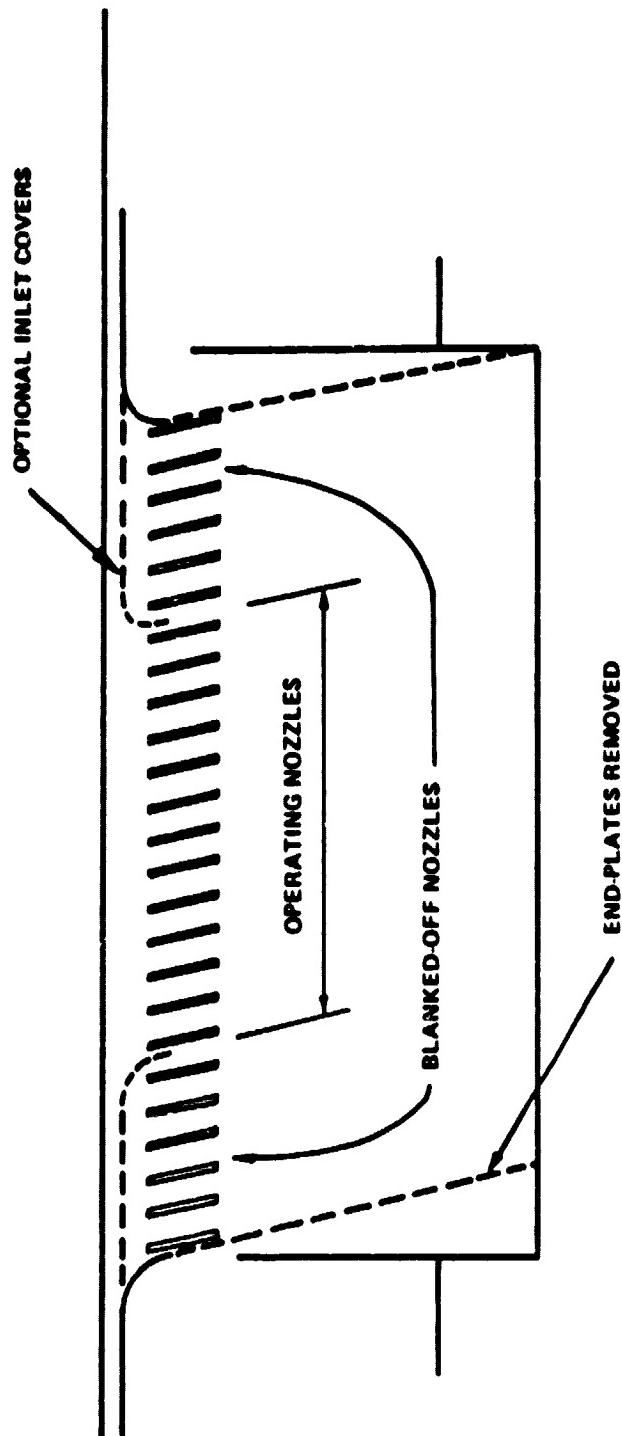
**SECTION 'A-A'**  
SECTION THROUGH AUGMENTER (OUTWARD)  
\* LOOKING FORWARD - L.H. SIDE \*



INLET VANE (VTOL-3 TESTS)



Fig. 8



FUSELAGE AUGMENTOR WITH REDUCED CHORDWISE LENGTH ("HALF-CENTRE" CONFIGURATION)

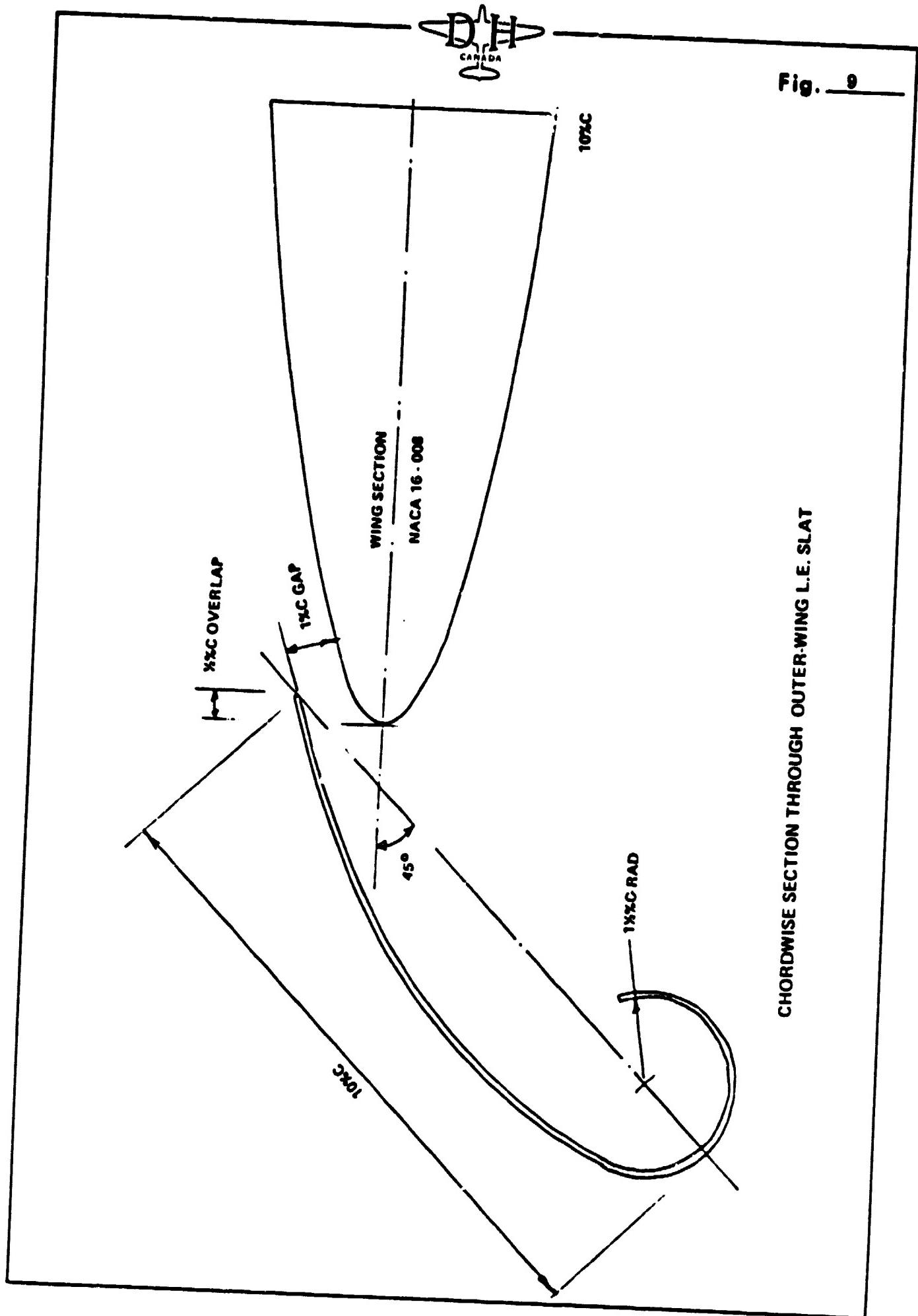
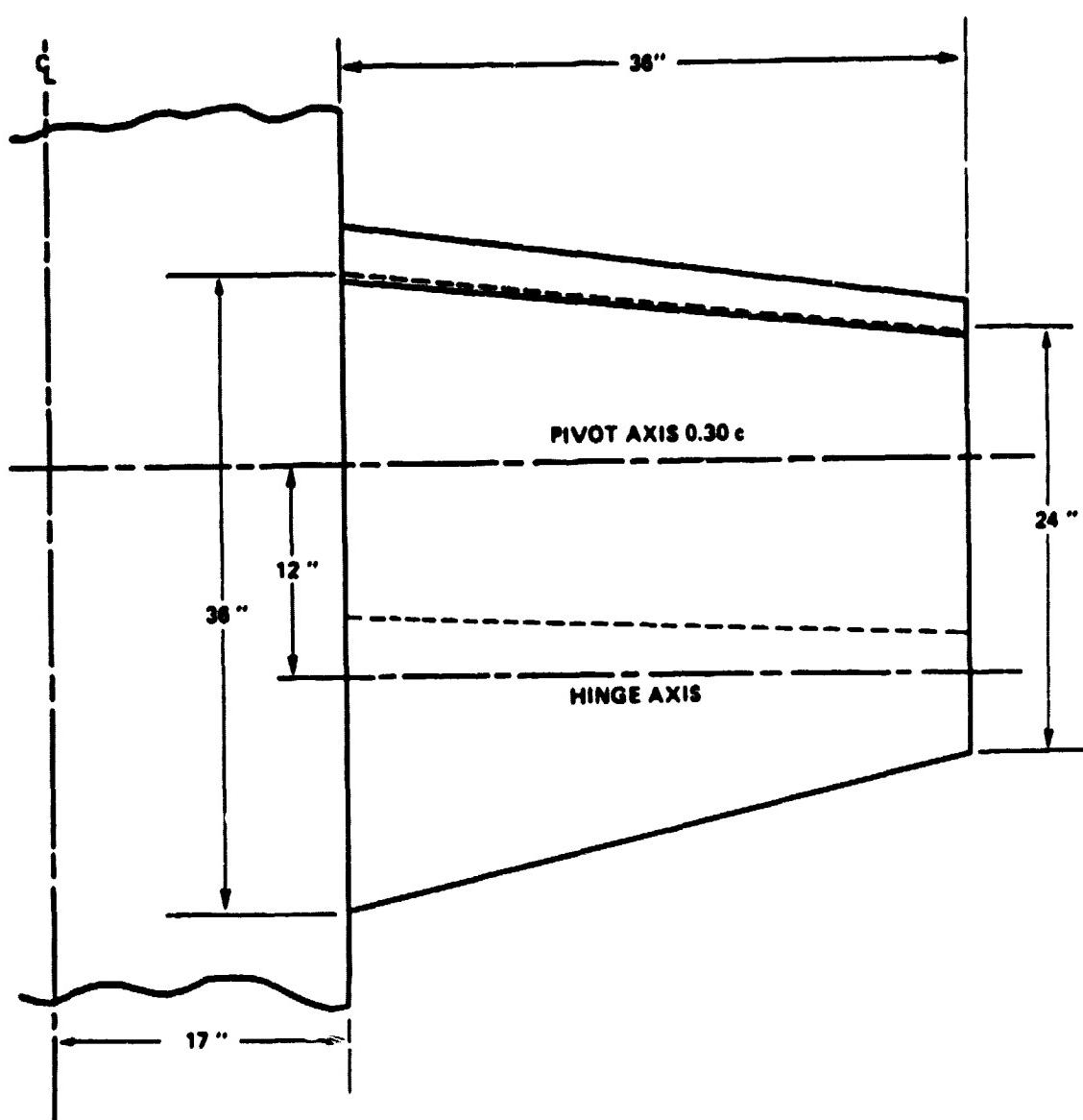
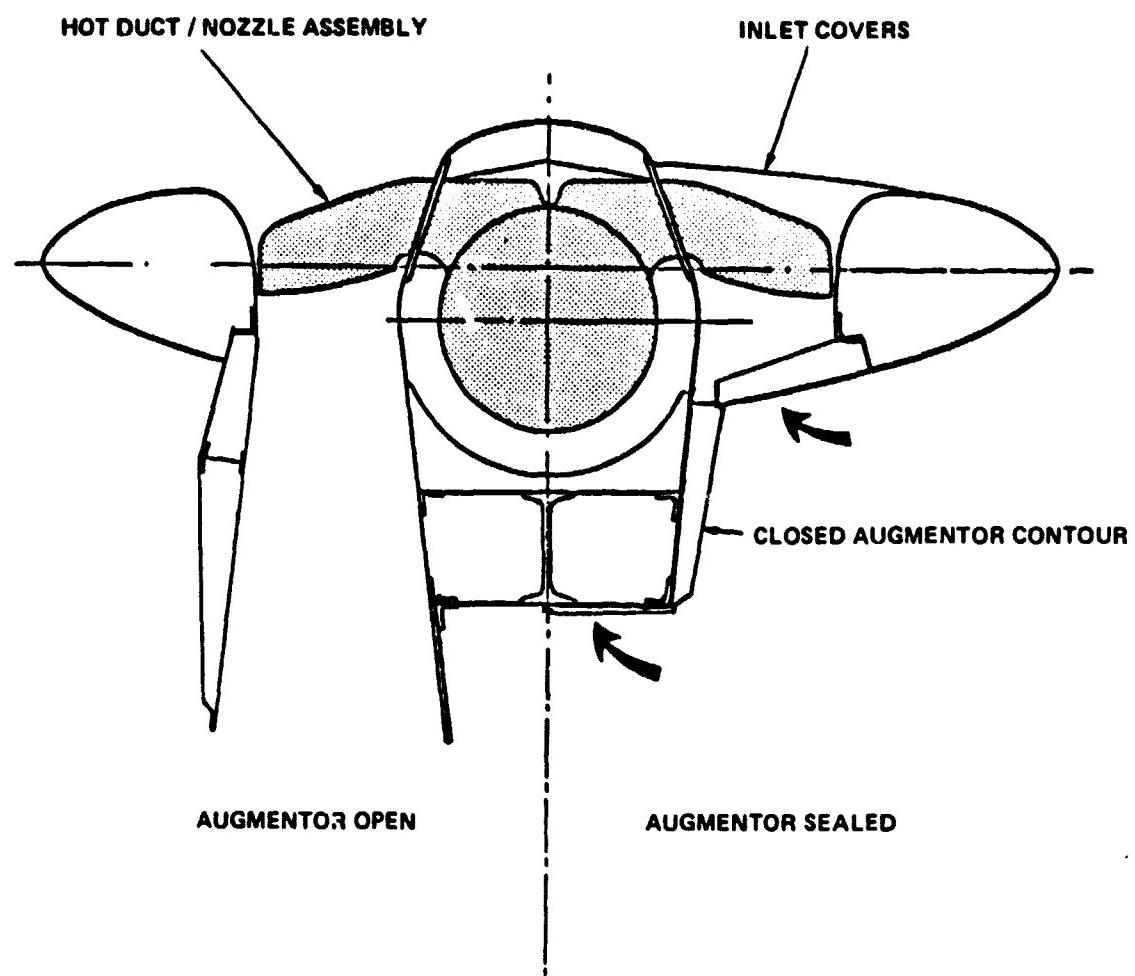




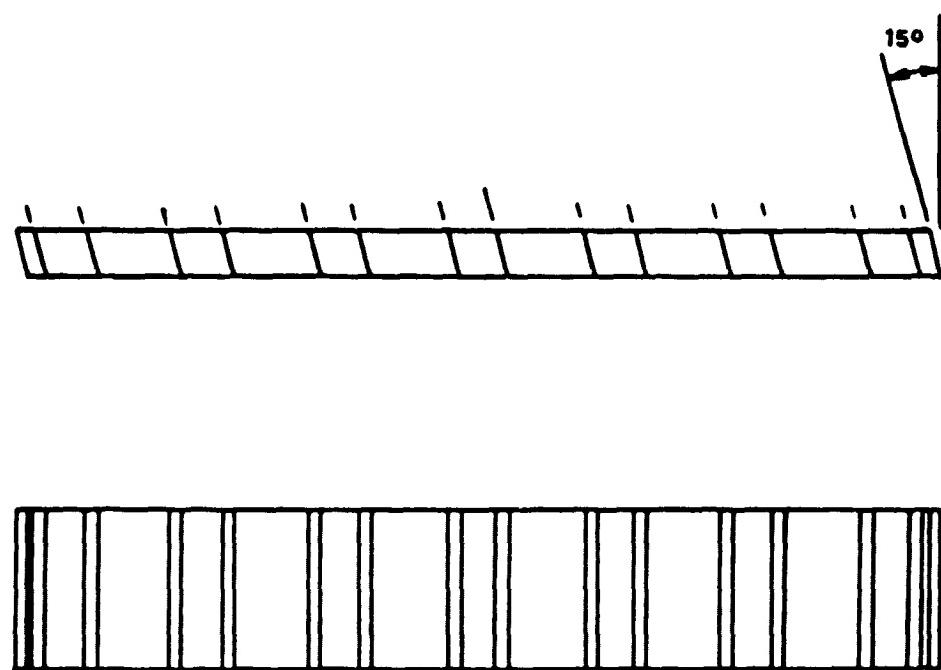
Fig. 10



CANARD PLANFORM AND SECTION



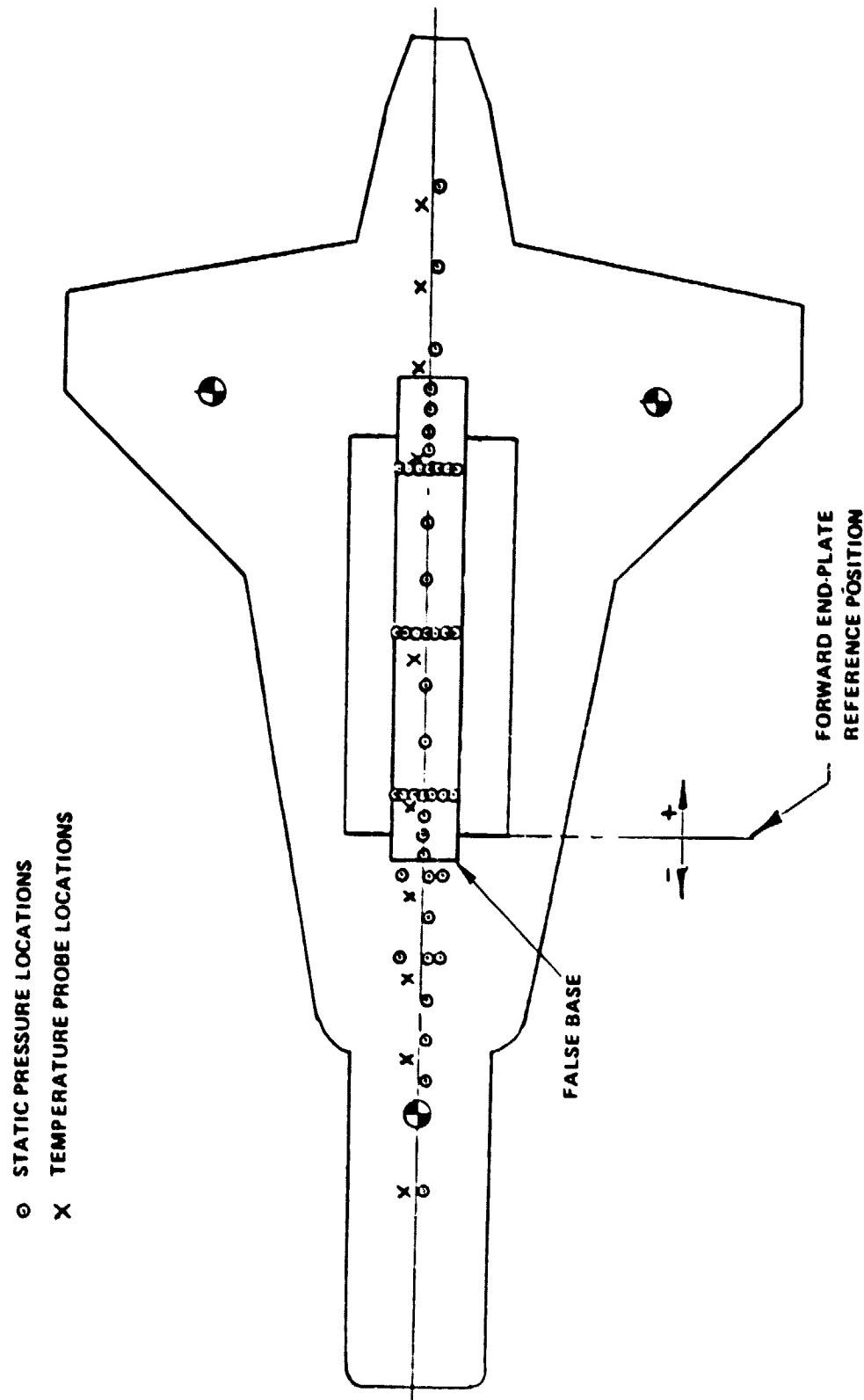
SECTION THROUGH FUSELAGE AUGMENTOR,  
SHOWING SEALED AUGMENTOR CONFIGURATION



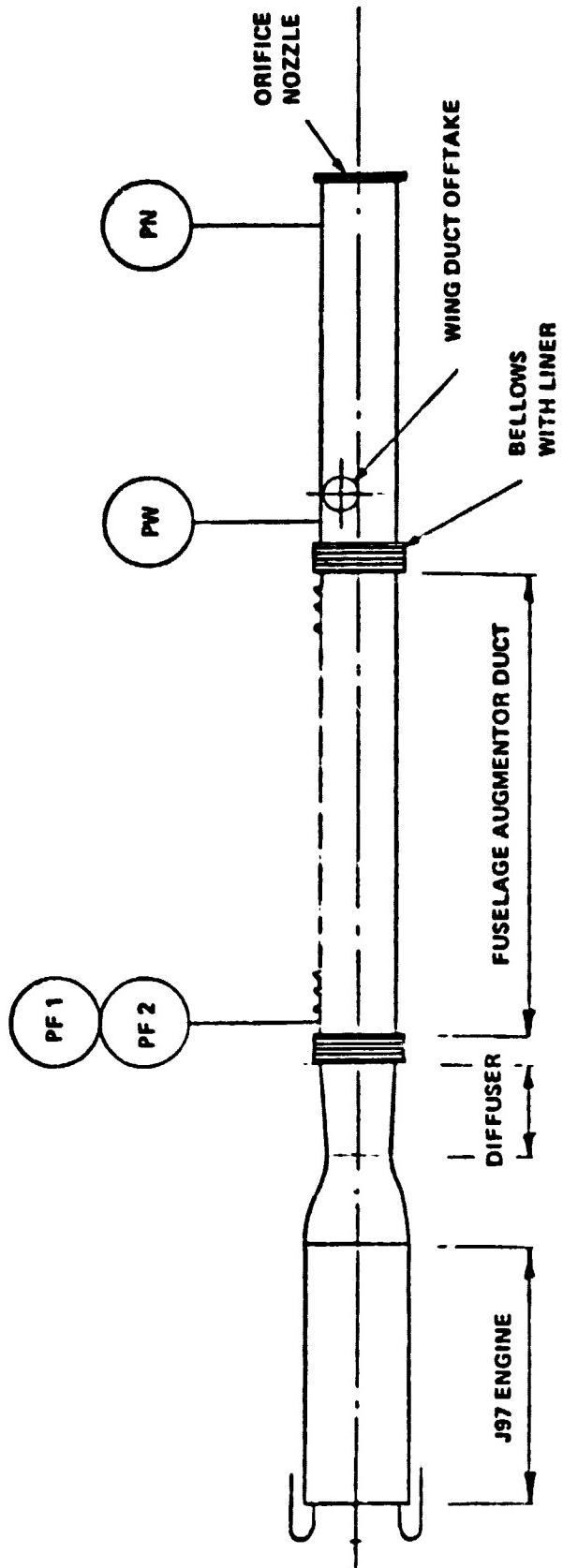
AUGMENTOR EXIT RAKE WITH CANTED PROBES



**Fig. 13**



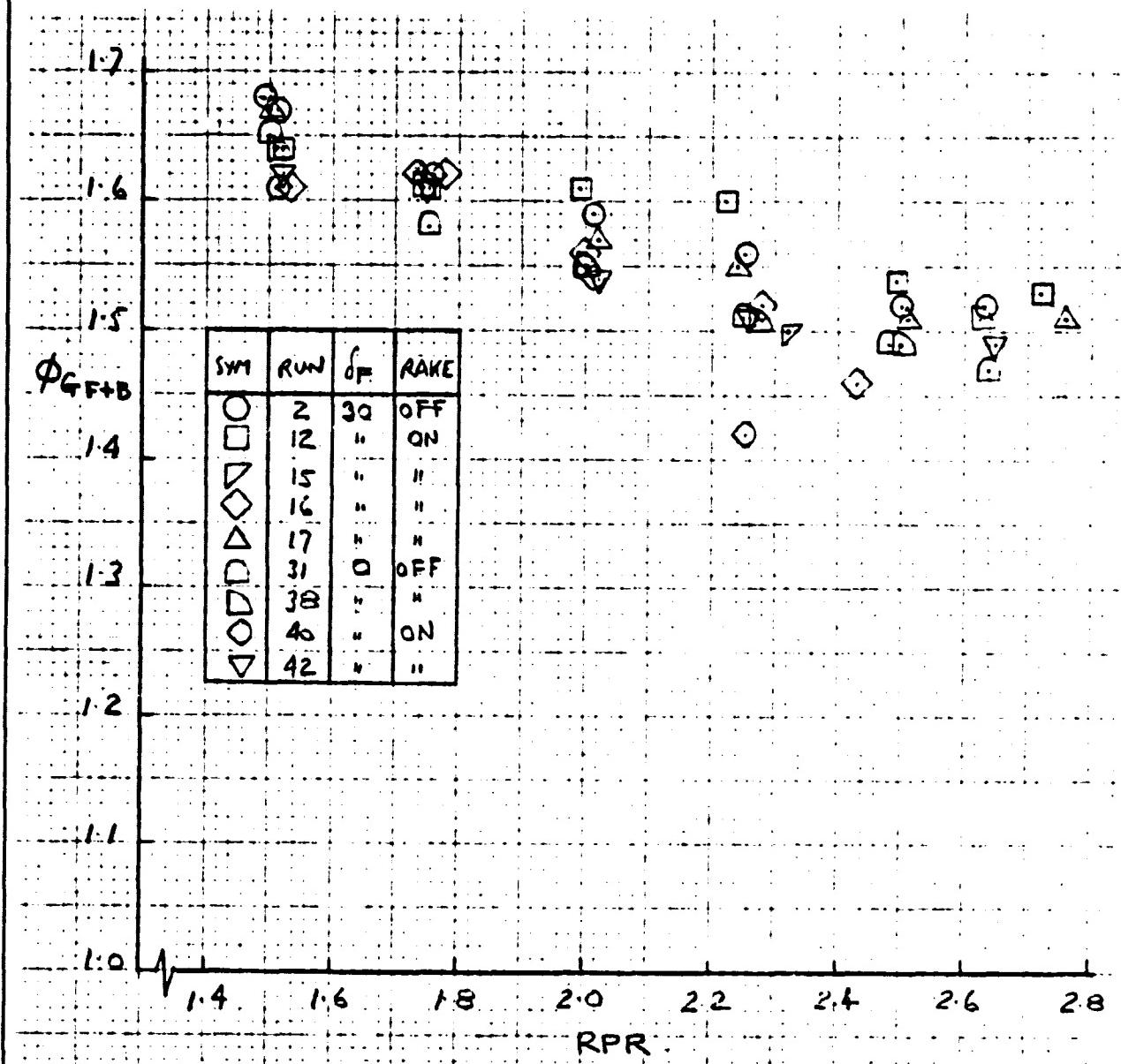
## **LOWER FUSELAGE INSTRUMENTATION (VTOL 3)**



LOCATION OF DUCT STATIC PRESSURE TAPS



Fig. 15(a)

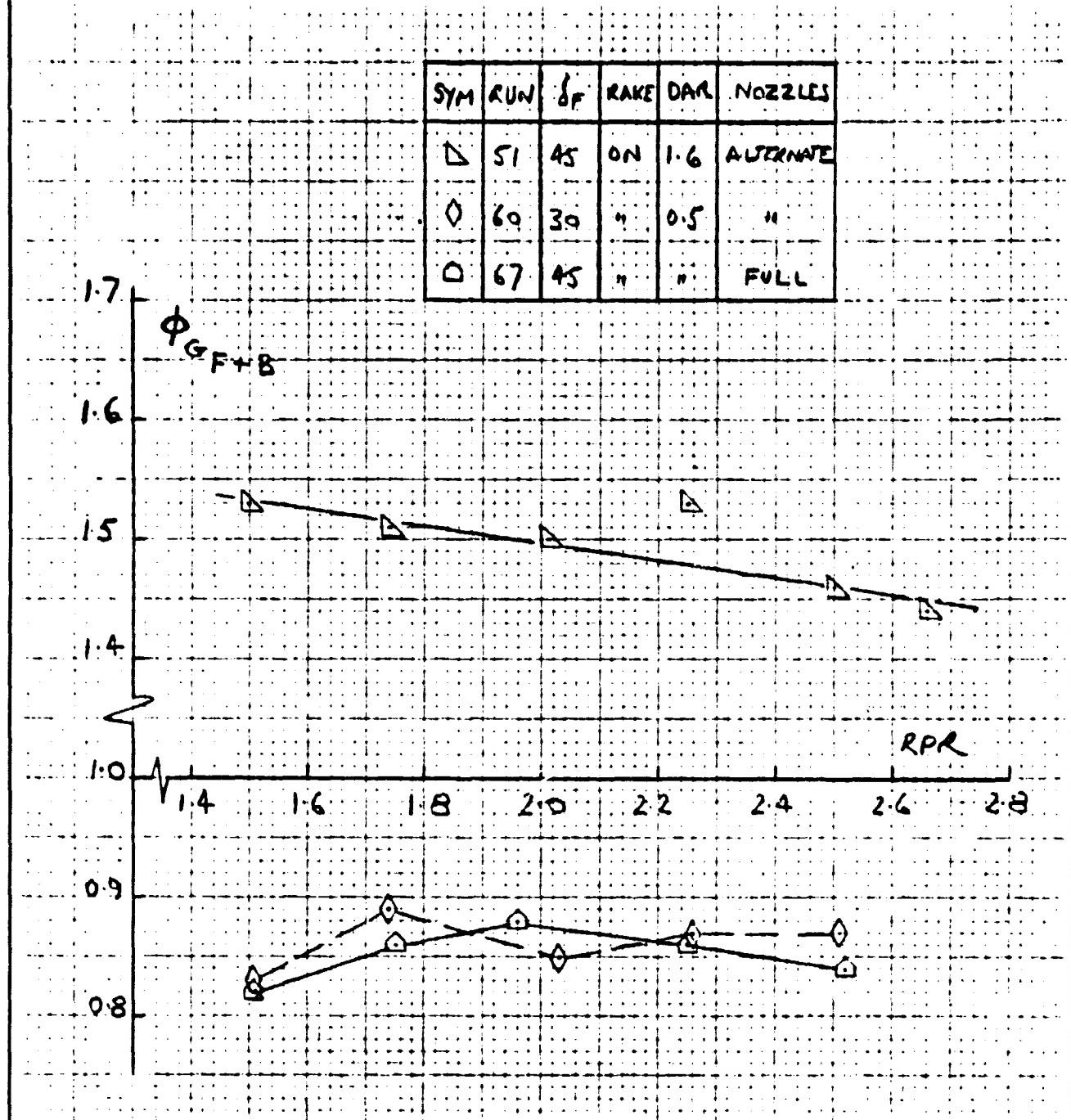


FUSELAGE AUGMENTOR STATIC THRUST AUGMENTATION RATIO

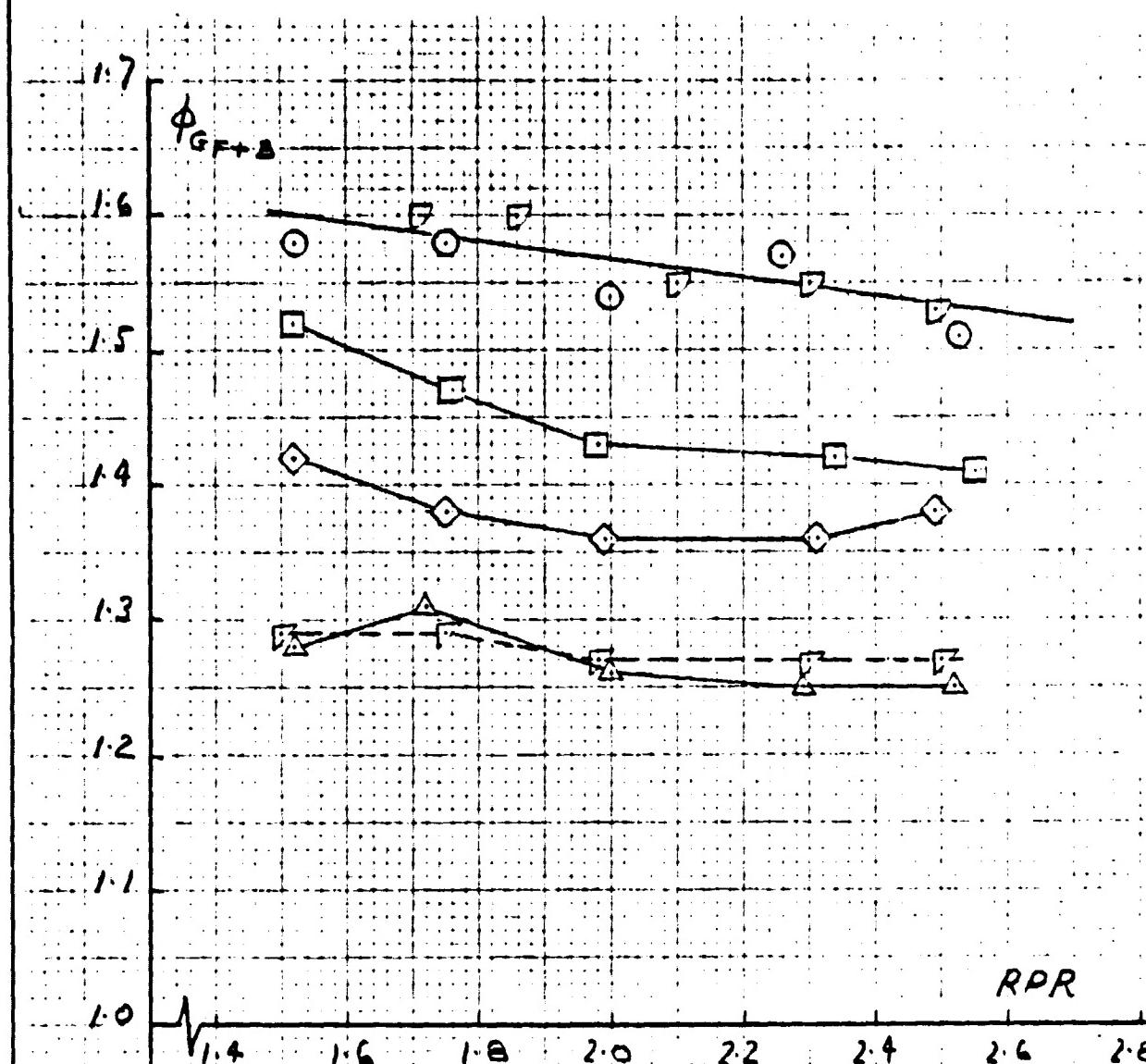
FULL NOZZLE SET      DAR = 1.6      END-PLATES ON  
(BASE THRUST INCLUDED)  
VTOL-2 TESTS

ORIGINAL PAGE IS  
OF POOR QUALITY

Fig. 15(b)



FUSELAGE AUGMENTOR STATIC THRUST AUGMENTATION RATIO

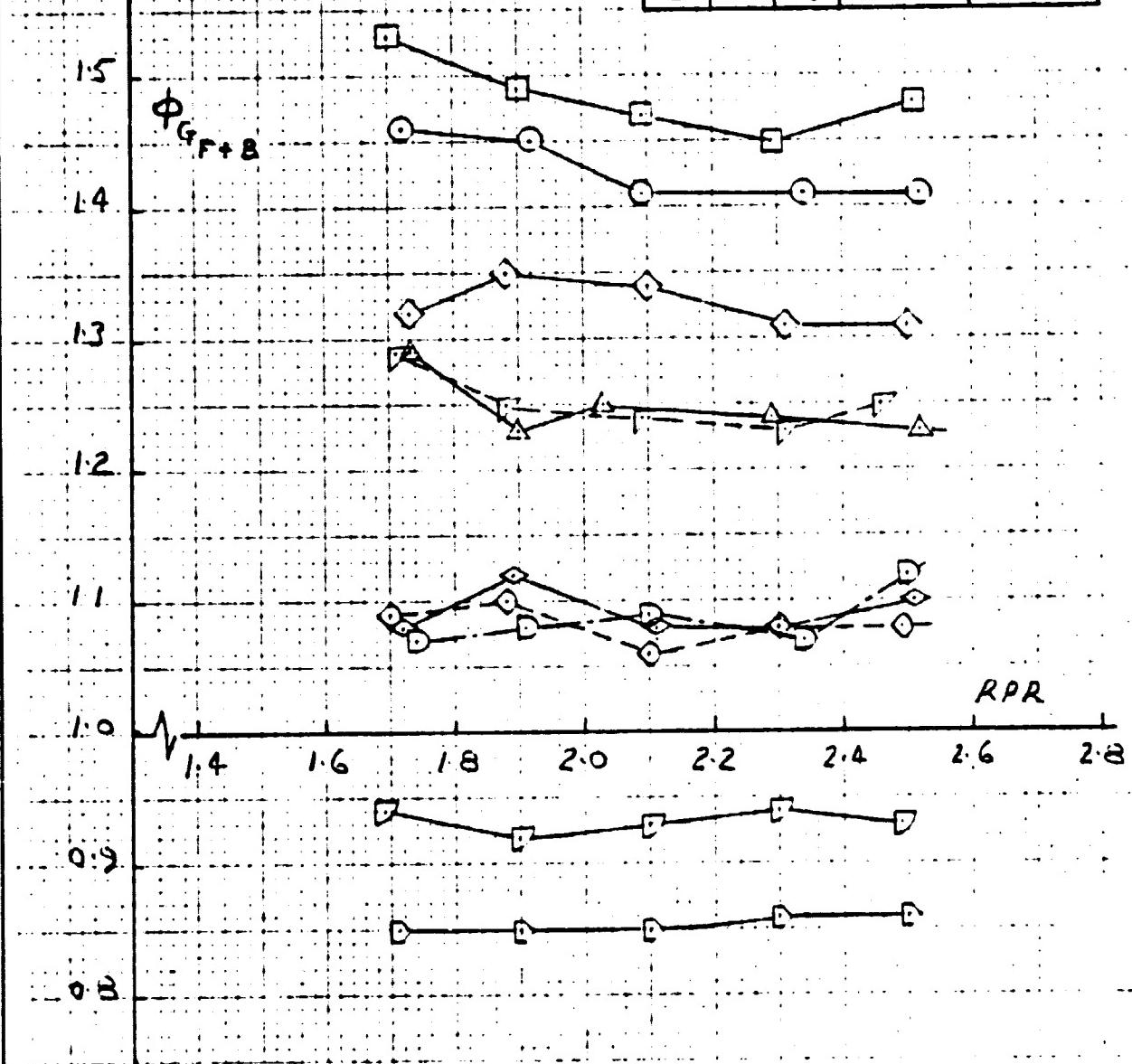


STATIC THRUST AUGMENTATION - VTOL 3 TESTS  
FULL NOZZLE SET



Fig. 15(d)

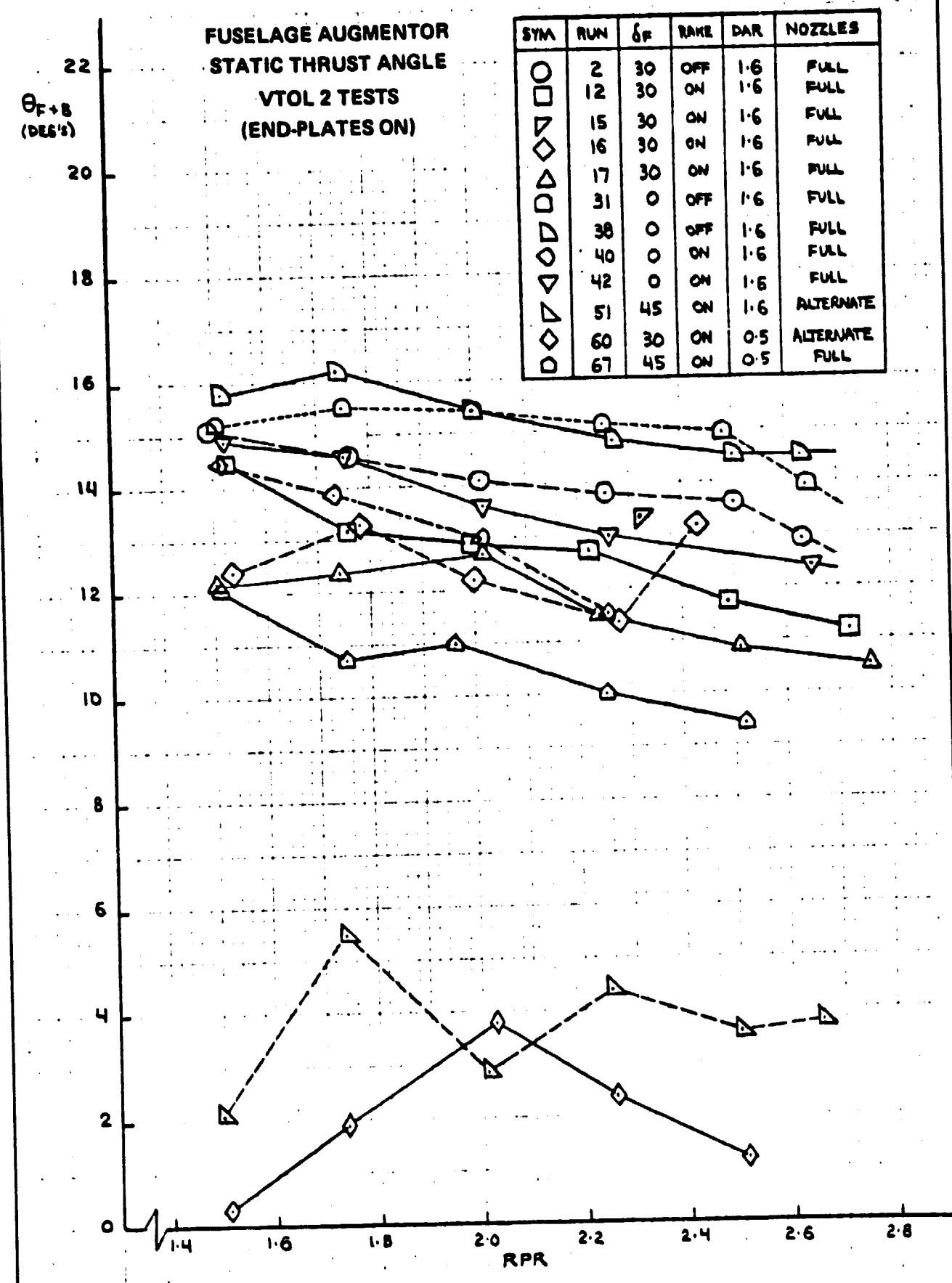
SYM	RUN	DAR	NOZZLES	END-PLATES
O	31	1.6	ALTERNATE	ON
□	32	"	"	"
△	49	"	"	FRONT OFF
▽	53	"	"	OFF
◆	58	1.0	"	"
◆	62	0.5	"	"
○	66	1.0	CENTRE	"
○	70	"	"	"
○	74	1.6	"	"
○	77	0.5	"	"

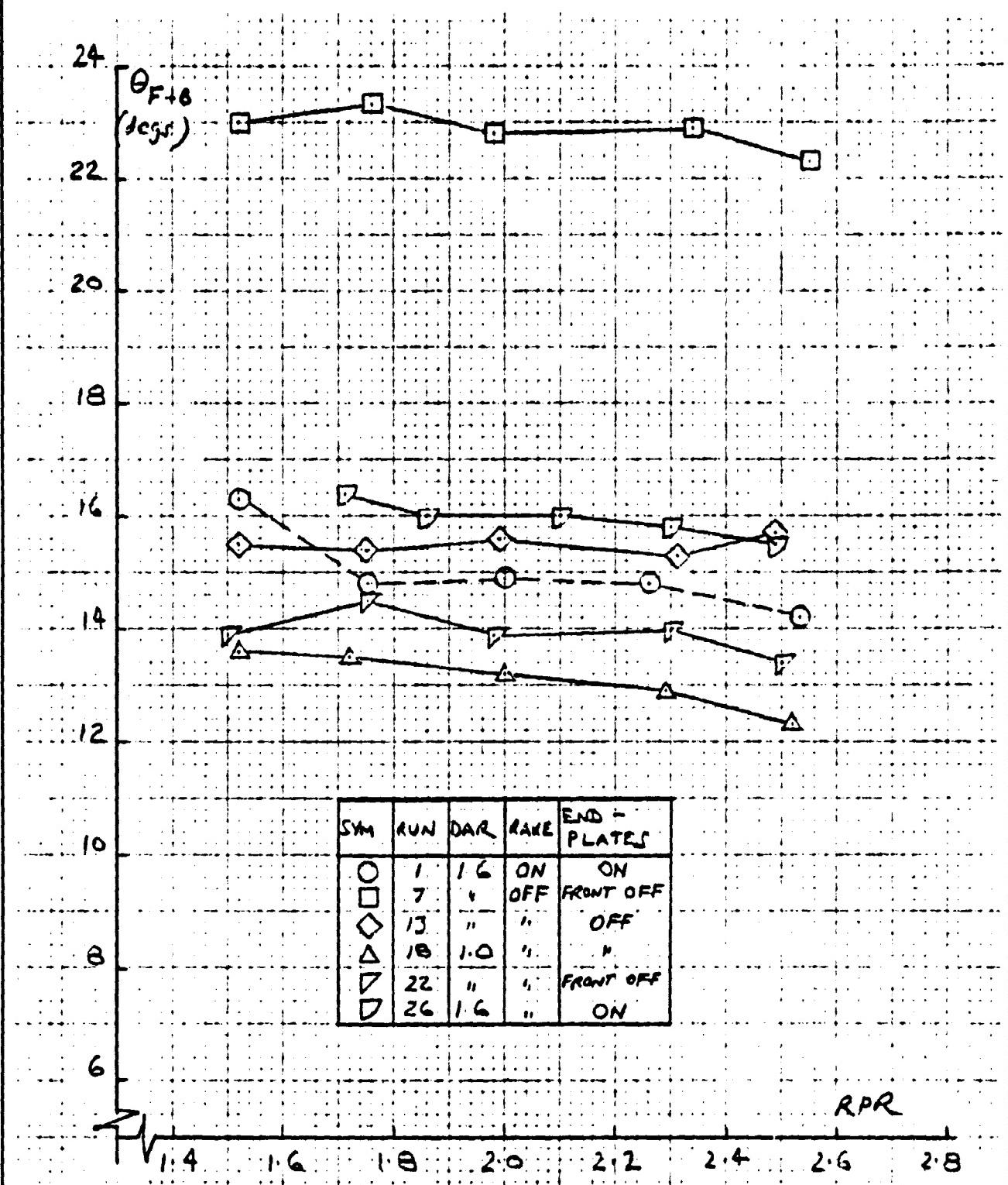


ORIGINAL PAGE IS  
OF POOR QUALITY

STATIC THRUST AUGMENTATION - VTOL 3 TESTS  
HALF NOZZLE TESTS (RAKE OFF)

Fig. 16(a)





FUSELAGE AUGMENTOR STATIC THRUST ANGLE - VTOL 3 TESTS  
FULL NOZZLE SET

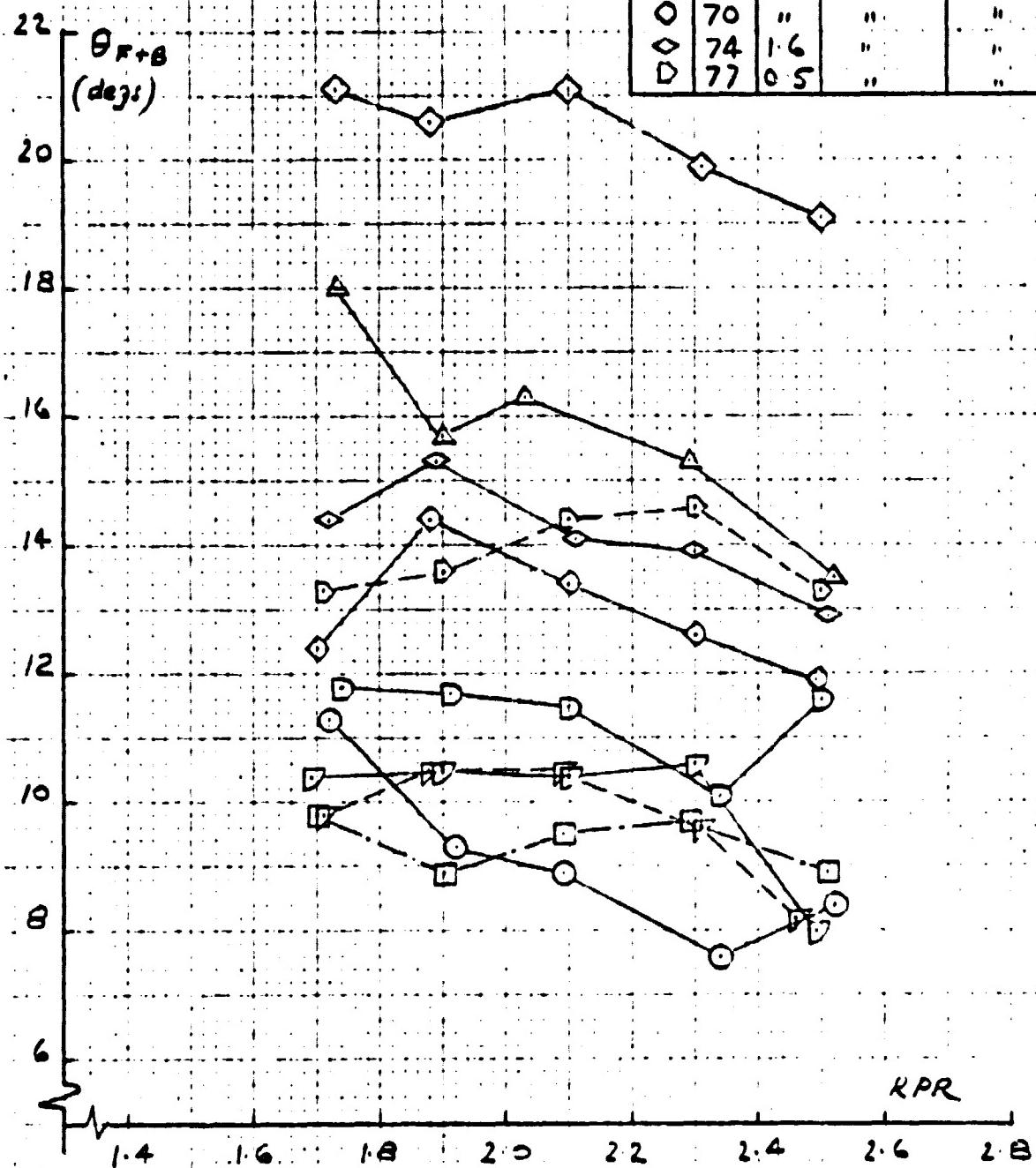
ORIGINAL PAGE IS  
OF POOR QUALITY



Fig. 16(e)

FUSELAGE AUGMENTOR STATIC THRUST ANGLE  
- VTOL 3 TESTS

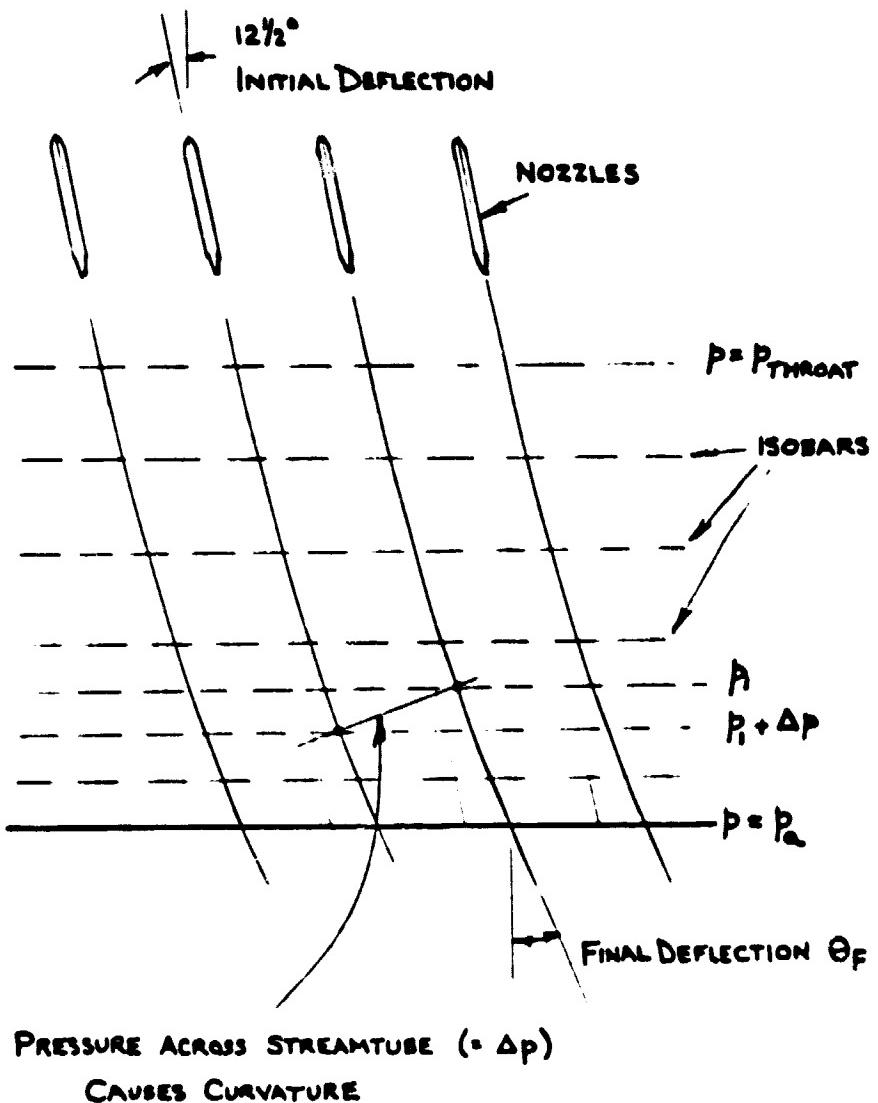
HALF NOZZLE TESTS  
(RAKE OFF)



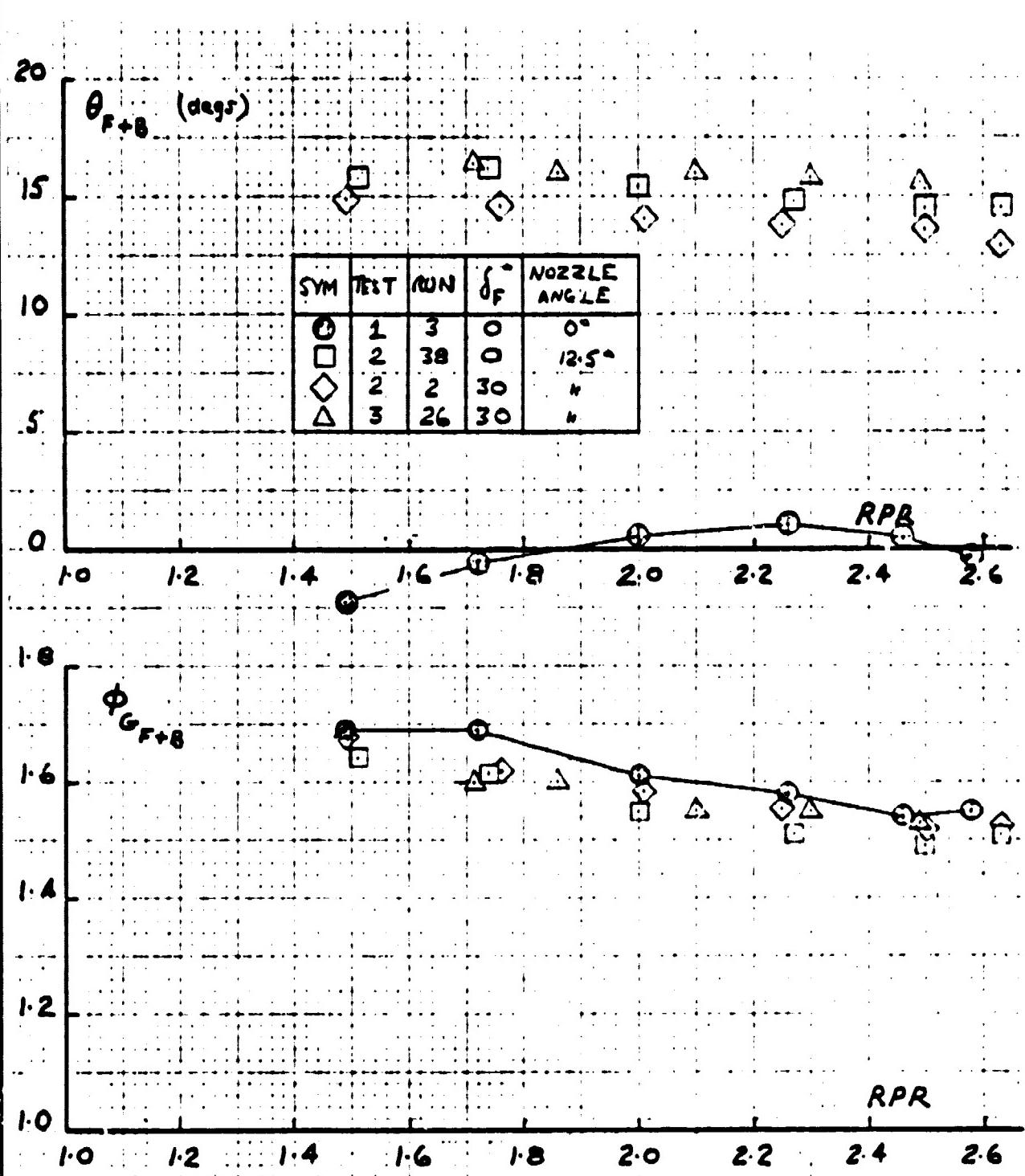
ORIGINAL PAGE IS  
OF POOR QUALITY



Fig. 17

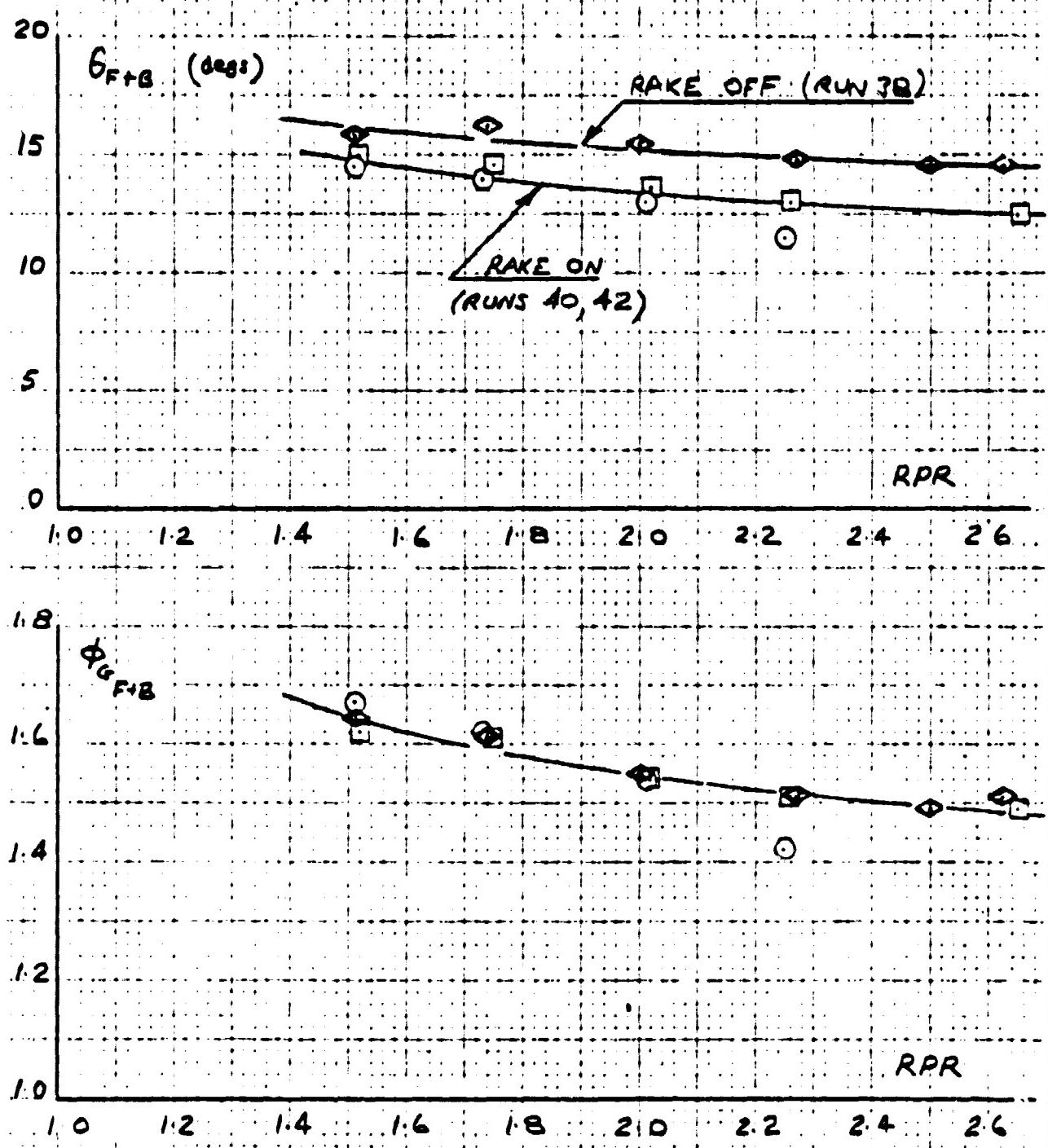


MECHANISM OF FLOW DEFLECTION  
IN  
FUSELAGE AUGMENTOR DIFFUSER



EFFECT OF FUSELAGE AUGMENTOR NOZZLE ANGLE ON STATIC PERFORMANCE

DAR = 1.6; FULL NOZZLE SET; EXIT RAKE OFF



EFFECT OF RAKE ON STATIC PERFORMANCE (VTOL 2 TESTS)

DAR = 1.6; FULL NOZZLE SET

ORIGINAL PAGE IS  
OF POOR QUALITY



Fig. 20

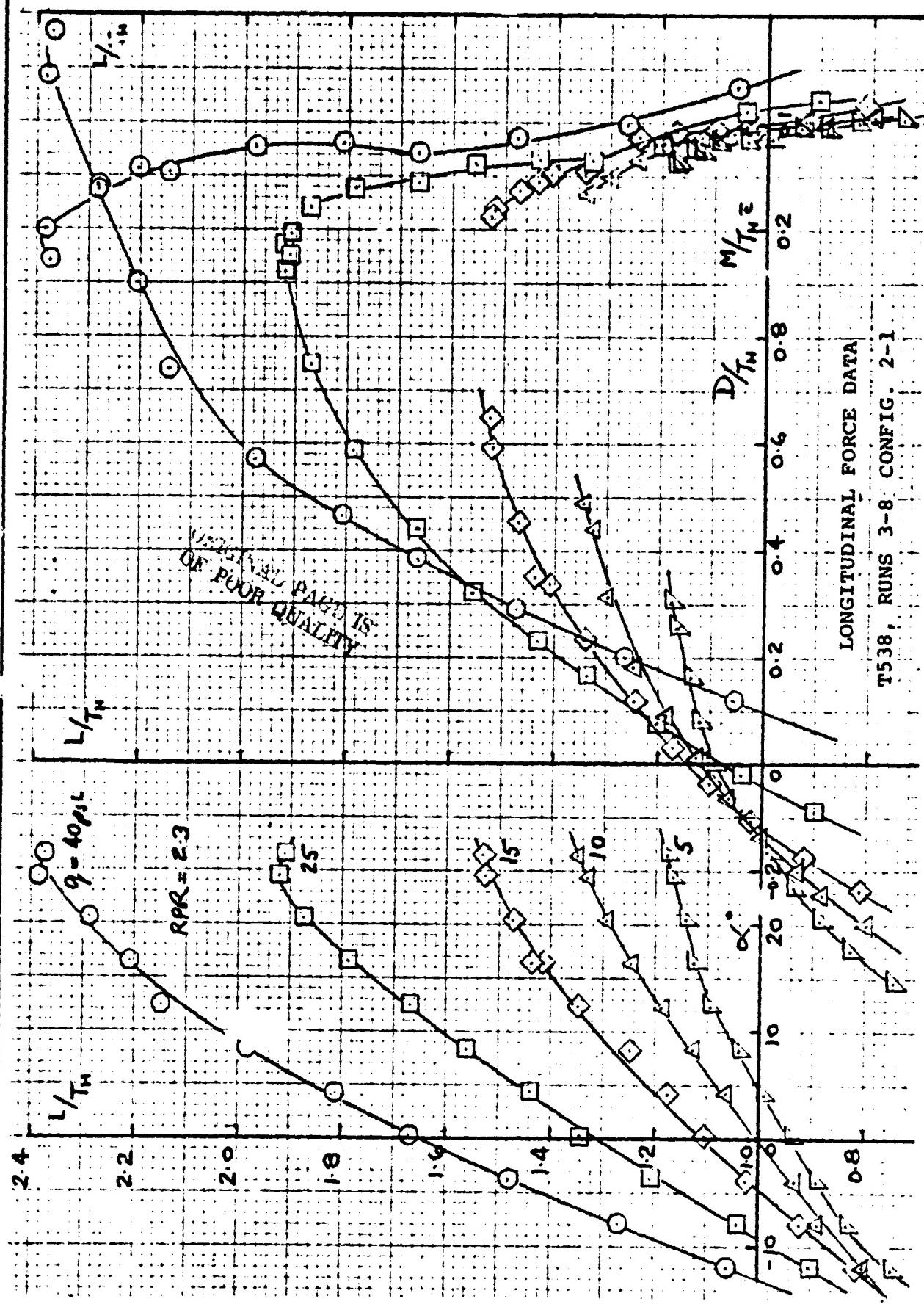




Fig. 21

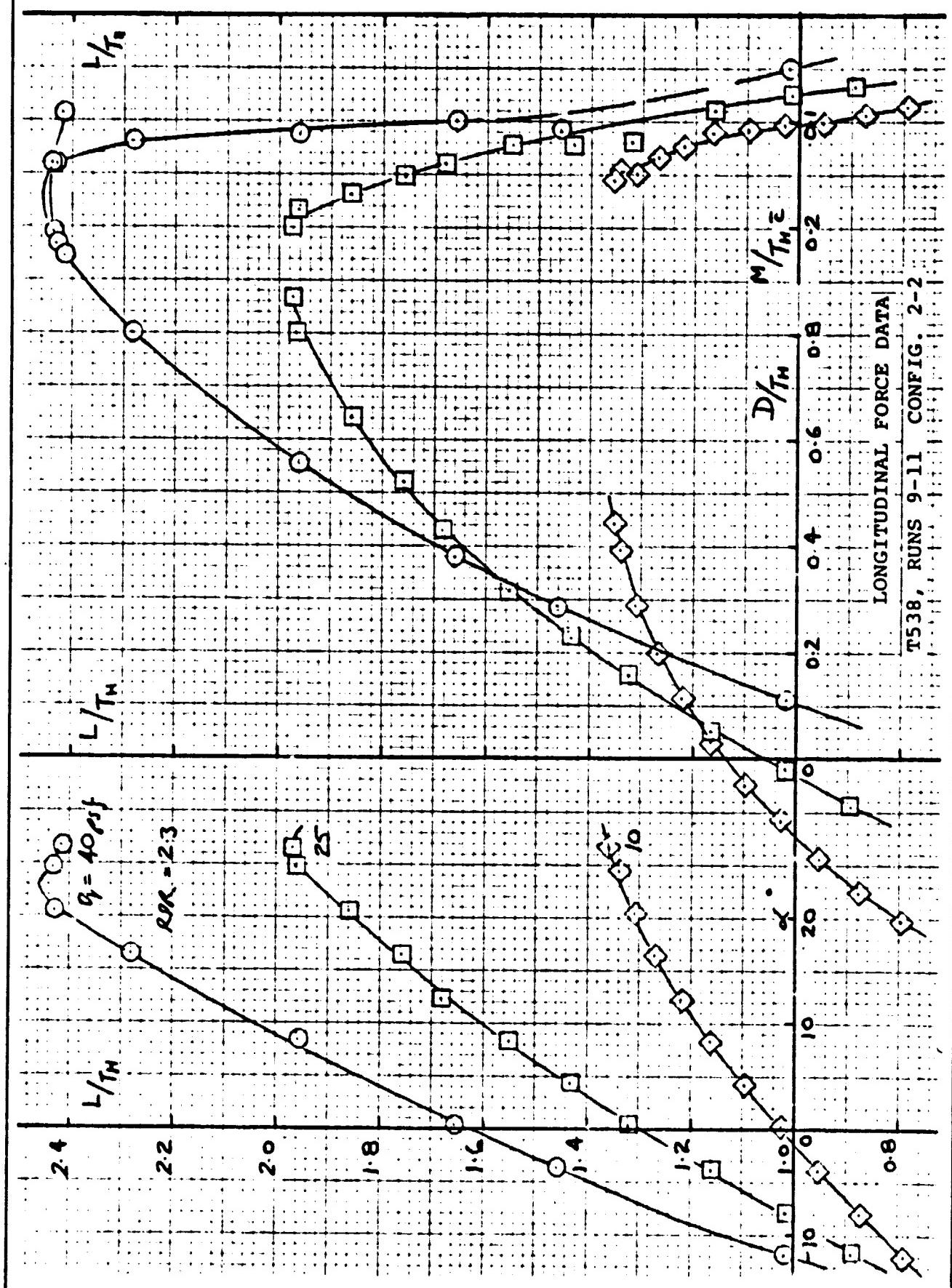




Fig. 22

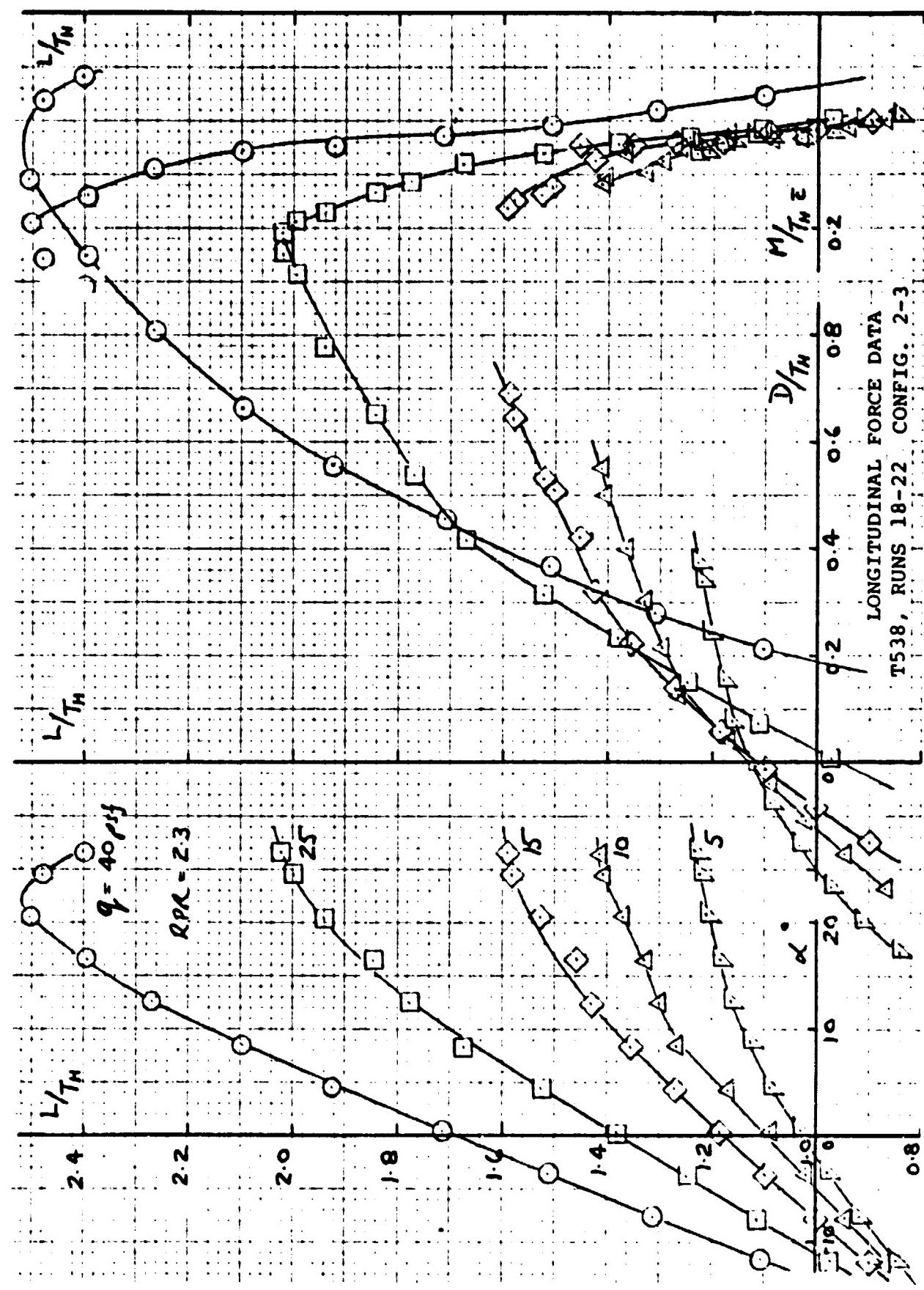




Fig. 23

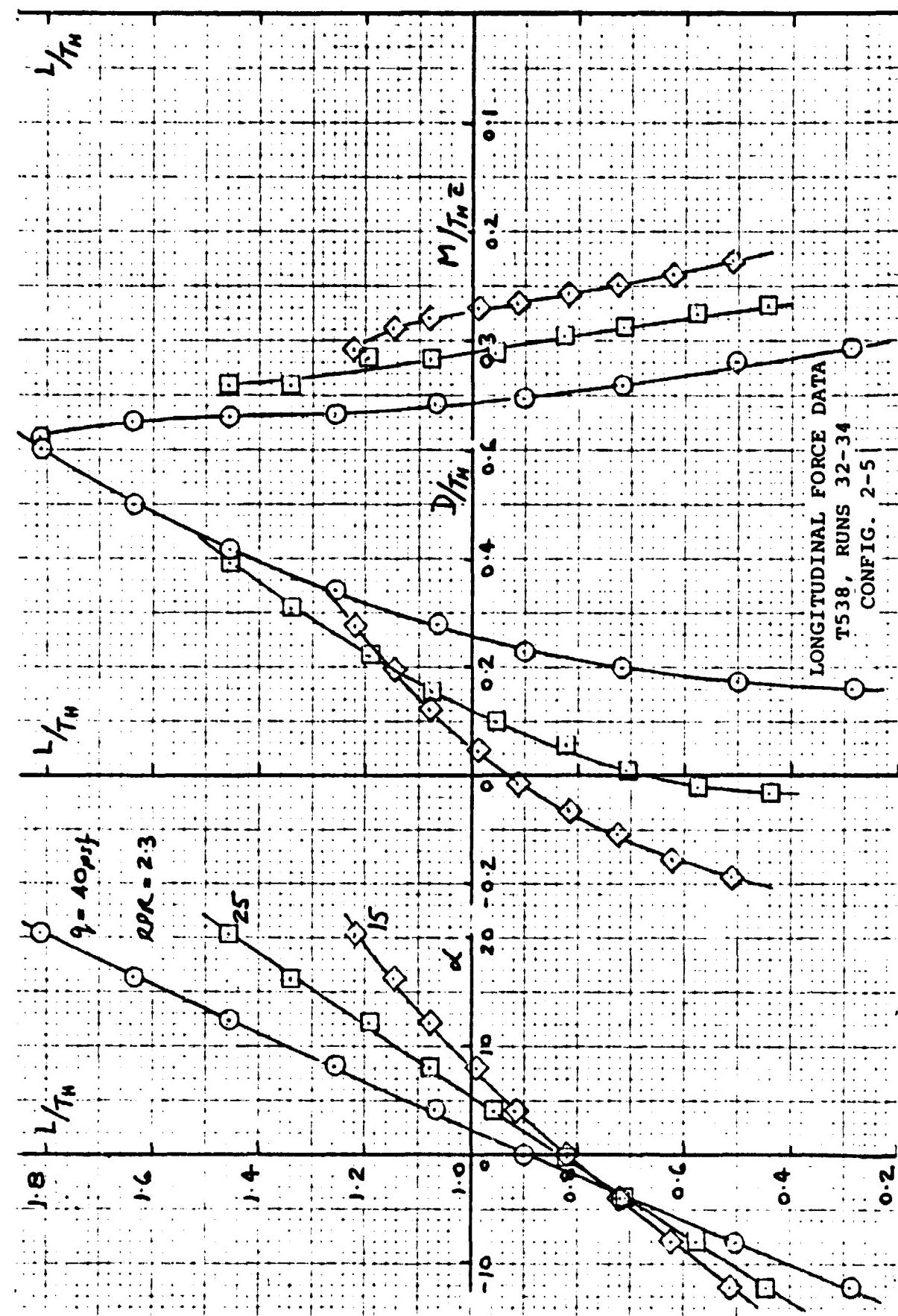




Fig. 24

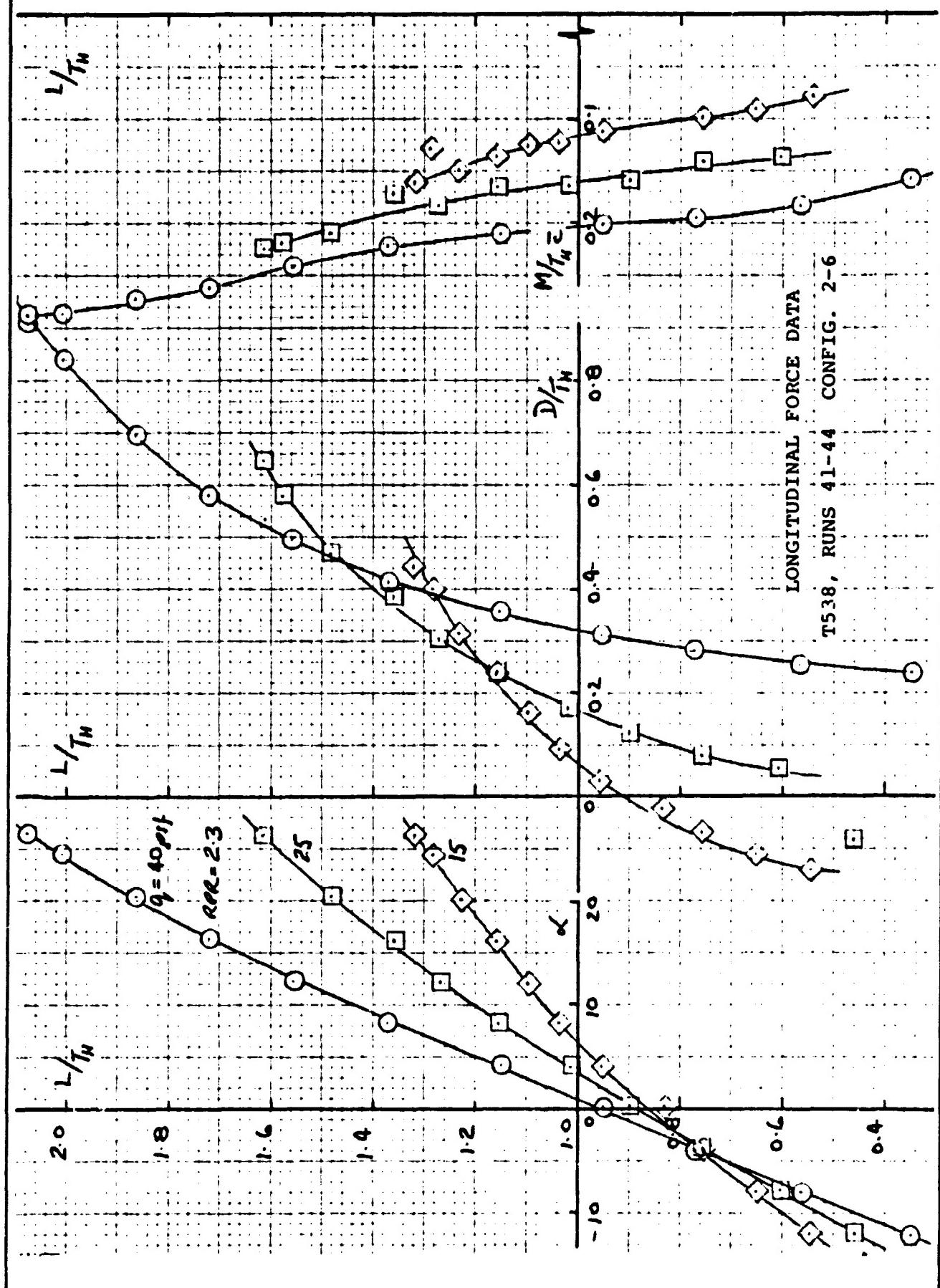




Fig. 25

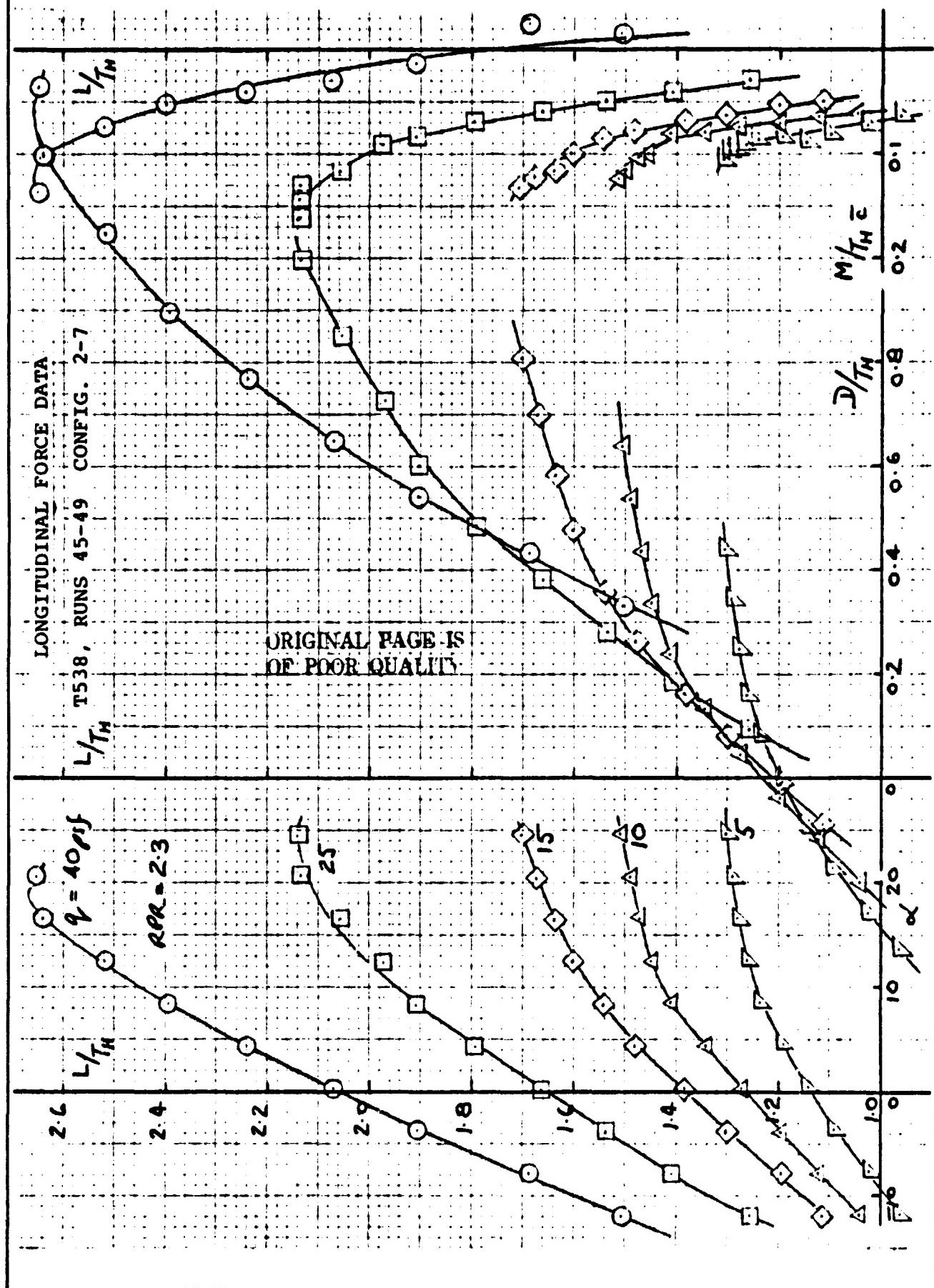


Fig. 26

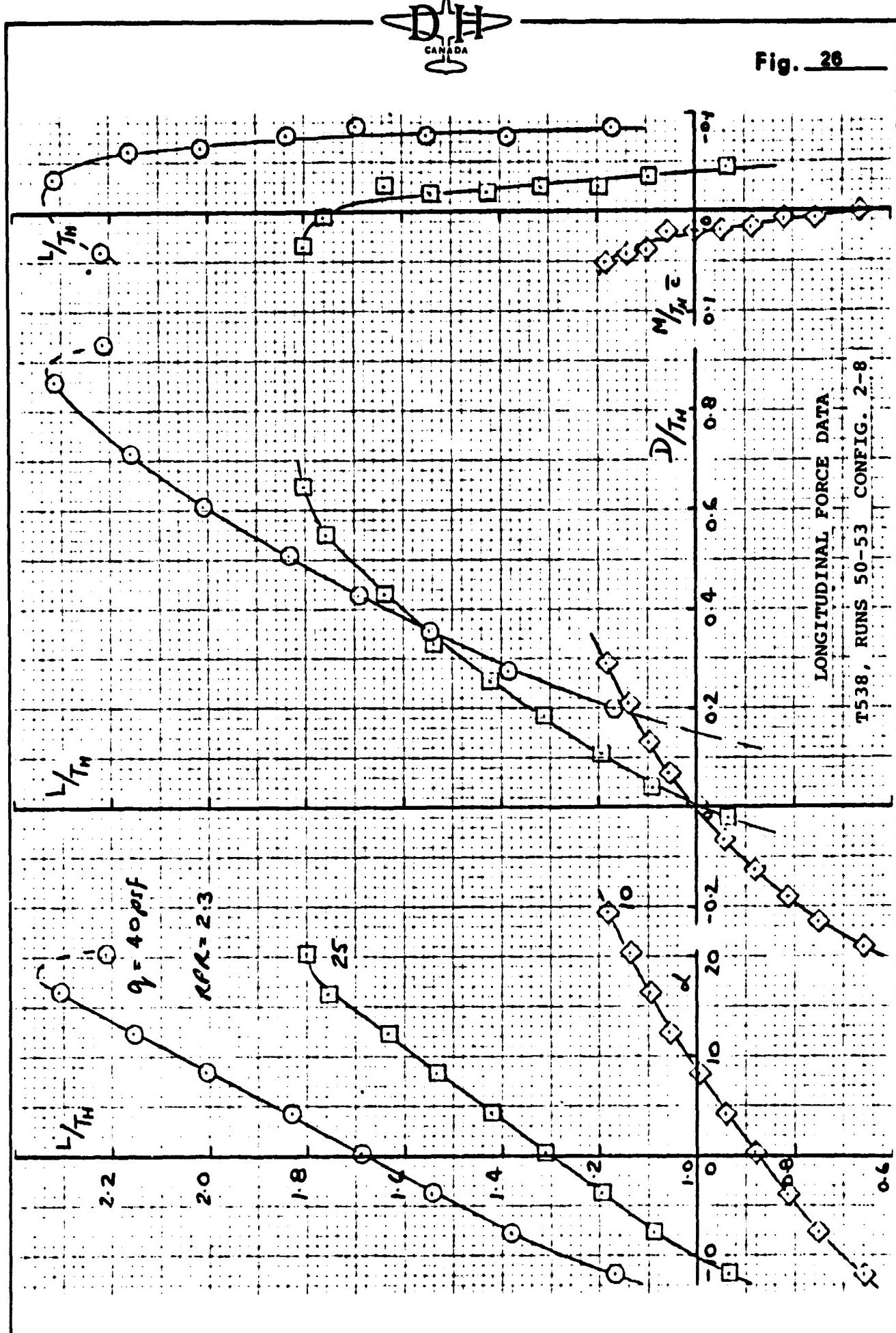


Fig. 27

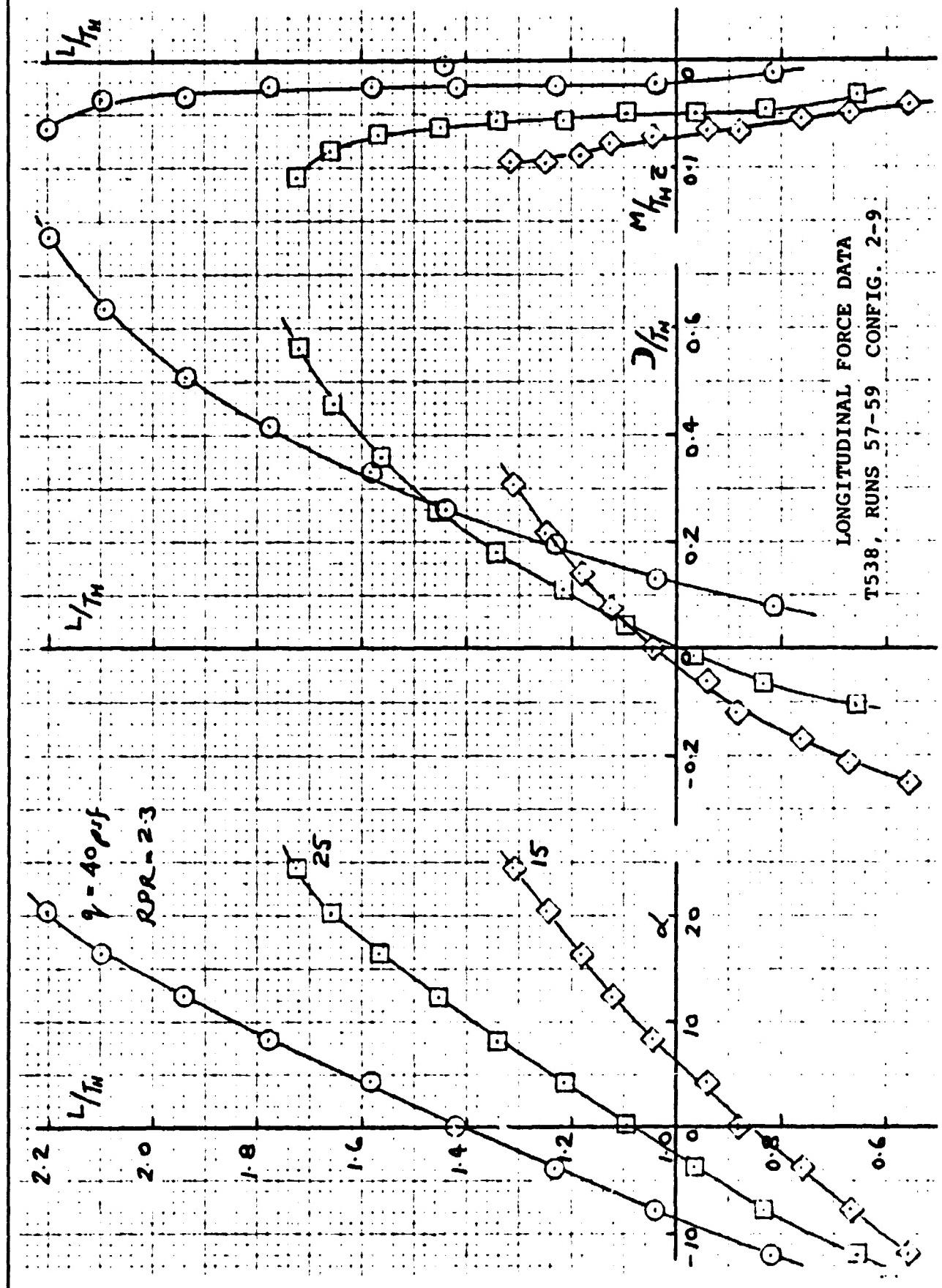




Fig. 28

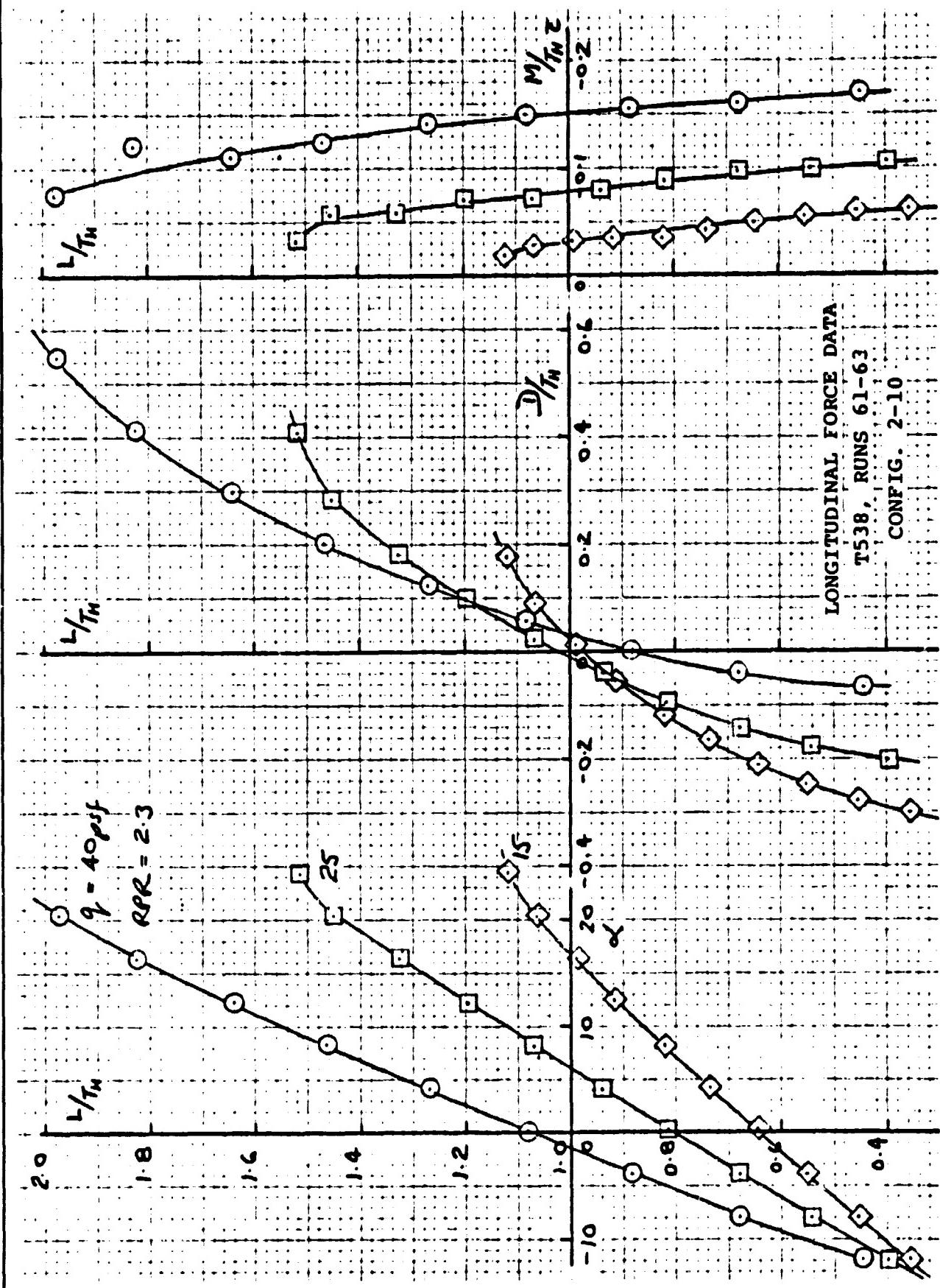




Fig. 29

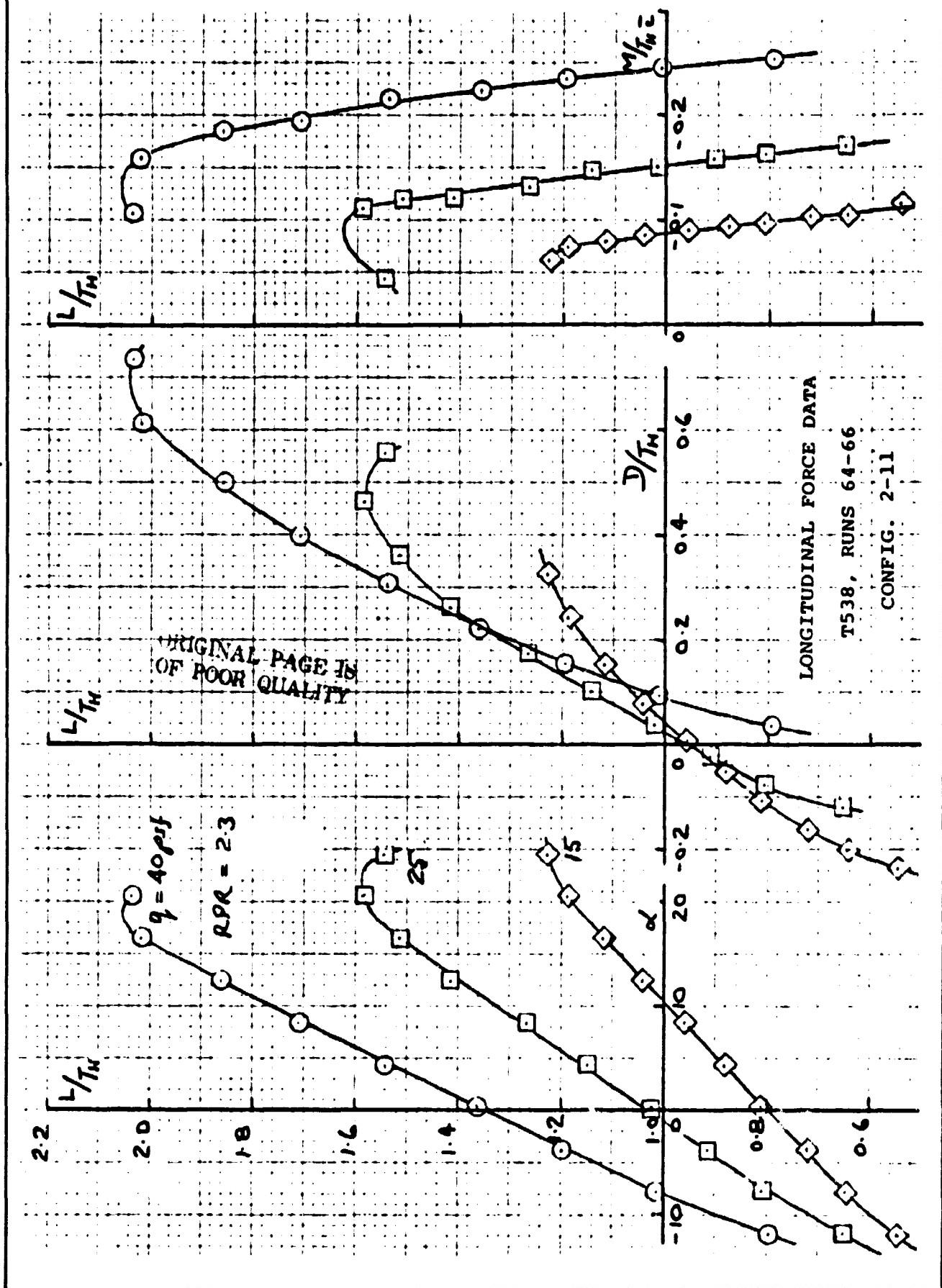
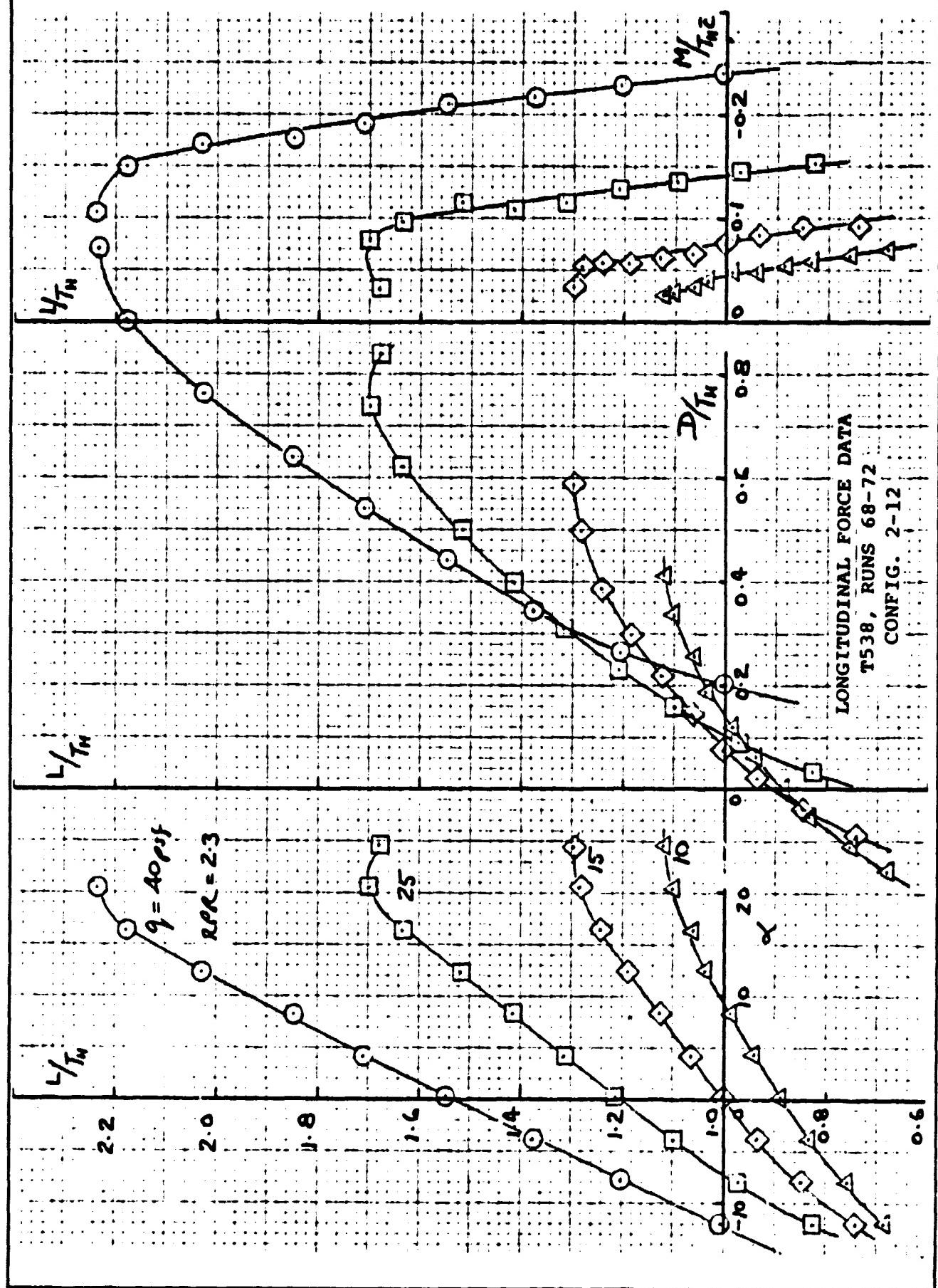




Fig. 30





**Fig. 31**

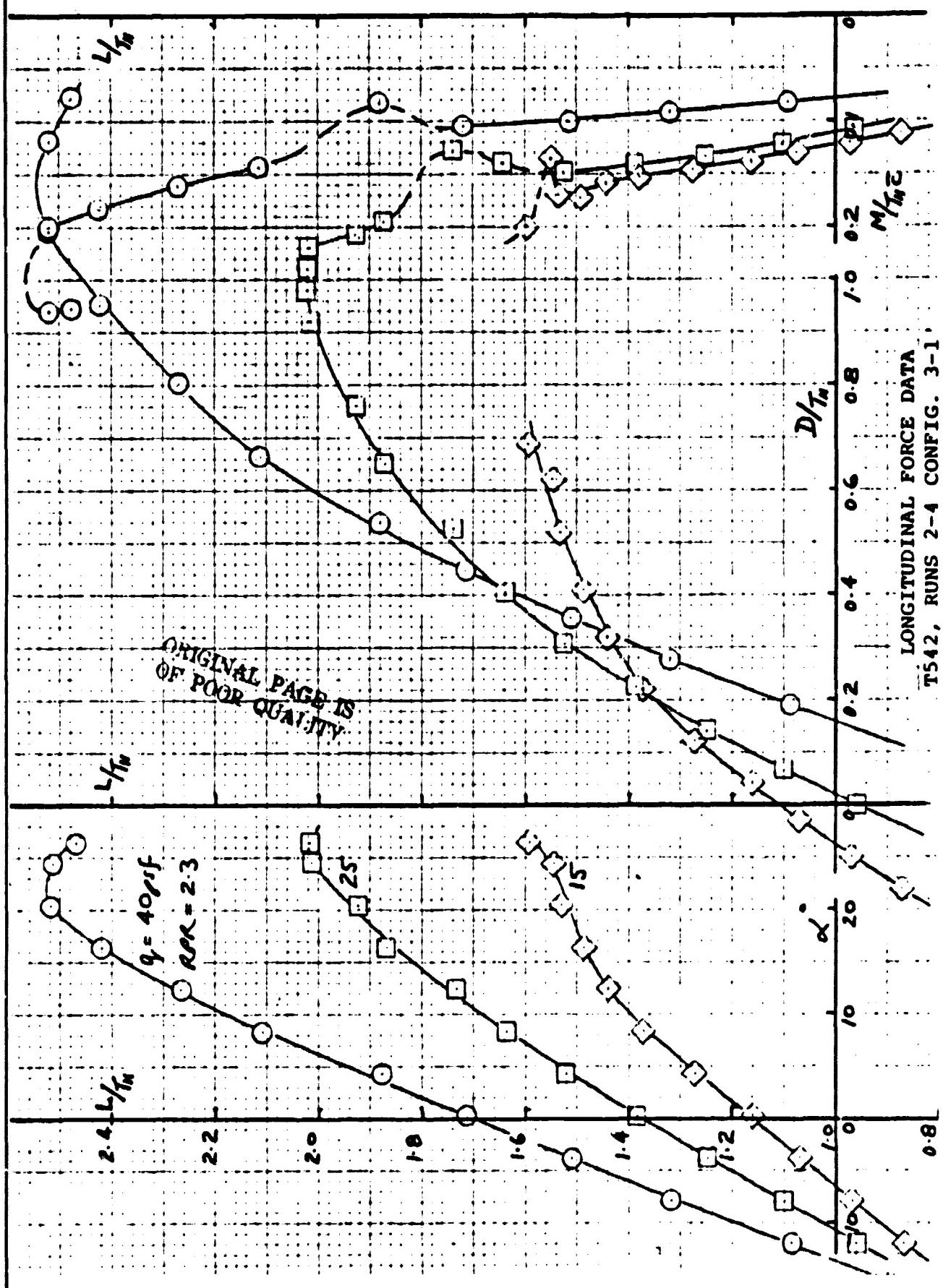




Fig. 32

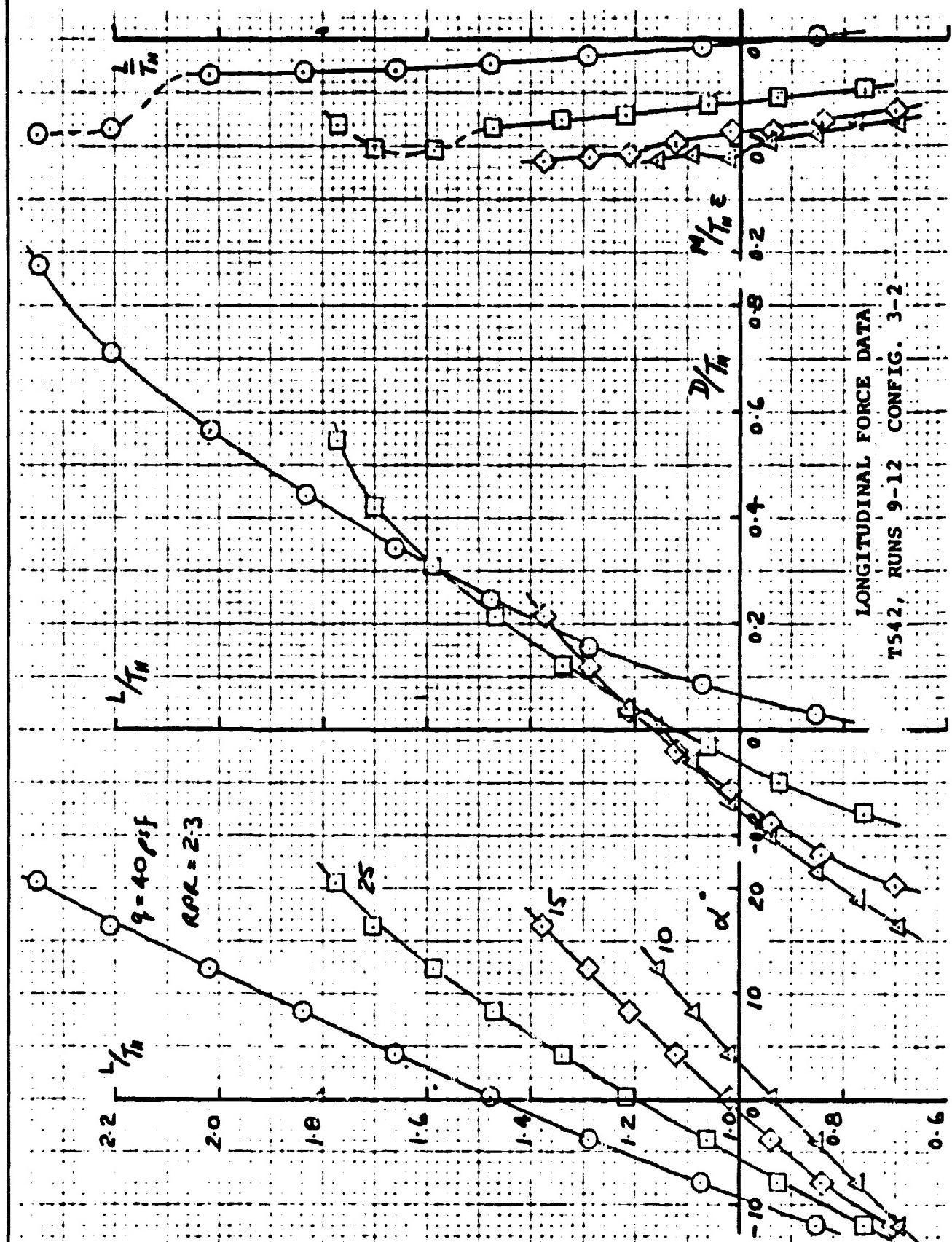


Fig. 33

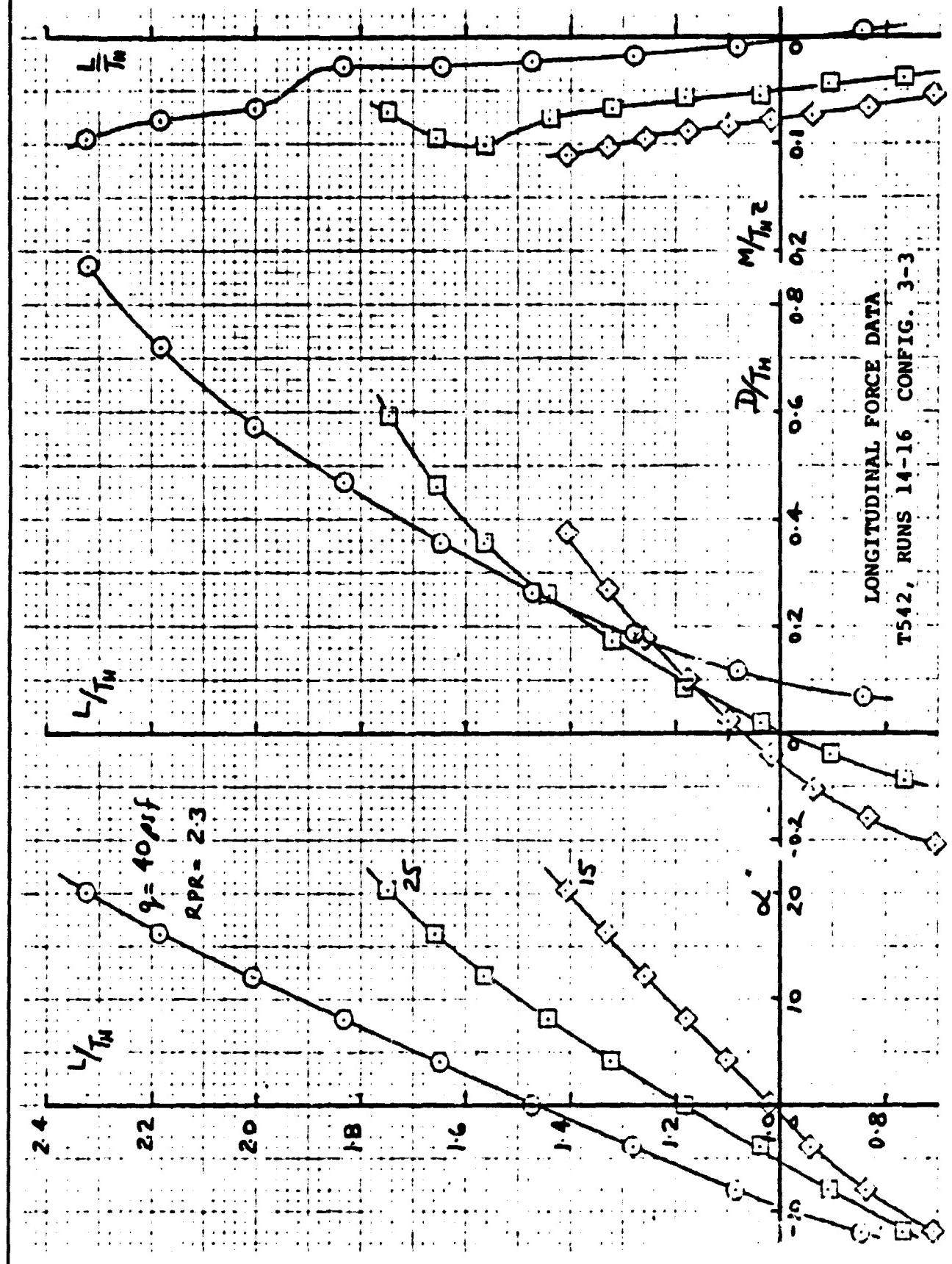




Fig. 34

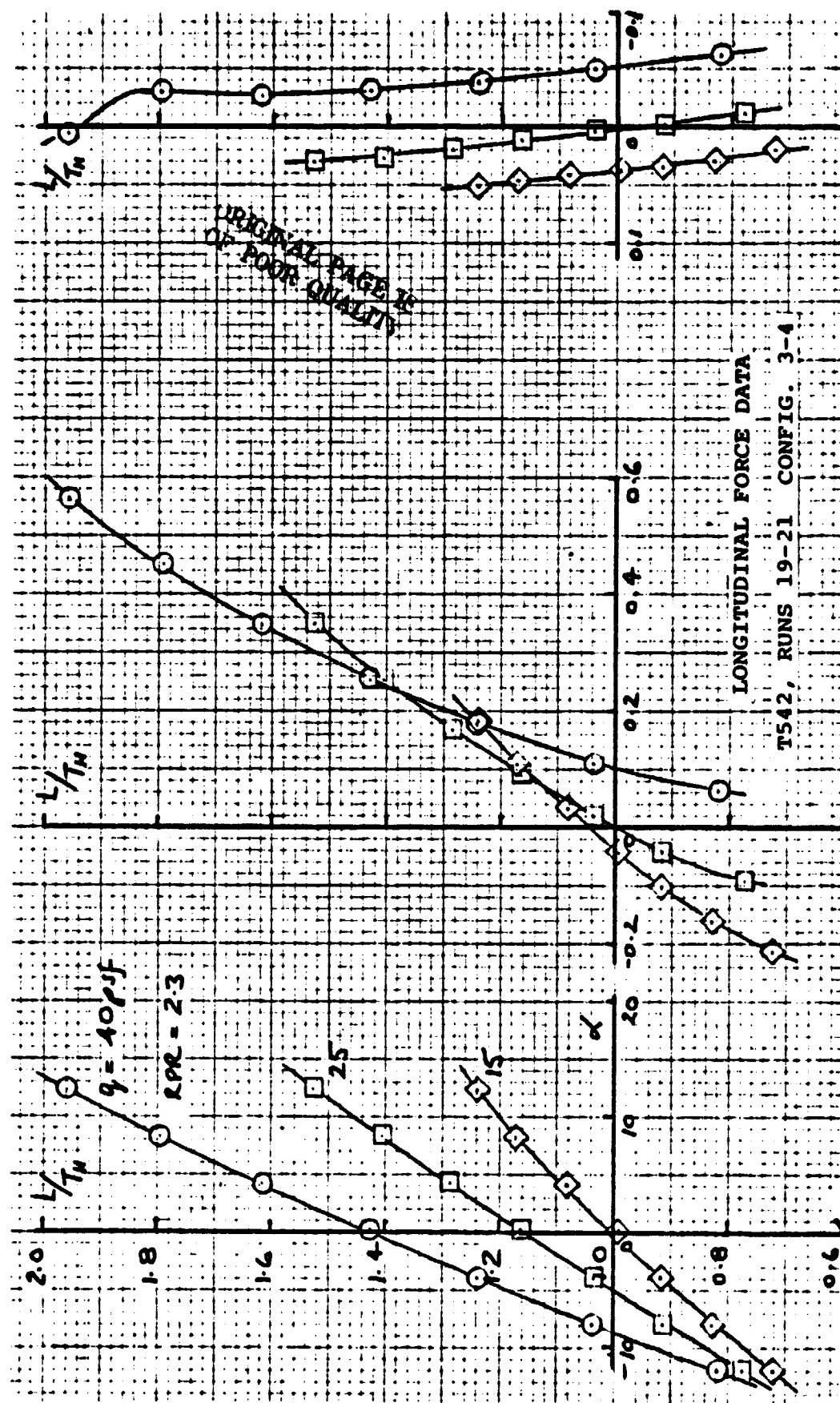


Fig. 36

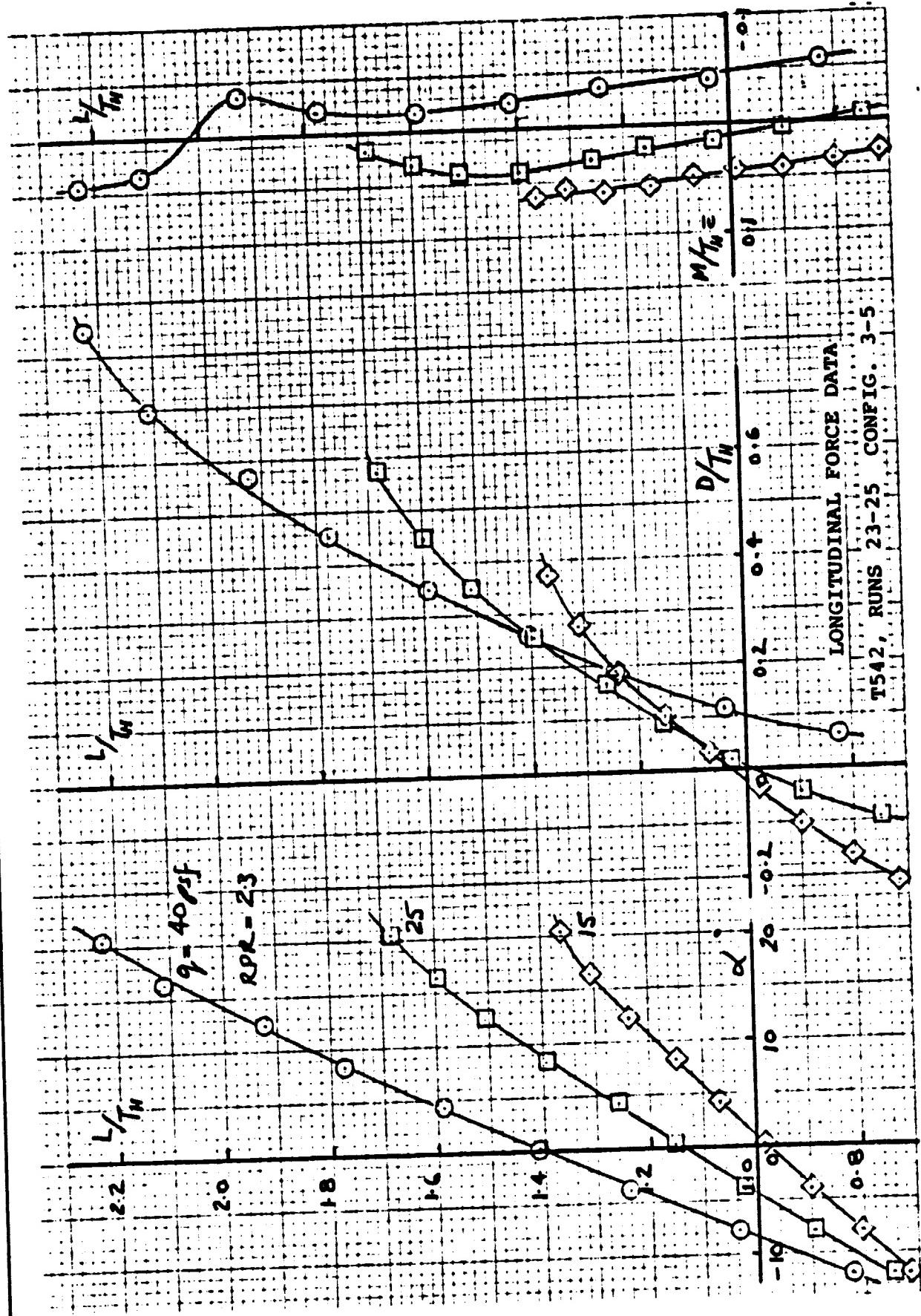
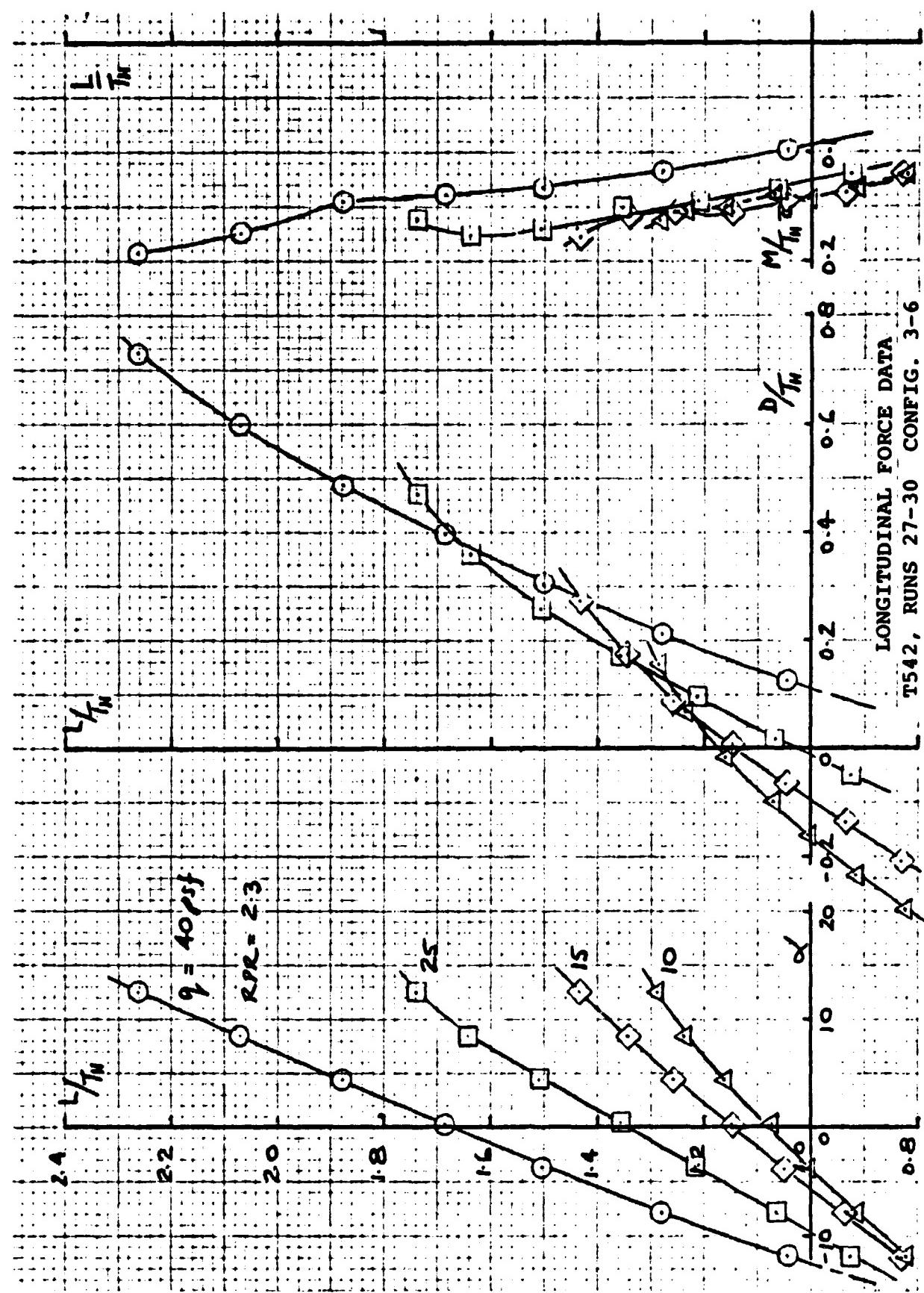




Fig. 36



ORIGINAL PAGE IS  
OF POOR QUALITY

Fig. 37

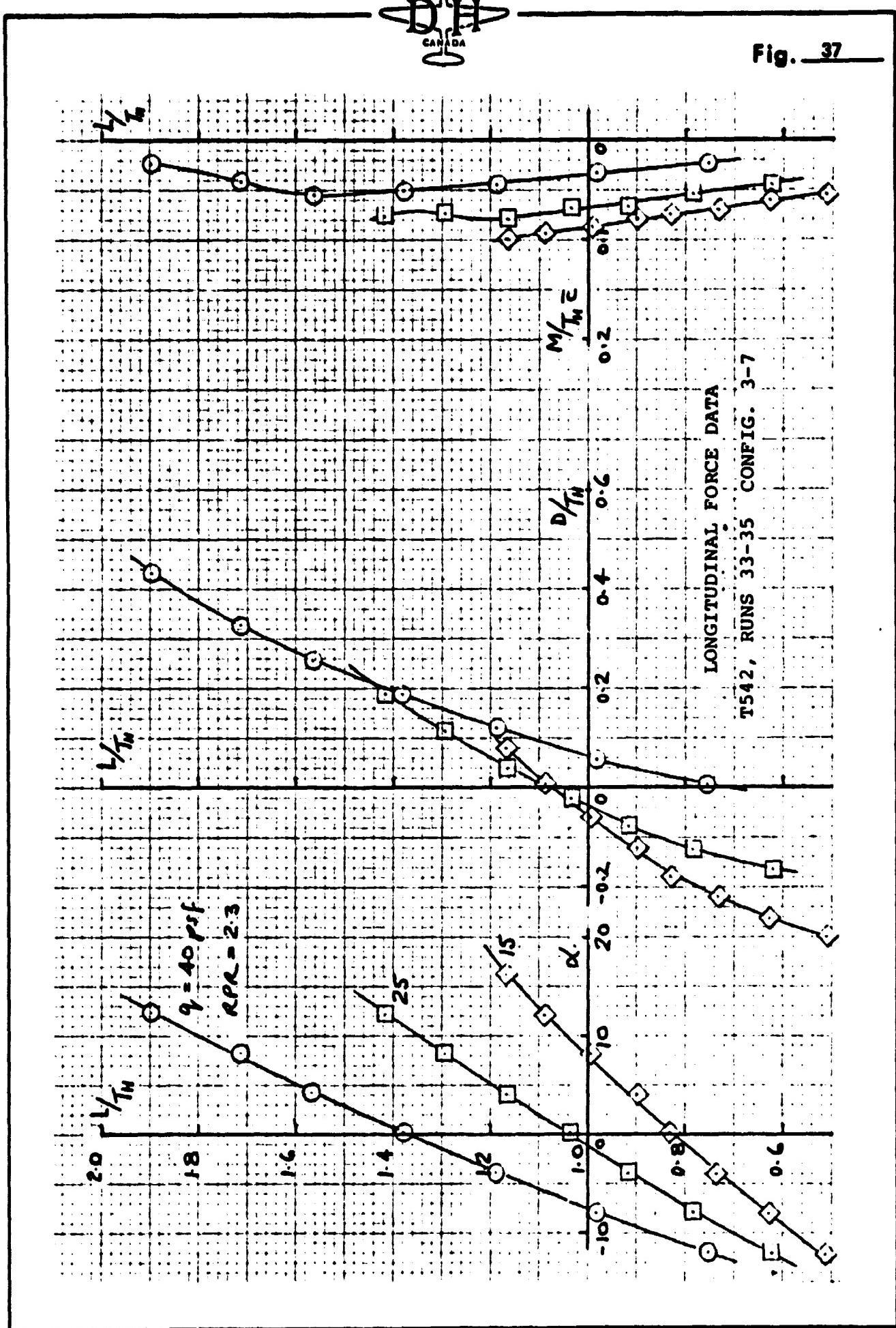
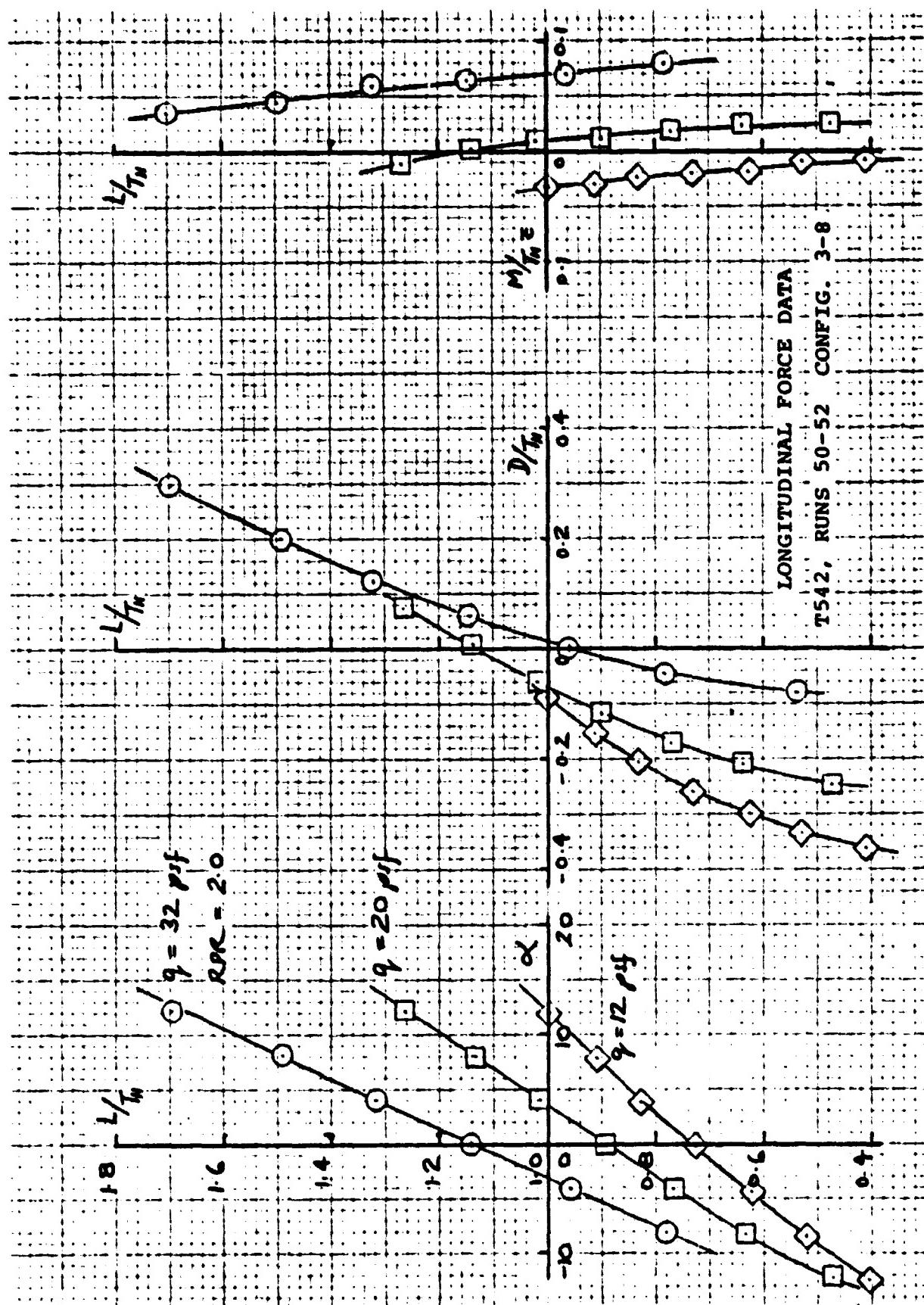




Fig. 38





**Fig. - 39**

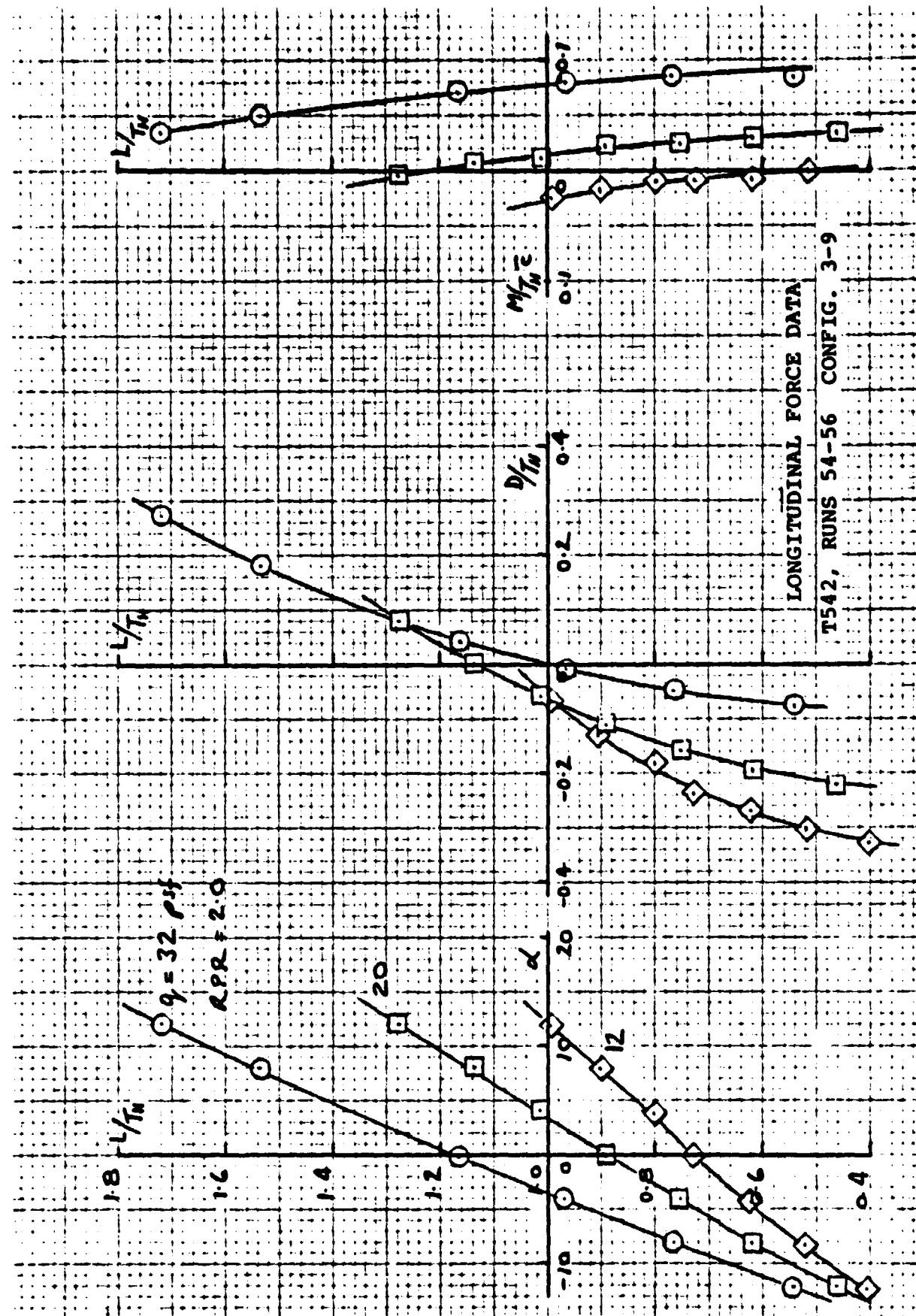




Fig. 40

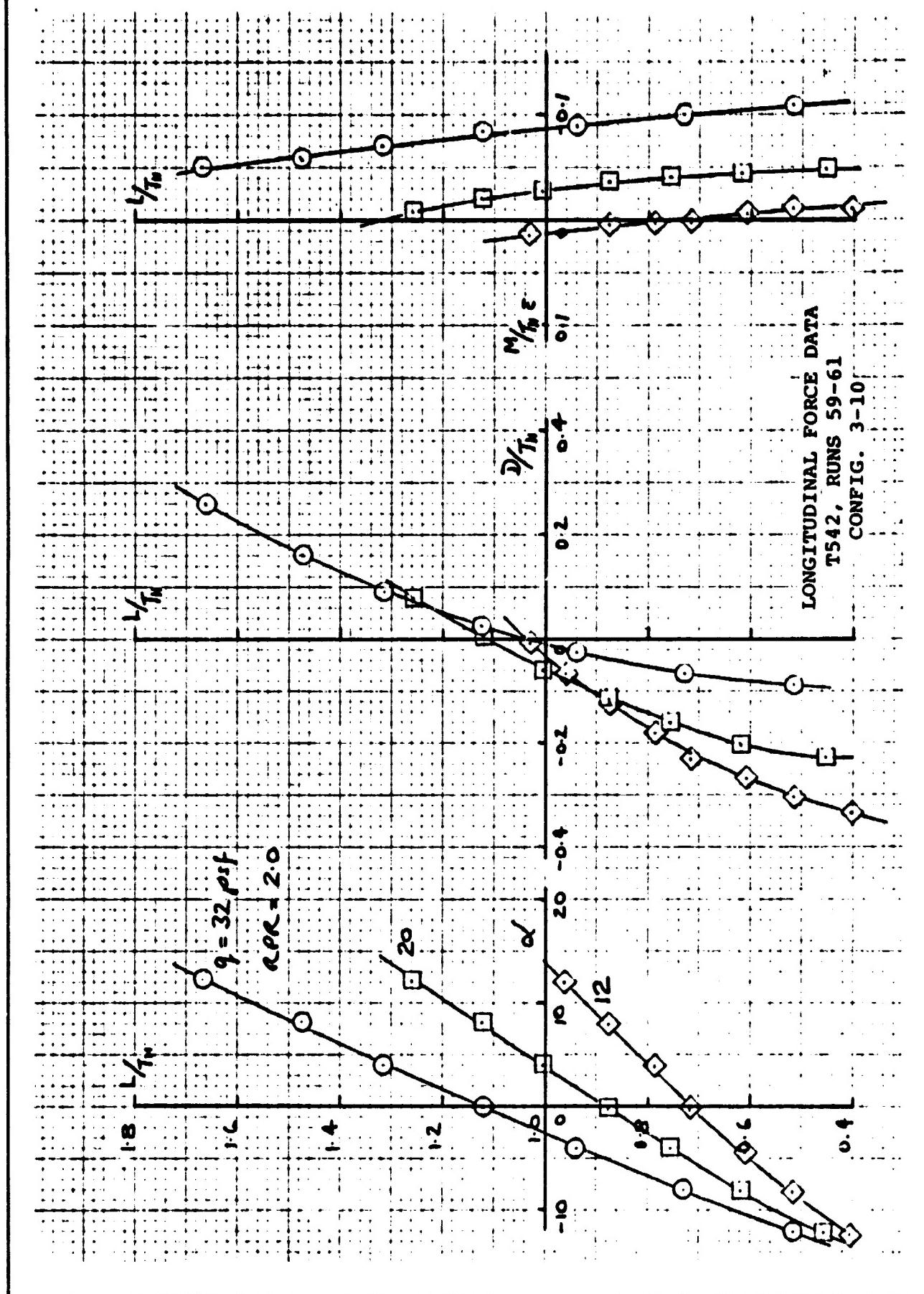


Fig. 41

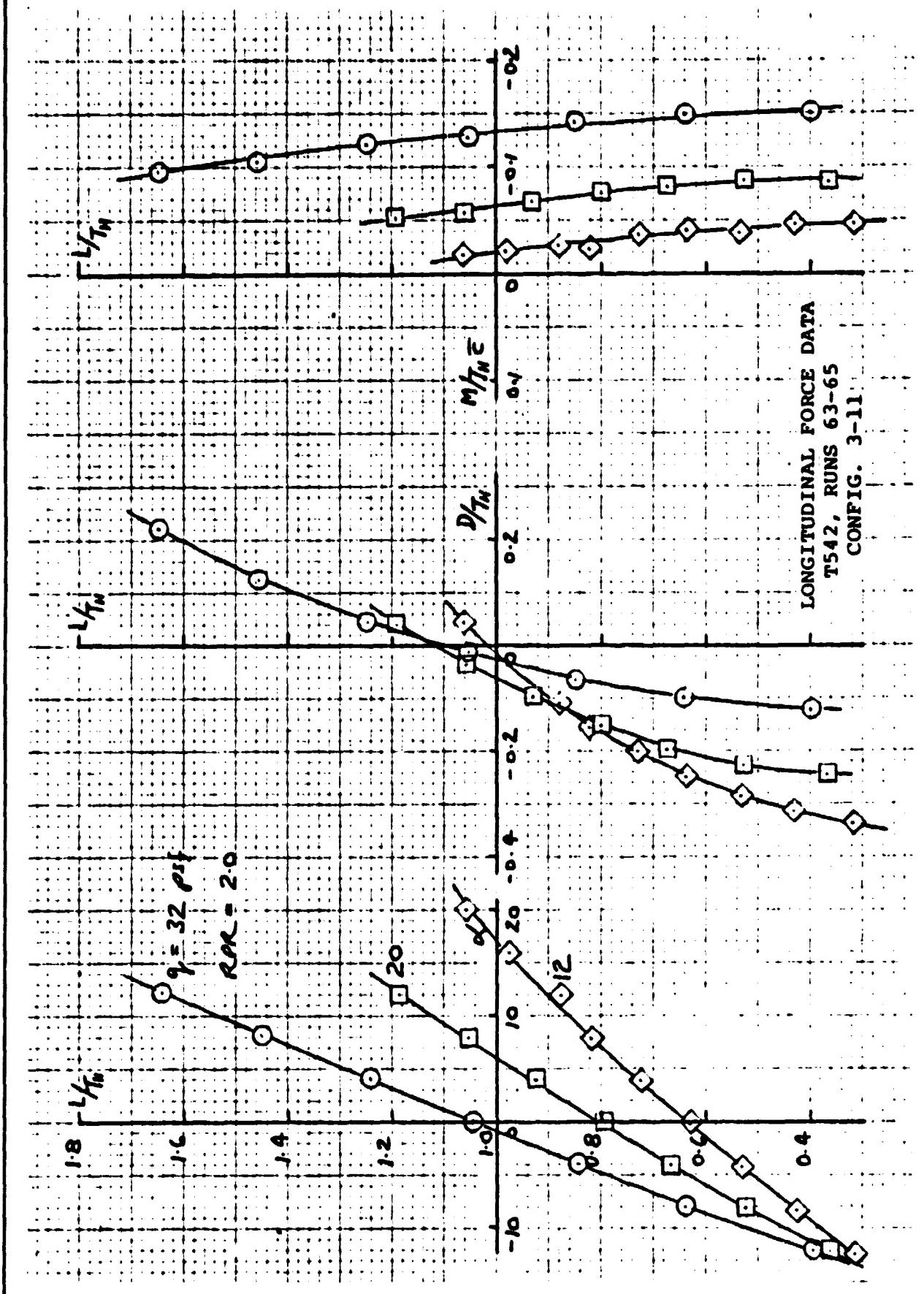
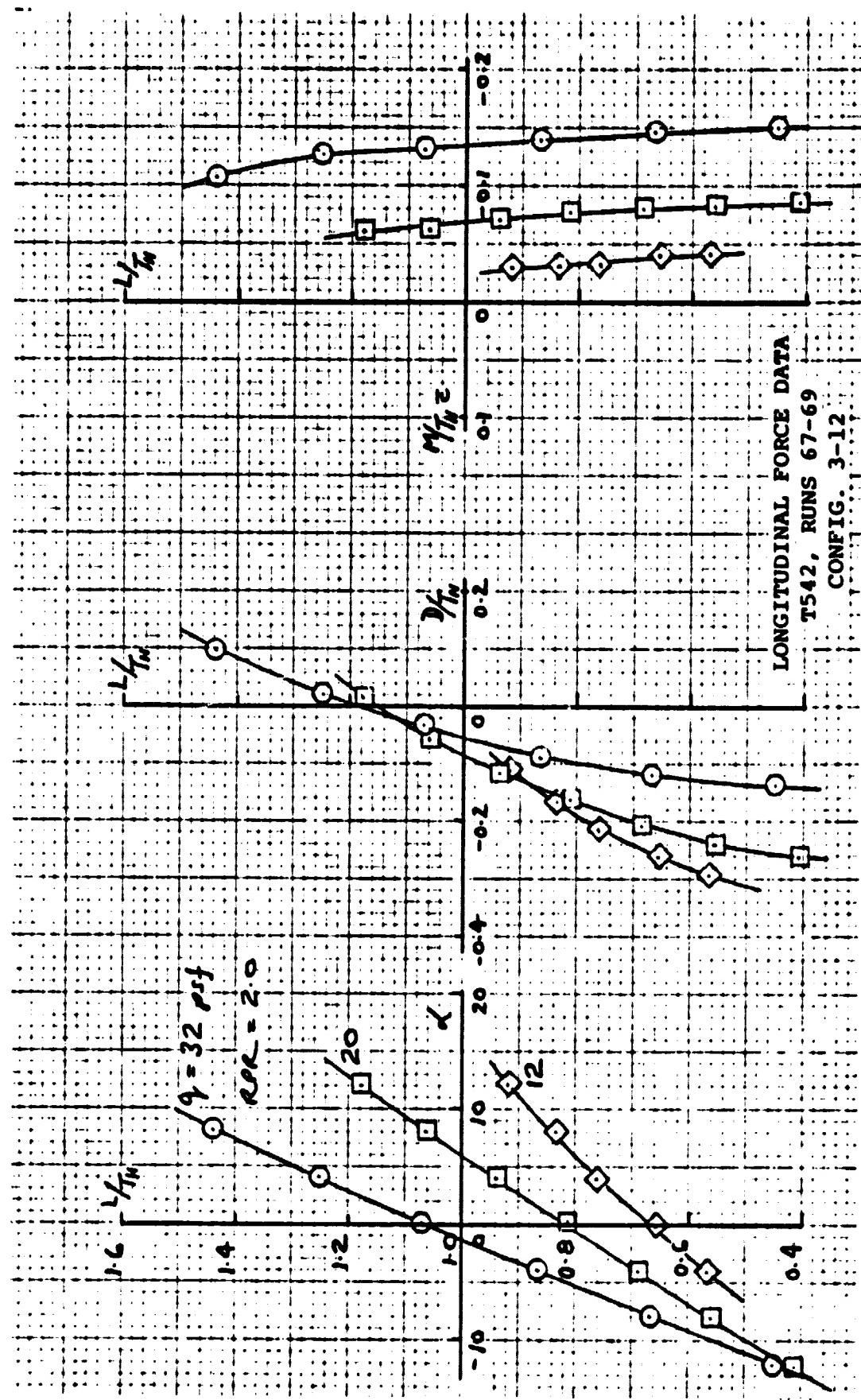




Fig. 42



The logo consists of a stylized letter 'D' above a letter 'H', with the word 'CANADA' written vertically between them.

**Fig. 43**

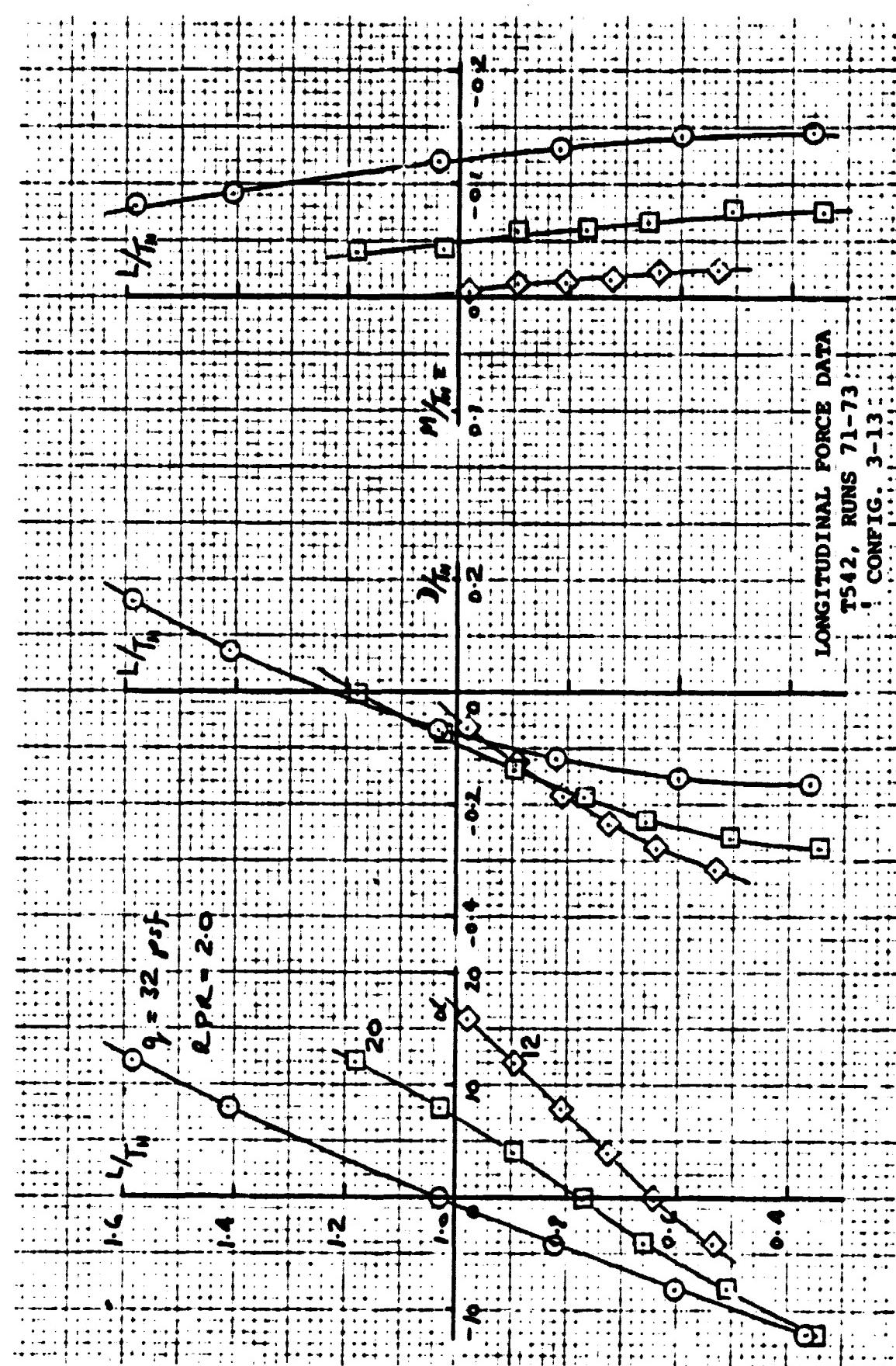


Fig. 44

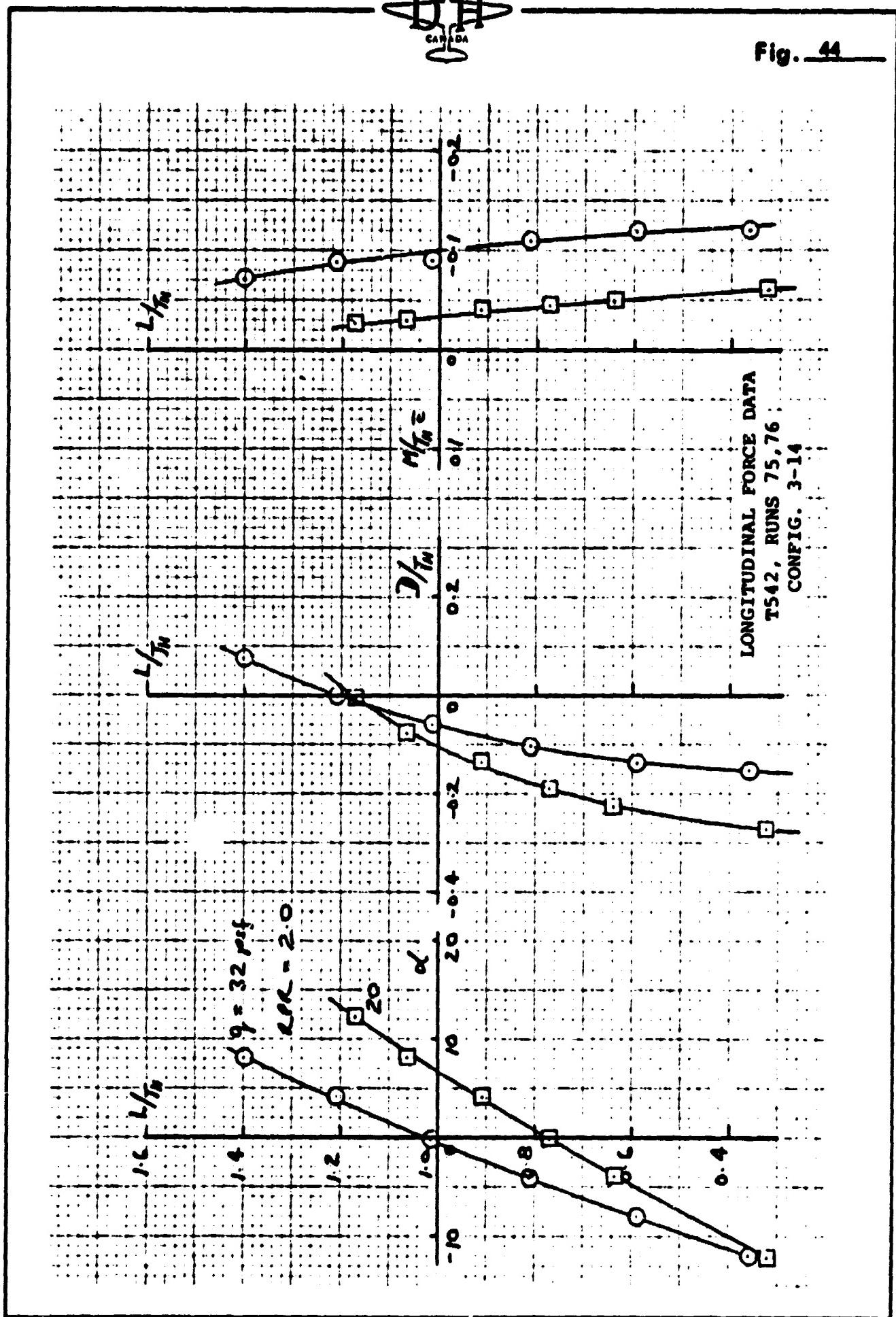


Fig. 45

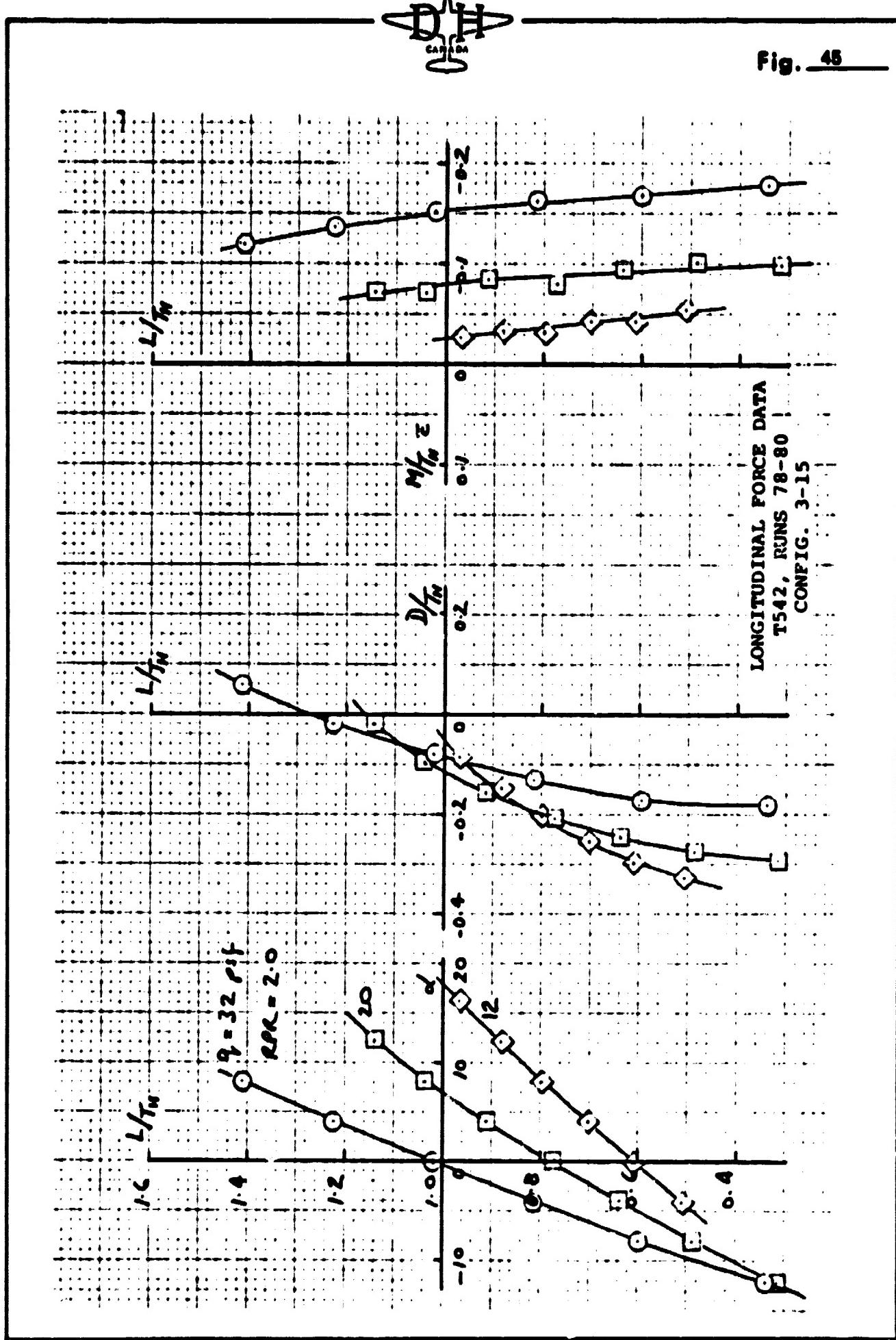
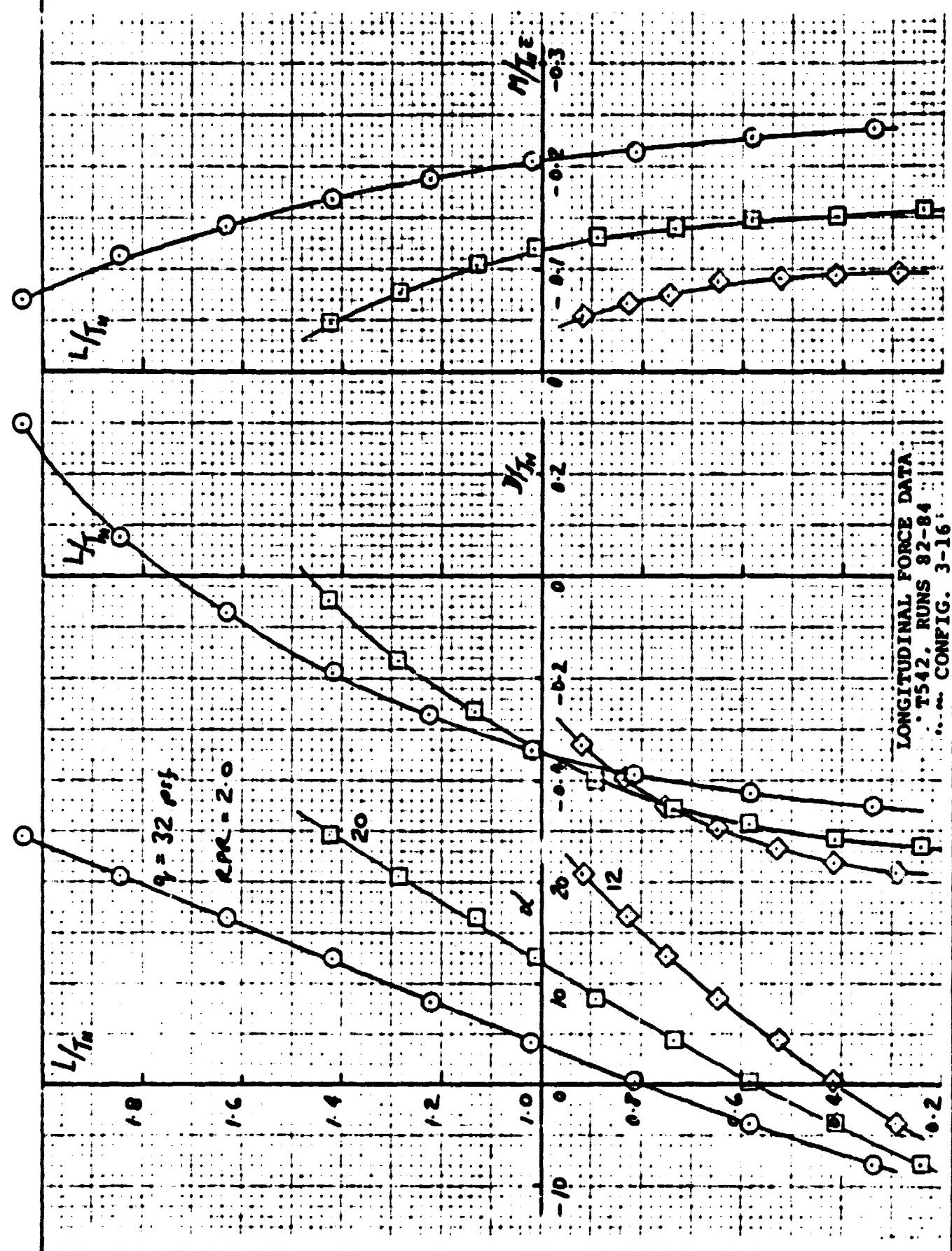


Fig. 48





**Fig. 47**

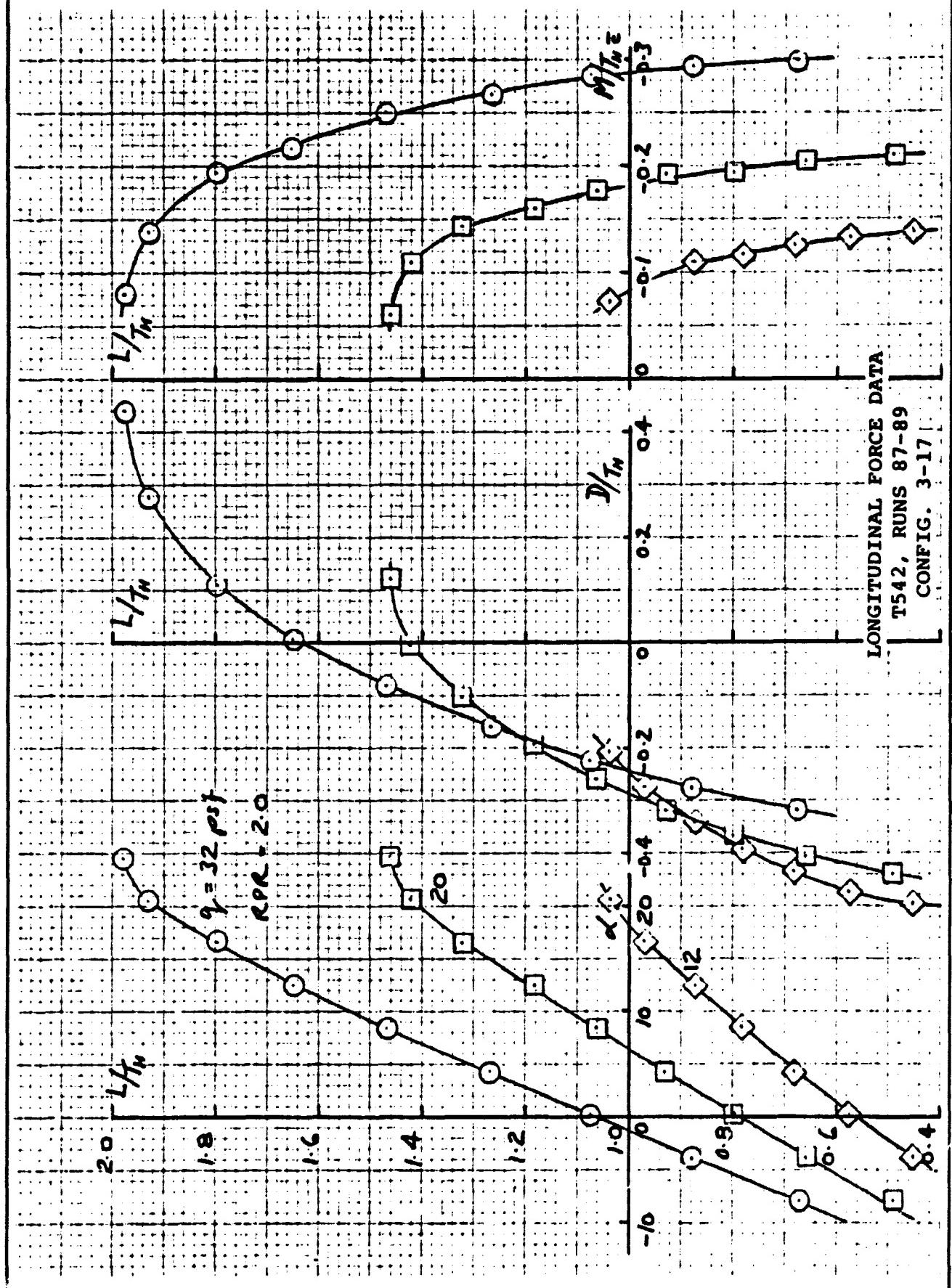
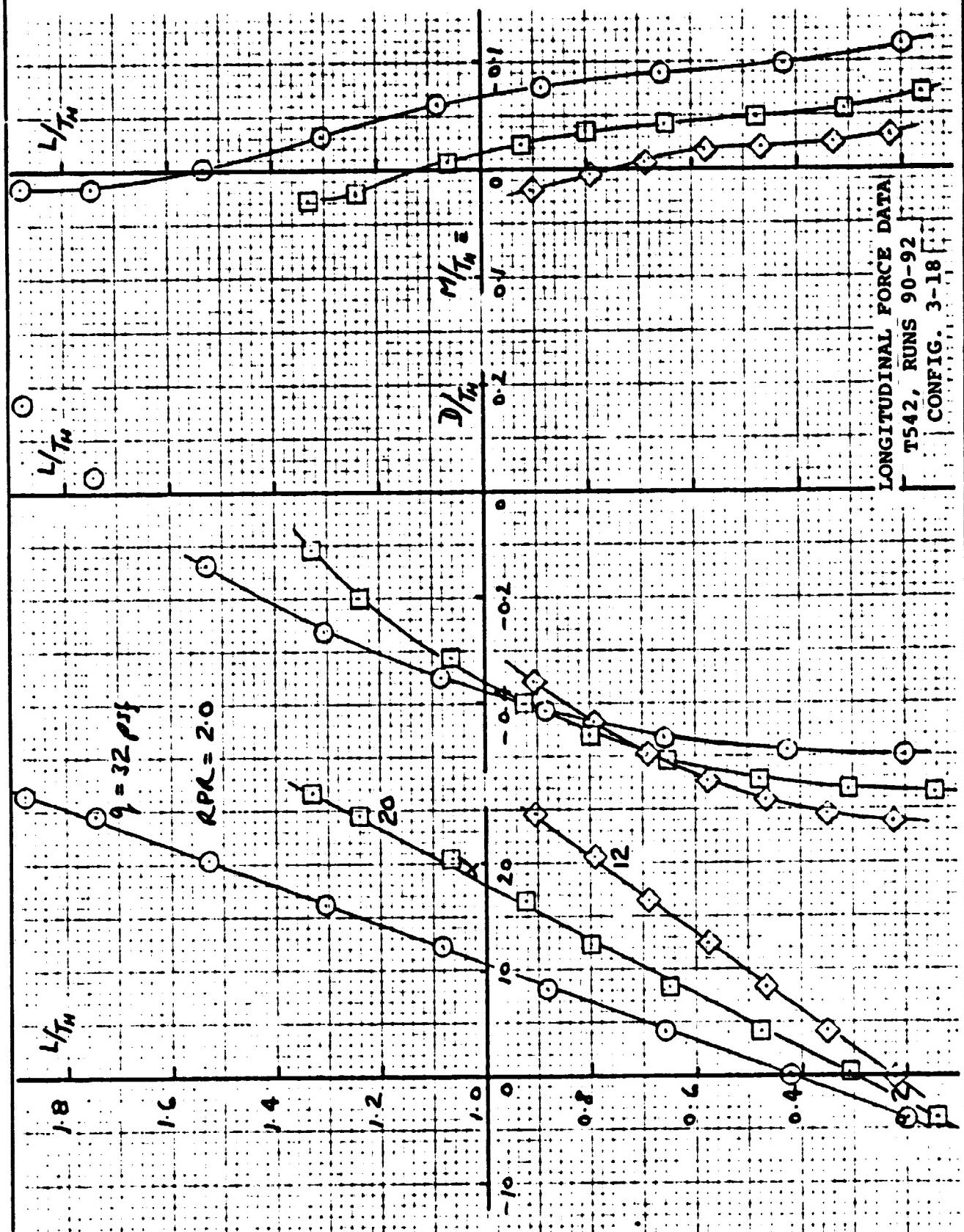




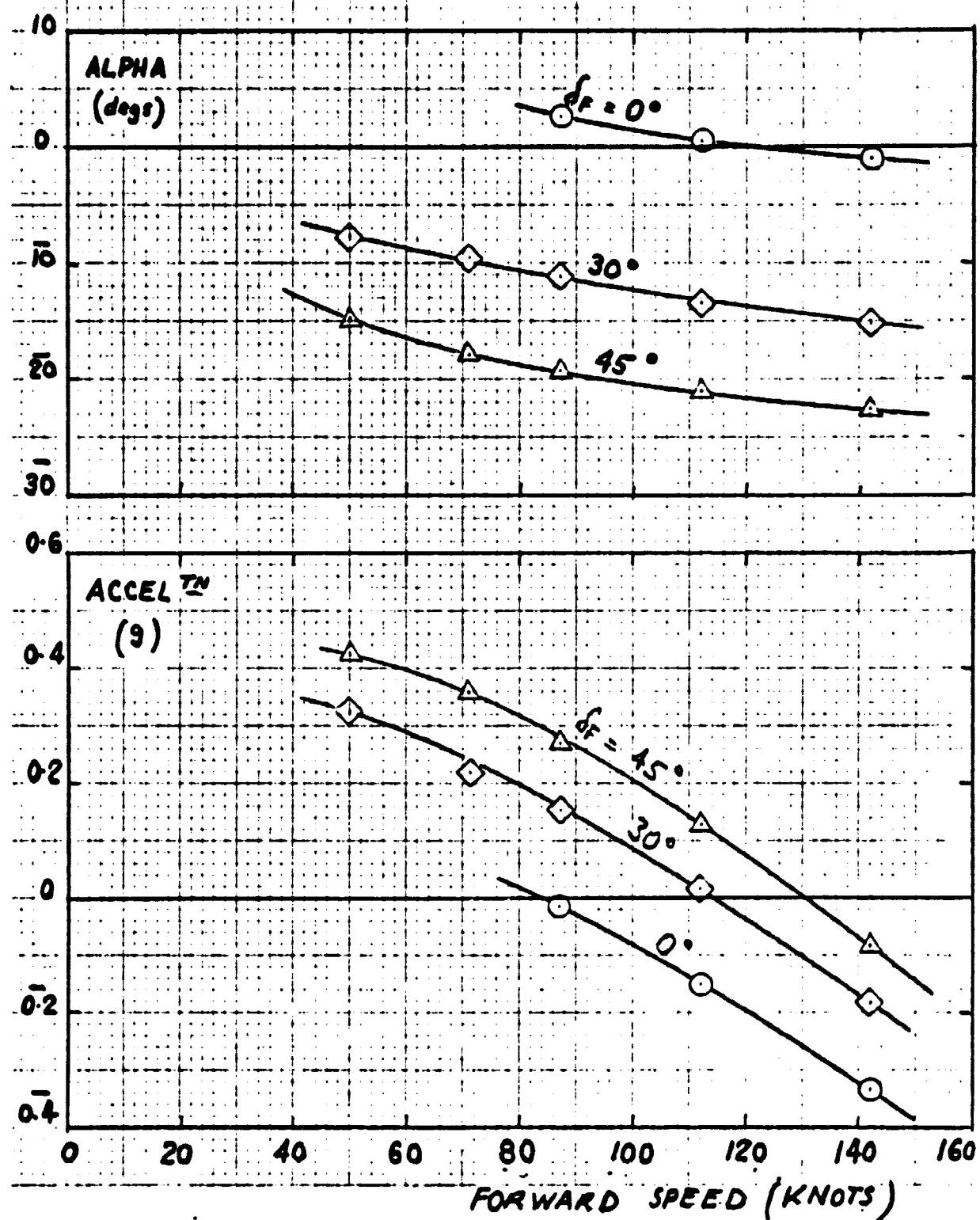
Fig. 48



ORIGINAL PAGE IS  
OF POOR QUALITY



Fig. 49(a)

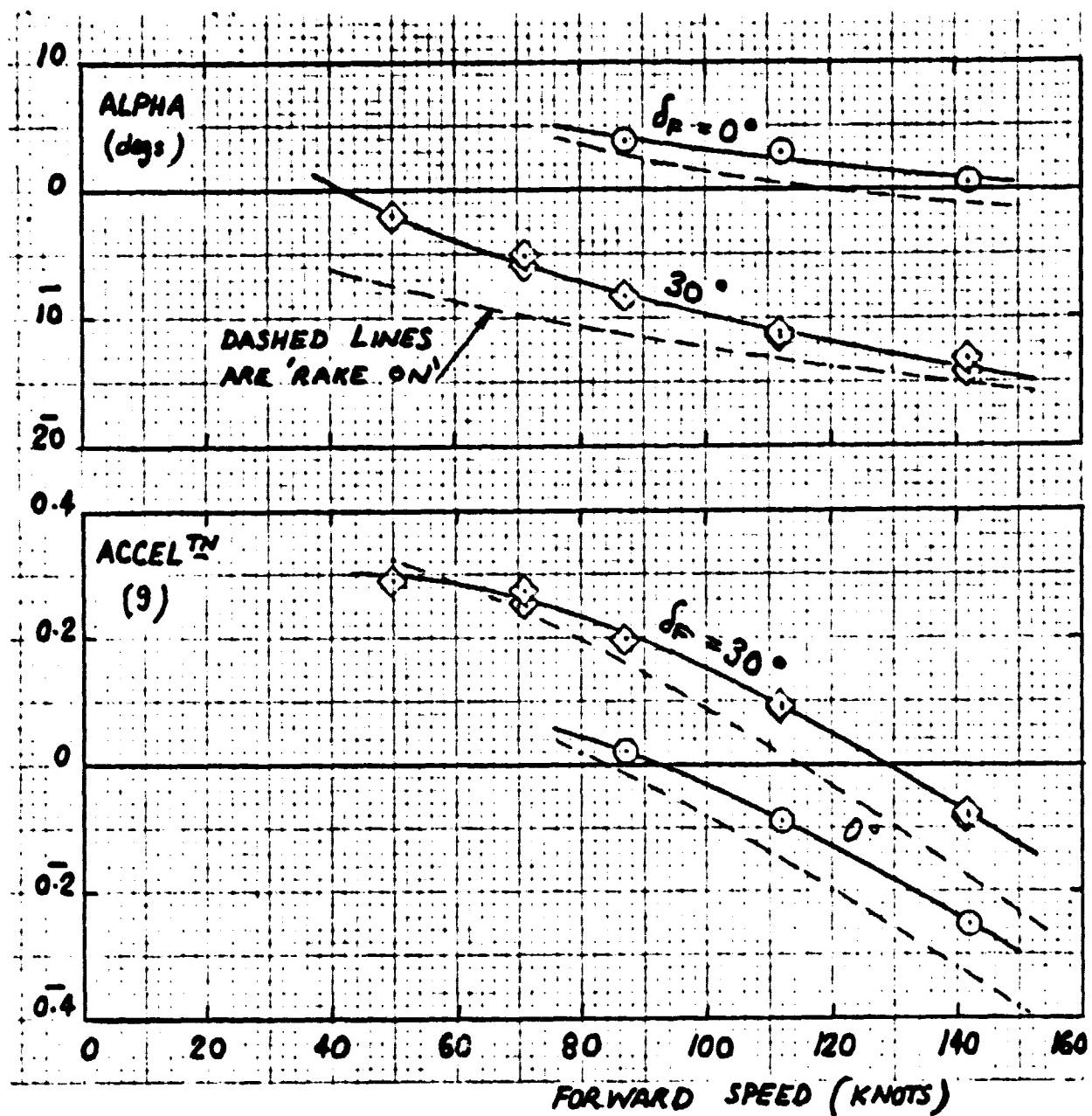


EFFECT OF FLAP ANGLE, BASIC AUGMENTOR  
RAKE ON

$$T_W/L = 1.10 \quad T_W/S = 60 \quad LB/FT^2$$



Fig. 49(b)

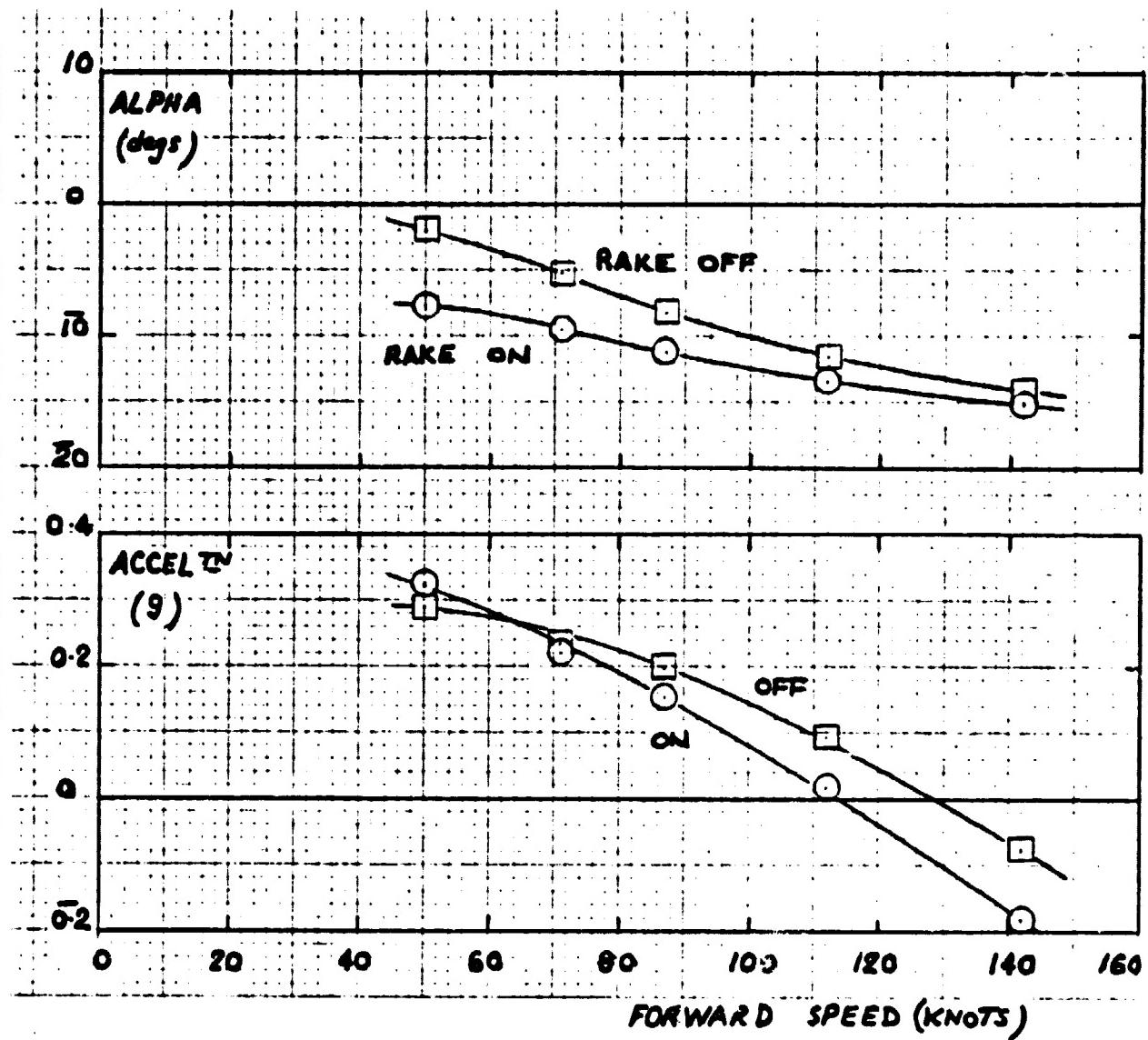


EFFECT OF FLAP ANGLE, BASIC AUGMENTOR  
RAKE OFF

$$T_h/L = 1.10 ; T_h/S = 60 \text{ lb/ft}^2$$



Fig. 50(a)



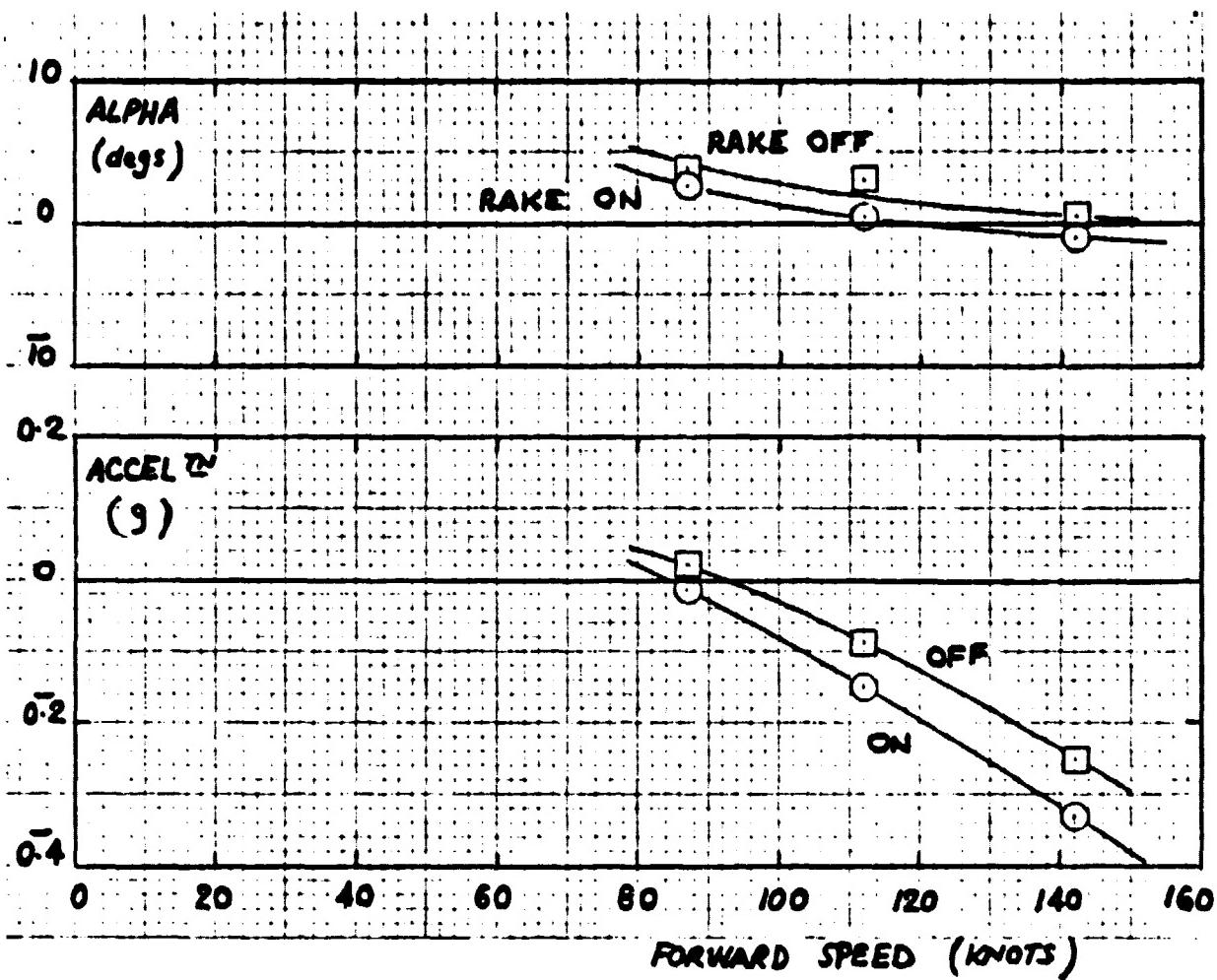
EFFECT OF EXIT RAKE, BASIC AUGMENTOR, VTOL 2 TESTS

END-PLATES ON       $\delta = 30^\circ$

$$T_H/L = 1.10 ; T_H/s = 60 \text{ LB/FT}^2$$



Fig. 50(b)



EFFECT OF RAKE; BASIC AUGMENTOR; VTOL 2 TESTS

END-PLATES ON

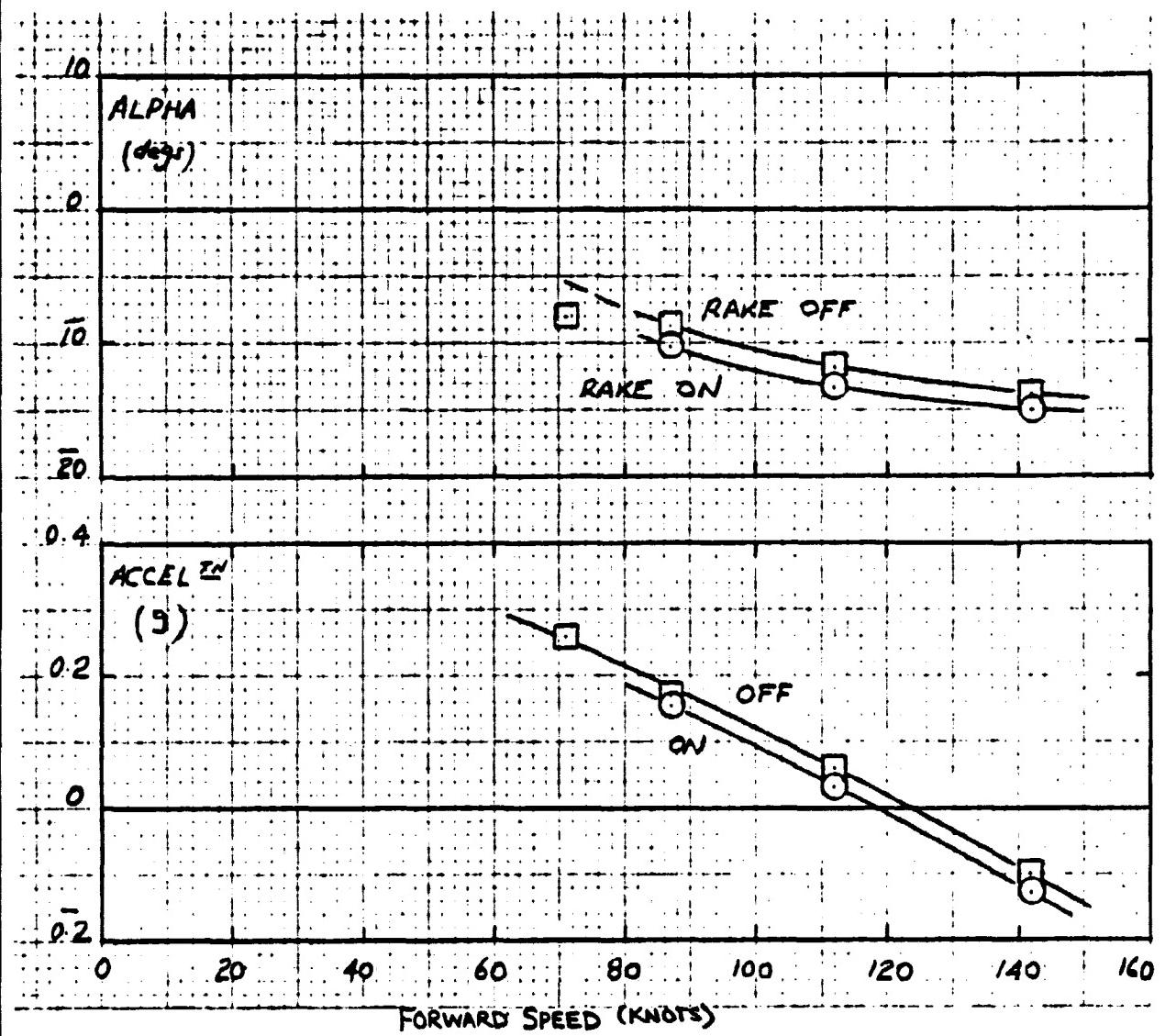
$\delta_F = 0^\circ$

$T_H/L = 1.10$

$T_H/S = 60 \text{ lb/ft}^2$



Fig. 50(c)



#### EFFECT OF EXIT RAKE, BASIC AUGMENTOR, VTOL 3 TESTS

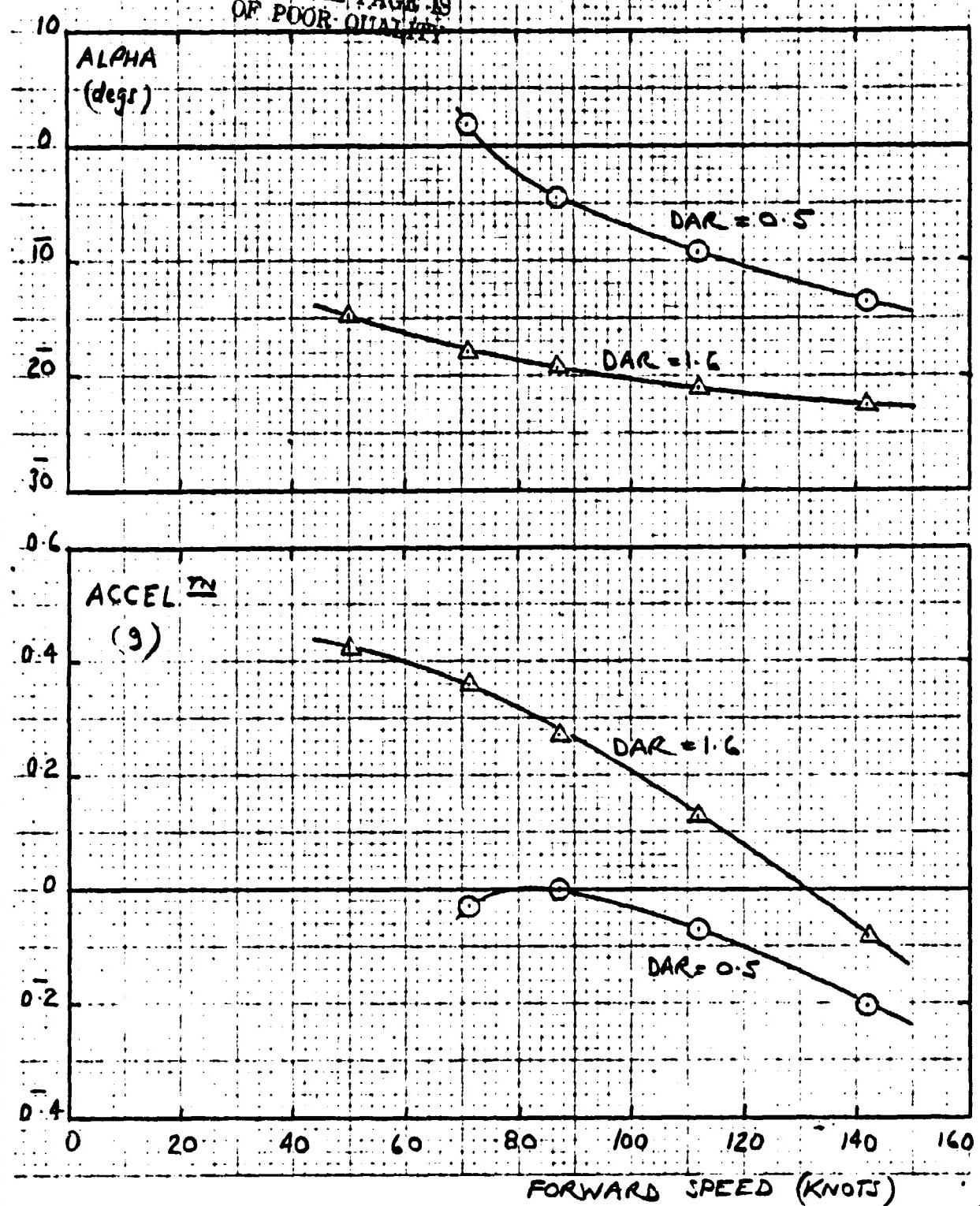
END-PLATES ON

$$\delta_F = 30^\circ$$

$$T_h/L = 1.10 \quad T_h/S = 60 \text{ lb/ft}^2$$



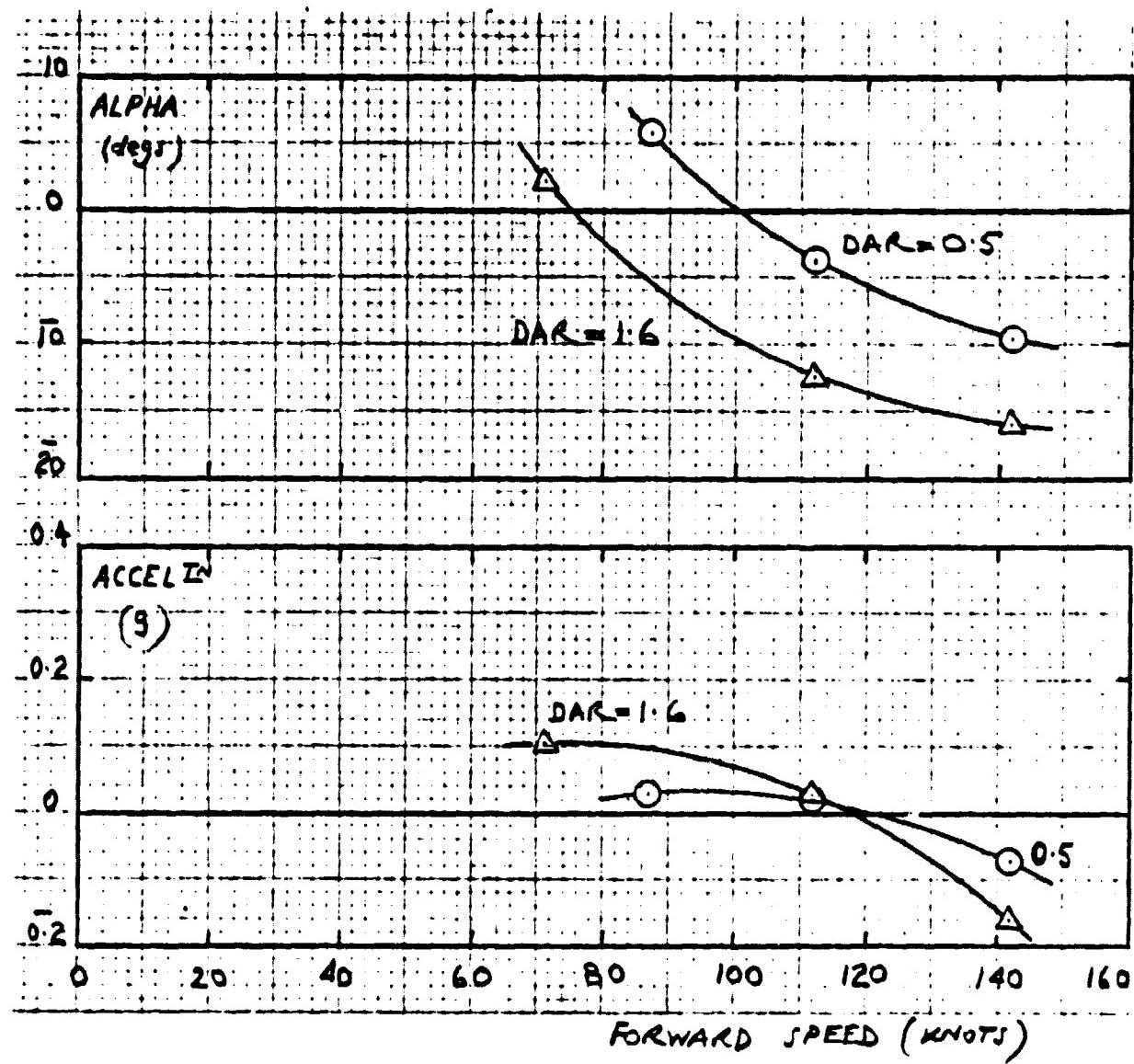
Fig. 51(a)



EFFECT OF DIFFUSER AREA RATIO, END-PLATES ON  
FULL NOZZLE SET  $\delta_F = 45^\circ$  RAKE ON  
 $T_H/L = 1.10$ ;  $T_H/S = 60 \text{ lb/ft}^2$



Fig. 51(b)

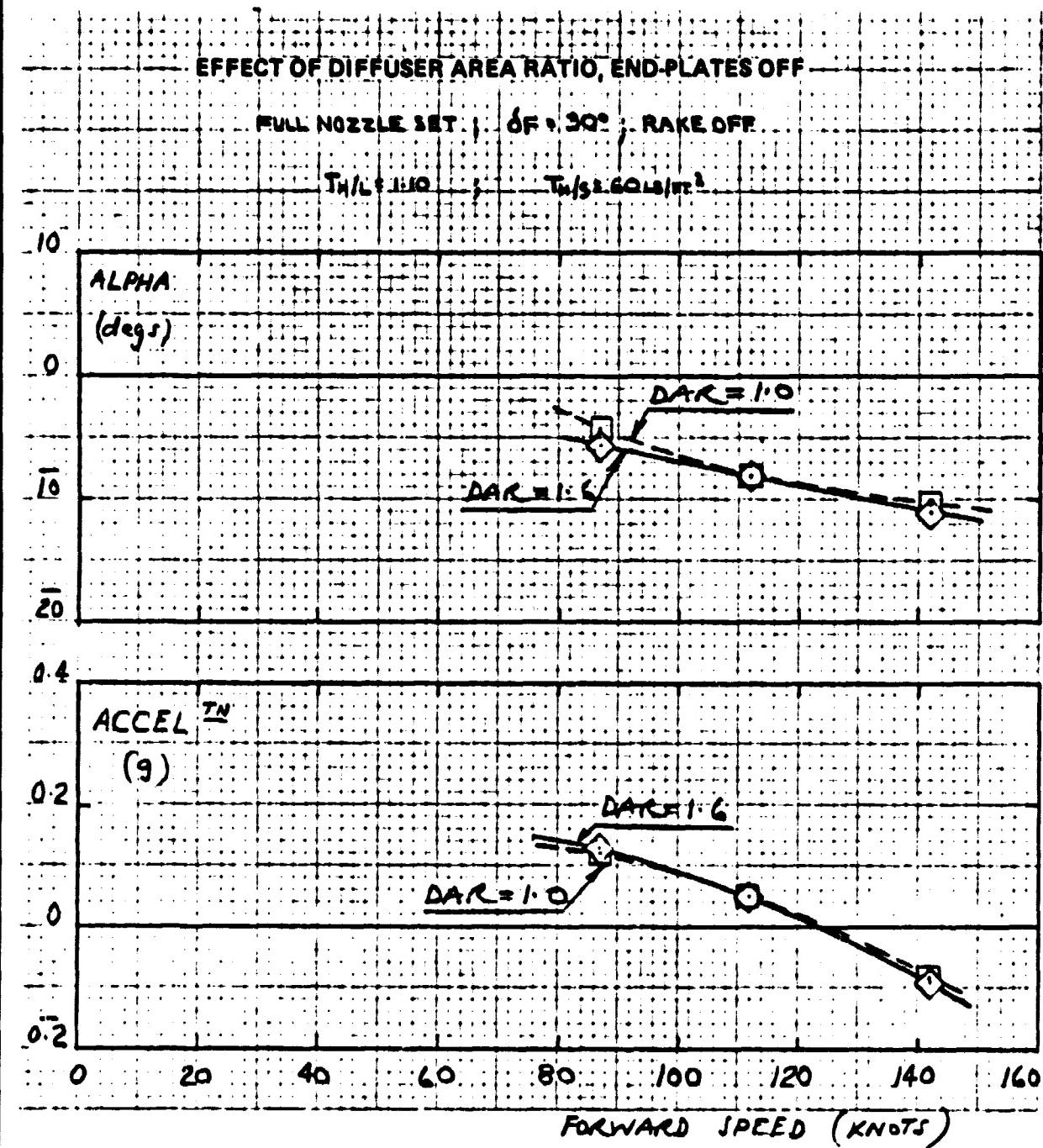


EFFECT OF DIFFUSER AREA RATIO END-PLATES ON  
ALTERNATE NOZZLES BLANKED RAKE ON

$$\delta_F = 45^\circ ; T_h/L = 1.10 ; T_h/S = 60 \text{ lb/ft}^2$$

DH  
CANADA

Fig. 52(a)



DH  
CARMAN

Fig. 52(b)

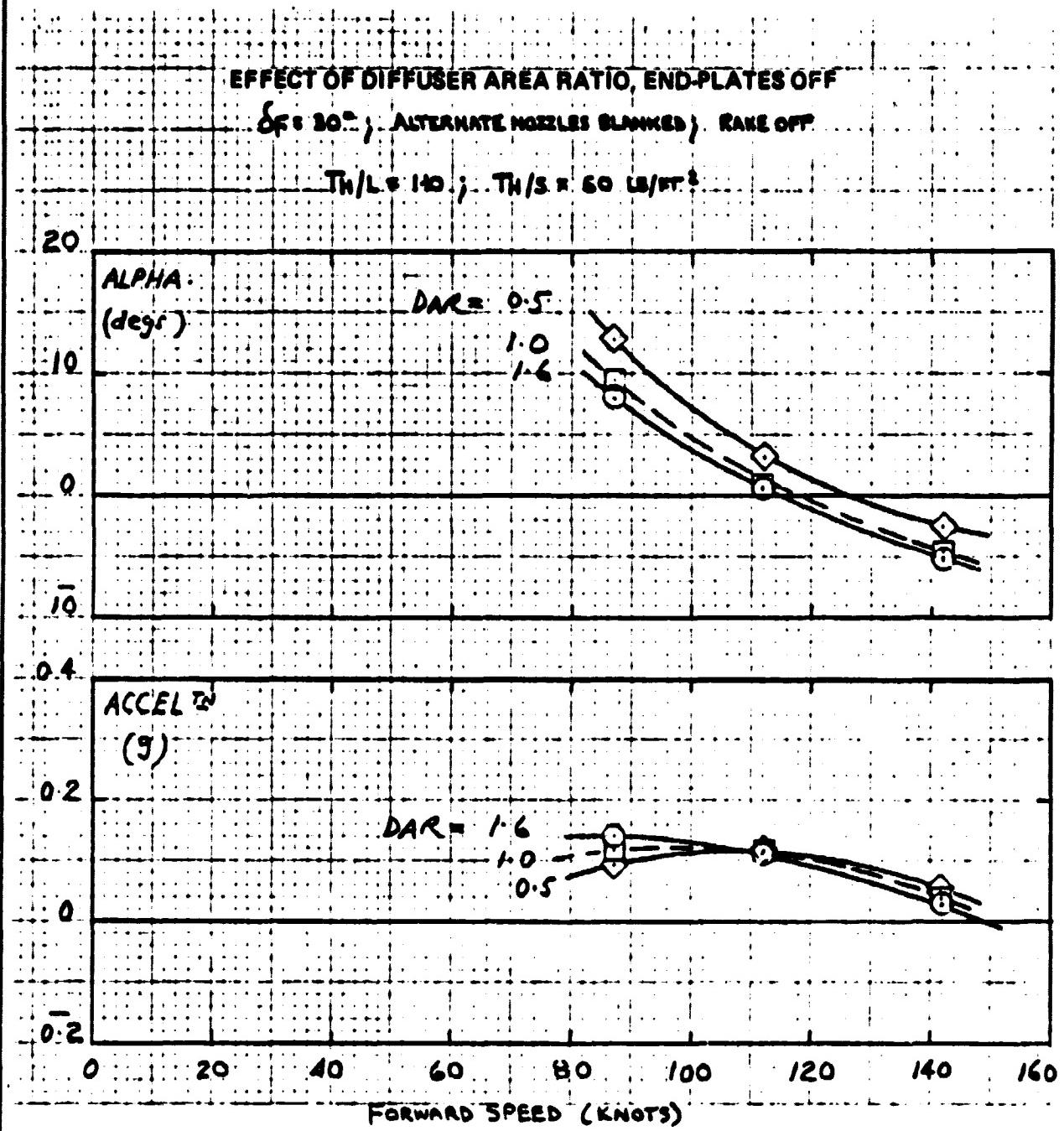
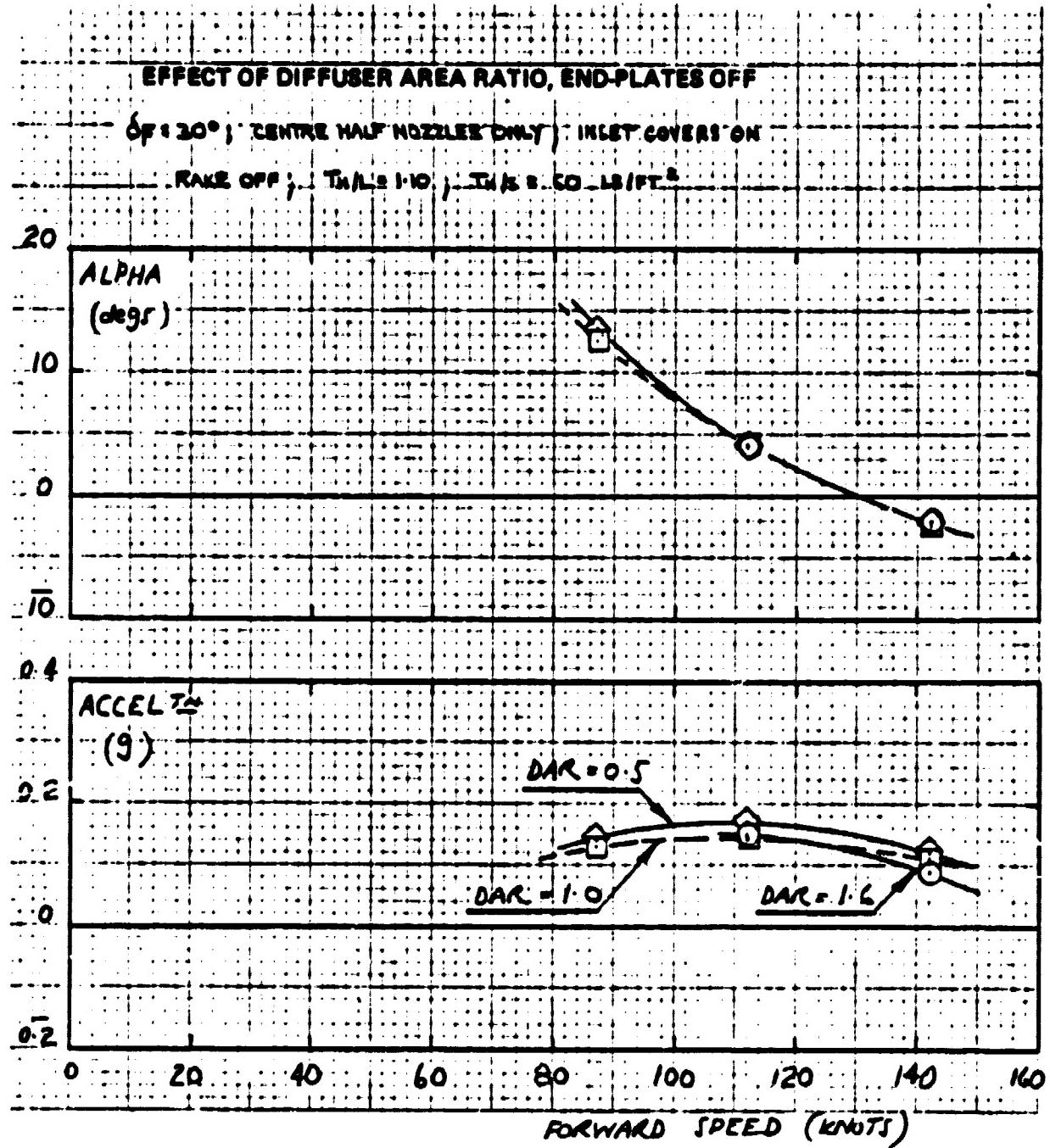




Fig. 52(c)



ORIGINAL PAGE IS  
OF POOR QUALITY



Fig. 53

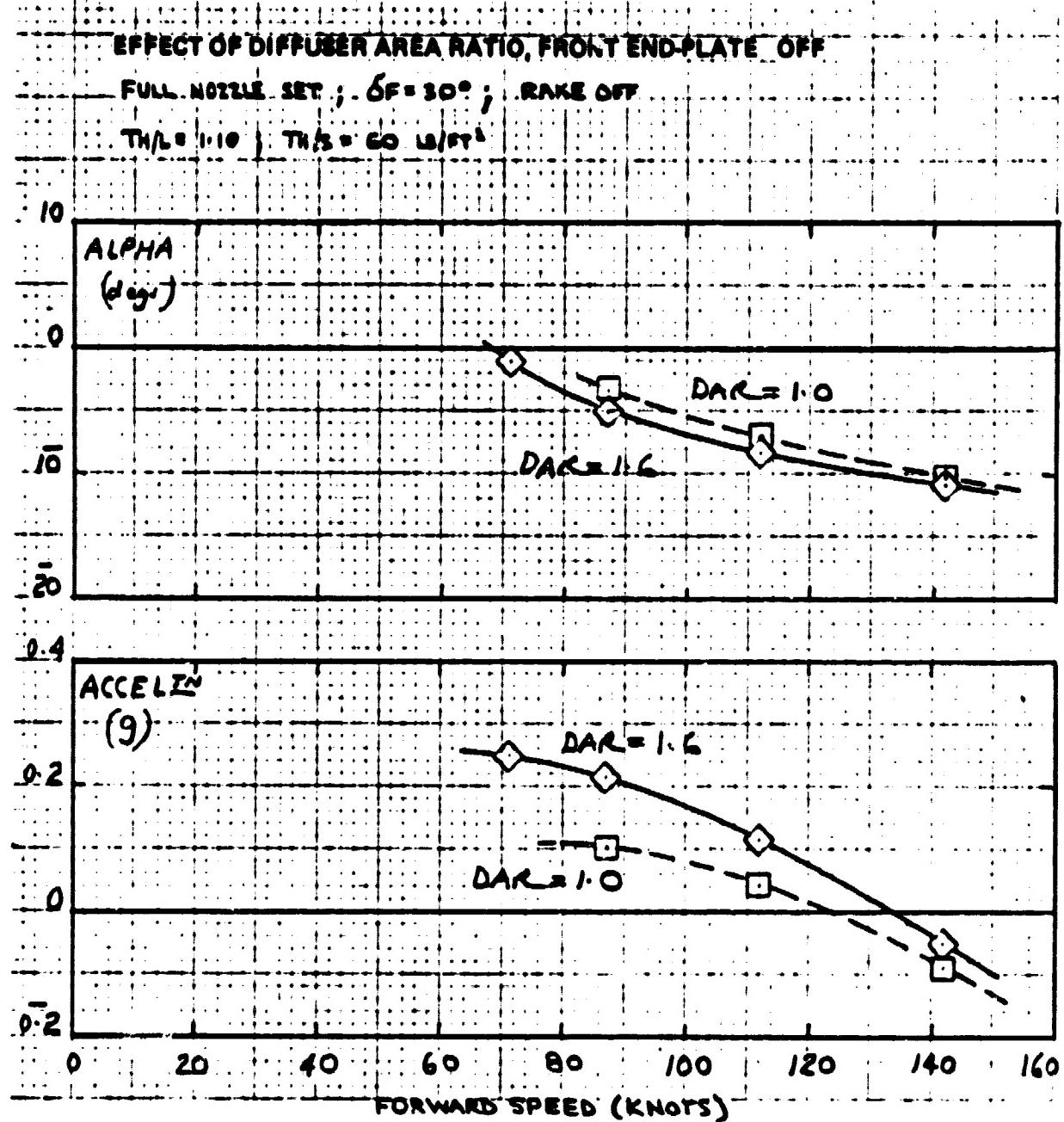




Fig. 54(a)

EFFECT OF AUGMENTOR END-PLATES, BASIC AUGMENTOR

$\delta F = 30^\circ$ ; RAKE OFF;  $T_h/L = 1.10$ ;  $T_h/S = 60 \text{ lb/ft}^2$

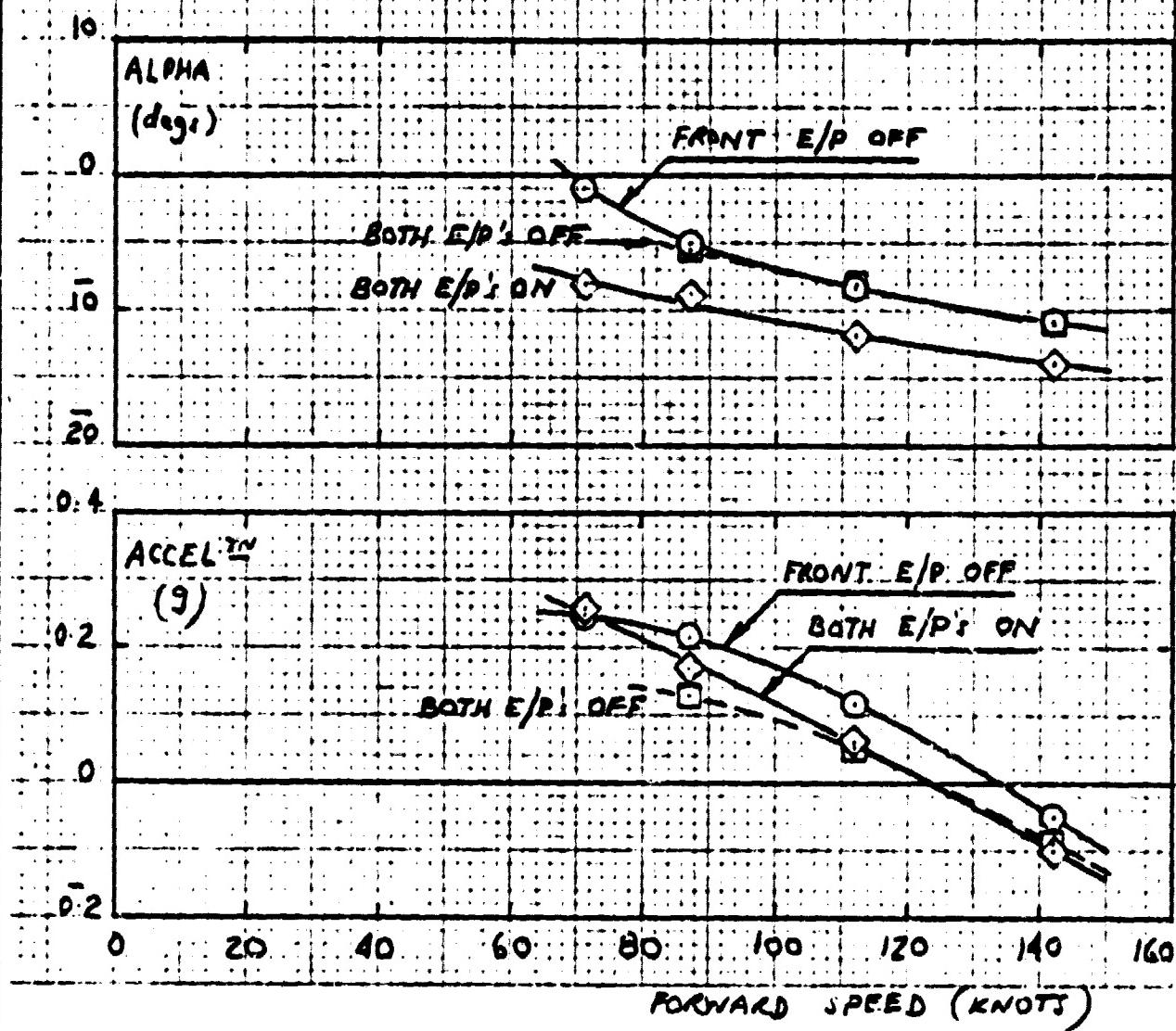




Fig. 54(b)

**EFFECT OF AUGMENTOR END-PLATES, ALTERNATE NOZZLES BLANKED**

$\delta F = 30^\circ$ ; RAKE OFF; DAR = 1.6

$TW/L = 1.10$ ;  $TW/S = 60 \text{ lb/ft}^2$

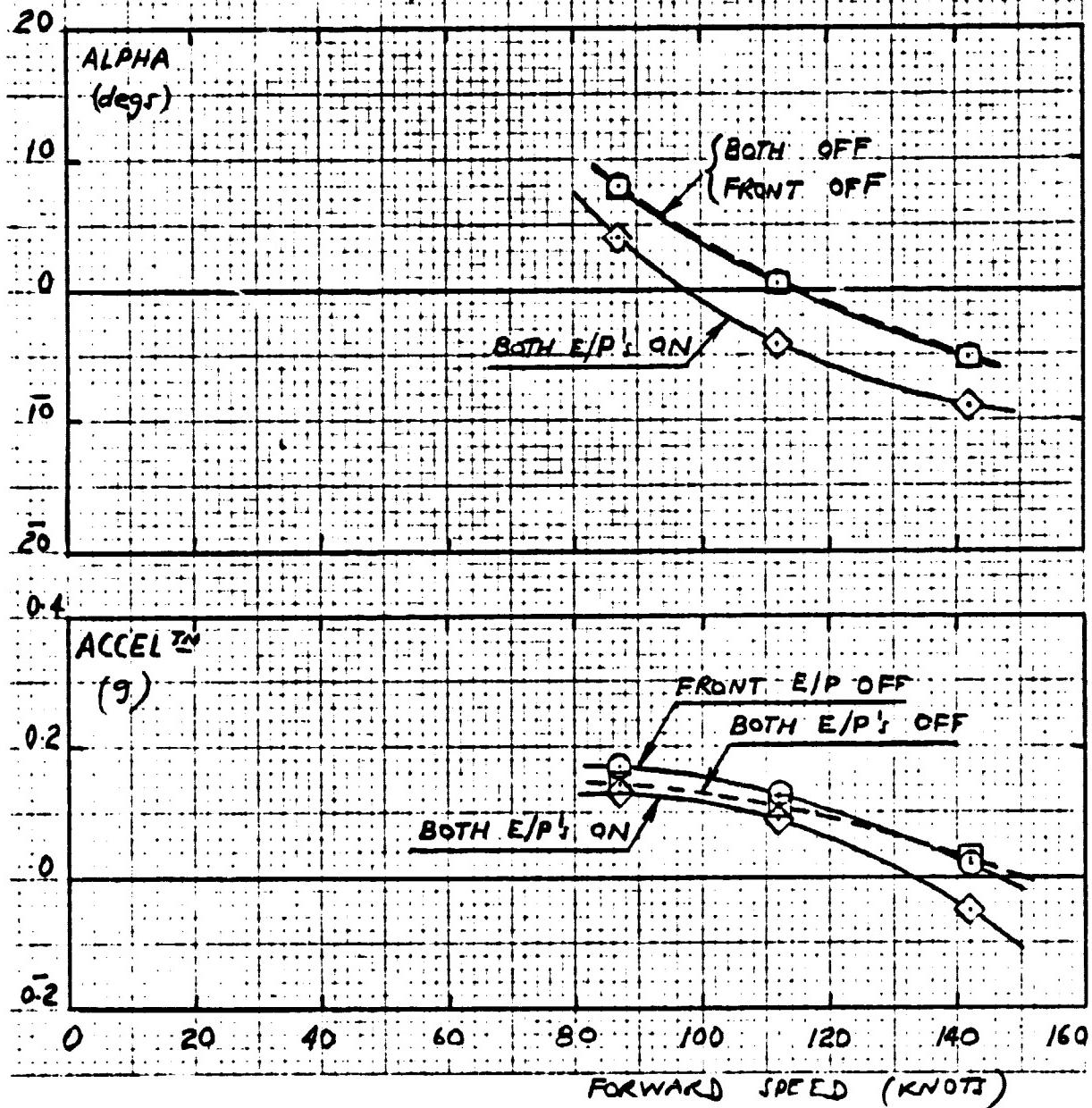
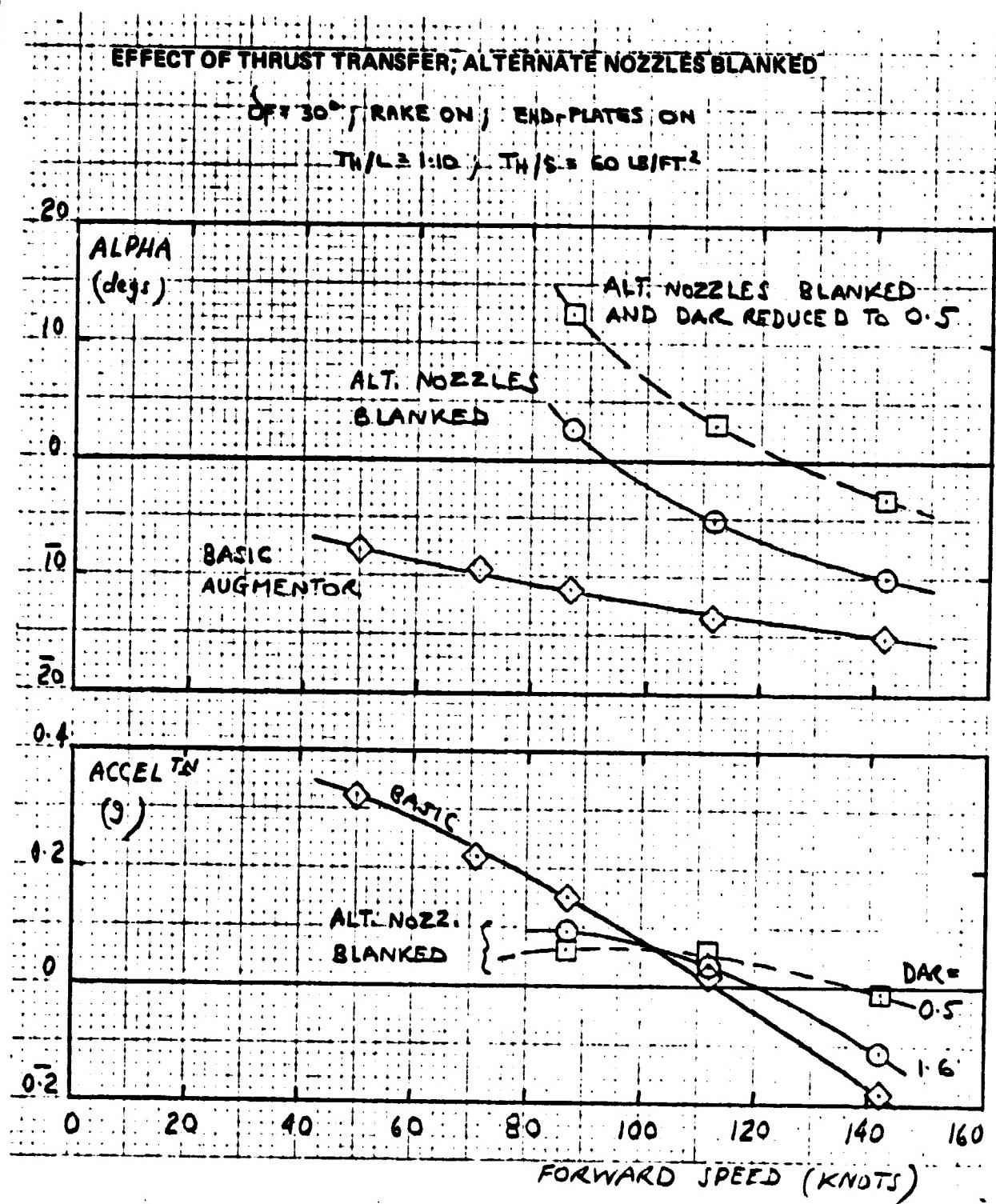


Fig. 55(a)



ORIGINAL PAGE IS  
OF POOR QUALITY

DH  
CANADA

Fig. 55(b)

EFFECT OF THRUST TRANSFER; ALTERNATE NOZZLES BLANKED

$\delta F = 45^\circ$ ; RAKE ON; E/P'S ON

$T_w/L = 1.10$ ;  $T_h/S = 60 \text{ lbf/in}^2$

10

ALPHA  
(deg)

0

10

20

30

0.6

ACCEL IN

(g)

0.4

0.2

0

-0.2

0

20

40

60

80

100

120

140

160

FORWARD SPEED (KNOTS)

ALT. NOZZ. BLANKED

DAR = 0.5

ALT. NOZZ.  
BLANKED

DAR = 1.6

BASIC  
AUGMENTOR

BASIC AUGMENTOR

ALT. NOZZ.

BLANKED

0.5

1.6



Fig. 55(c)

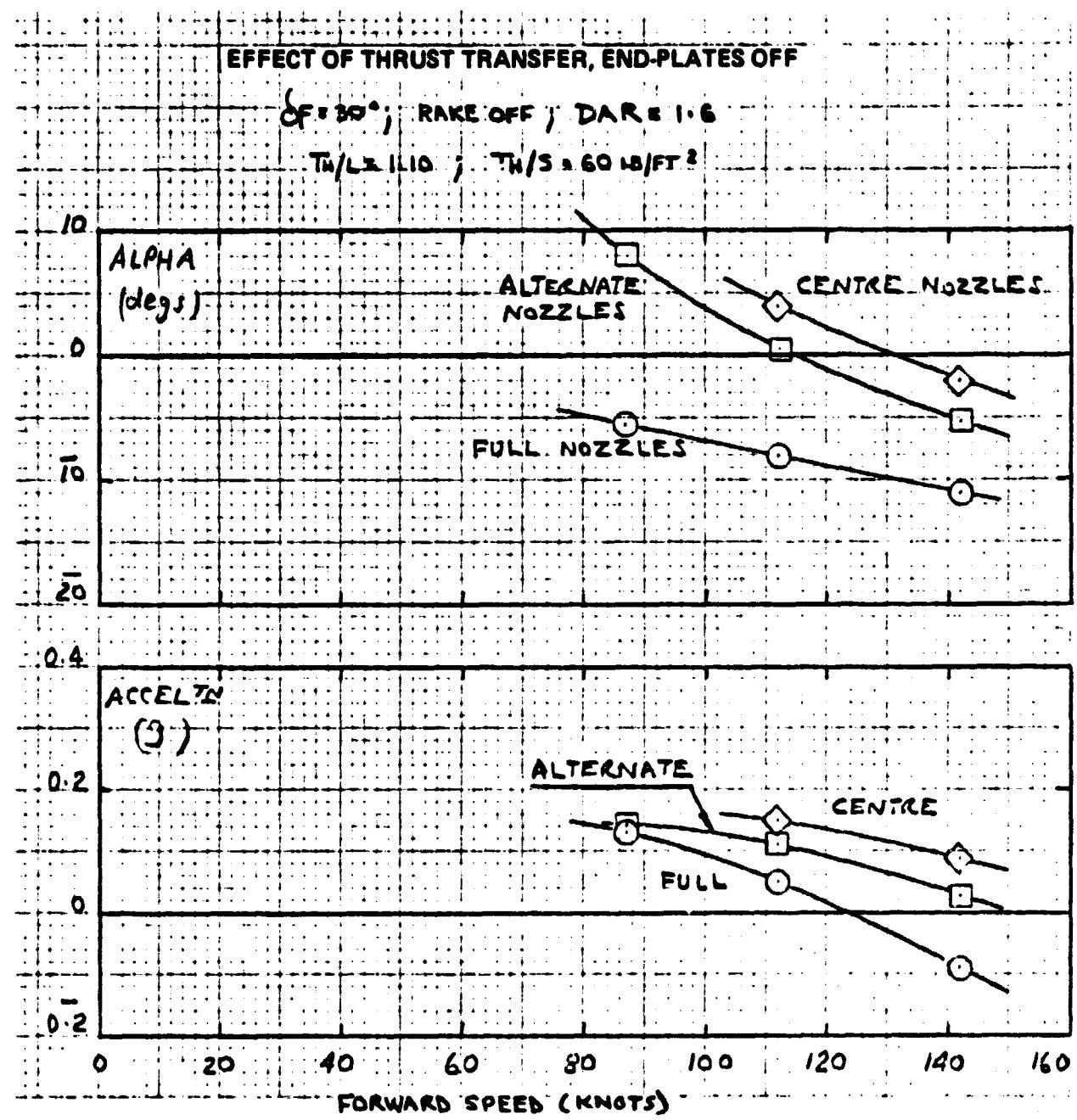
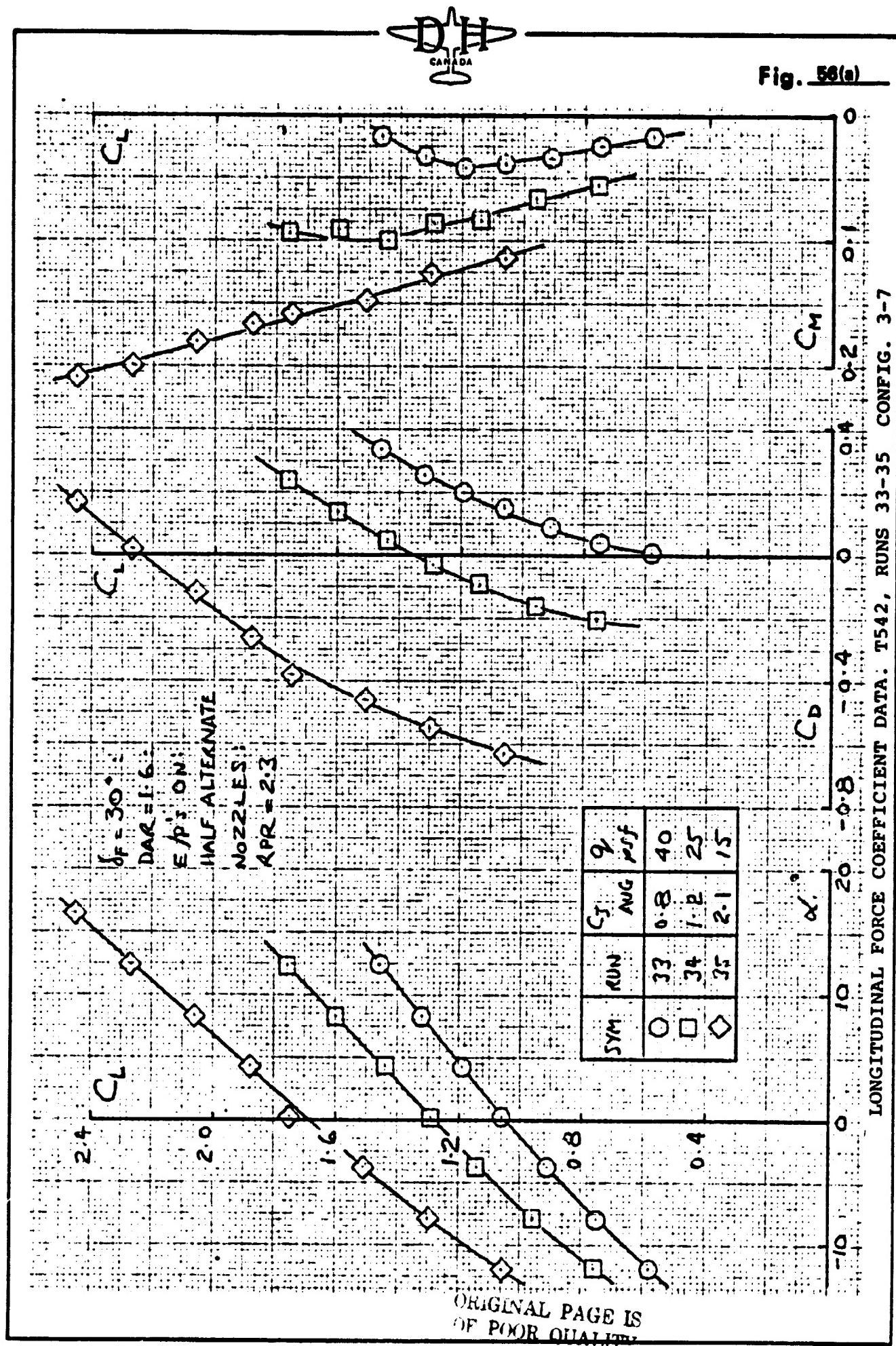


Fig. 58(a)



LONGITUDINAL FORCE COEFFICIENT DATA: T542, RUNS 33-35 CONFIG. 3-7

Fig. 56(b)

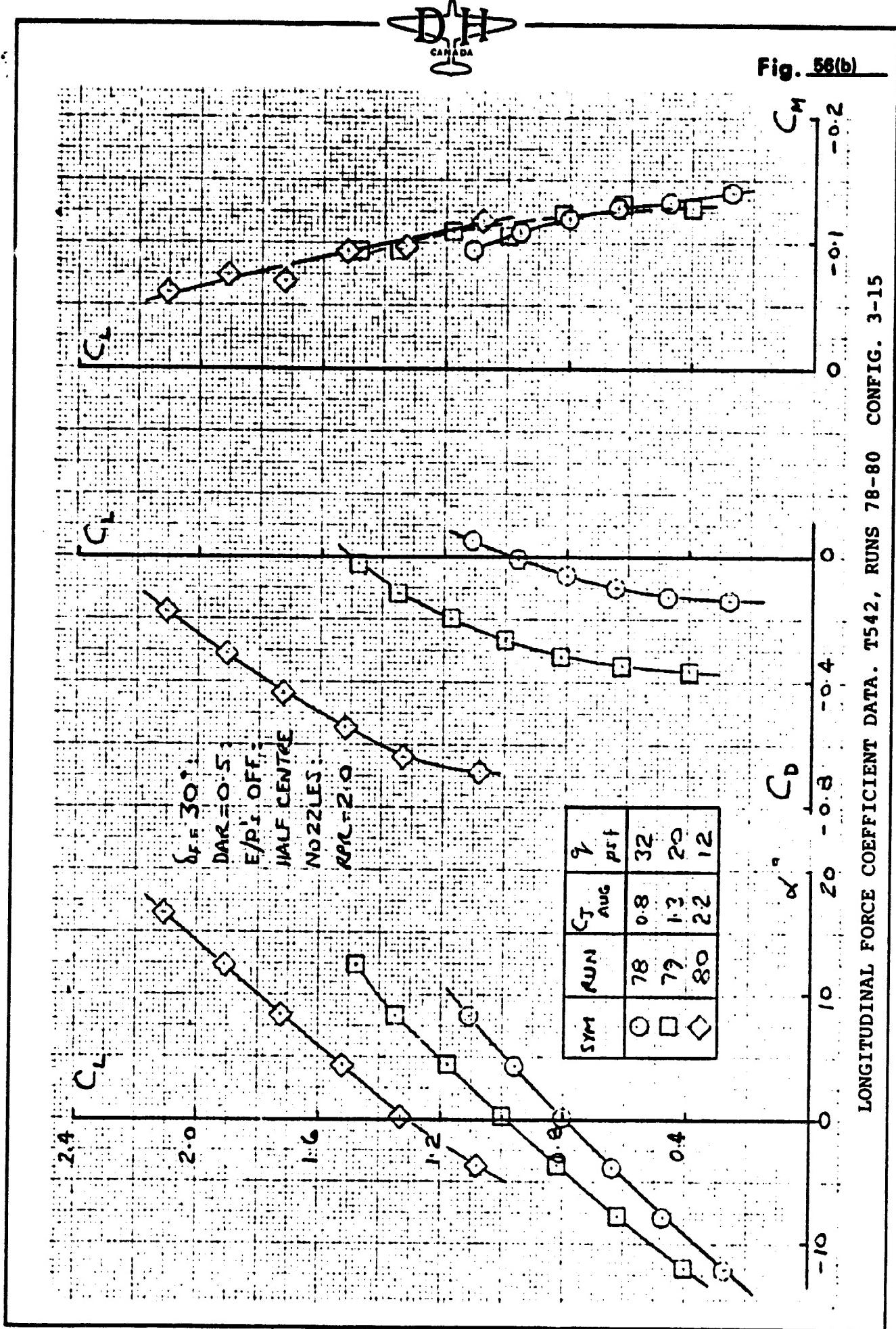




Fig. 57.

### EFFECT OF FLAP ANGLE, WING-BORNE

FUSELAGE AUGMENTOR SEALED

$T_h/L = 1.10$ ;  $T_w/s = 60 \text{ lb/ft}^2$

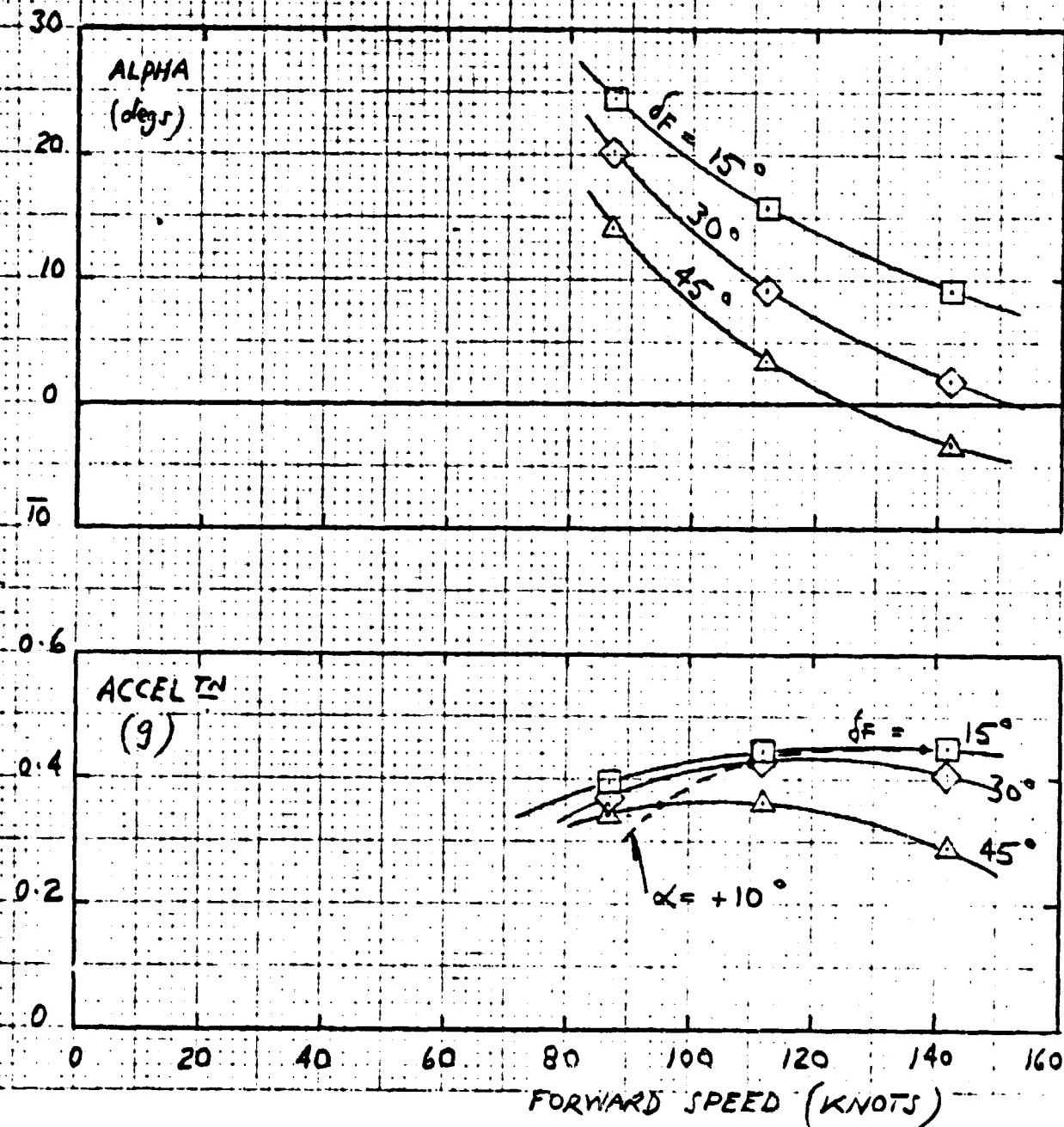
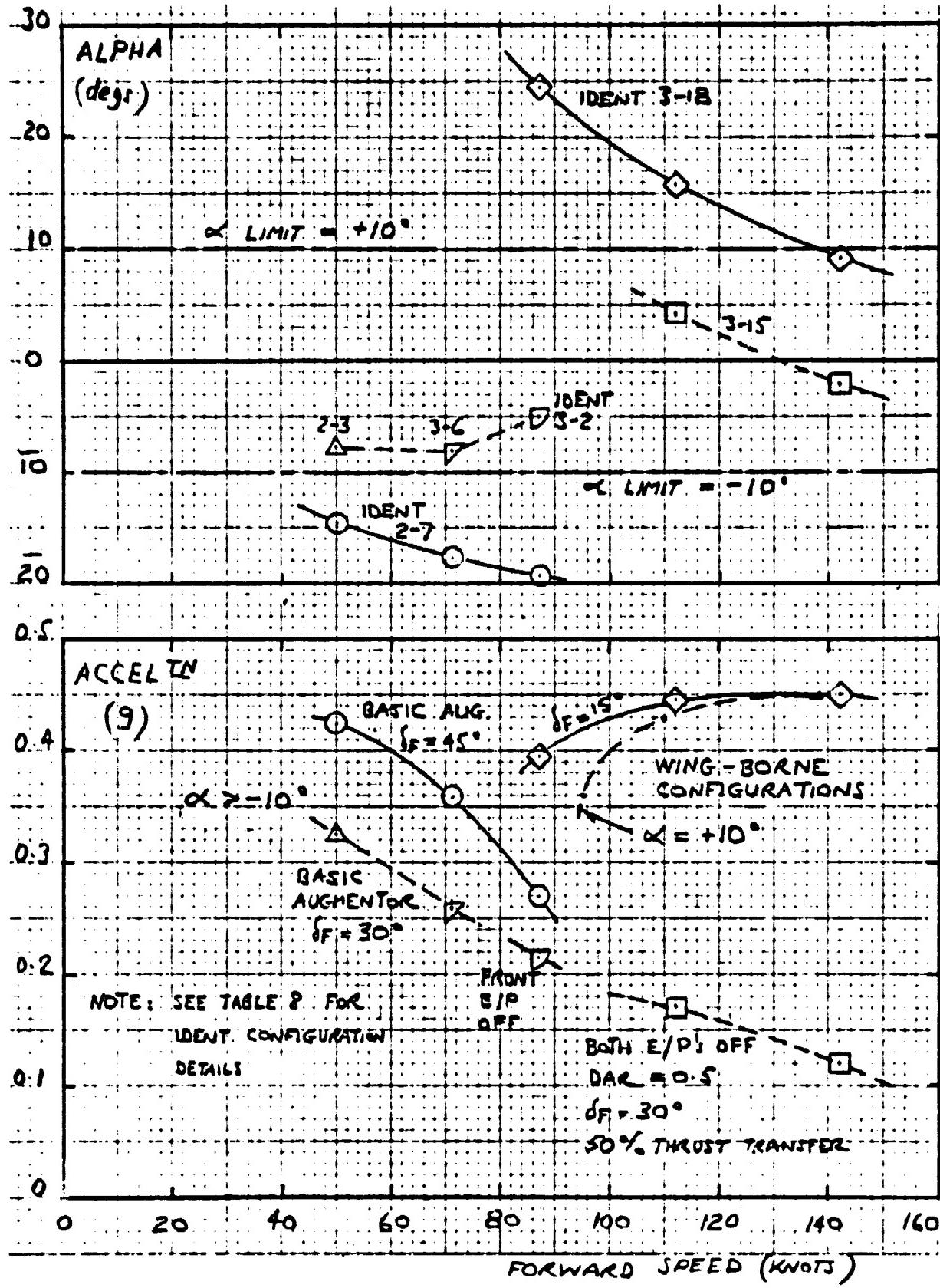




Fig. 38

### DEMONSTRATED ACCELERATION CAPABILITY





**Fig. 59**

## TRANSITION CONFIGURATION PITCHING MOMENTS

$$TH/L = 1.10 \quad ; \quad TH/S = 60 \text{ } \mu\text{s/ft}^2$$

$\alpha$  LIMITS:  $\pm 10^\circ$

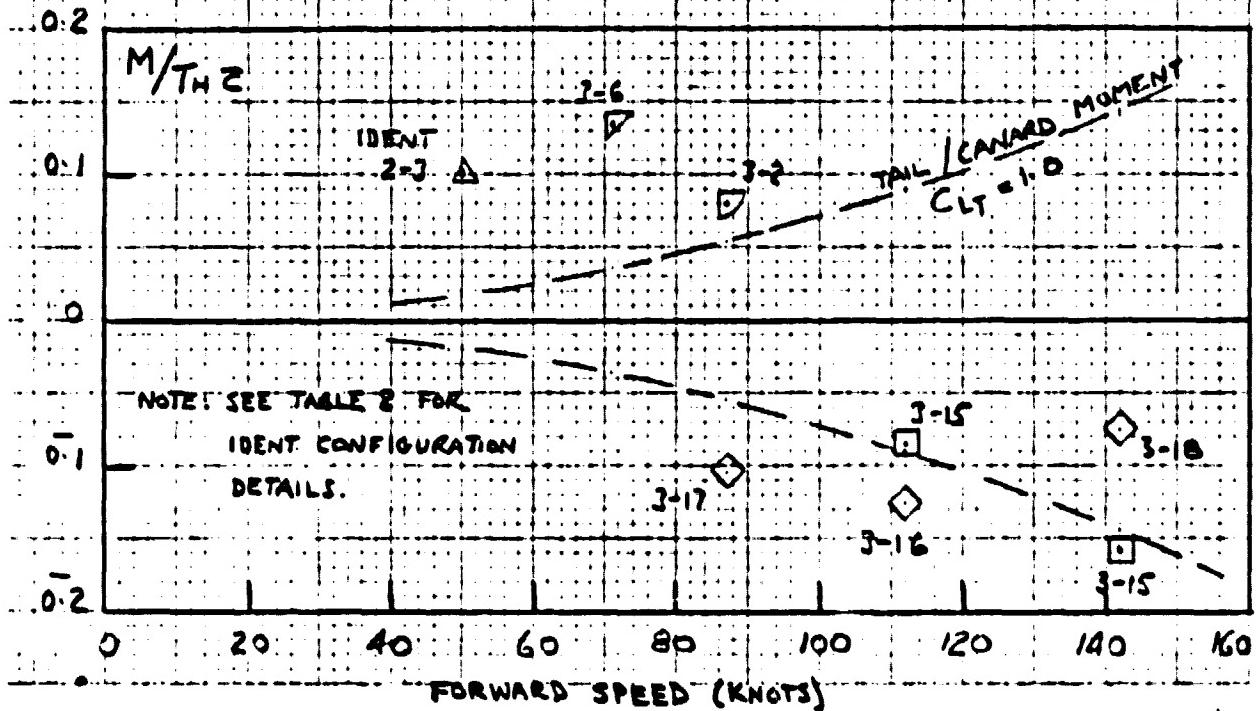


Fig. 60(a)

EFFECT OF WING LEADING-EDGE SLAT ON LONGITUDINAL CHARACTERISTICS

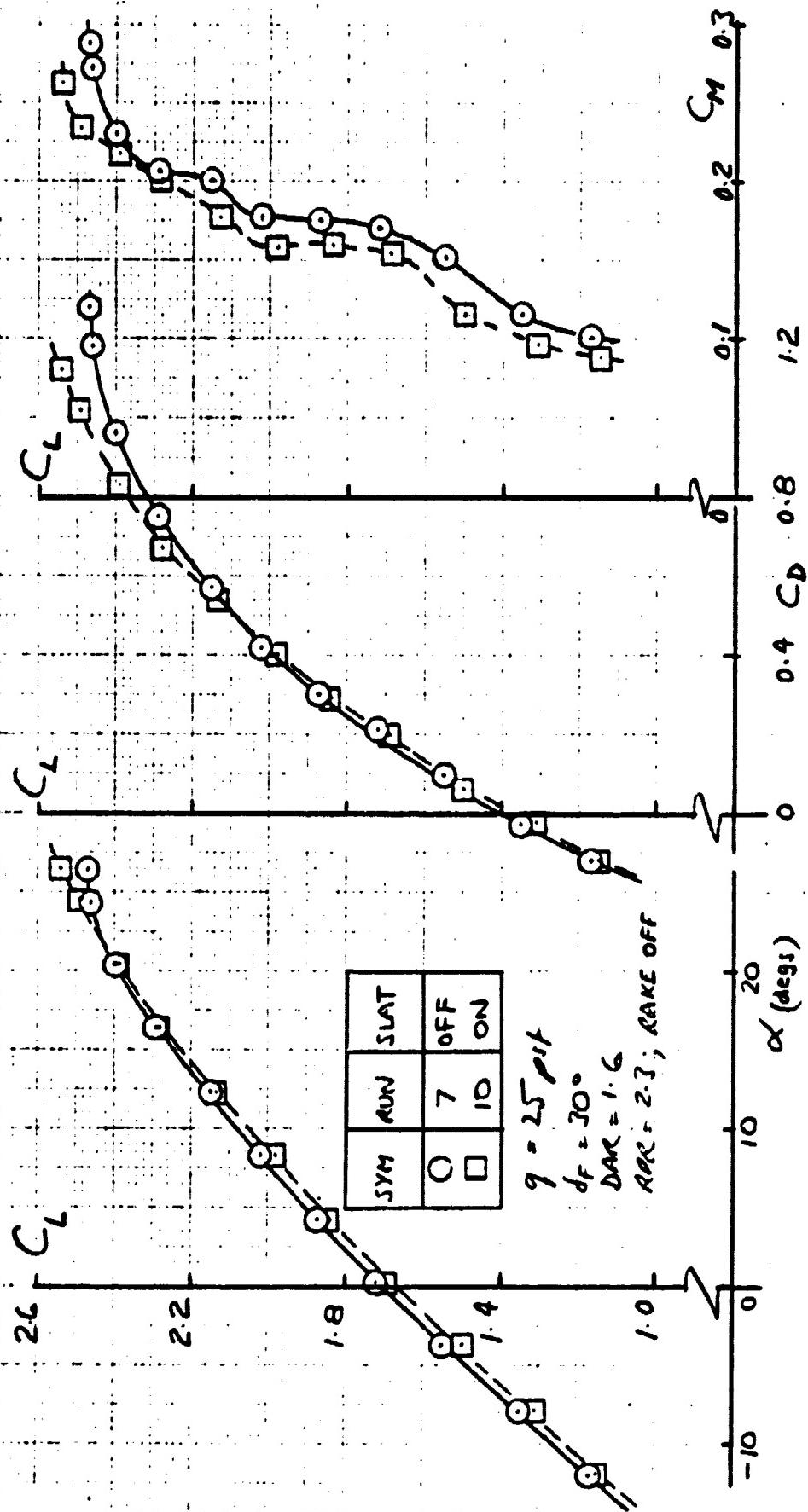


Fig. 60(b)

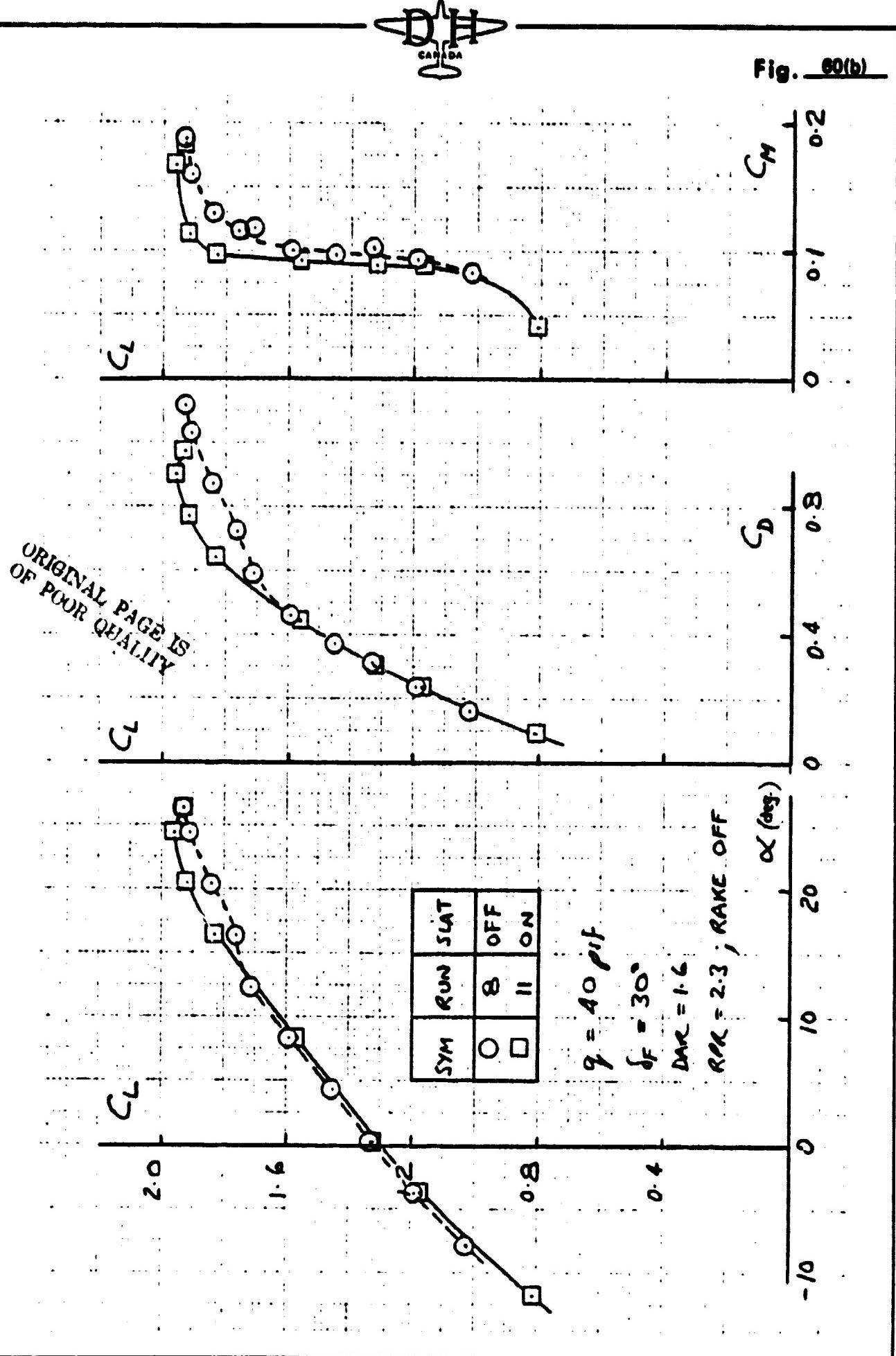




Fig. 61(a)

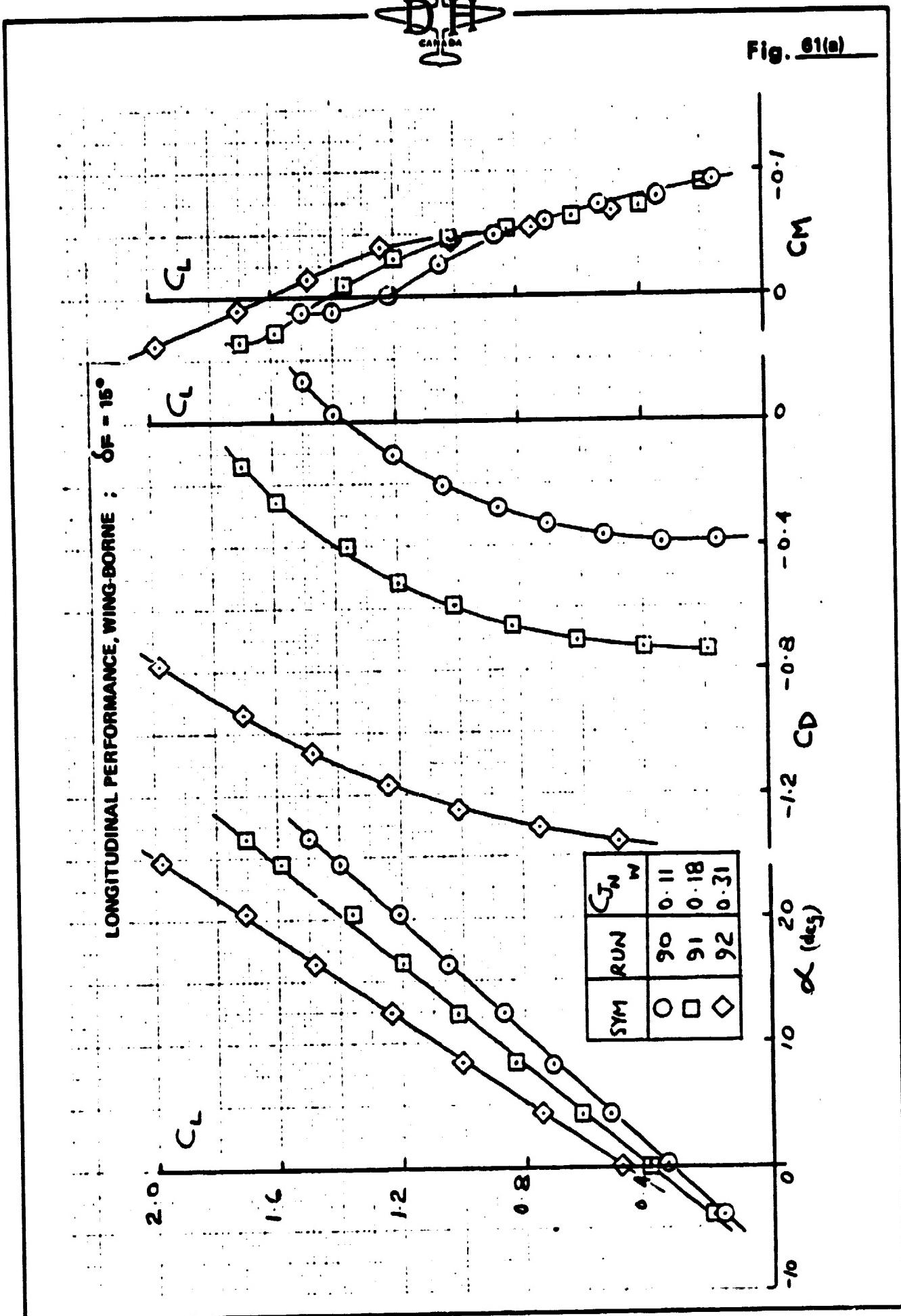


Fig. 61(b)

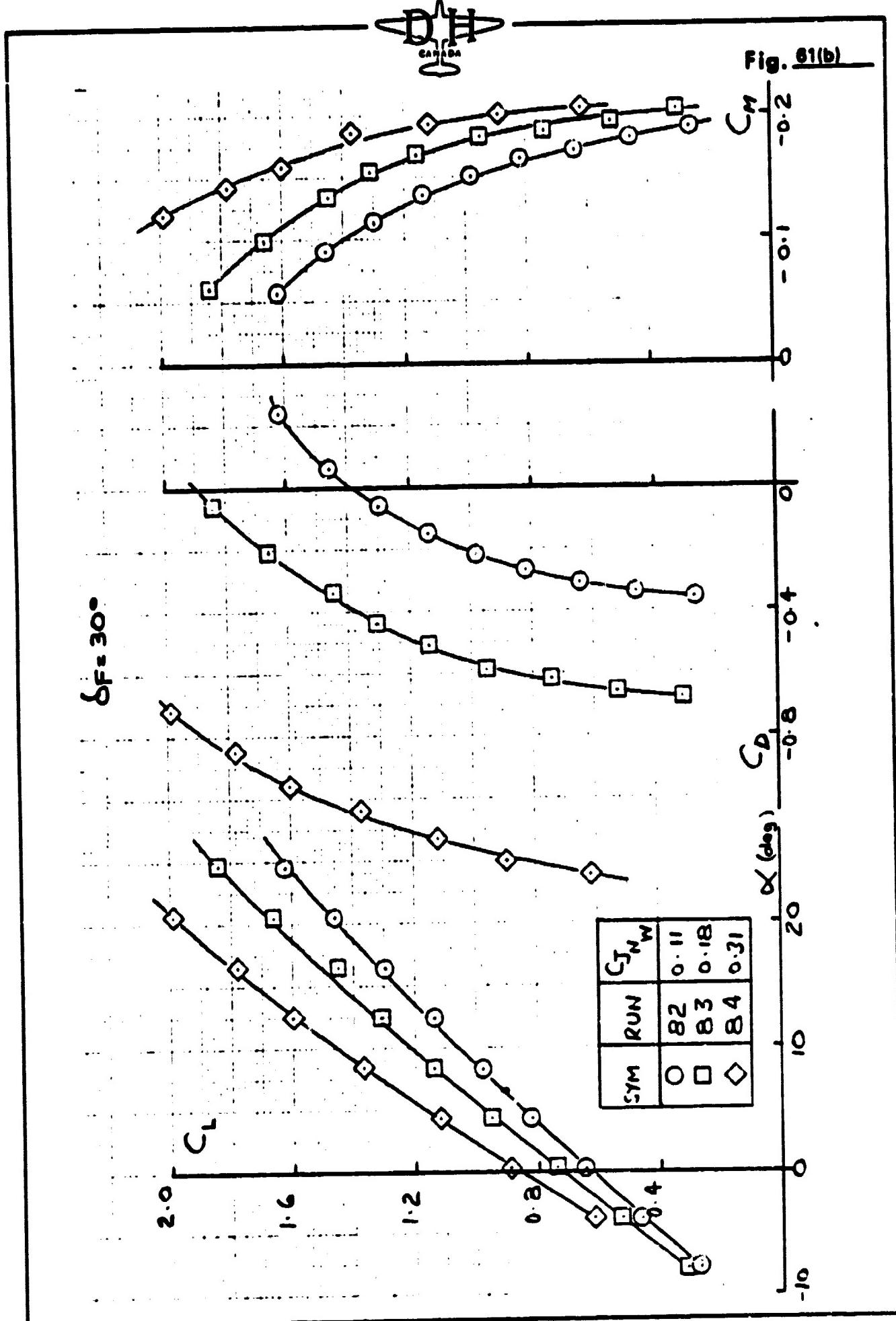


Fig. 61(c)

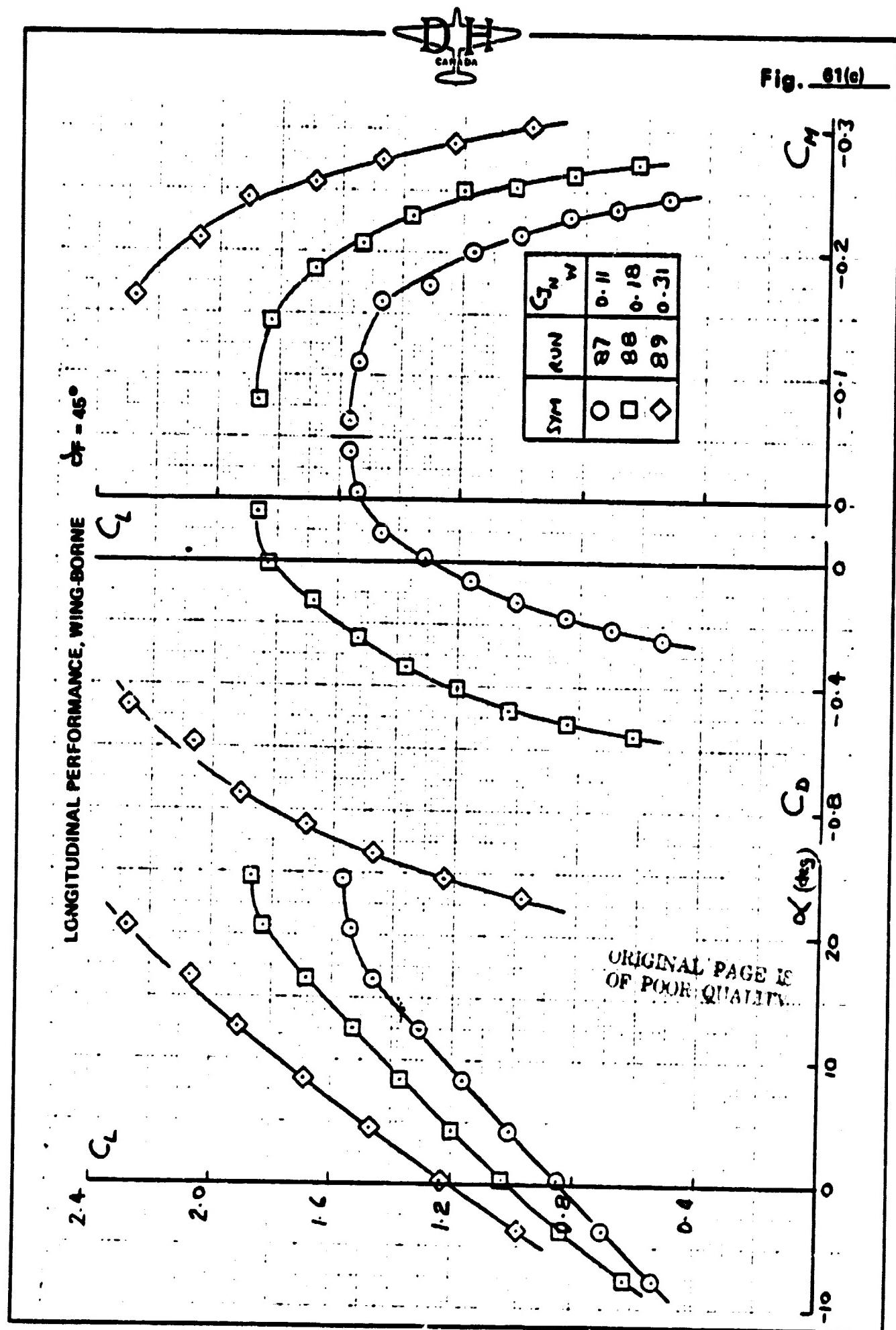




Fig. 62(a)

EFFECTIVE LIFT, WING-BORNE;  $\delta_F = 15^\circ$

(FUSELAGE AIRMVENTOR SEALED)

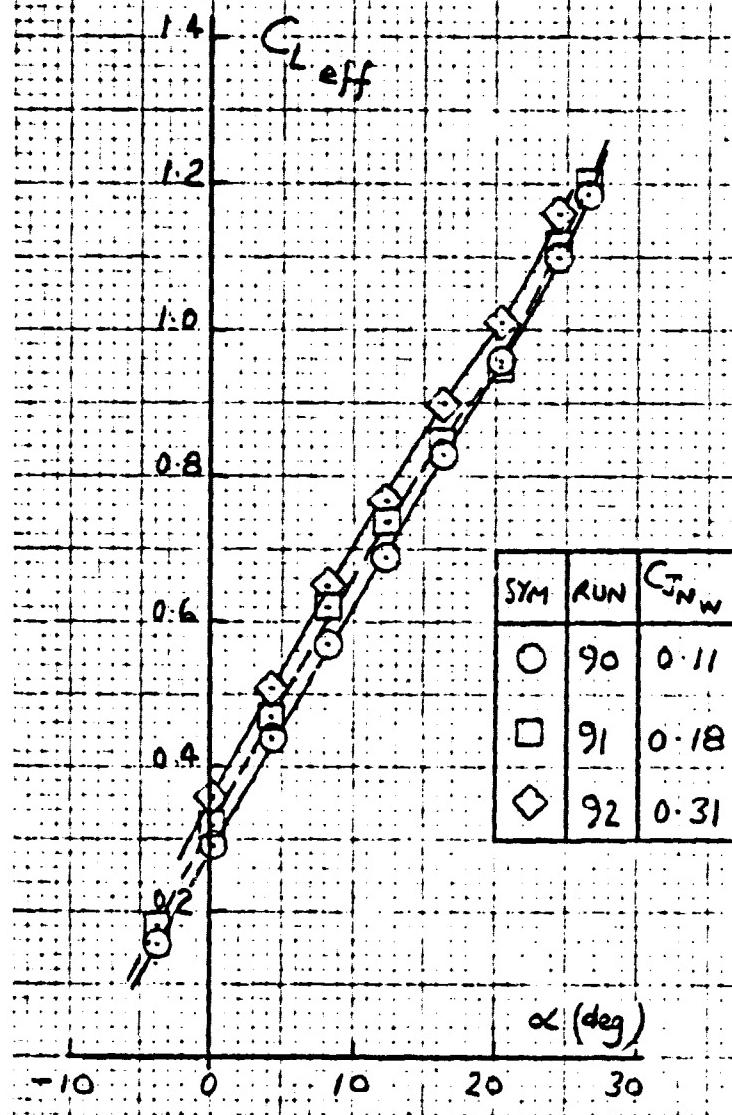




Fig. 62(b)

EFFECTIVE LIFT, WING-BORNE ;  $\delta_F = 30^\circ$   
(FUSELAGE AUGMENTOR SEALED)

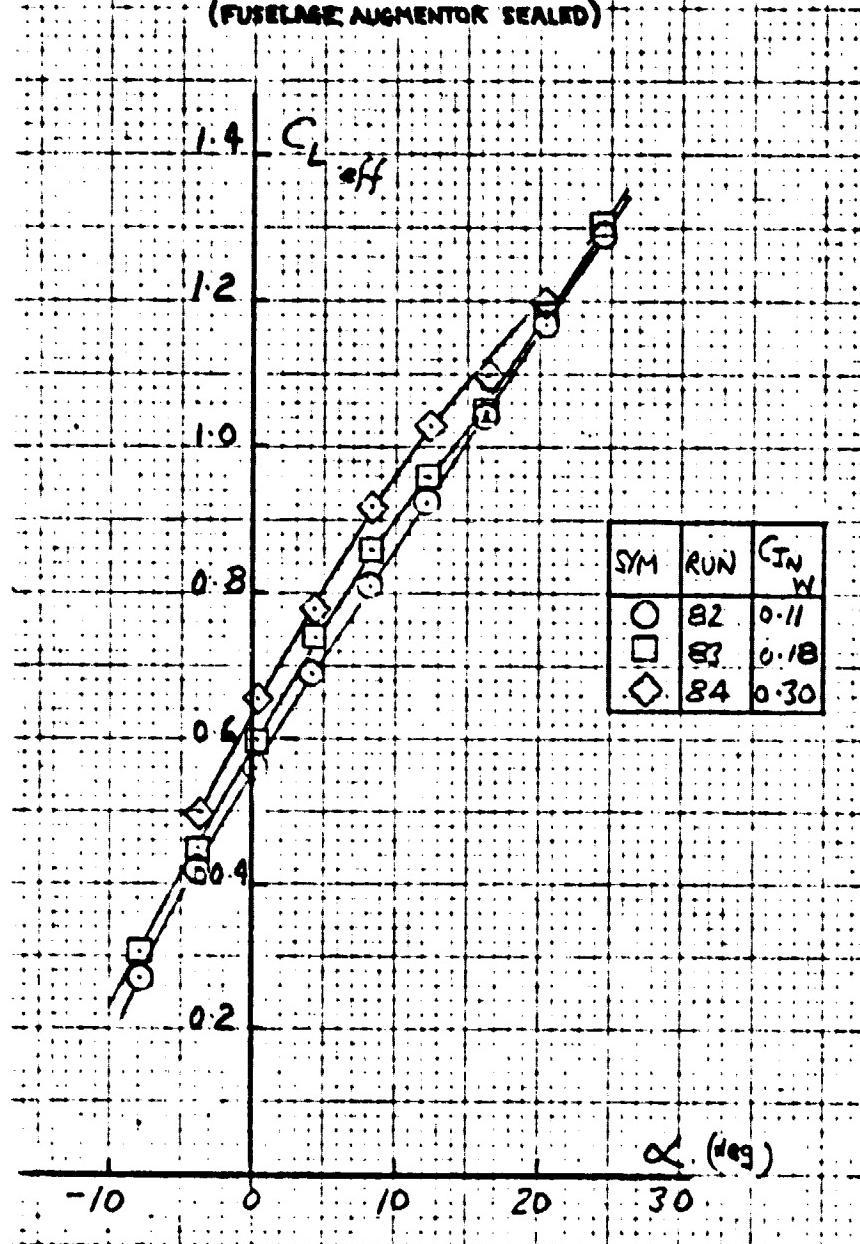
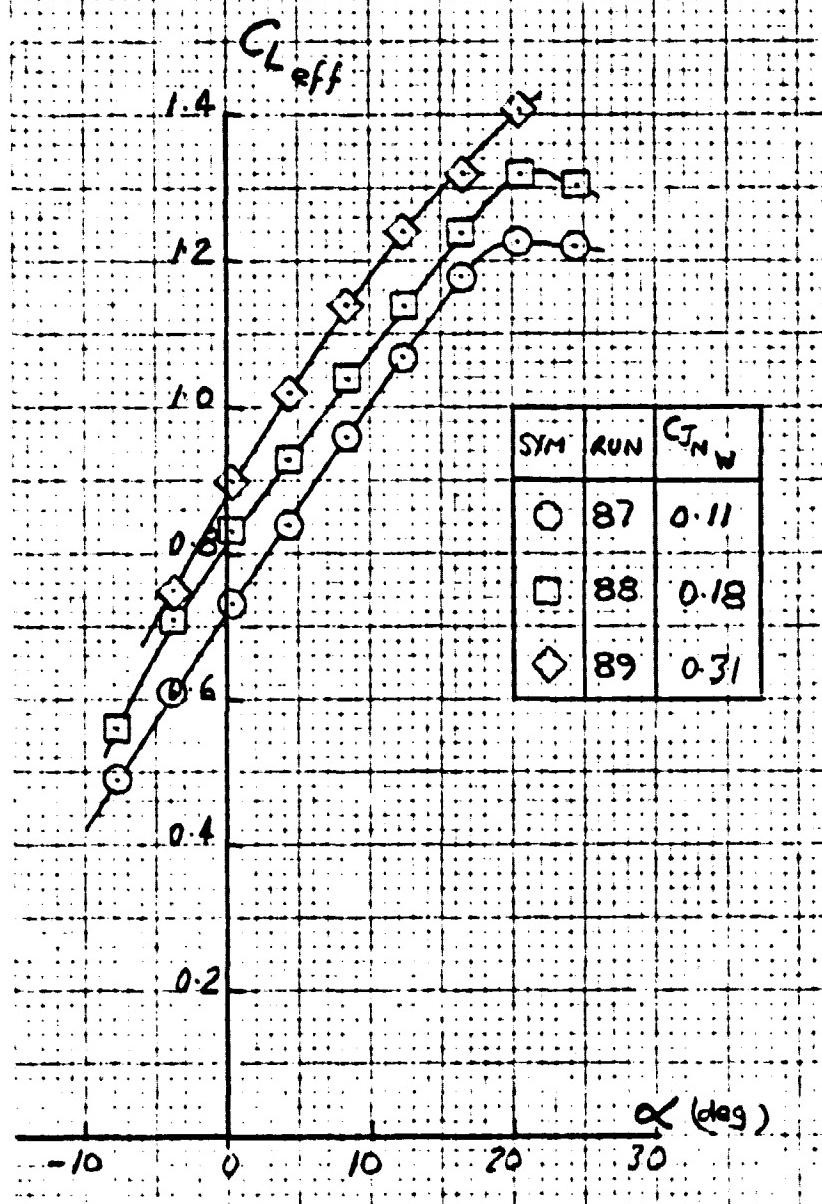




Fig. 62(c)

EFFECTIVE LIFT, WING-BORNE;  $\delta_F = 45^\circ$

(FUSELAGE AUGMENTOR SEALED)



## EFFECT OF FLAP ANGLE ON EFFECTIVE LIFT

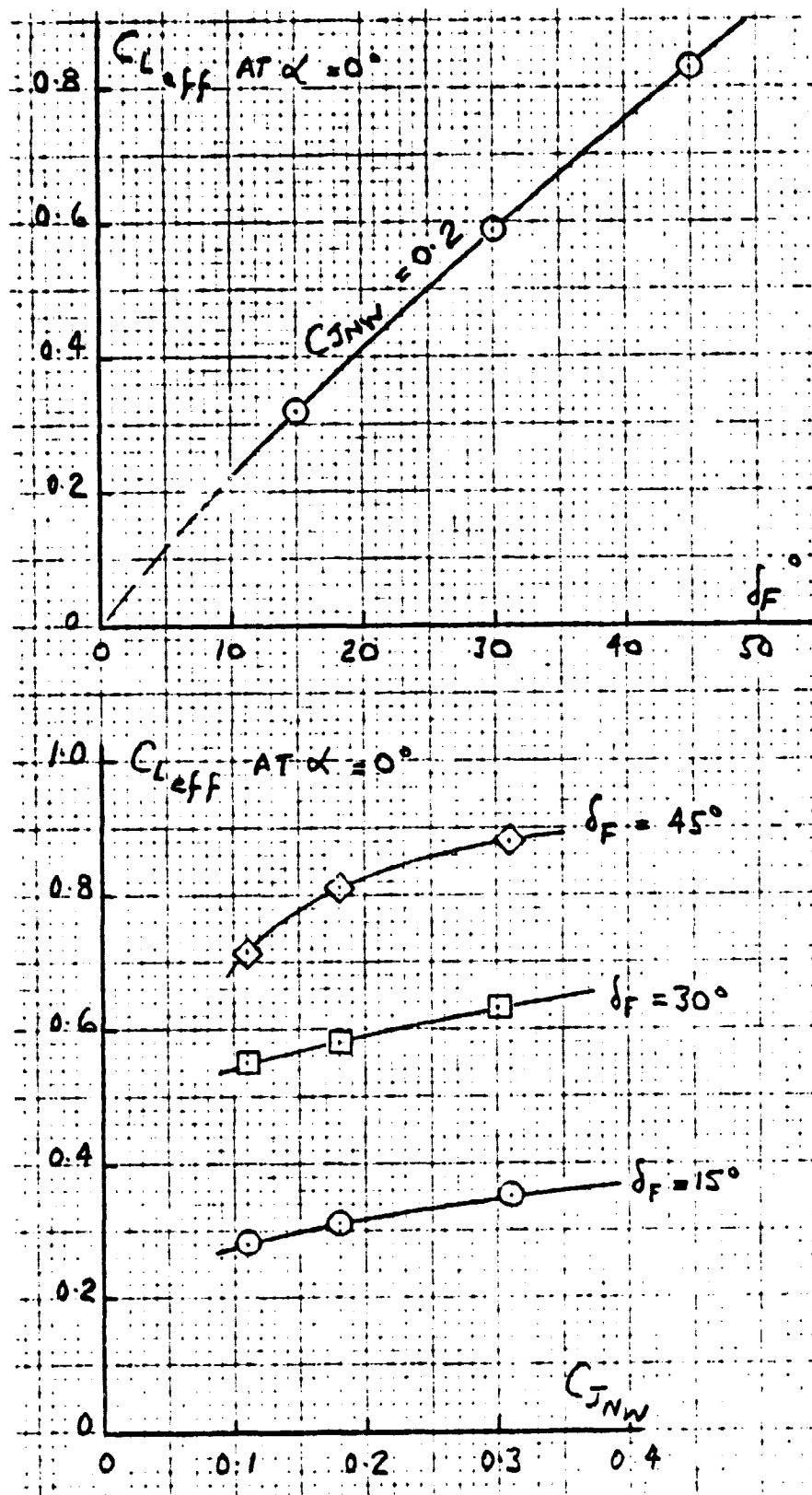
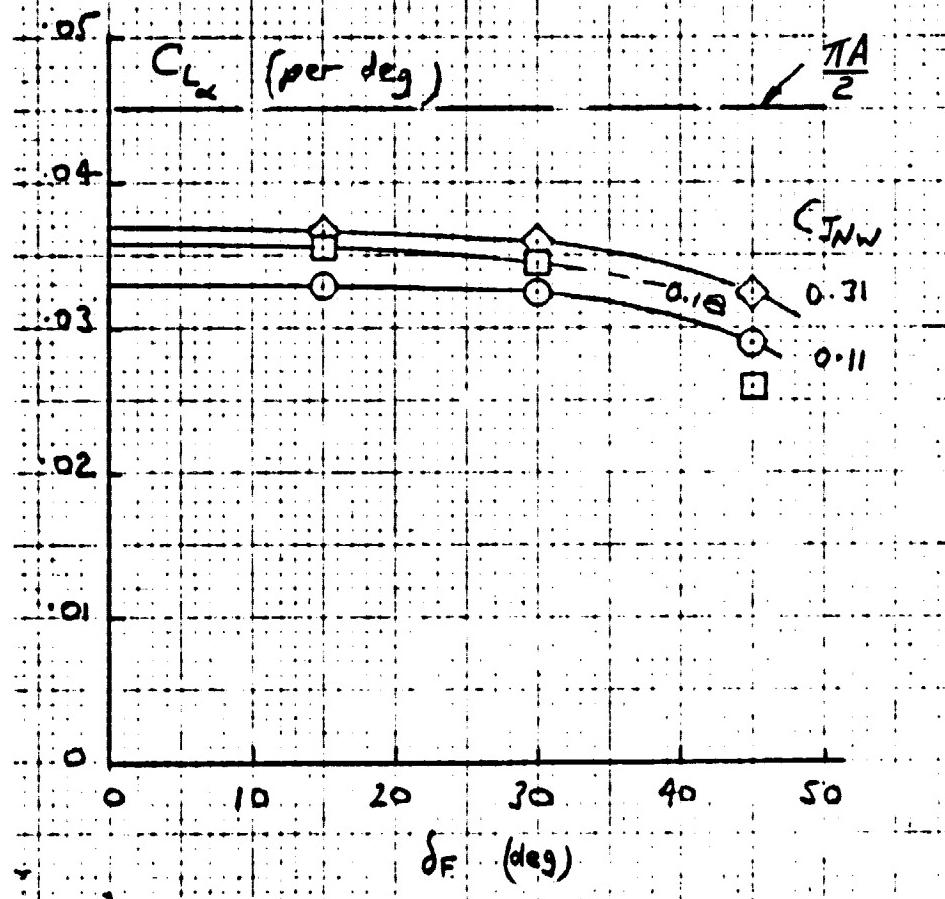


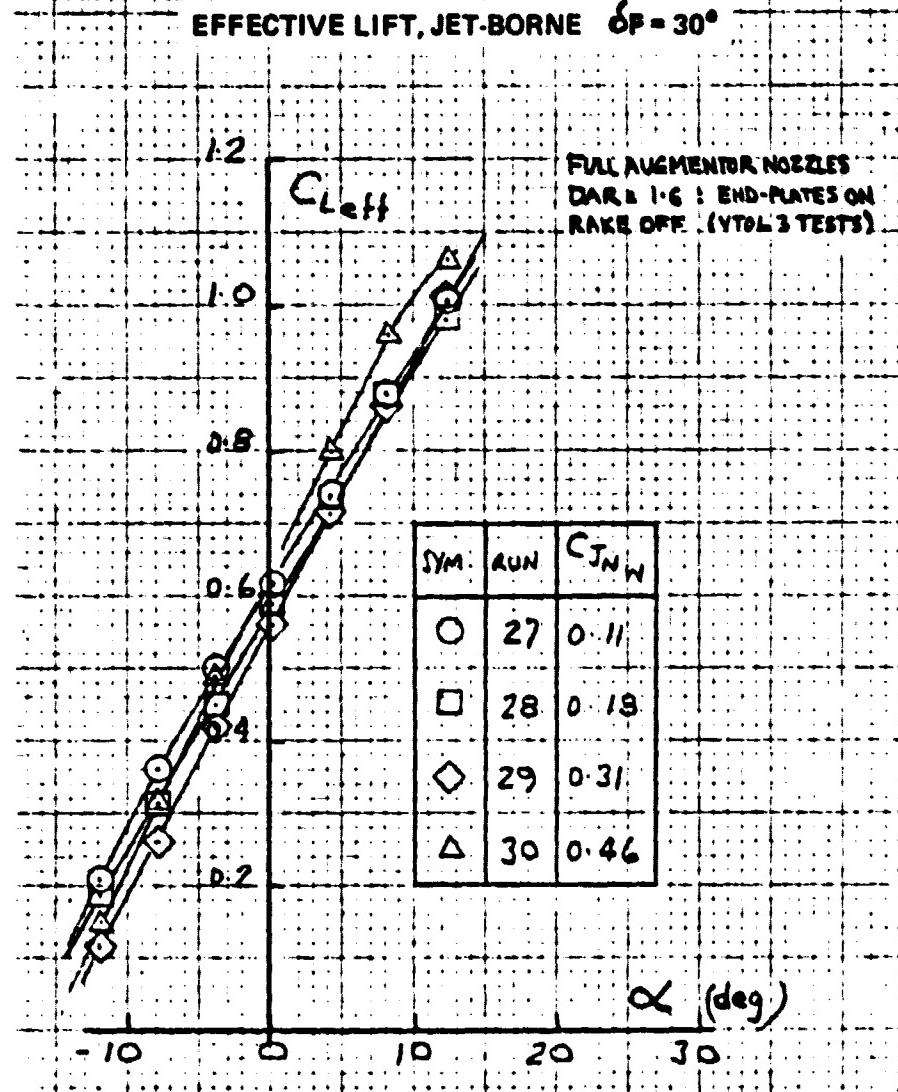


Fig. 64

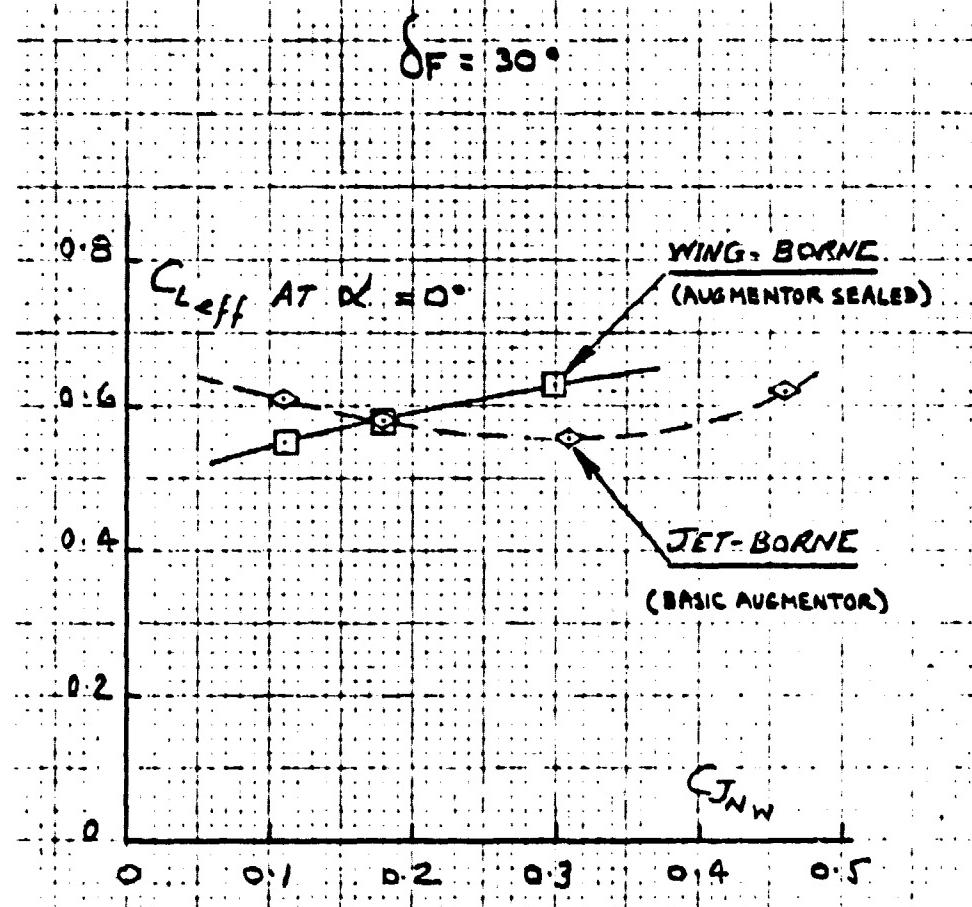
EFFECT OF FLAP ANGLE ON LIFT CURVE SLOPE

$(\partial C_{L_{\infty}} / \partial \alpha)_{\alpha=0^\circ}$  • [WING-BORNE] •





INTERFERENCE OF FUSELAGE AUGMENTOR ON LIFT



## INTERFERENCE OF FUSELAGE AUGMENTOR ON LIFT CURVE

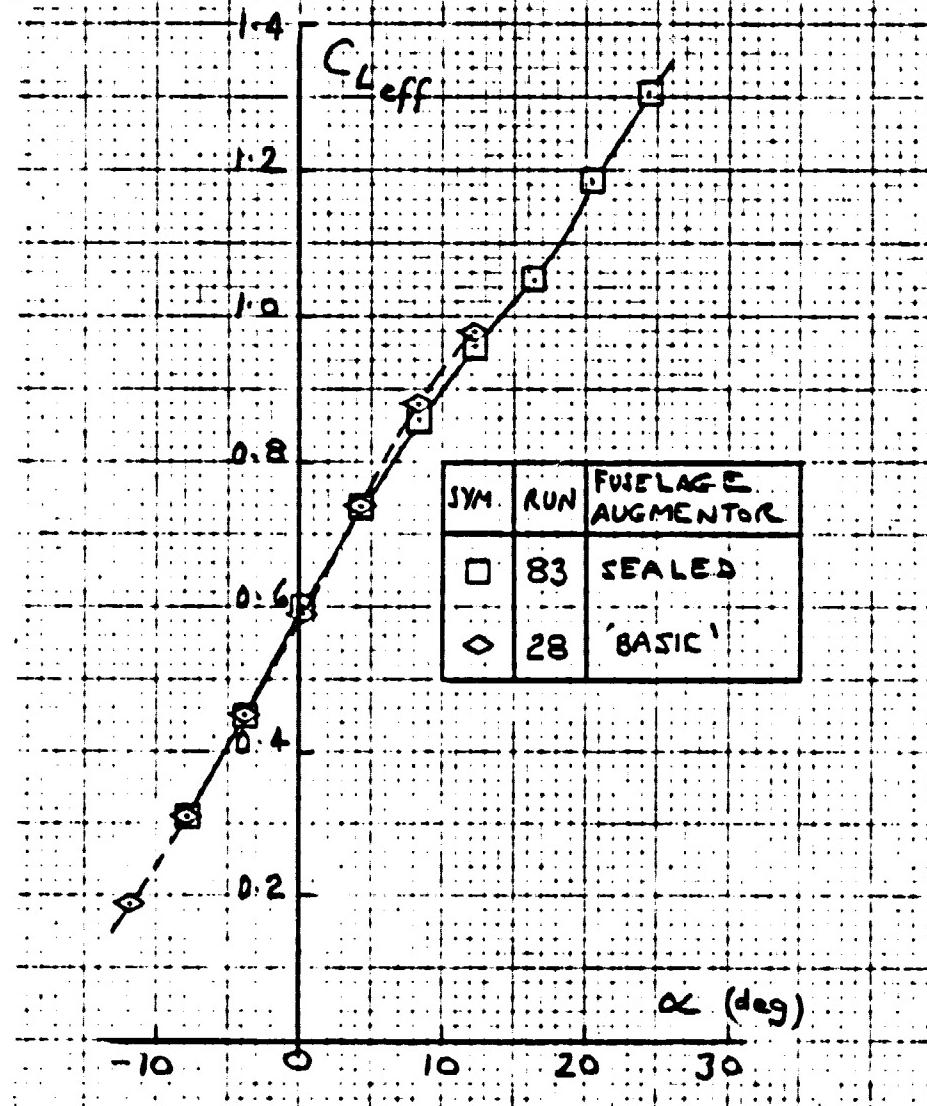
 $\delta_F = 30^\circ$ 
 $C_{J_{NW}} = 0.18$ 




Fig. 68(a)

EFFECTIVE DRAG, WING-BORNE  $\delta_F = 15^\circ$  (FUSELAGE AUGMENTOR SEALED)

ORIGINAL PAGE IS  
OF POOR QUALITY

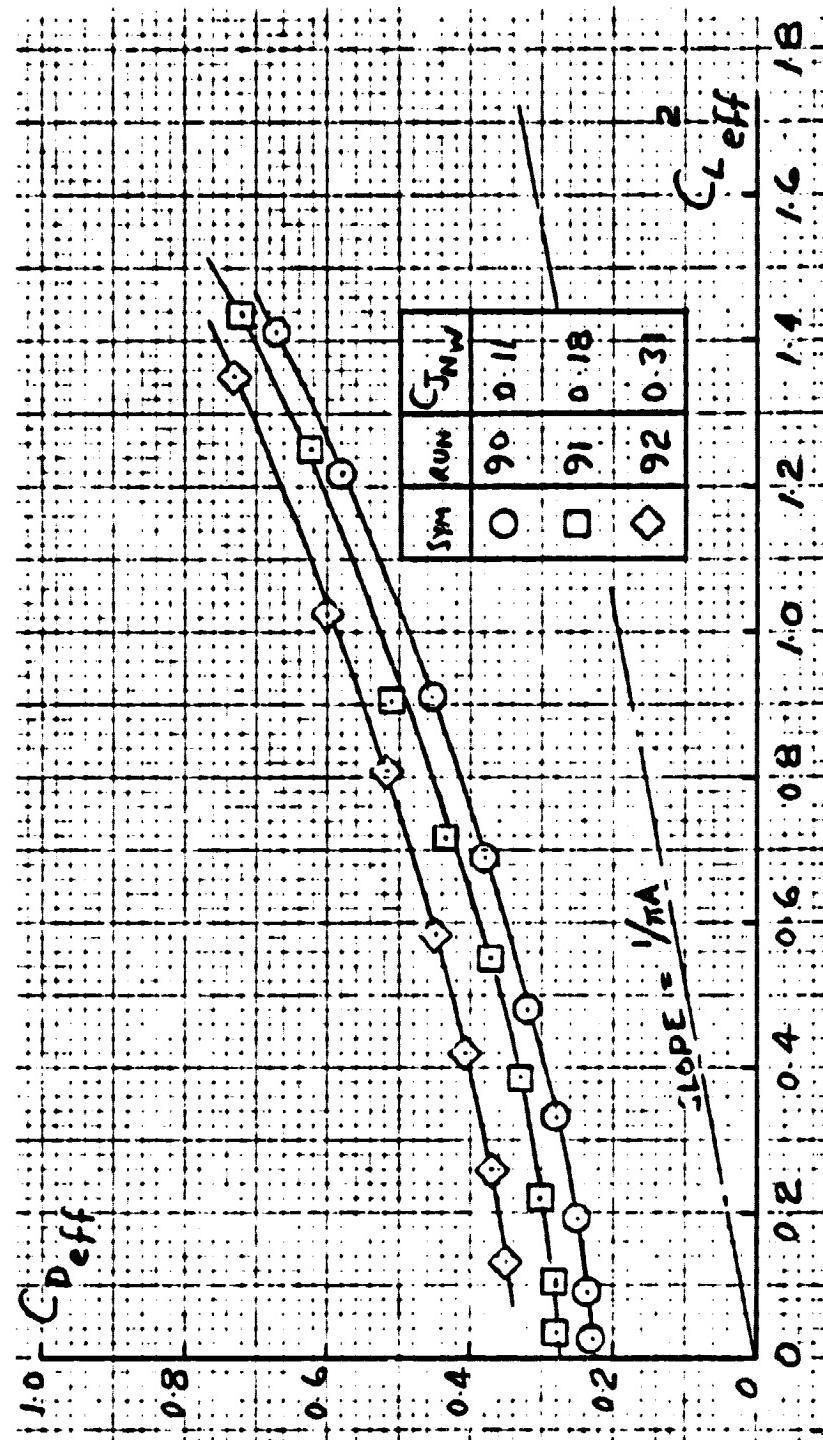


Fig. 68(b)

EFFECTIVE DRAG, WING-BORNE       $\delta_F = 30^\circ$  (FUSELAGE AUGMENTOR SEALED)

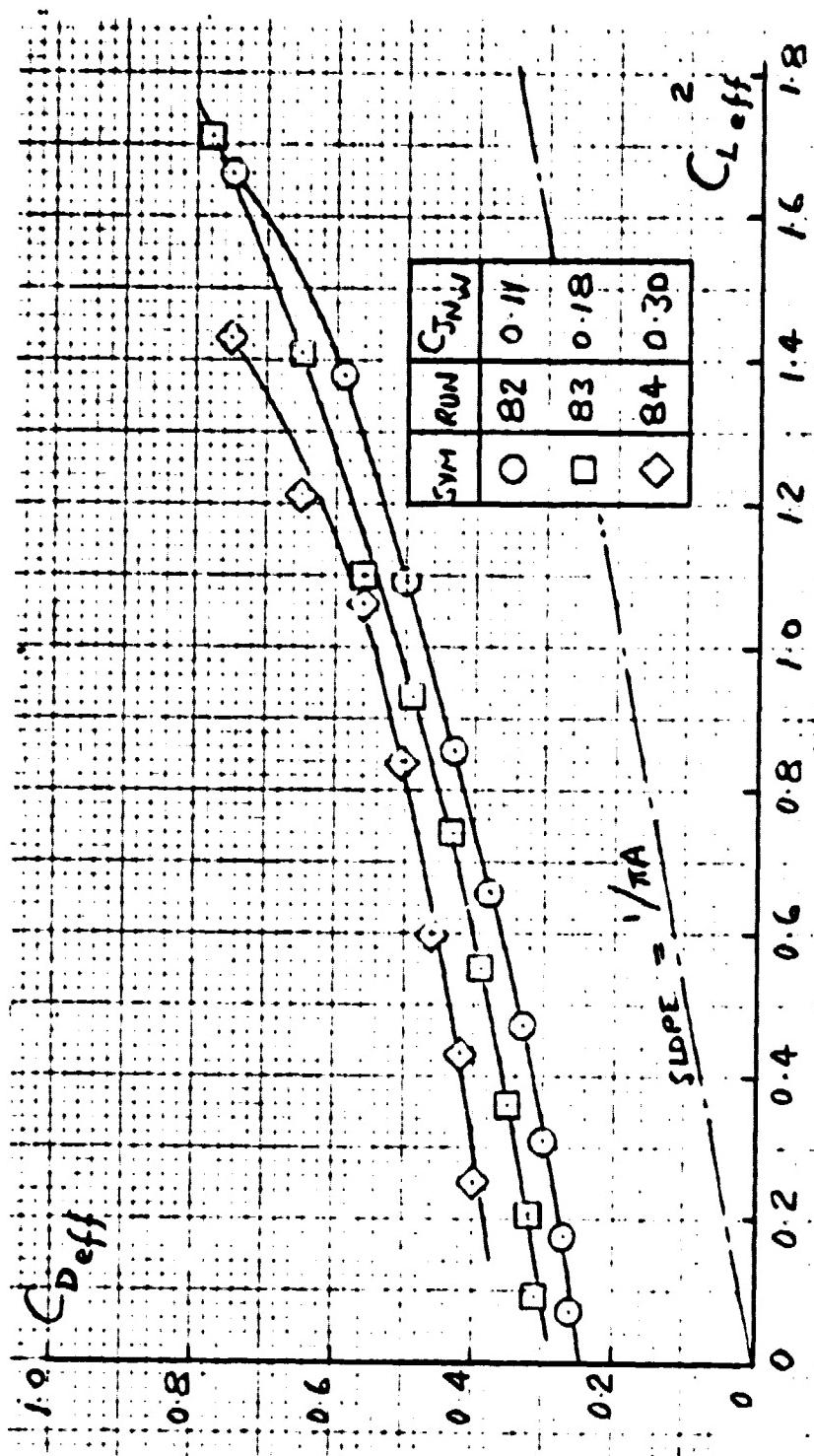


Fig. 68(c)

EFFECTIVE DRAG, WING-BORNE  
 $\delta_F = 45^\circ$  (FUSELAGE AUGMENTOR SEALED)

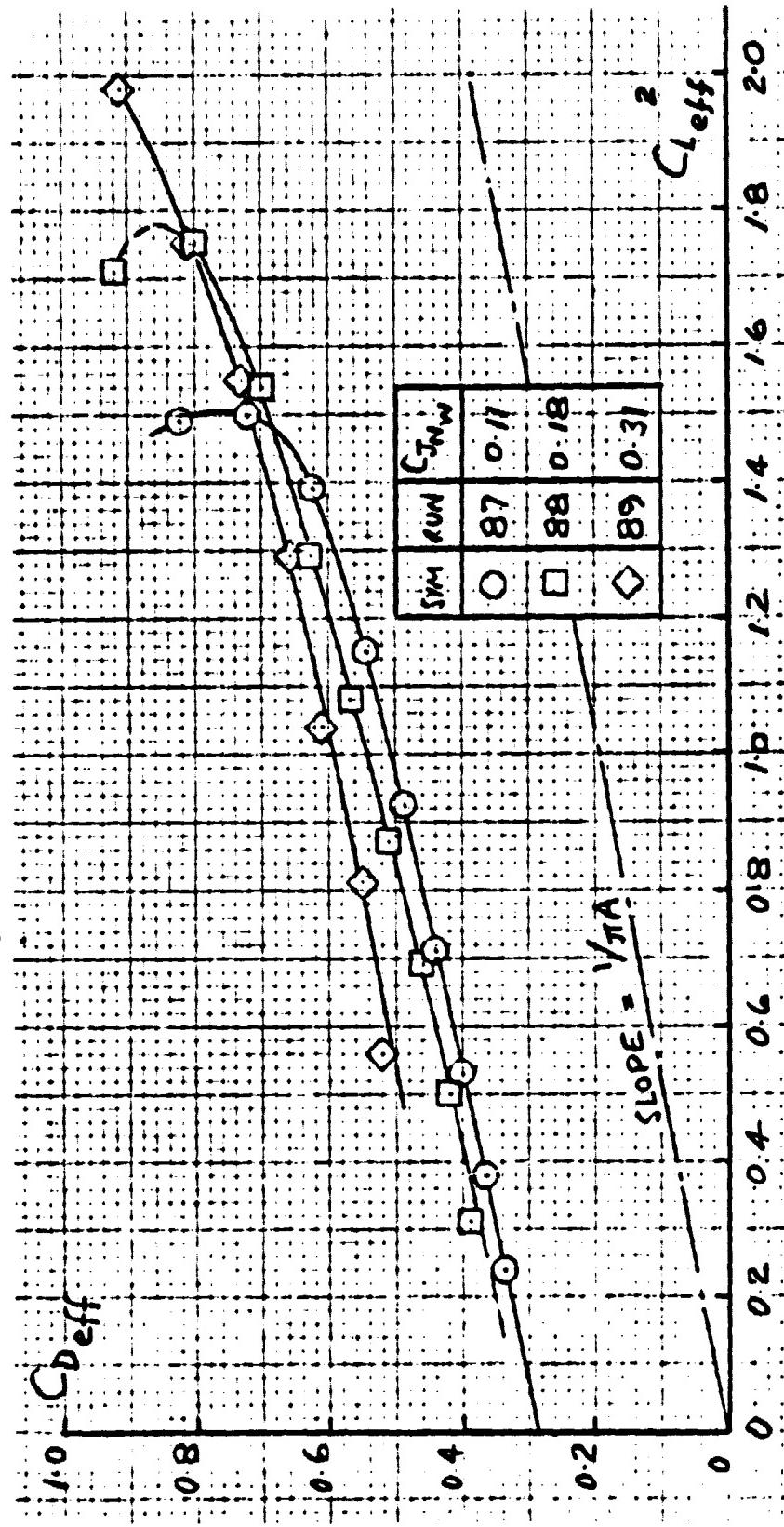
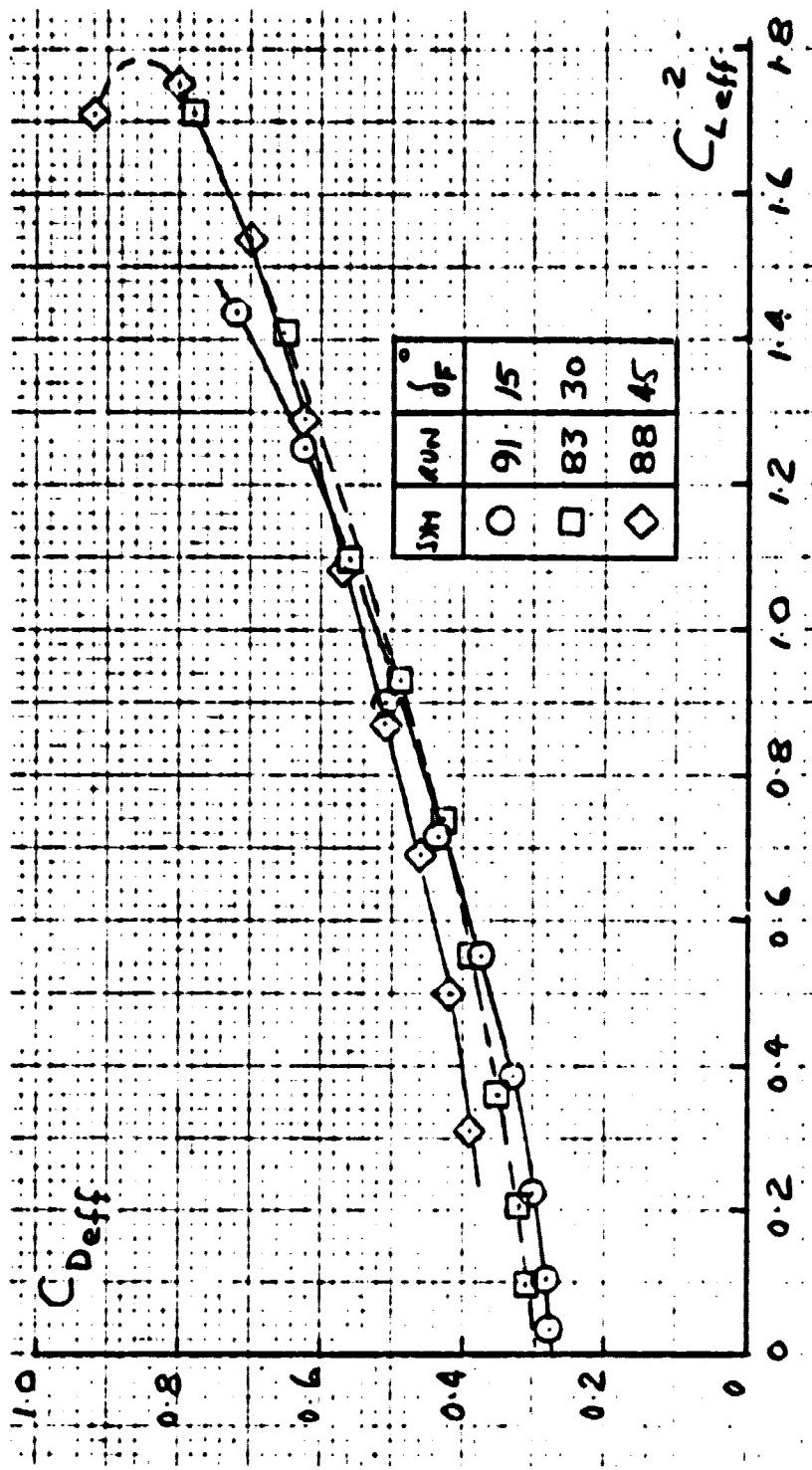




Fig. 69

EFFECT OF FLAP ANGLE ON EFFECTIVE DRAG, WING-BORNE  
(FUSELAGE AUGMENTOR SEALED)  $C_{D_{eff}} = 0.18$



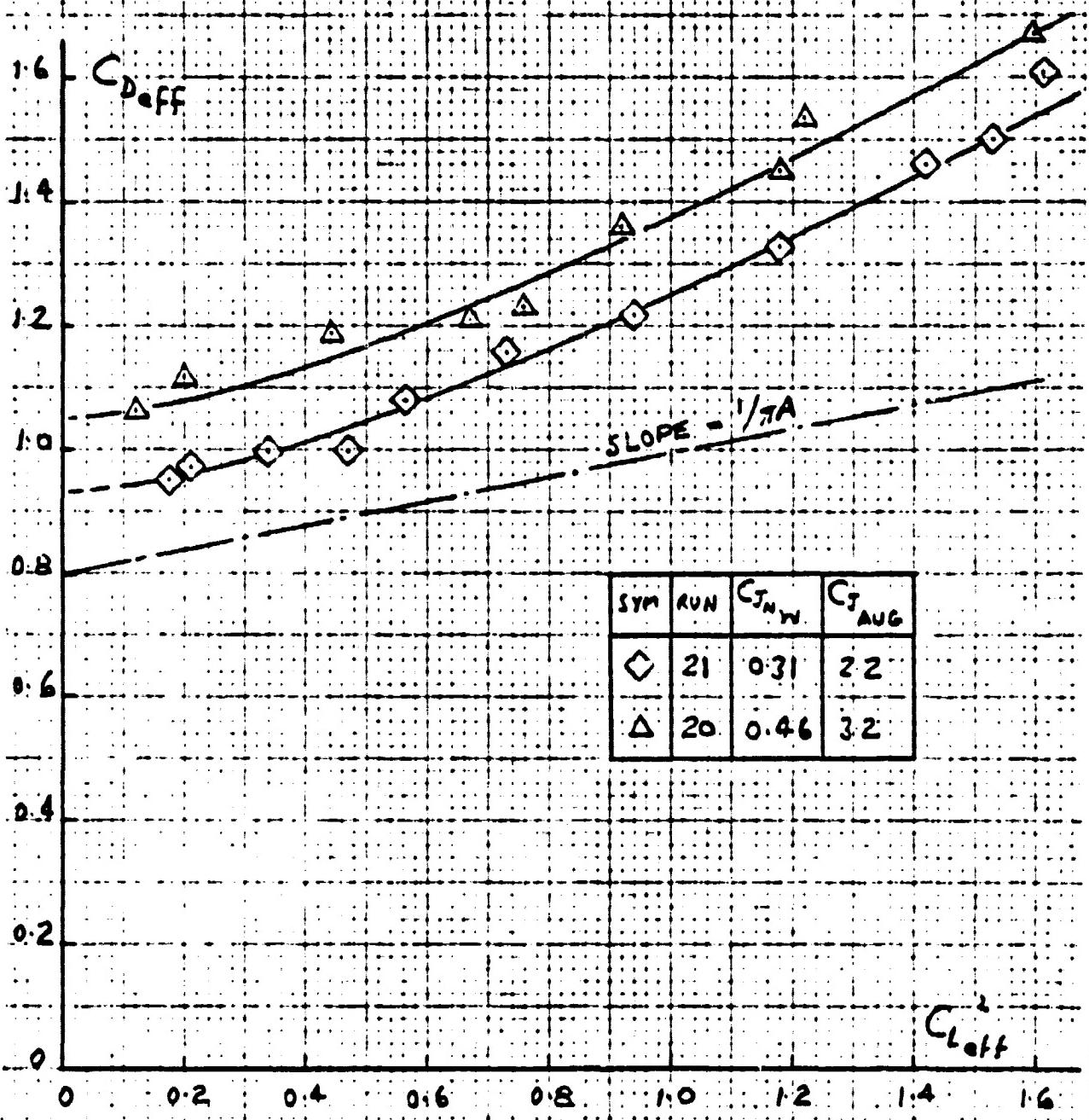
ORIGINAL PAGE IS  
OF POOR QUALITY



Fig. 70

EFFECTIVE DRAG, JET-BORNE;  $\delta_F = 30^\circ$ ; VTOL 1 TESTS

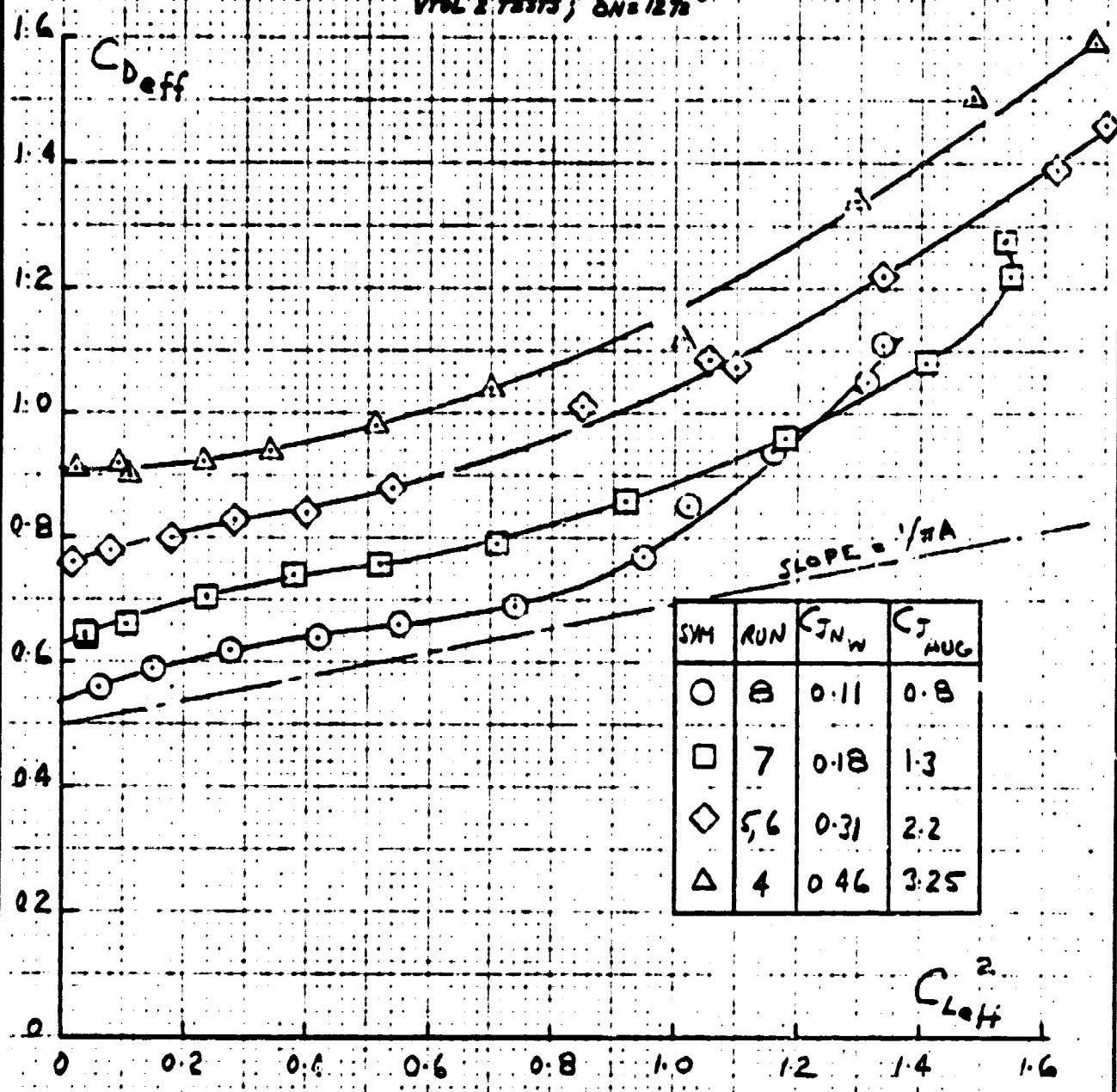
PULL AUGMENTOR NOZZLES  
DAR = 1.6, END-PLATES ON  
RAKE OFF; L/E SLAT OFF  
 $\delta_{DN} = 0^\circ$



EFFECTIVE DRAG, JET-BORNE

$\delta F = 30^\circ$

FULL AUGMENTOR NOZZLES  
 $DAR = 1.6$ ; END-PLATES ON  
 RAKE OFF; 1/2 SLAT OFF  
 VTOL 2 TESTS;  $\Delta h = 12\%$

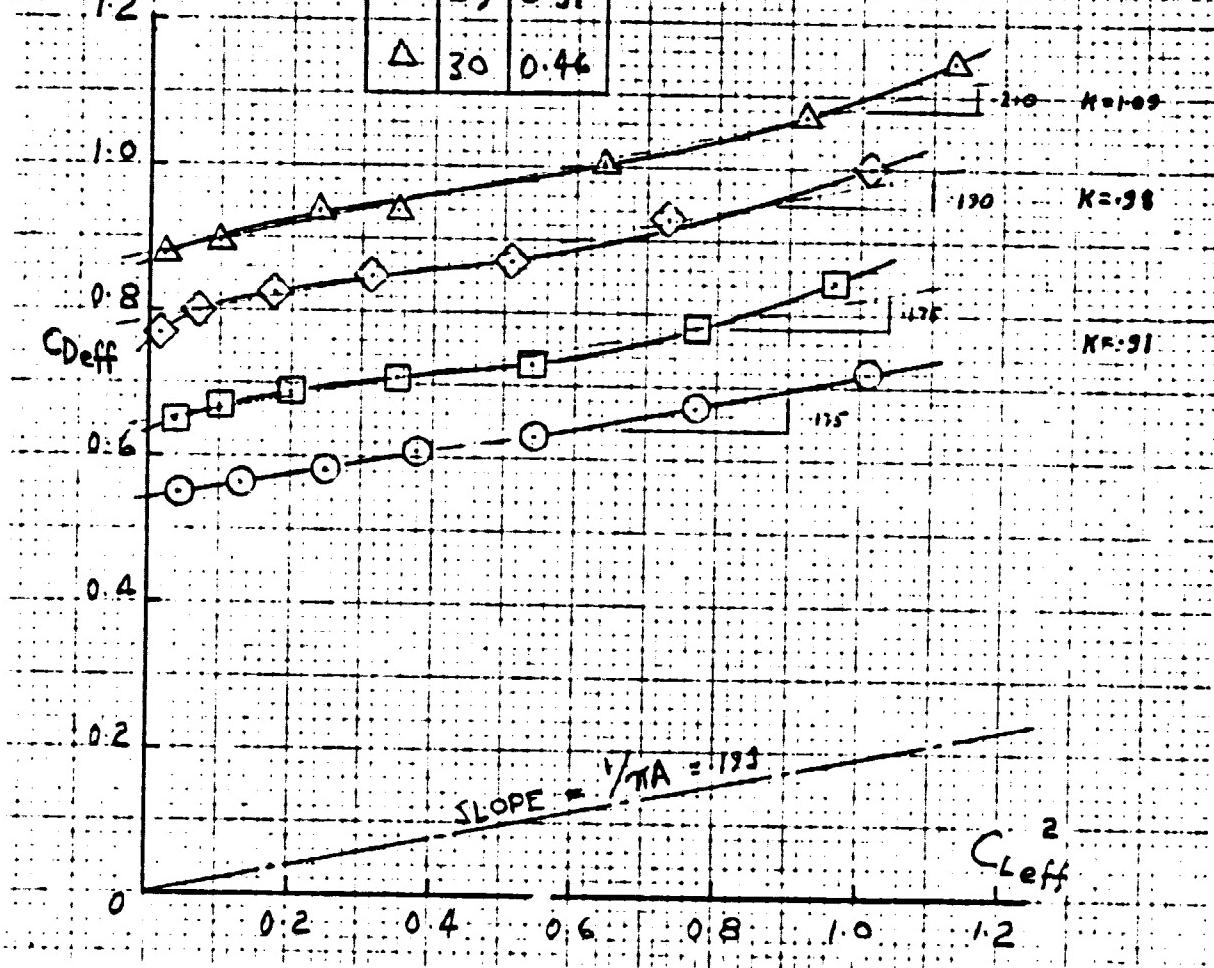


EFFECTIVE DRAG, JET-BORNE

$\delta F = 30^\circ$

FULL AUGMENTOR NOZZLES  
 $DAR = 1.6$ ; END-PLATES ON  
 RAKE OFF (VTOL 3 TESTS)  
 L/E SLAT ON

SYM	RUN	$C_{J_{NW}}$
○	27	0.11
□	28	0.18
◇	29	0.31
△	30	0.46

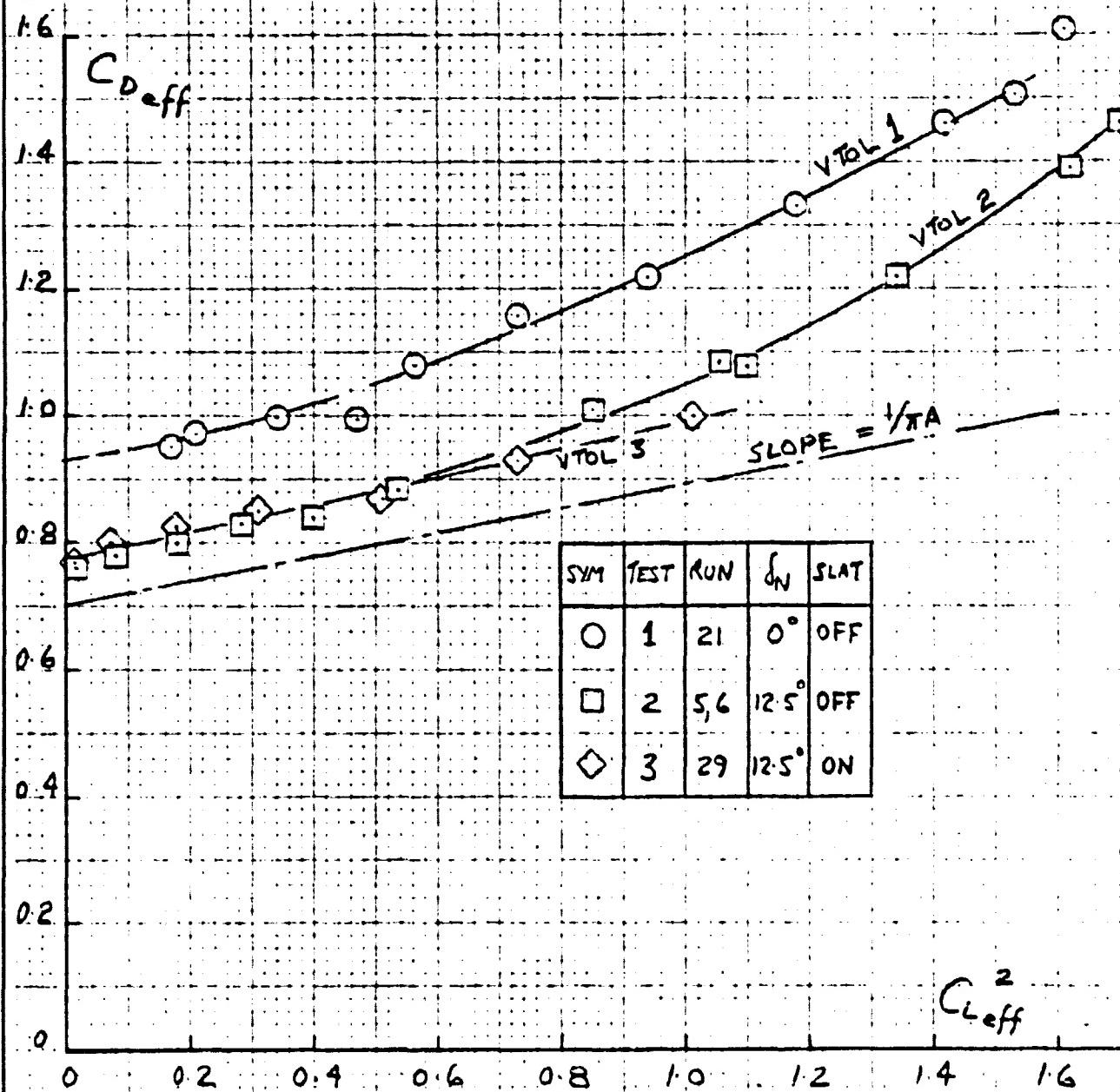


ORIGINAL PAGE IF  
 OF POOR QUALITY

EFFECT OF FUSELAGE AUGMENTOR NOZZLE ANGLE  
 ON EFFECTIVE DRAG

 $\delta F = 30^\circ$ ,  $C_{JW} = 0.31$ ,  $C_{JAU} = 2.2$ 

FULL AUGMENTOR NOZZLES

 DAR = 1.6; END-PLATES ON  
 RAKE OFF

 ORIGINAL PAGE IS  
 OF POOR QUALITY



**Fig. 74**

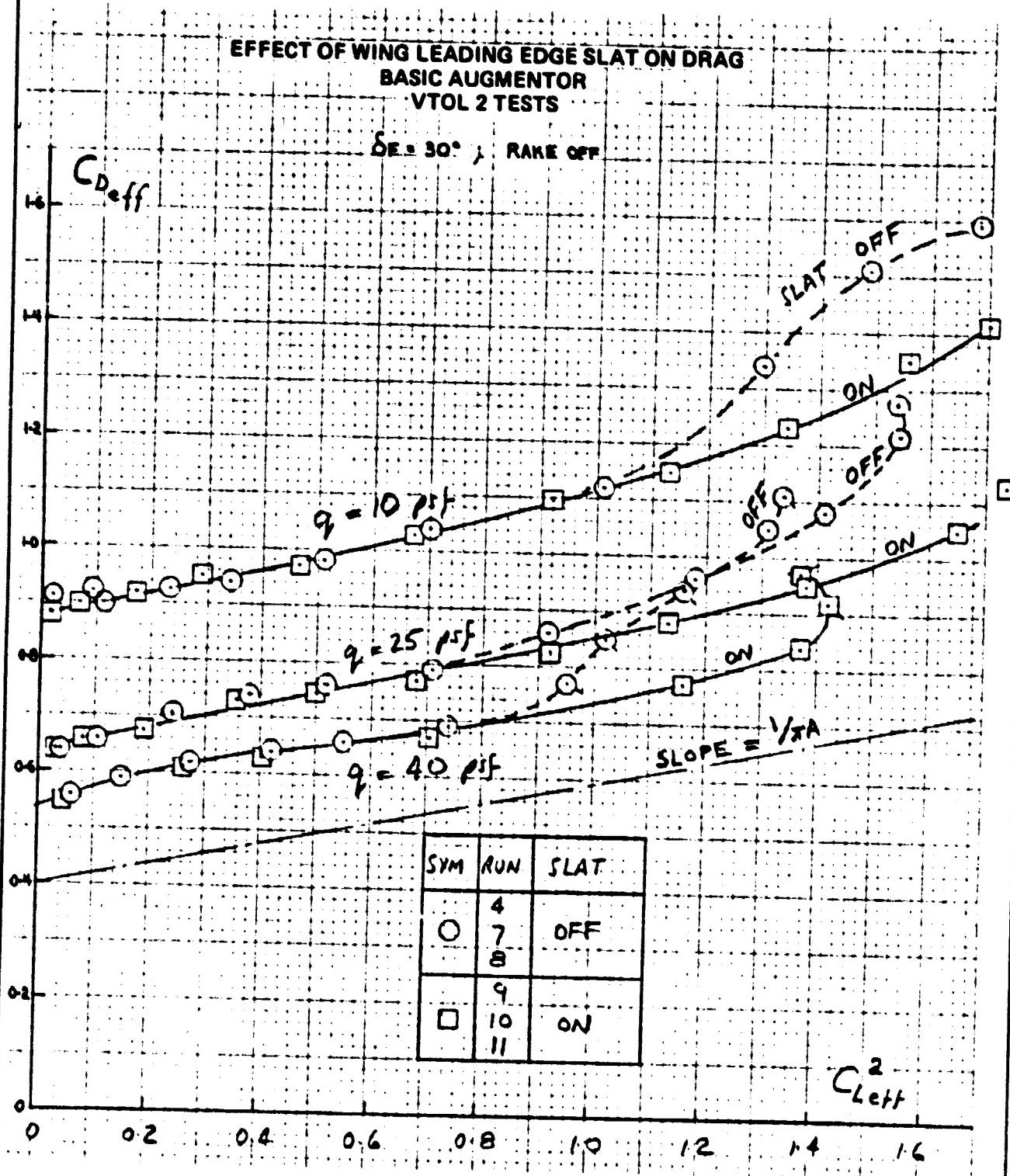




Fig. 75(a)

EFFECT OF POWER SETTING ON LATERAL/DIRECTIONAL CHARACTERISTICS

$\delta_F = 30^\circ$ ;  $q = 107 \text{ ft/lb}$ ; DAR = 1.6; FULL NOZZLES; RAKE ON

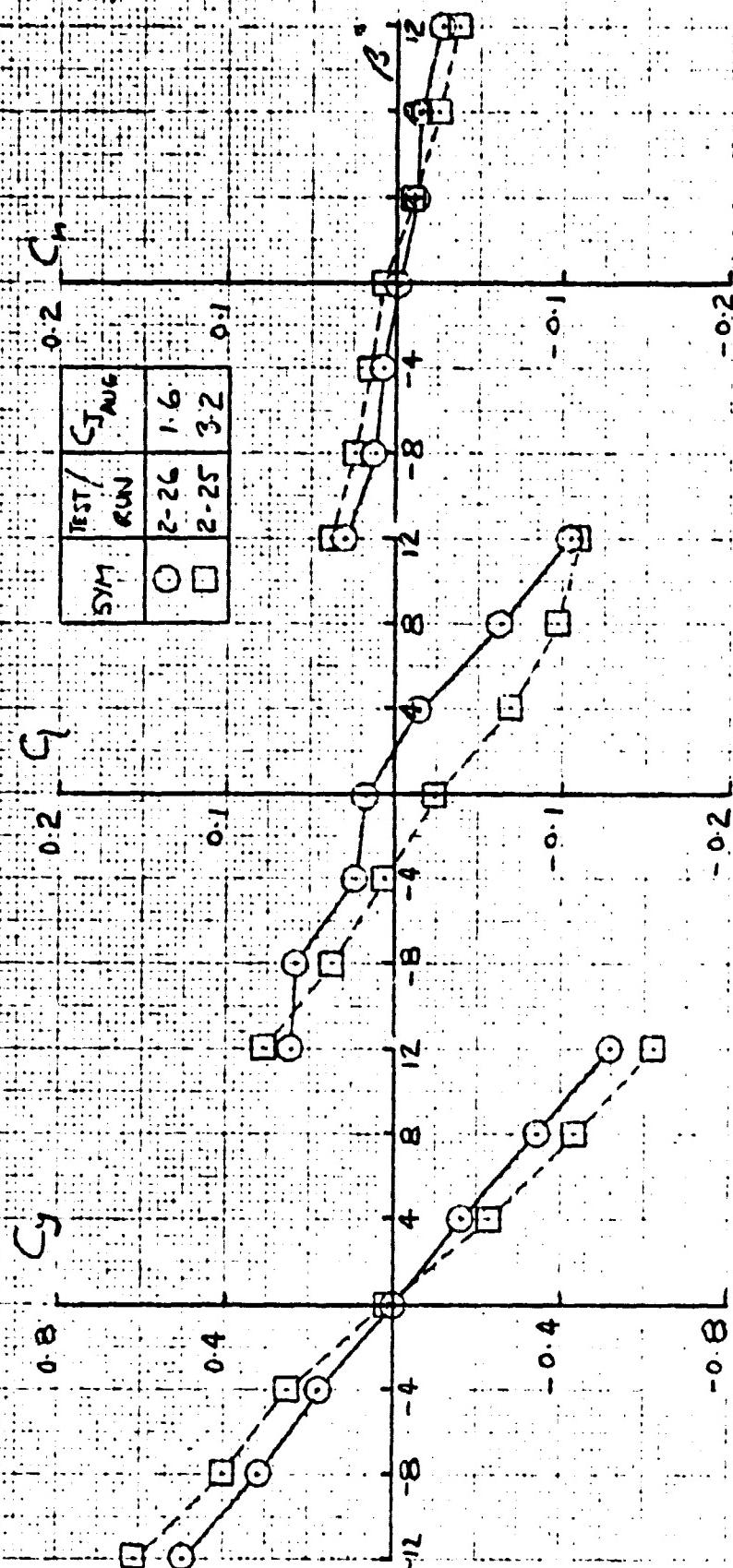
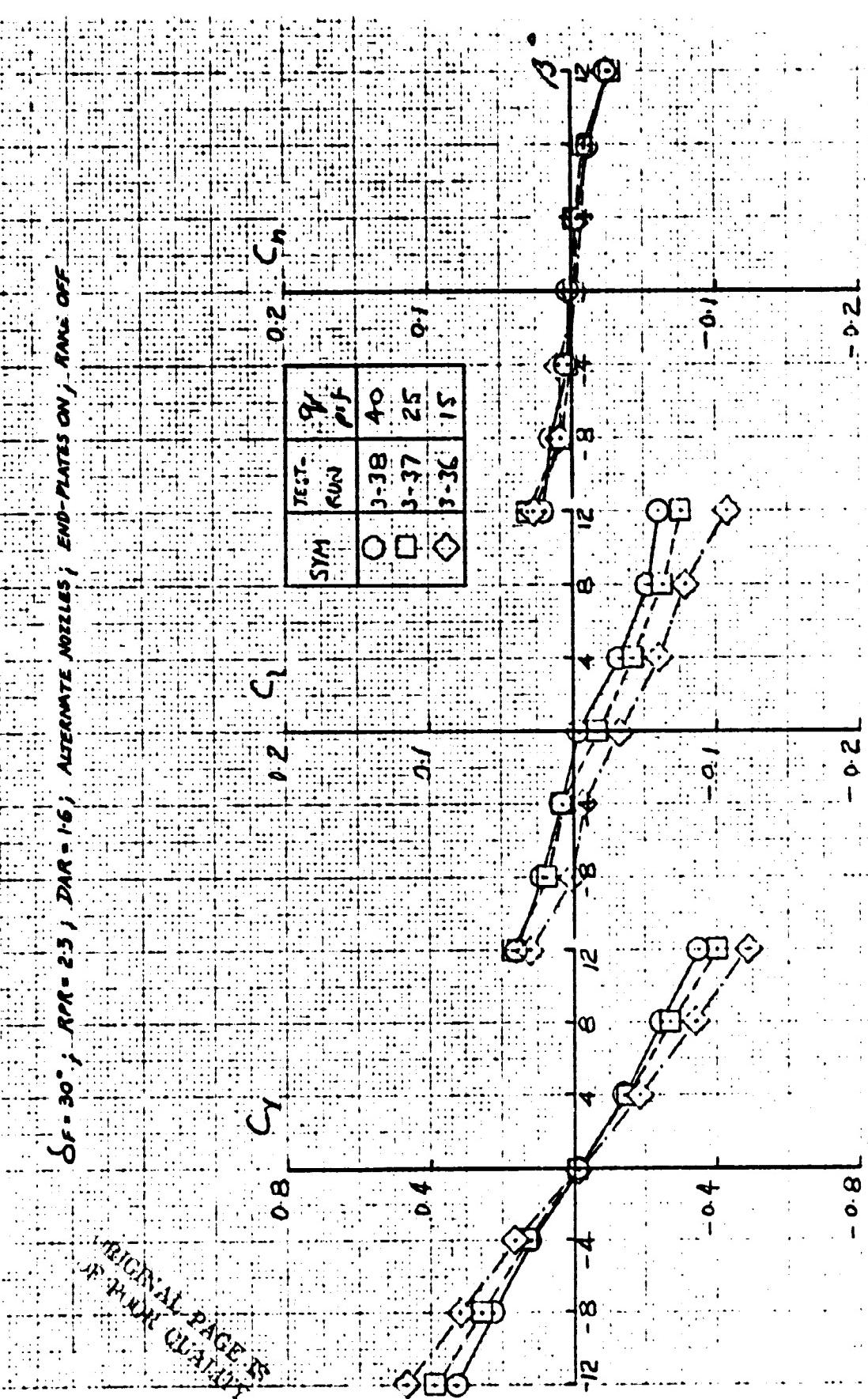




Fig. 75(b)

$\delta_F = 30^\circ$ ;  $RPR = 2.3$ ;  $DAR = 1.6$ ; ALTERNATE NOZZLES; END-PLATES ON; RAKE OFF



REPRODUCED BY  
PHOTOCOPIES  
EXCEPT AS  
NOTED

Fig. 76



EFFECT OF FUSELAGE AUGMENTOR NOZZLE ANGLE ON LATERAL/DIRECTIONAL CHARACTERISTICS

$\delta_F = 30^\circ$ ; RPR = 2.3;  $q = 10$ ; DAR = 1.6; FULL NOZZLES, RAKE ON

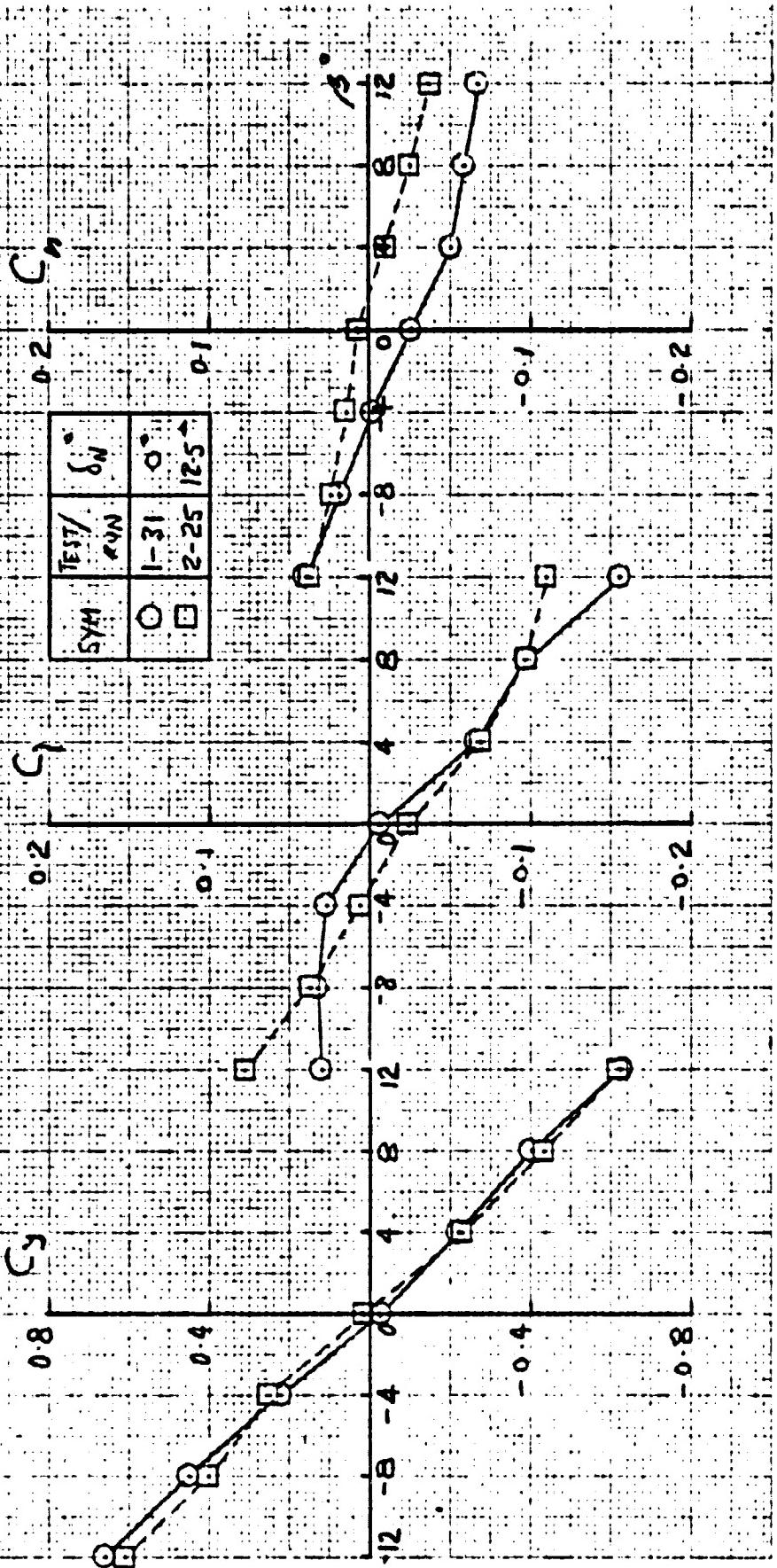


Fig. 77

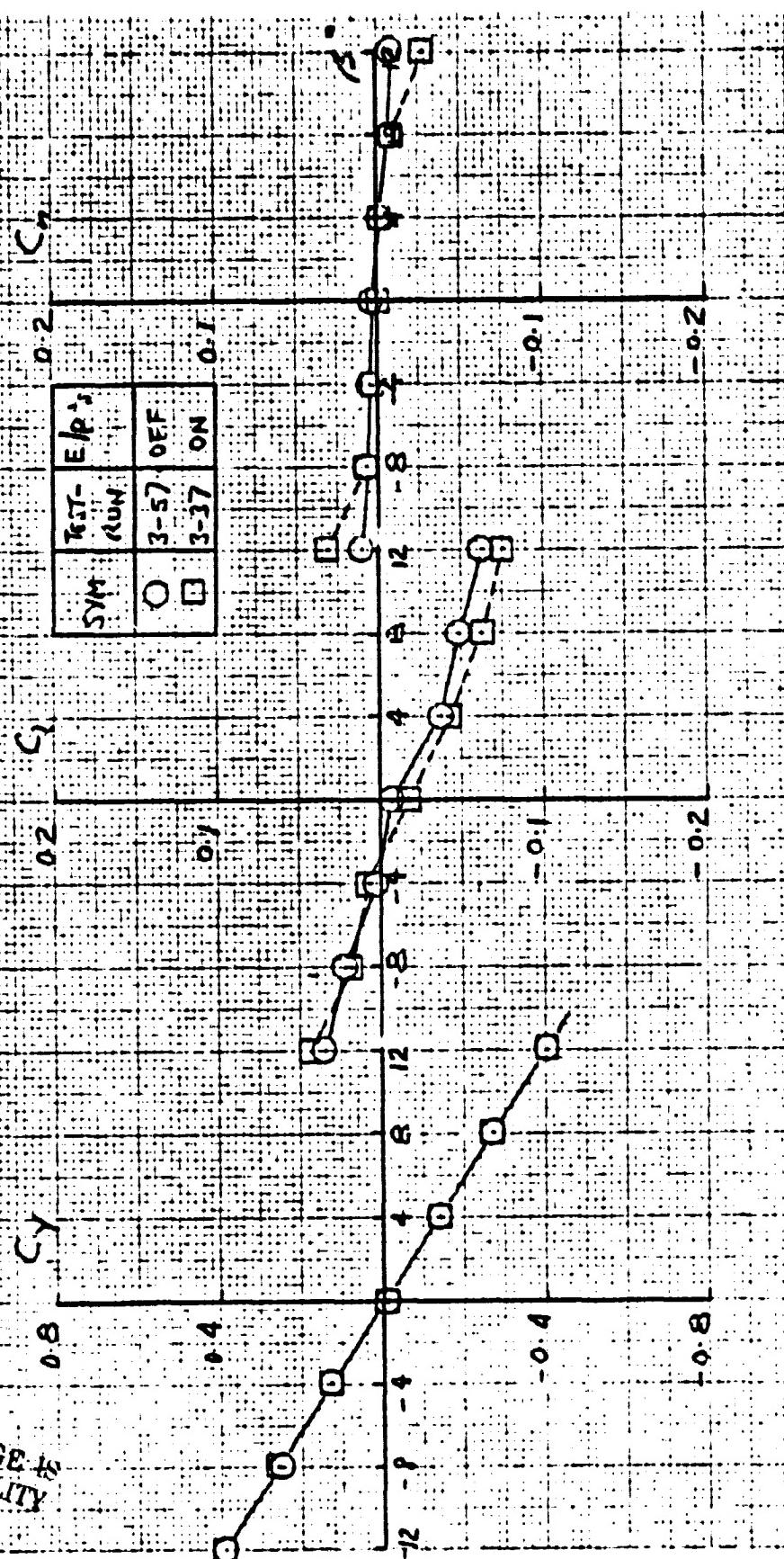


EFFECT OF FUSELAGE AUGMENTOR END-PLATES ON LATERAL / DIRECTIONAL CHARACTERISTICS

$\delta F = 30^\circ$ ; DAR = 1.6; ALTERNATE NOZZLES; RAKE OFF

SYM	TEST RUN	$E/\rho_A^2$
O	3-57	OFF
□	3-37	ON

ORIGINAL PAGE IS  
OF POOR QUALITY



EFFECT OF FORWARD SPEED ON LONGITUDINAL DISTRIBUTION OF THRUST AT AUGMENTOR EXIT

VTOL 2 RESULTS (RUNS 17-22) DAR = 1.6 : FULL NOZZLES

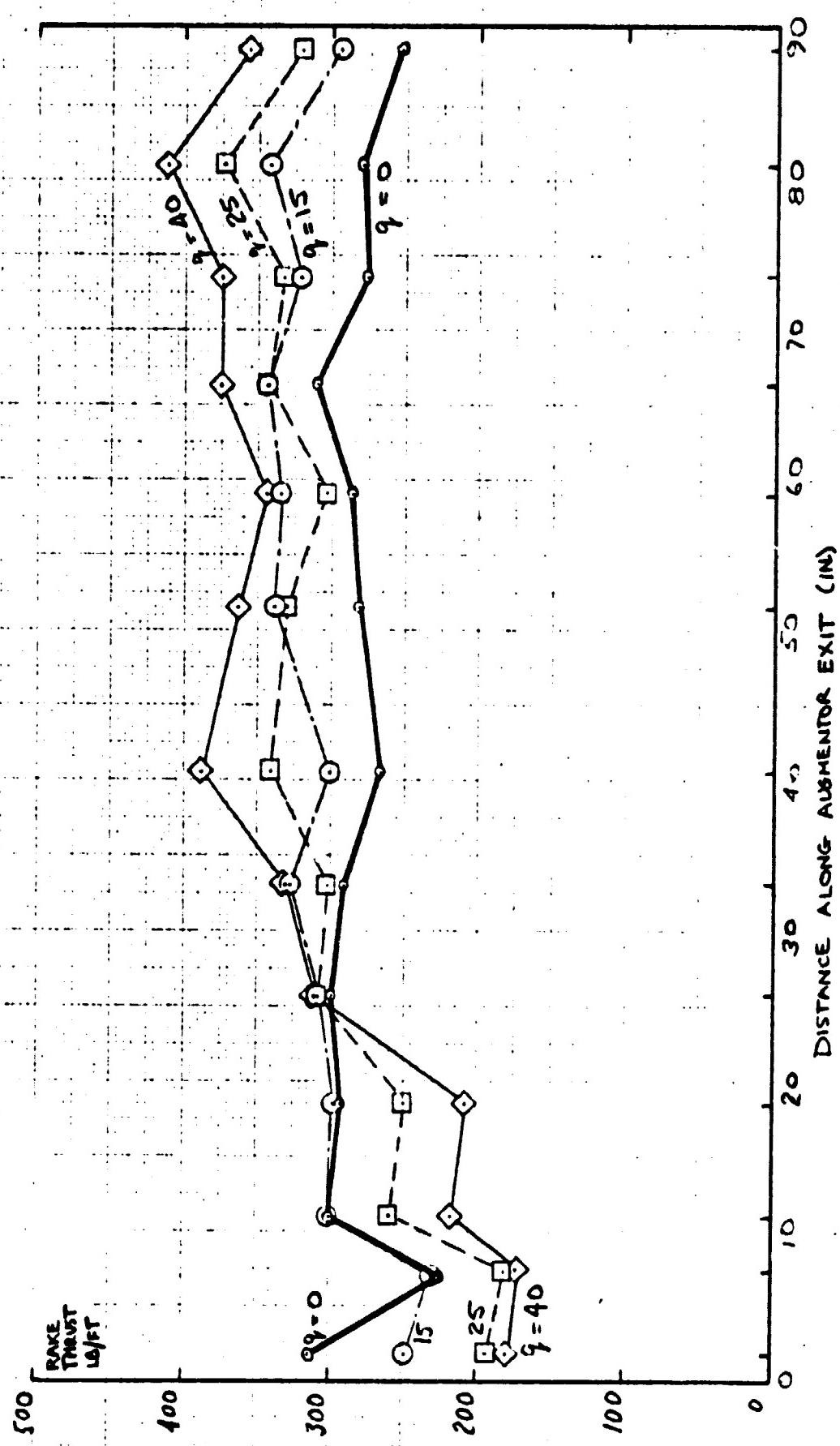


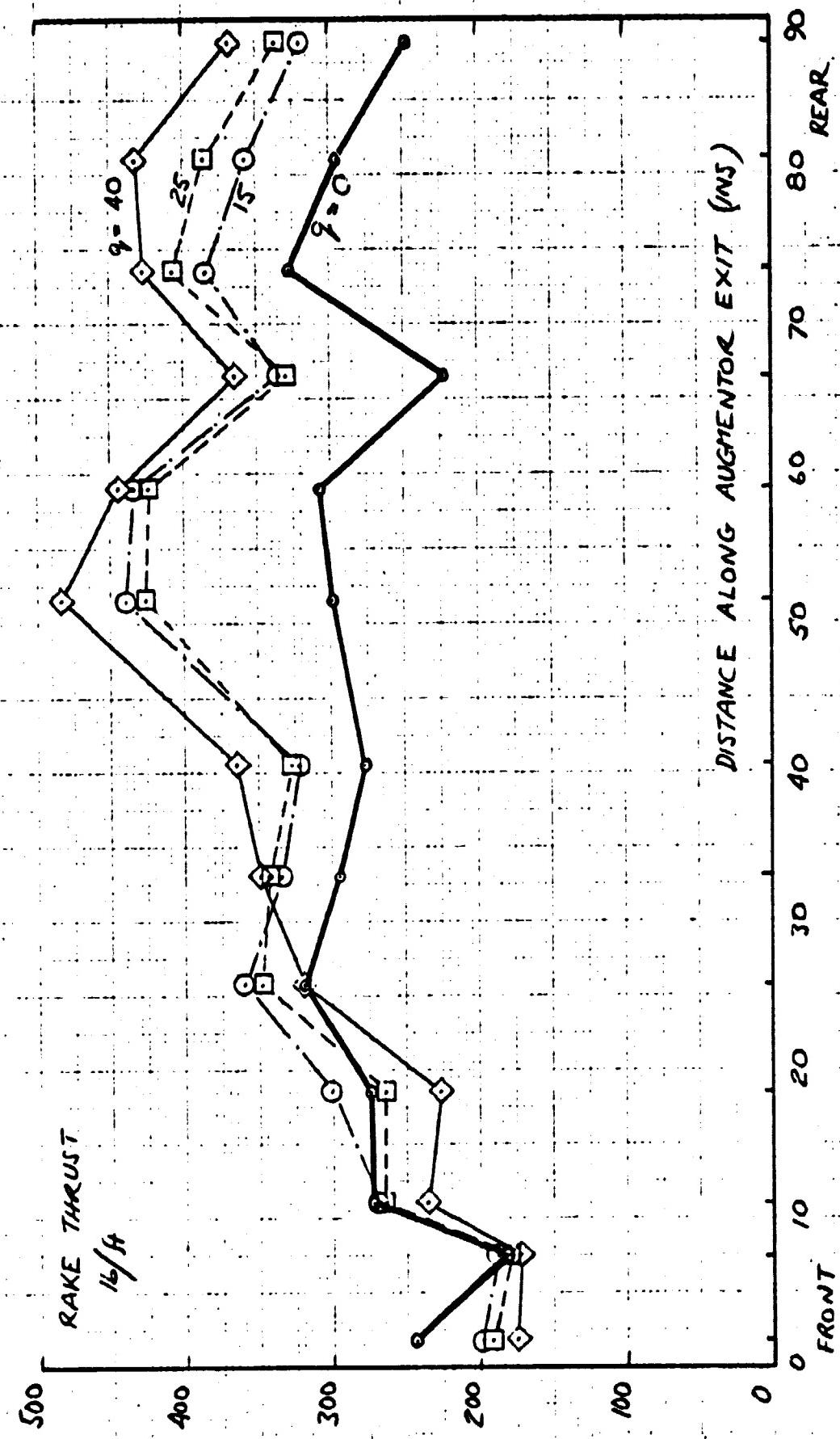
Fig. 78





Fig. 79

EFFECT OF FORWARD SPEED ON LONGITUDINAL DISTRIBUTION OF THRUST  
AT AUGMENTOR EXIT  
VTOL 3 RESULTS (RUNS 1-4) DAR = 1.6 : FULL NOZZLES



EFFECT OF FORWARD SPEED ON RAKE THRUST

$\alpha = 0^\circ$ ,  $1 \text{ DAR} = 1.6$ , FULL NOZZLES

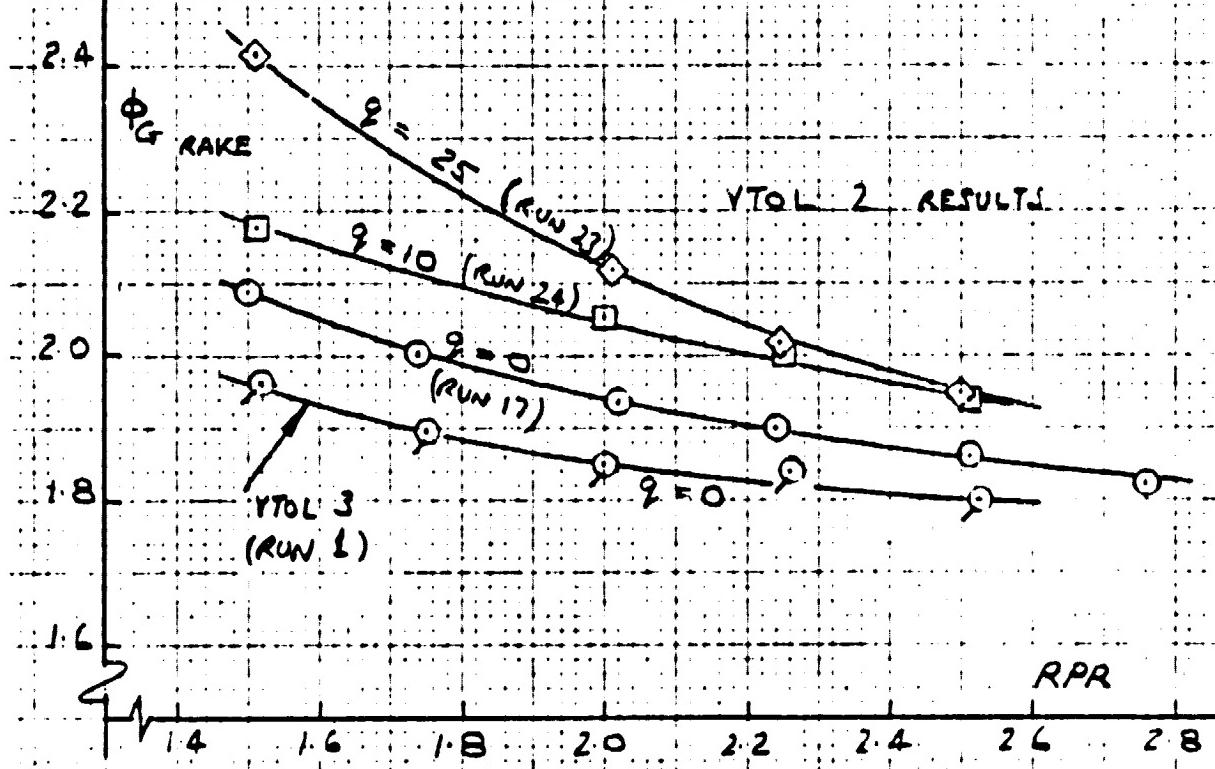
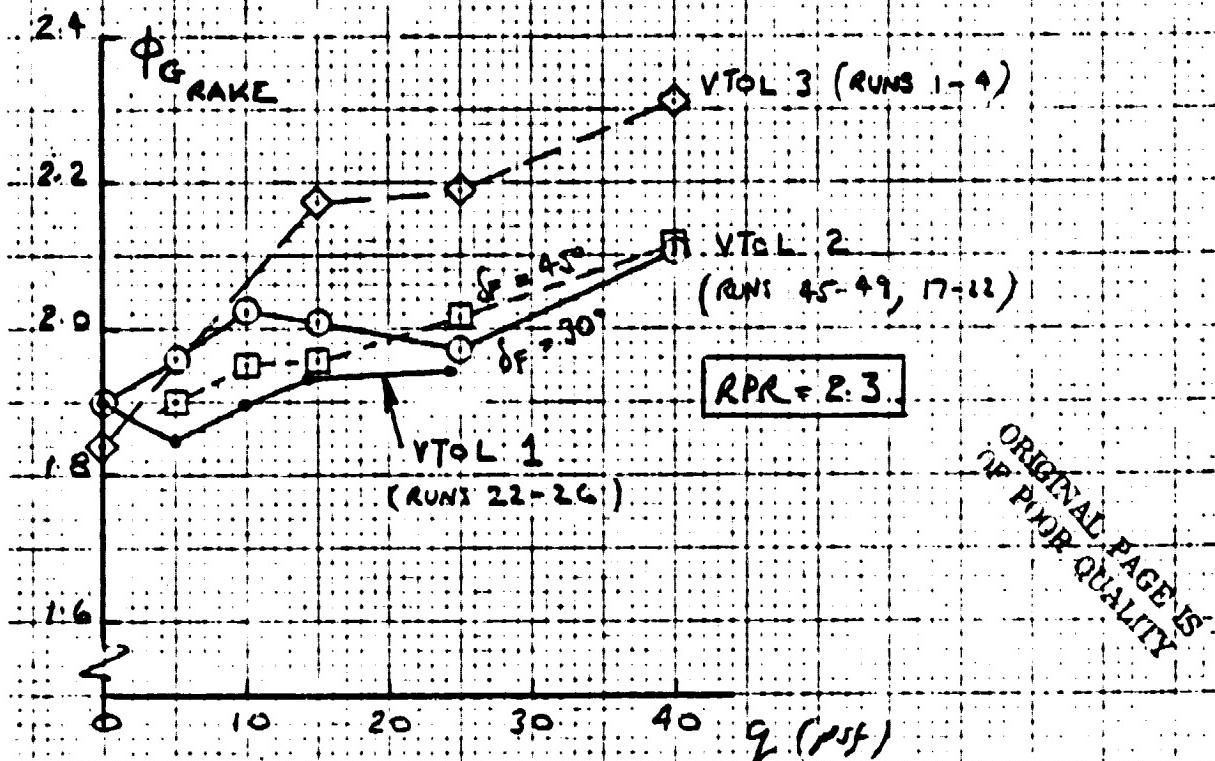
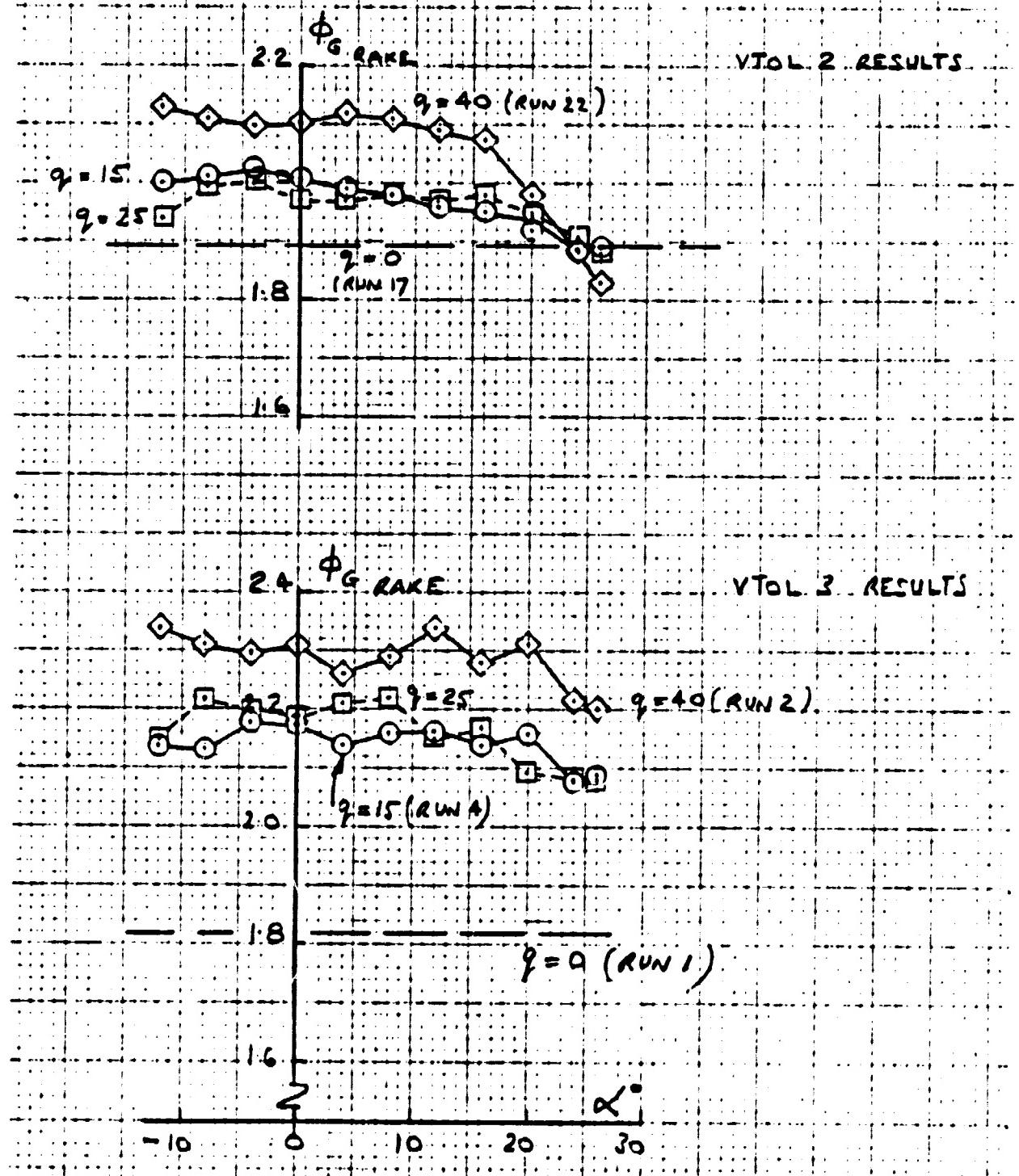




Fig. 81

EFFECT OF ANGLE OF ATTACK ON RAKE THRUST

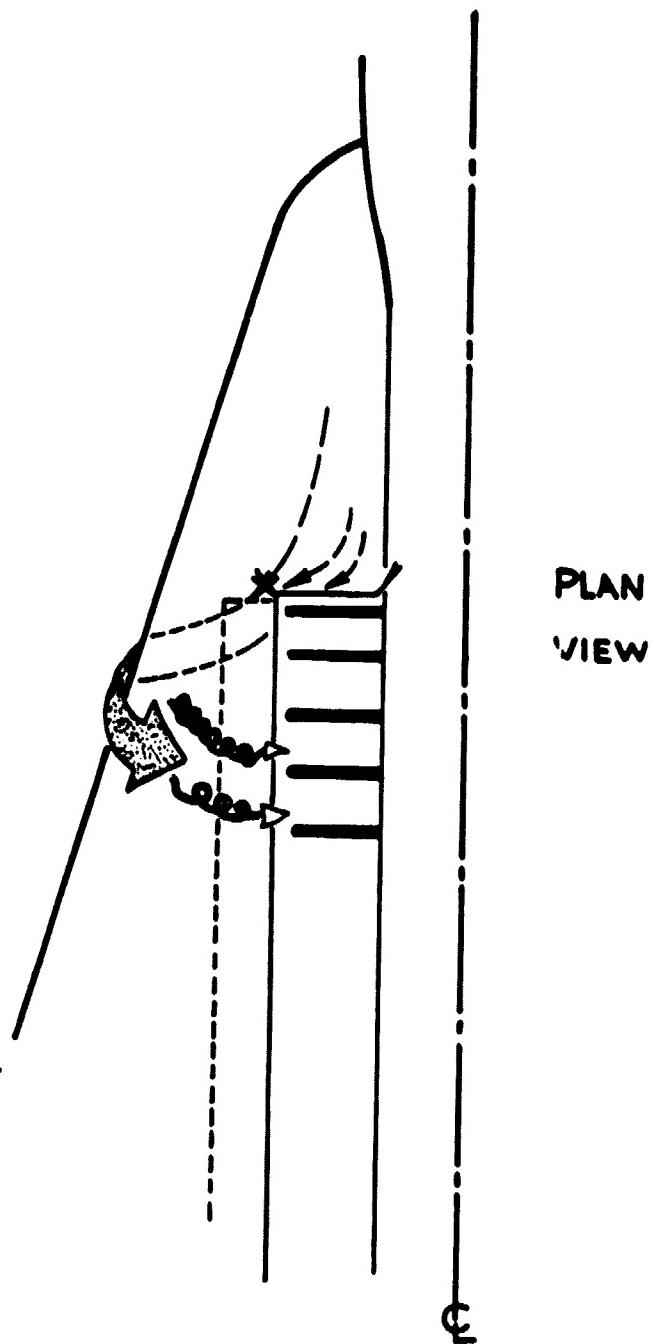
DAR = 1.6 FULL NOZZLES RPR = 2.3



ORIGINAL PAGE IS  
POOR QUALITY



Fig. 82



**FLOW SEPARATION FROM FRONT  
END-PLATE AND INGESTION BY AUGMENTOR**

Fig. 83(a)

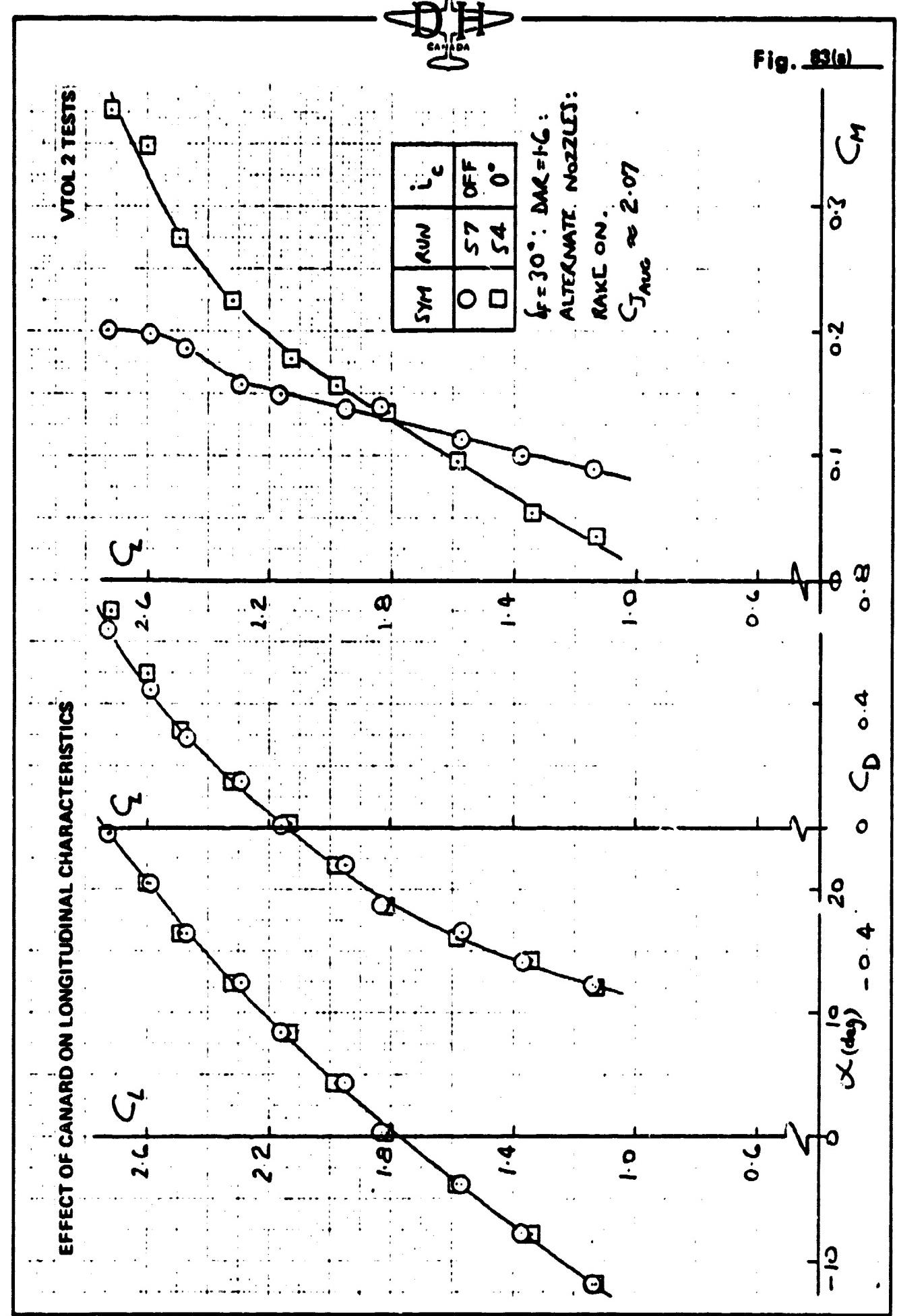


Fig. 83(b)

EFFECT OF CANARD ON LONGITUDINAL CHARACTERISTICS

VTOl 2 TESTS

ORIGINAL PAGE IS  
OF POOR QUALITY

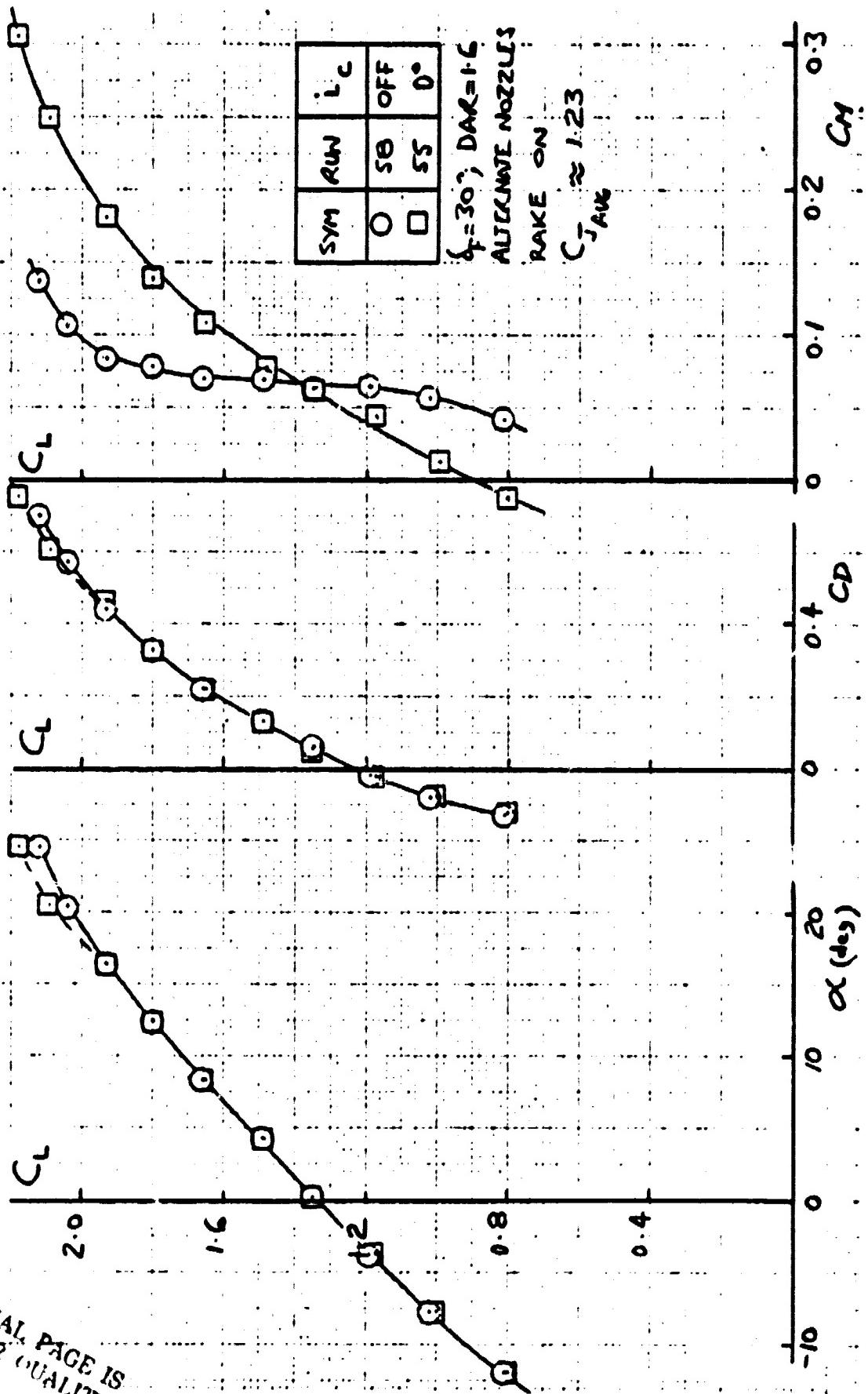
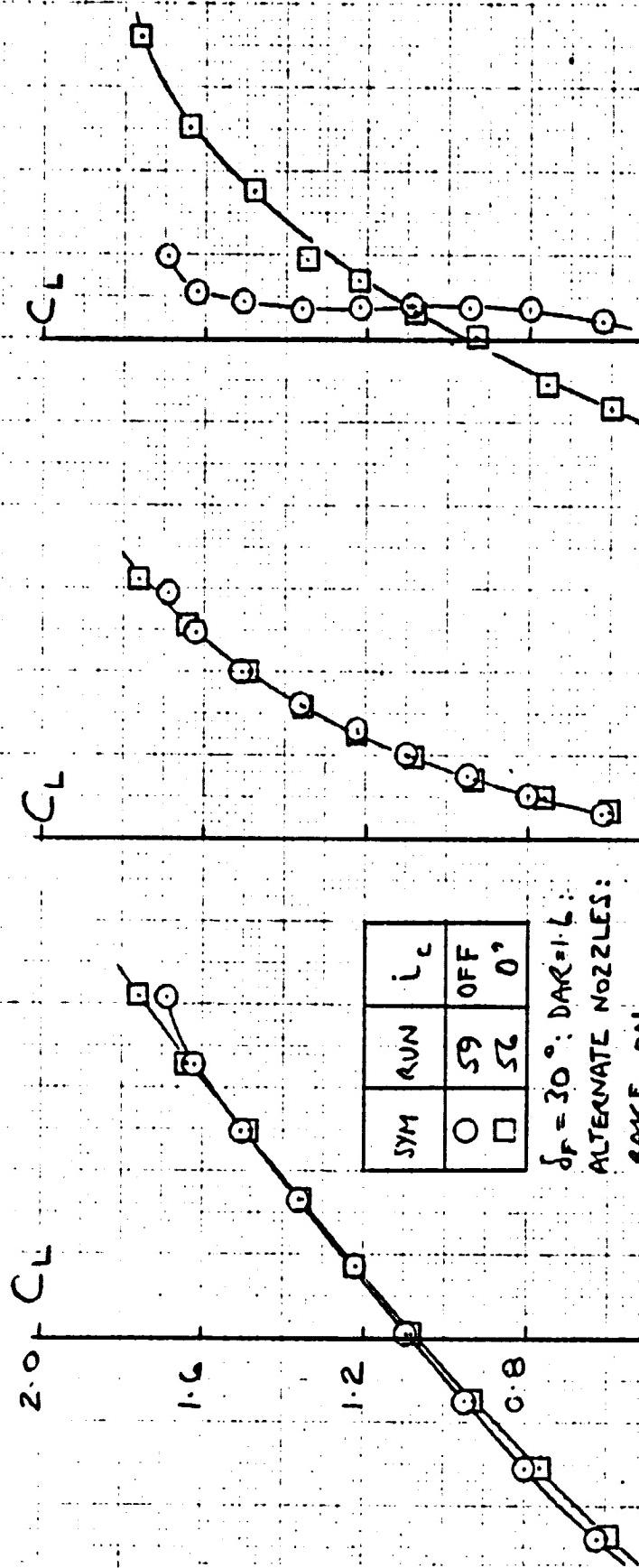


Fig. 83(c)

EFFECT OF CANARD ON LONGITUDINAL CHARACTERISTICS

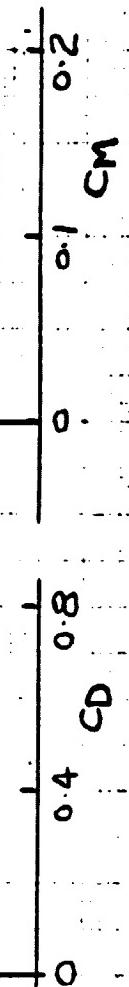
VTOL 2 TESTS

$2.0 \cdot C_L$

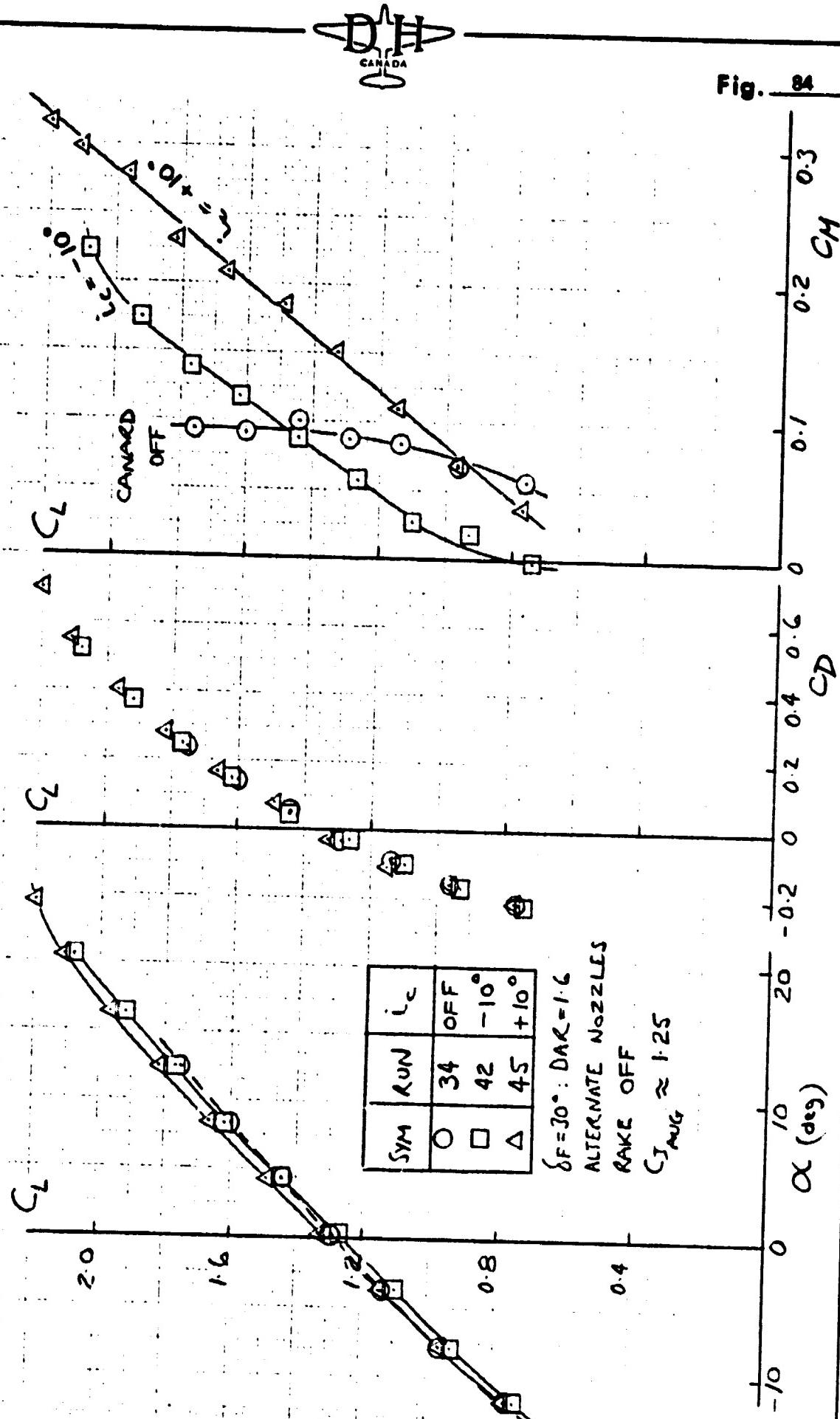


$\delta_F = 30^\circ$ ; DAR = 1.6;  
ALTERNATE NOZZLES:  
RAKE AN.

$C_{T_{AVG}} \approx 0.77$

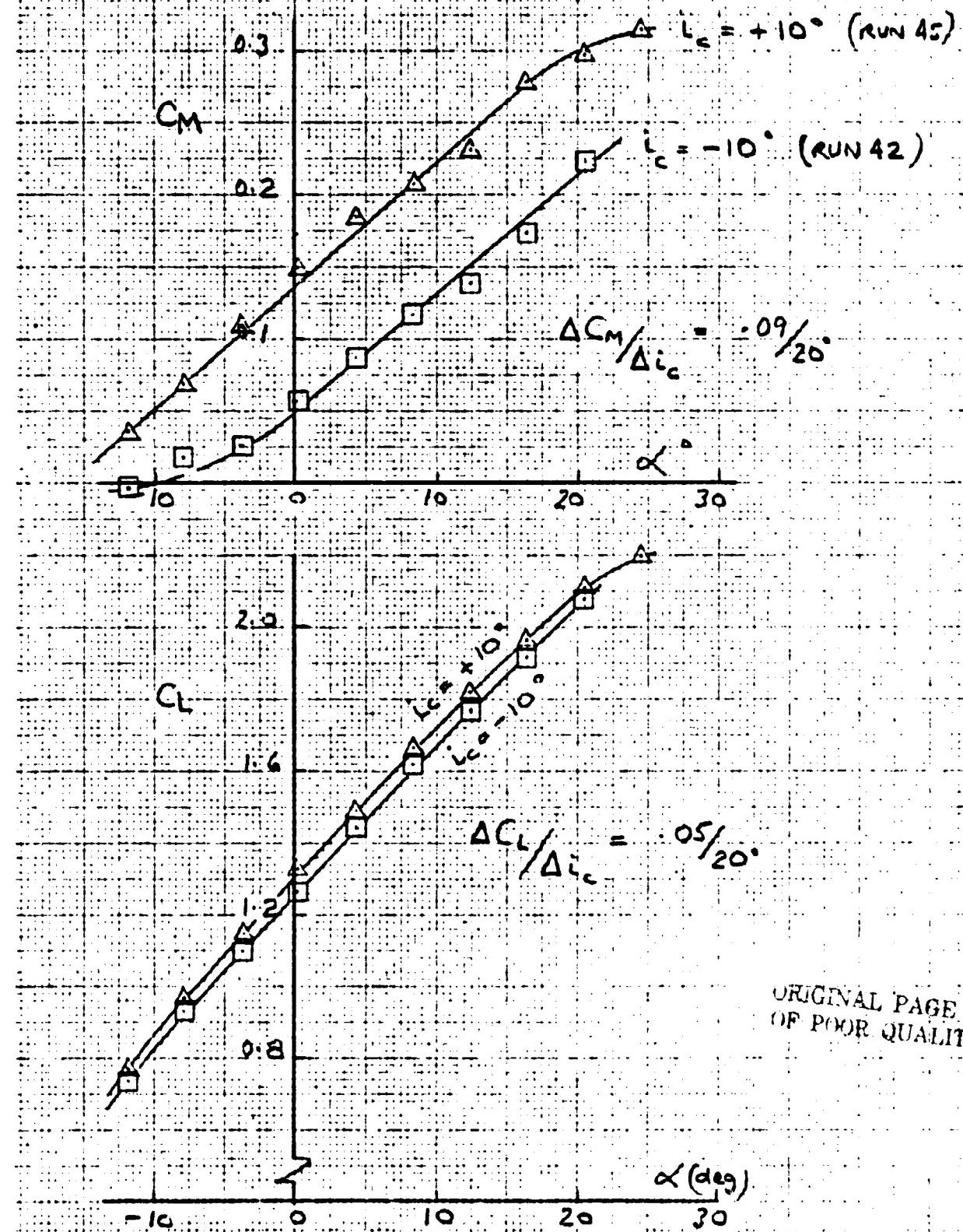


## VTOL 3 TESTS    EFFECT OF CANARD SURFACE ON LONGITUDINAL CHARACTERISTICS

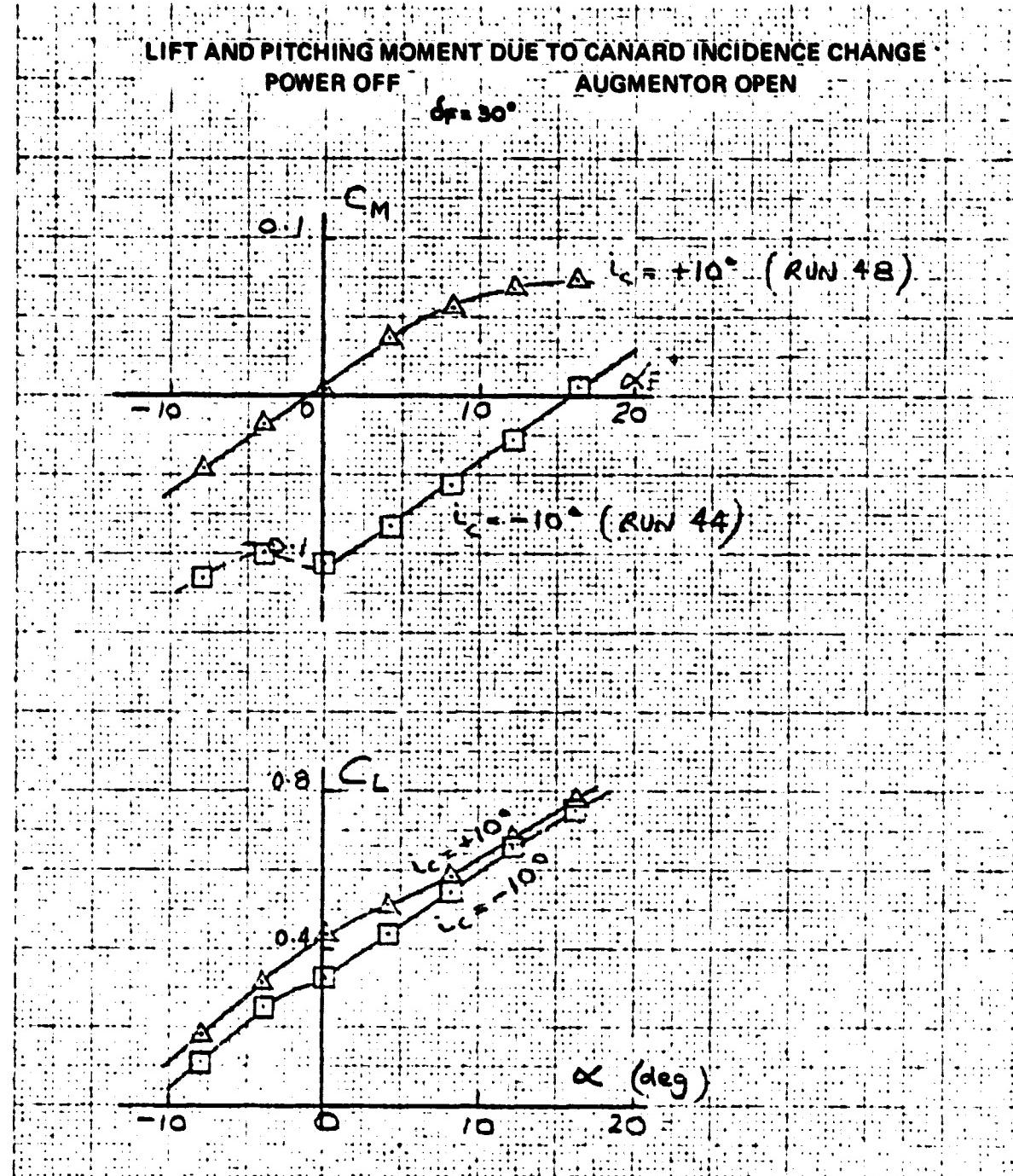


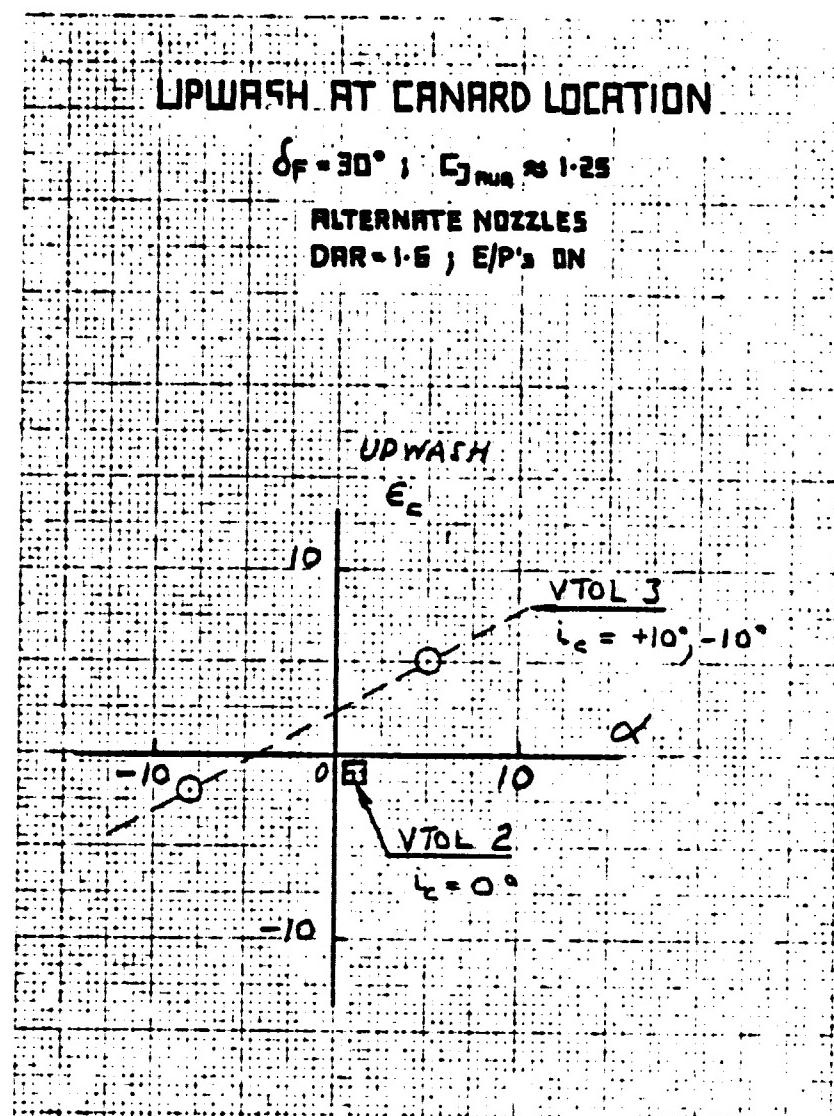
LIFT AND PITCHING MOMENT DUE TO CANARD INCIDENCE CHANGE

$C_{L\text{can}} = 1.25$ ;  $\delta_F = 30^\circ$



ORIGINAL PAGE IS  
OF POOR QUALITY





EFFECT OF CANARD FLAP ON  $C_L$ ,  $C_D$ ,  $C_M$ 

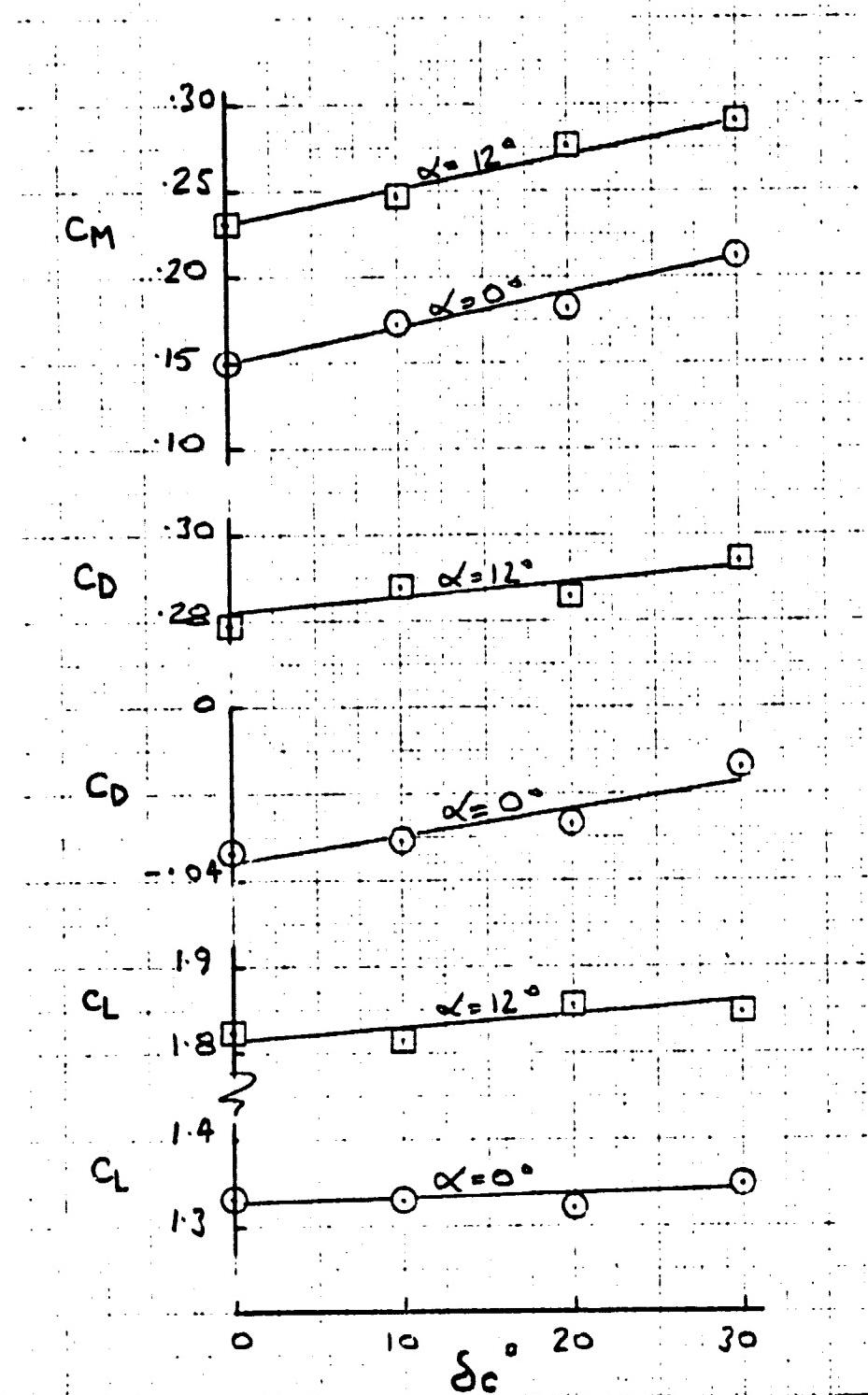
 RUN 43, VTOL 3 TESTS;  $\delta_F = 30^\circ$ 

 ORIGINAL PAGE IS  
OF POOR QUALITY

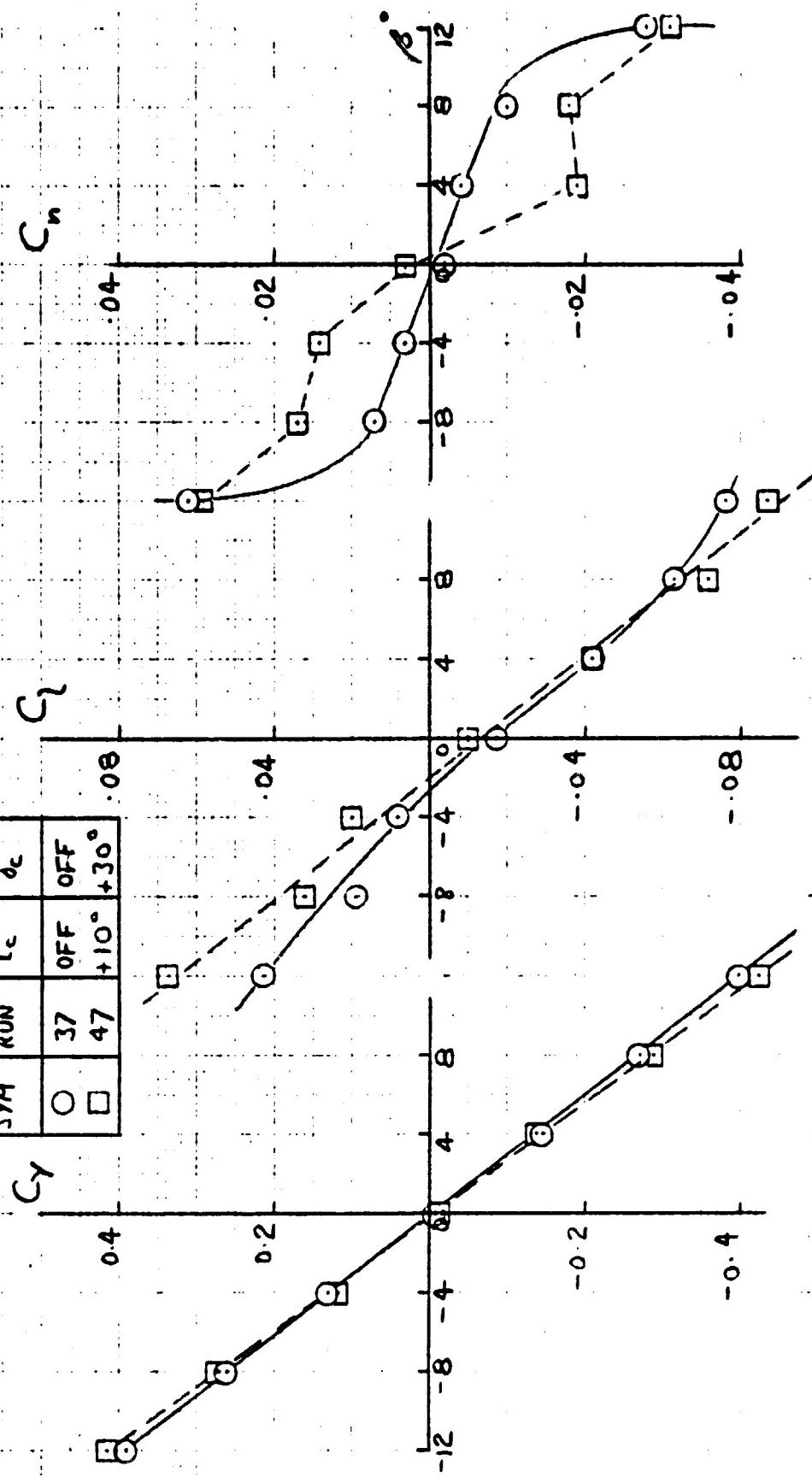


Fig. 89

EFFECT OF CANARD ON LATERAL/DIRECTIONAL CHARACTERISTICS

$$(\gamma_{TOL}, \beta) = 0^\circ; C_{J, AVG} \approx 1.25$$

SYN	RUN	$i_c$	$\delta_c$
○	37	OFF	OFF
□	47	+10°	+30°



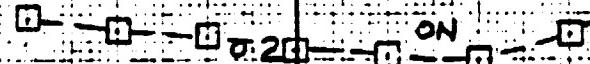
SYM	RUN	$L_c$	$\delta_c$
○	3-37	OFF	OFF
□	3-47	+10°	+30°
◇	3-43	-10°	0°

$\alpha = 0^\circ : C_{AUG} \approx 1.25$

$\delta_F = 30^\circ$

0.3

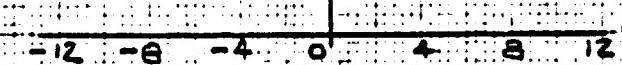
$C_M$



0.1

CANARD

OFF



-0.4

$C_D$

-0.2



1.4

1.0

EFFECT OF CANARD ON LONGITUDINAL  
CHARACTERISTICS WITH YAW ANGLE

ORIGINAL PAGE IS  
OF POOR QUALITY